PHOTOGRAPH THIS SHEET

A131684

DTIC ACCESSION NUMBER

II

LEVEL

I

INVENTORY

Deterioration of Synthetic Fiber Rope During Marine Usage.

DOCUMENT IDENTIFICATION

1 Jan. - 31 Dec. '81

Progress Rpt., Project R/T-11

31 Dec '81

DISTRIBUTION STATEMENT A
Approved for public release;
Distribution Unlimited

DISTRIBUTION STATEMENT

ACCESSION FOR		
NTIS	GRA&I	☒
DTIC	TAB	☐
UNANNOUNCED		☐
JUSTIFICATION		
BY		
DISTRIBUTION /		
AVAILABILITY CODES		
DIST	AVAIL AND/OR SPECIAL	
A		

DISTRIBUTION STAMP

DTIC
ELECTE
S AUG 24 1983 D
D

DATE ACCESSIONED

DTIC COPY INSPECTED

83 08 01 022

DATE RECEIVED IN DTIC

PHOTOGRAPH THIS SHEET AND RETURN TO DTIC-DDA-2

DTIC FORM OCT 79 70A

DOCUMENT PROCESSING SHEET

DETERIORATION OF SYNTHETIC FIBER ROPE

DETERIORATION OF SYNTHETIC FIBER ROPE DURING MARINE USAGE

PROGRESS REPORT PROJECT R/T-11

PERIOD JANUARY 1 - DECEMBER 31, 1981

PREPARED FOR

SEA GRANT OFFICE

MASSACHUSETTS INSTITUTE OF TECHNOLOGY

CAMBRIDGE, MASSACHUSETTS 02139

FUNDED BY

NAVAL SEA SYSTEMS COMMAND

U. S. NAVY

Document was not prepared under a contract number but was prepared under a sea grant per Mr. George Prentice, NAVSEA

PRINCIPAL INVESTIGATORS

STANLEY BACKER

FREDERICK J. McGARRY

JAMES H. WILLIAMS, JR.

ACKNOWLEDGMENT

Investigators in this project acknowledge with appreciation the considerable guidance and encouragement received from Mr. George Prentice of the Naval Sea Systems Command. Mr. Steve Roush and Mr. Ken Bitting of the U. S. Coast Guard have also provided needed assistance in our studies.

PARTICIPANTS IN STUDY OF DETERIORATION OF SYNTHETIC FIBER ROPE DURING MARINE USAGE

POLYMERS LABORATORY

Professor Frederick J. McGarry
Dr. John Mandell
Mrs. Maryann Kenney*

COMPOSITE MATERIALS AND NDE LABORATORY

Professor James H. Williams, Jr.
Dr. Samson Lee

FIBERS AND POLYMERS LABORATORY

Professor Stanley Backer
Professor Giuliana C. Tesoro
Mr. Peter Hsu*
Mr. Moon Seo*

*Full time Research Assistants

OUTLINE OF CONTENTS

		Page Number
1.	GENERAL INTRODUCTION	1.1
2.	ENVIRONMENTAL DEGRADATION OF NYLON AND POLYESTER GIULIANA C. TESORO	2.1
3.	PATHOLOGICAL STUDY OF WORN ROPES STANLEY BACKER, PETER HSU and MOON SEO	3.1
4.	NONDESTRUCTIVE EVALUATION OF SYNTHETIC ROPE JAMES H. WILLIAMS, JR. and SAMSON LEE	4.1
5.	FATIGUE LOADING AND ENVIRONMENTAL EFFECTS JOHN F. MANDELL and MARYANN KENNEY	5.1
6.	MECHANICAL STUDIES OF NEW ROPE STANLEY BACKER, PETER HSU and MILOS NEBESAR	6.1

TABLE OF CONTENTS

	Page Number
1. GENERAL INTRODUCTION	1.1
Objectives of Program	1.1
Research Plan	1.2
Summary of Progress	1.2
2. ENVIRONMENTAL DEGRADATION OF NYLON AND POLYESTER	2.1
Introduction and Scope	2.1
Mechanisms of Chemical Degradation	2.6
Photochemical Degradation	2.10
Oxidative and Thermo-Oxidative Degradation	2.34
Immersion in Water and Aqueous Solutions	2.37
Assessment of Chemical Degradation in Fibers	2.46
Summary/Conclusions and Recommendations	2.55
3. PATHOLOGICAL STUDY OF WORN ROPES	3.1
Introduction	3.1
Structural composition of Used Ropes	3.1
Tensile Properties of Fibers and Yarns	3.3
Molecular Weight Studies	3.11
Differential Scanning Calorimetry	3.15
Effect of Water Immersion	3.16
Microscopic Studies	3.19
Summary/Conclusions	3.27
Future Plans	3.28
References	3.29
4. NONDESTRUCTIVE EVALUATION OF SYNTHETIC ROPES	4.1
Introduction	4.1
Ultrasonic Characterizations	4.1
Acoustic Emission Characterizations	4.3
Conclusions	4.7
Future Plans	4.7
References	4.8

TABLE OF CONTENTS

	Page Number
5. FATIGUE LOADING AND ENVIRONMENTAL EFFECTS	5.1
Introduction	5.1
Experimental Procedures	5.3
Results and Discussion	5.4
Conclusions	5.8
Future Plans	5.9
References	5.9
6. MECHANICAL STUDIES OF NEW ROPE	6.1
Structural Changes Incurred During Loading	6.3
Crushing of Filaments	6.5
Self-Induced Twisting of Running Ropes	6.6
Structural Mechanics of Rope Structures	6.7
Summary/Conclusions/Future Plans	6.9
References	6.11

DETERIORATION OF SYNTHETIC FIBER ROPE

DURING MARINE USAGE

1. GENERAL INTRODUCTION

This three-year program was initiated on a limited basis in October 1980. By February 1, 1982, three distinct laboratory groups at M.I.T. had become active in various phases of the study. Cooperating groups included the Polymers Laboratory of the Department of Materials Science and Engineering, as well as the Composite Materials and Nondestructive Evaluation Laboratory and the Fibers and Polymers Laboratory of the Department of Mechanical Engineering.

OBJECTIVES OF PROGRAM

The overall objectives of this three-year program are:

- To identify the sources and corresponding rates of deterioration of mechanical properties during usage or storage of synthetic-fiber marine cordage.
- To evaluate or develop nondestructive tests capable of detecting and quantifying:
  - (a) average rope deterioration due to general stress applications and to overall exposure,
  - (b) local deterioration due to excessive stresses incurred during handling.
- To analyze and verify experimentally the modes of local deformation and the stress distributions which occur in rope structures during usage under various marine conditions.
- Based on results obtained above, prepare recommendations relating to:
  - (a) development of nondestructive test devices for shipboard evaluation of rope deterioration,
  - (b) development of new material/structural combinations to enhance rope behavior and to reduce deterioration rates,
  - (c) modification of usage and handling procedures to extend the safe life of marine ropes.

RESEARCH PLAN

The research plan of the study is subdivided into seven phases as follows:

(1) Survey of (a) rope literature to identify mechanisms of failure and (b) textile literature to determine treatment of similar problems in apparel and industrial materials.

(2) "Pathological" study of worn ropes to confirm presence of failure mechanisms cited in rope and textile literature and to identify new modes of deterioration.

(3) Development of nondestructive evaluation methods to identify (a) local faults, (b) uniform degradation.

(4) Analytical studies of deformation modes and stress distributions during typical rope loading procedures.

(5) Investigation of the role of stress-corrosion cracking in fiber-deterioration.

(6) Experimental studies to confirm predicted deformation modes and stress distributions.

(7) Preparation of design recommendations for:

   (a) NDE techniques for shipboard use,

   (b) new material/structures combinations,

   (c) modification of rope usage and handling procedures.

SUMMARY OF PROGRESS

This section contains the individual executive summaries of progress to date in each of the study phases which were active during the first year of the program.

Environmental Degradation of Nylon and Polyester

A critical evaluation of the literature in context of Ocean Engineering applications

A critical evaluation of concepts and results discussed in the literature on environmental/chemical degradation of nylon and of polyester is presented, with emphasis on investigations that may be relevant to the problems of rope degradation in use. The objective is to provide a basis for enhanced understanding of the role of chemical and structural changes of fibers in the deterioration of rope properties during use.

The effects of ultraviolet radiation, of oxygen, and of aqueous environments on the chemical degradation of nylons and of polyester have been studies in depth by many investigators; some of the important variables have been defined, and attempts have been made to establish correlations between observed changes in the chemical structure, or in the supramolecular structure, and specific properties of polymers or fibers. It is extremely difficult, however, to apply the results obtained and knowledge gained in laboratory experiments under controlled conditions to the realistic situation of ropes in ocean engineering applications.

This report summarizes current knowledge on the mechanisms of chemical degradation of primary importance in nylon and in polyester, and on the numerous variables which must be considered in interpreting results of exposure to environments causing degradation. In the case of exposure to ultraviolet radiation, it has been shown that in the presence of oxygen, photochemical degradation of polyamides and of polyesters involves photosensitized oxidation processes in which chain scission is the dominant degradative reaction. Chain scission is reflected in decreased average molecular weight of polymer chains, and is accompanied by microstructural changes and by changes in mechanical properties which have particular significance in the case of fibers. Photochemical degradation is accelerated in the presence of titanium dioxide delustrant. It can also be retarded or inhibited by fiber additives which operate by one of several mechanisms.

In the case of interaction with aqueous media, the changes that occur in fibers as a result of exposure to high relative humidity, or of immersion in water, or of prolonged contact with solutions of specific inorganic salts can accelerate the degradative effects of other factors under some conditions.

The experimental assessment of environmental degradation in fibers requires consideration of changes on a molecular level, and on the level of supramolecular structure. Methodology for evaluation includes analysis of specific functional groups by instrumental techniques; measurements of molecular weight averages and of molecular weight distribution; evaluation of moisture response, swelling, and dye diffusion; scanning electron microscopy; and assessment of mechanical properties. The correlation of the conditions of exposure with the extent of degradation can be attempted in laboratory experiments carried out on well characterized materials under controlled conditions. For materials exposed to degradative environments in use, the methods of evaluation and criteria indicated may be used with reference to appropriate controls, only to suggest the magnitude of change over specified periods of usage.

Pathological Study of Worn Ropes

Structural Composition of Used Ropes

Each of the worn ropes selected for study in this first year has been analyzed as to its structural composition. The step-by-step build-up of the rope, starting with the fiber producers' basic yarn, has been documented. While most of the 3-strand lines had the same basic structure and were composed throughout of a given singles and plied yarn, one rope was observed to use different sized yarns in the strand core vs. the peripheral section of the strand. The base filament employed in most ropes studied was 6-denier, high tenacity (bright) nylon 66, although, in the case of two ropes, other deniers were used--13-denier and 8-denier. One rope was composed of nylon 6 filaments and another of polyester.

Tensile Properties

The purpose of these studies of the tensile properties of fibers and yarns taken from worn ropes has been to provide empirical data on local rope deterioration during marine usage and to furnish the basis for formulating a realistic model of ropes in service to be used in subsequent applied mechanics studies. Both short span (0.5-in) and long span (8-in to 12-in) tensile tests were conducted.

The short span tests were used to probe the extent and distribution of tensile loss over the cross section of the rope at a given location along its length. Short span tests were again employed to determine the distribution of residual filament strength along the lengths of selected yarns in a full twist period in the rope structure. Such tests were conducted at various locations over the rope cross section. Long span tests were then carried out to identify the distribution and severity of weak spots along 8-in to 12-in yarn lengths extracted from inner and outer sections of the rope. And, in one case, repeat tests were made on already tested filament lengths to identify a second weak spot.

The data indicate that core fibers of the 3-strand ropes manifest fairly constant values of tensile strength along their length and fiber rupture locations are spread uniformly along the 8-in to 12-in lengths. Tensile rupture locations in layers closer to the strand surface are no longer uniformly spread along the filament lengths. At the surface, and, in some cases, at the first sublayer of the strand, the average tensile value decreases significantly, the spread of breaking strength increases markedly and the failure locations tend to congregate. Such groupings can reflect either highly concentrated damage due to local external wear, or periodic damage, indicating more uniform external deterioration condition interacting with the periodic geometric availability of the yarns at the rope surface.

In double braided ropes, filaments taken from the inside of

plied yarns of the rope core manifest higher strengths than those from the surface layers of the same yarns. The inner zone fibers also display a more uniform spread of rupture locations. Distinct rupture location groupings for the outer zone filaments of the rope core yarns reflect the likelihood of internal rope abrasion between outer surface fibers of the core and the inner surface of the cover braid.

Evidence of the role of internal rope abrasion is also seen in the data from short span tests taken over the cross section of some 3-strand ropes. In particular, filaments extracted from the closely packed "hard" spots in the surface and subsurface strand layers (at rope center locations) show strength reductions, which, in some cases, are significant. Microscopic examination confirms that internal abrasion does contribute to these reductions.

The goal of these first year mechanical pathological studies has been reached to a reasonable extent and sufficient data are now at hand to enhance further studies of rope mechanics. It is expected that some limited studies of filament damage distribution will be continued, particularly in the case of rope samples for which more precise wear and exposure histories are available.

Molecular Weight Studies

The purpose of the molecular weight measurements was to establish whether there is prima facie evidence of chemical degradation (chain scission) for fibers in regions of maximum wear, in which visual and microscopic observation and testing of mechanical properties suggest that extensive degradation may have occurred in use. After initial trials with various analytical systems, it was decided to use Gel Permeation Chromotography (GPC) for determination of molecular weight changes, a method capable of providing precise and reproducible number-average ($\bar{M}_n$) and weight-average ($\bar{M}_w$) molecular weight values, as well as a measure of polydispersity index relating to the broadness of the molecular weight distribution. Samples of unused rope, comparable age and similar filaments were not available for use as controls in these tests. Accordingly, it was decided to use the GPC values for the core fibers of the strands as a control "stand-in". And fiber specimens were then selected from various locations in the worn ropes for the GPC evaluation of molecular weight parameters. Conclusions of the GPC studies are as follows:

Use of strand-core $\bar{M}_n$ data as a basis for normalized comparisons of changes in number average molecular weights is a valid procedure. This follows from the observation that differences in $\bar{M}_n$ values for strand core fibers of ropes varying in age from 3 to 16 years are well within the range of experimental error about their mean. Similarly, the average M_n for the one nylon 66 rope tested is not significantly greater than the mean $\bar{M}_n$ of the core fibers of the older, worn ropes.

Fibers taken from the outermost surface of worn ropes

3 and 4 years old did not evidence significant reductions in M_n as compared to strand core fibers from corresponding ropes.

Consistently significant reductions in $\bar{M}_n$ are not observed in fibers taken from the underpart of the exposed surface yarns and from the first subsurface layers.

On the basis of published results for the correlation between effect of UV exposure on $\bar{M}_n$ and on tensile strength, it is concluded that chain scission is an important component in the deterioration of outermost fibers in the marine ropes. (It has been suggested that the per cent loss in $\bar{M}_n$ due to UV exposure may be multiplied 2.5 times to provide an estimate of the corresponding loss in tensile strength.)

The fact that measured losses in tensile strength exceed the losses thus estimated in 5 out of 6 of the "old" ropes, would suggest that chemical scission is not the sole factor in deterioration of the outermost fibers. Mechanical action must contribute the remaining damage, as is evidenced in Scanning Electron Microscopy studies.

The absence of control specimens and the lack of detailed information on actual exposure (UV, immersion, and mechanical) of each rope precludes the generalization of conclusions in a form more useful for marine applications. Further chemical tests are warranted based on other techniques as cited in the literature survey of Section 2.

Differential Scanning Calorimetric Measurements (DSC)

DSC measurements were made on all specimens of rope studied in the program. The data confirm the presence of one nylon 6 specimen among the worn rope and one polyester, the remainder being nylon 66. Additional information furnished reflects on differences in crystal structure, a subject to be studied further in the coming year.

Effect of Water Immersion

The effect of water immersion at various temperatures is well documented in the literature as relates to textile processing. However, most of this information deals with water immersion at high temperatures for relatively short times and under light loads. In applications of synthetic fibers to marine ropes, the immersions are at lower temperatures for long periods and under relatively heavy loads, both axial and lateral (to the filament). To date only preliminary data have been obtained concerning immersion behavior, but enough to indicate some reduction in breaking strengths and elongations as a result of heavy load immersion in fresh or in sea water. In contrast, long term heavy loading of filaments in air does not appear to affect strength to a significant degree but, as expected, subsequent elongations to rupture are noticeably reduced. There is some fractography evidence of structural changes in the filament in

heavy-load sea-water immersions, but considerably more work is required for definitive answers. Finally, it appears that residual shrinkage of filaments from worn specimens varies significantly with position in 3-strand rope--a subject which will be considered further in future studies.

Microscopic Studies

Microscopic studies of the ten worn rope specimens have documented the various types of degradation which occur during marine usage of synthetic fiber lines. The appearance of filaments at the outermost location of the 3-strand twisted rope varies from strand to strand, sometimes manifesting an encrustation and coating, or surface attack. Etching is seen in some fibers leading to a porous spongy structure. Surface gouging, abrasion, and/or filament crushing are frequently in evidence. In many cases, photomicrographs are accompanied by filament load-elongation curves, to permit a subjective correlation between the extent of filament-surface encrustation or other non-mechanical filament modifications and stress/strain behavior. Fractography studies show a marked conversion in surface-exposed filaments from the scallop-shaped crack spreading-failure of a new synthetic fiber to the cup and cone, sheath/core, longitudinal splitting and occasional brittle failure characteristic of chemically or photochemically degraded fibers.

It has also been demonstrated that filaments in relatively protected sections of the rope can undergo significant mechanical damage through friction and filament-filament abrasion. Depending on the location in the rope cross-section, this type of mechanical attrition can take place in some cases with little accompanying contamination. In other cases, the presence of sand, grit, and, possibly, salt deposits adds to the intensity of mechanical attack.

Finally, it is seen that internal pressures within the rope center, i.e. between strands, can be so intense as to cause "welding" of parallel filaments, adding locally to the bending rigidity of the rope and focusing frictional damage to fibers at the boundaries of the "welded" zones. Such pressures often result in lateral filament compression and in locations where filaments are not parallel, to embossing of individual fibers. Such compression/embossing is sometimes accompanied by the opening of surface cracks in the filament and, in extreme cases, to significant reductions in filament strength.

Nondestructive Evaluation of Synthetic Rope

Preliminary nondestructive (NDE) characterizations have been obtained from new Samson double-braided 2-in-1, 0.635 cm (1/4-in) diameter nylon rope in the dry condition at room temperature. The NDE techniques so far considered include ultrasonics and acoustic emission (AE).

In ultrasonic attenuation testing where the transmitting and receiving transducers are on the side along a straight line on the rope, the output signal amplitude decreases with increasing frequency and increases with increasing rope tension in an unflawed rope. In ultrasonic "stress wave factor" (SWF) testing, a correlation is found between the SWF and the load level at which the measurement is taken if the load level is normalized with respect to the ultimate load of each individual rope sample having various numbers of cut core yarns.

In AE testing, a parameter called the "AE load delay" has been defined as the tensile load required to produce a specified low baseline level of the AE activity. It has been observed that the AE load delay can be correlated with the ultimate rupture load of ropes having various numbers of cut core yarns and a variety of stress concentrating knots. Table 4.3 is a summary of the ultimate rupture load and AE load delay data for Samson double-braided 2-in-1, 1/4" nylon rope with various numbers of cut core yarns. The AE ringdown counts load delay is plotted vs. the ultimate rupture load as shown in Fig. 4.6. A similar correlation can be obtained for the AE event counts load delay. Table 4.4 is a summary of the ultimate load, AE load delay, and knot efficiency data for various knotted ropes. The industry's suggested knot efficiency is also shown and is found to be in general agreement with the data. Correlations between the AE load delay vs. ultimate load similar to Fig. 4.6 are also found.

Fatigue Loading and Environmental Effects

Marine ropes may be subjected to a complex variety of static and cyclic loads under varying environmental conditions. This part of the project is intended to determine the effects of short and long term static and cyclic loads in air and sea water environments. Nylon and other synthetic fibers are known to be degraded by cyclic loading, and polymers are also degraded by specific environmental agents which can lead to very low stress fractures. The plan for this study is to test single fibers, yarns, and small ropes to characterize their static and cyclic fatigue properties in air and sea water environments. Changes in residual properties will be followed during the course of the tests. The results will be combined with microscopy and other studies to establish an understanding of the causes of rope degradation under these conditions.

Work during the first year of the study has concentrated on establishing the basic fatigue S-N curves and residual properties for single fibers and yarns. Both air and sea water environments have been used, but only short-term exposure to sea water has been studied to date. Nylon fibers and yarns are found to lose a significant fraction of their strength when subjected to cyclic fatigue loads. Single fibers appear to fall according to the total time under load, regardless of the frequency or stress amplitude. Yarns are more sensitive to cyclic loading than are single fibers, losing approximately 60% of their initial strength after 10^5 cycles; yarn failure appears dominated by the number of cycles rather than total time under load, possibly due to fiber-fiber interactions. Dry yarns go through a shakedown process which results in a plateau on the S-N curve at high loads. Short term sea water immersion causes a modest reduction in lifetime under some conditions, but also may lubricate yarn structures. The residual strength of fibers and yarns remains close to the initial strength up to at least 75% of their lifetime; the residual strain to failure is reduced by approximately 40% in cycling, but the cumulative strain to failure is close to the strain to failure in a single cycle. Preliminary fractographic work indicates possible fiber-fiber damage and fracture surfaces which are not unique to fatigue loading.

2. ENVIRONMENTAL DEGRADATION OF NYLON AND POLYESTER

A critical evaluation of the literature in the context of ocean engineering applications of rope

INTRODUCTION AND SCOPE

A discussion of problems of environmental degradation in synthetic fibers (nylons and polyester), and in ropes made from them, requires consideration of some factors governing the properties of fibers, of effects of chemical and structural changes resulting from environmental exposure on mechanical properties, and of the relationships of fiber properties to the performance of yarn and assemblies made from them. While it is not possible to present this multifaceted subject in depth, it is useful to review briefly the salient concepts underlying the material discussed, the rationale used in its selection, and the objectives of this document.

1. Factors governing fiber properties. The properties of fibers may be thought of as encompassing macroscopic or geometrical (e.g. length, cross-section, surface roughness), physical (e.g. density, thermal, optical, electrical), chemical (e.g. response to heat, to oxidative environment, moisture sorption), and mechanical (e.g. tensile properties) characteristics. The chemical, physical, and mechanical properties of the semicrystalline, irreversibly oriented polymers which constitute most fibers, are primarily determined by the molecular structure of the fiber-forming polymer and by the crystallinity and orientation, or supramolecular structure. For fibers made from a given polymer (e.g. nylon 6.6; polyethylene terephthalate), important parameters of molecular structure include molecular weight, and molecular weight distribution; many essential structural features which result from ordering of macromolecular chains are controlled by processing variables during spinning and other manufacturing steps.

Several levels of structure thus contribute to and govern the properties of fibers. In use, and more specifically, upon exposure to chemical degradative environments, changes may occur independently on each level, but are more likely to occur in various simultaneous, sequential, or interdependent combinations, according to the state of the material, and the causative factors it encounters.

In early work on environmental degradation of fibers, there has been a tendency to consider any observed deterioration of mechanical properties (e.g. strength losses) as the result of bond scission reactions, and of decreased molecular weight of the polymer chains. However, this limited chemical concept does not reflect the diversity and complexity of degradative processes, nor the consequences of changes on a supramolecular level which may be associated with, or dependent on, chemical reactions in the polymer molecule.

In the context of current concepts of the supramolecular structure of polyamide and polyester fibers (Morton and Hearle, 1975, pp. 60-71), some qualitative conclusions have been formulated regarding the effects of chemical and structural changes on the mechanical properties of these fibers. It has been proposed, for example, that stress is borne primarily by polymer chains in the less ordered regions of the fiber, that the distribution of stress in these regions depends on orientation and on attendant structural details, and that rupture of chains subjected to disproportionate stress will thus occur almost exclusively in the intercrystalline, or amorphous regions.

The sorption and diffusion of oxygen, or of other gaseous or liquid contaminants, is restricted to the amorphous regions, and therefore, chemically mediated chain scission processes will also be localized in the regions which have the major stress-bearing role.

The sorption of moisture also takes place in the amorphous regions. The plasticizing action of sorbed moisture may affect elastic deformation and resistance to impact stress. Under some conditions, it may increase fiber tenacity or elongation, offsetting the effect of simultaneous adverse changes. It has been suggested (Figucia, 1968), that in this case, the fiber may exhibit no change in normal mechanical characterization for a considerable period of time, and yet may be undergoing internal processes which predispose it to change by subsequent influences.

It is evident from these examples that the microscopically heterogeneous nature of fibers is such that even small chemical and/or physical changes can exert significant effects on their properties.

2. Causative factors in environmental degradation. Chemical degradation of fibers may result from a number of causative factors which may interact, and may produce changes in properties through separate, concurrent or sequential effects. The following are of major interest in the framework of the subject matter covered in this report.

- Ultraviolet radiation (light exposure)
- Heat (moderate temperatures)
- Oxygen (air)
- Gaseous contaminants in air (e.g. SO_2)
- Water (high relative humidity)
- Aqueous solutions of salts.

The effects of UV radiation, of oxygen and of aqueous environments on the chemical degradation of nylons and of polyester have overwhelming importance in the case of rope. Many variables in the conditions of experiments designed to study the effect of the above factors on chemical degradation of nylons and of polyesters have been investigated, and their effects have been reported. Some are discussed under the appropriate heading in this report. The great number of variables is mentioned here only to point out the complexity of the problem--and the inherent difficulty in applying results obtained and knowledge gained in laboratory experiments under controlled conditions to the realistic situation of ropes in ocean engineering applications.

3. Chemical composition (additives) and geometry. Several additional factors must be considered in reviewing, interpreting, and attempting to extrapolate or generalize results reported in the literature on the chemical degradation of polymers and fibers to the problems of rope.

The presence of additives (e.g. delustrants, UV stabilizers) in the fibers may have significant effects on chemical degradation processes. However, the chemical structure of additives present in commercial fibers is not often disclosed, and the effect of added compounds cannot always be separated from that of the programmed environment. Attempts to circumvent this difficulty may have been made in some instances by carrying out experiments on oriented polymer films of controlled chemical composition

prepared in the laboratory, but this approach has other limitations and pitfalls. In the context of rope applications, the focus of interest is on drawn, undyed fibers, with emphasis on bright (free of delustrant) fibers. In the discussion which follows, data on dull (TiO_2 delustered) fibers are included for the purpose of comparison, and/or with reference to mechanisms of degradative processes in the presence and in the absence of the additive.

Difficulties in relating results of laboratory experiments to "real life" are common. They are, however, particularly great in this case, because of the large number of variables that must be considered in the materials, in the modes of exposure, in the interactions of factors causing degradation, and in the assessment of effects. Furthermore, difficulties are encountered in the "translation" of changes in fiber and yarn properties to the expected behavior of rope structures designed to withstand stress under exacting and diverse service conditions.

In considering environmental degradation of ropes in ocean engineering application, dimensions and geometry of the rope play important roles in that they govern the extent to which fibers and yarns in specific locations within the rope are exposed to the degradative influence of external causes. Effects of rope diameter, and of yarn location are illustrated, for example, by the data summarized in Table 2.1 (Hawkins and Tipson Ltd., unpublished results, 1981) which are presented here primarily to demonstrate some of the problems associated with predictions of rope performance based on data obtained in laboratory experiments on fibers or yarns.

With all the possibilities for changes within the fibers, with the numerous variables in test conditions, and with the problems of translation efficiency, it is obvious that conventional test values obtained on fiber or yarn samples exposed to controlled environments in the laboratory cannot be considered predictive of practical performance--but only suggestive of events that may occur in use, on a different scale.

4. Scope and objectives of the report. Within the limitations briefly outlined above, a study of the literature on

Table 2.1

Approximate Range of % Strength Retained

(From Hawkins and Tipson Ltd/ICI Exposure Trials)

	Diameter (mm)	% Strength Retained
Polyester rope(*)	8	87-90
	24	90-92
	48	92-100
(Stabilized) Nylon rope(*)	8	60-78
	24	80-87
	48	~ 100

	Location of Yarns	% Strength Retained
Yarns from 24mm diameter Polyester rope(**)	inside (core)	92-100
	outside (surface)	74-78
Yarns from 24 mm diameter (stabilized) Nylon rope(**)	inside (core)	72-82
	outside (surface)	60-62

(*) Exposed in India, Canada, U.K. for 12 months

(**) Exposed in Canada, U.K. for 18 months.

environmental/chemical degradation of nylon and polyester provides a wealth of information and knowledge. A critical evaluation of concepts and results that are, or may be, relevant to the problems of rope degradation in use is presented here. The objective is to summarize in a single document the highlights of current knowledge on the subject as a basis for enhanced understanding of the events leading to wear and, eventually, failure, in the use of rope, and for future research investigations specifically designed to improve resistance to chemical degradation and wear life through the selection of materials in which degradative reactions may be suppressed or retarded. The selection of literature references, and of data drawn from them, has been guided in large measure by the author's experience and knowledge in polymer and fiber chemistry. To the extent that the selection of facts constitutes opinion, the material discussed in this report, the conclusions and recommendations reflect this author's opinion regarding the importance of those aspects of degradation which are, or may be, related to property changes and wear in fibers, yarns, and cordage during use.

MECHANISM OF CHEMICAL DEGRADATION

The chemical reactions occurring in nylon and polyester fibers exposed to environmental conditions which may be encountered in use are complex, and governed by a large number of factors. An in-depth review of these reactions, and of the mechanisms underlying them, is beyond the scope of this report. However, the insight gained in investigations of chemical degradation in the polymer molecules of major interest in the context of synthetic fiber rope provides an appropriate background for a discussion of experimental observations made under controlled conditions of laboratory exposure, and of relationships established between exposures of fibers and yarn assemblies to specific environments, and effects on properties.

Depending on the polymer, and on the conditions of exposure, chemical degradation may result in chain scission or, in some instances, in crosslinking of polymer chains. The determination of changes in molecular weight by well established analytical

techniques has been extensively used to characterize reactions associated with breaking of chain bonds, formation of oligomers, and changes in properties associated with these processes. Consideration of simultaneously occurring crosslinking reactions complicates the problem of characterizing the changes in molecular structure which occur in the initial stages of degradation. The identification of low molecular weight degradation products formed under extreme conditions of exposure, coupled with analytical techniques applied to partially reacted polymer and oligomers, ultimately provide a framework in which the reaction paths and mechanisms of degradation under specific conditions of polymer exposure are postulated and interpreted.

1. Nylon (polyamides). The mechanism of chemical degradation of polyamides was studied in early work (Achhammer et al., 1951), in which films prepared from copolymers of nylon salts (6.6 and 6.10), and ε-caprolactam were exposed to elevated temperature, ultraviolet radiant energy, and different atmospheric conditions. The results of examination by many analytical techniques of films degraded under different conditions, led to the conclusion that degradation of polyamides may involve changes in molecular orientation, and in the amount of molecularly associated material which has a plasticizing effect, such as water, as well as chemical change in the polymer molecules.

The mechanism of photochemical degradation of polyamides was elucidated, and discussed in detail more than a decade later (Moore, 1963) in an investigation of nylon films (6.6; 6.10; 10.6 and 6), and of related model N-alkylamides, which remains a classic to this date. This work addressed the mechanisms of UV-induced reactions of polyamides in direct photolysis of the molecules, which occurs independently of the atmosphere, and even in the absence of oxygen, on exposure to light of shorter wavelength (below 3000 Å), and in photochemical oxidation (photosensitized oxidation) which requires the presence of oxygen, and occurs on exposure to light of longer wavelength.

In the process of photolysis, evidence was obtained for scission of polyamide chains involving the amide bond, and also

or crosslinking. The "probable" photolytic scission reactions of nylon 6.6 chains are shown in the equations below:

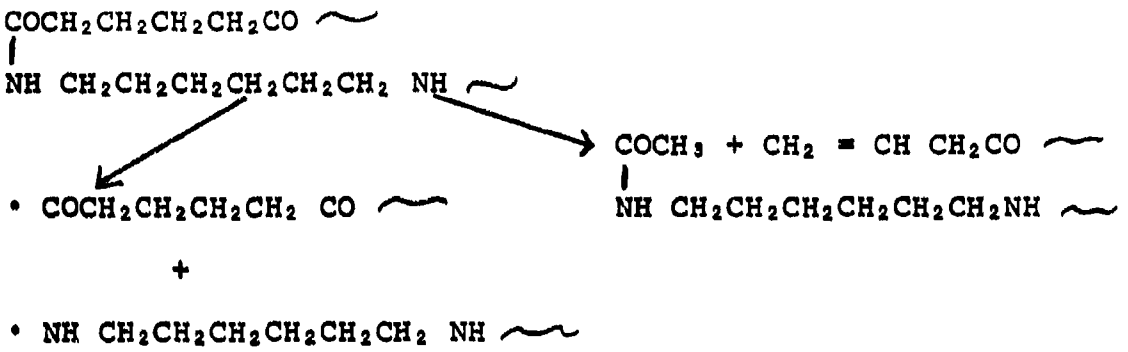

In photo oxidation reactions of polyamides, oxidative attack was shown to occur at the methylene group adjacent to the nitrogen atom, with subsequent decomposition of the —CHOH radical formed and formation of aldehyde groups (end groups) as shown below for nylon 6.6.

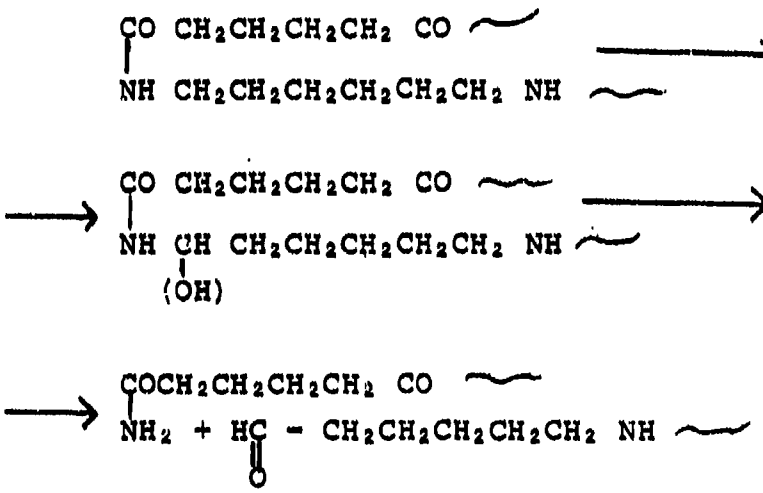

The results of this work also showed that the presence of Titanium dioxide delustrant in nylon polymer enhanced photodegradation only above 3000 Å in the presence of oxygen: The TiO_2 did not change the nature of the oxidation process, but appeared to act as a photosensitizer.

The results of an electron spin resonance (ESR) study of the degradation of nylon 6 filaments irradiated at liquid nitrogen temperatures with wavelengths in the region of solar radiation support the hypothesis that the first step in the photolytic degradation of nylon is the cleavage of amide bonds (Heuvel

and Lind, 1970). On the other hand, work on the mechanism of degradation of nylon 6 fibers caused by thermal oxidation (dry air at 200 ± 10°C) showed that, under the conditions used, the preferred site of attack and chain scission is the N-vicinal methylene group, as proposed by Moore for the case of photo oxidation (Valk et al., 1970).

2. Polyethylene terephthalate (PET) and polyesters. The mechanism of thermal and thermo-oxidative degradation of PET has been reviewed (Peters and Still, 1979). However, the investigations cited in this review have entailed exposure to temperatures above the melting point of PET, and results are thus of limited relevance to the problems and exposure modes of PET considered in this report.

The photolysis of PET films has been studied in vacuo with light of wavelengths 2537 Å and 3130 Å (Marcotte et al., 1967). Similar quantum yields for CO and CO_2 formation, and other similarities in results led the authors to the conclusion that gross chemical effects of in vacuo exposure to light of different wavelength are closely similar, even though in the case of 2537 Å light, they occur in a much "thinner" layer. The mechanism of photolytic degradation of PET proposed by Marcotte is based on primary reactions leading to the formation of CO and CO_2, according to the equation below.

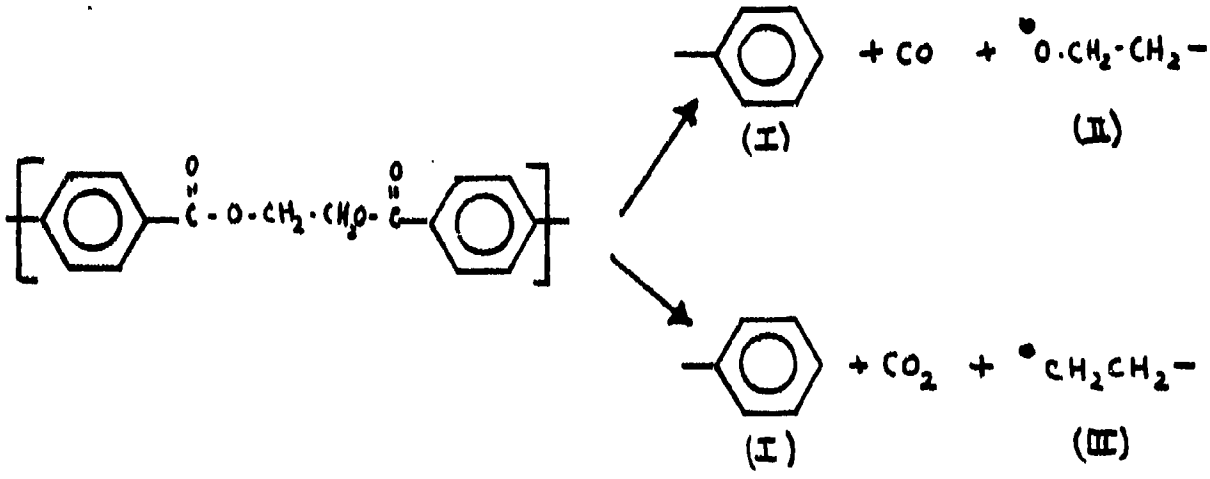

Radicals I, II, III may then combine, disproportionate or abstract hydrogen atoms from neighboring molecules. An important

consequence of hydrogen abstraction would be the formation of free radicals, which could account for crosslinking reactions. The photodegradation of PET is a complex process, involving photo-oxidative reactions in addition to photolysis, and including chain scission, formation of gaseous products (CO and CO_2), and changes in the concentration of carboxylic acid end groups. Some aspects of the reactions are discussed in a later section of this report in conjunction with the observed effects of photochemical degradation of PET on polymer properties.

PHOTOCHEMICAL DEGRADATION

While it is well known that sunlight causes chemical degradation in organic polymers and fibers, the meaningful investigation of degradative effects under controlled conditions of exposure in the laboratory is a difficult task. The publications documenting results of research investigations and progress in this field generally cover specific aspects of the problem and specific approaches. Results and conclusions apply within narrowly defined limits, and, in most instances, it is not possible to formulate generalizations, to establish definitive inter-relationships of results obtained by different investigators, and to "translate" the results reported for a given system and mode of exposure to more realistic systems and situations. The discussion which follows should be viewed in the framework of these limitations.

The variables which must be considered in interpreting results of exposure to ultraviolet radiation are those of the environment, including radiation wavelength, method of exposure, oxygen, moisture, and temperature, and those of the exposed material which, in addition to the polymer molecule, include physical form (e.g. fiber, film) and dimensions of the material, supramolecular structure, and additives (e.g. delustrants, inhibitors).

A thoughtful review of the variables and of the problems encountered in evaluating the effect of irradiation by natural and artificial light on the breaking strength of polyester and

nylon filaments has been presented (Kaufmann, 1971) in conjunction with experimental results obtained in the study.

1. Light sources and spectral distribution. The intensity of sunlight varies with wavelength and with season, hour and atmospheric conditions. The schematic drawing reproduced in Fig. 2-1 (Stowe et al., 1974) indicates that 3500 Angstrom is the wavelength mid-way in the ultraviolet portion of sunlight reaching the earth's surface (near - UV). In standard methods developed for outdoor exposure of materials, the seasonal fluctuation in the UV light reaching the earth is a major problem. Measurements of exposure periods in terms of total radiation in Langleys (cal/cm^2) do not provide accurate comparisons of tests performed in the same locations at different seasons of the year. Singleton et al. (1965, 1969) have proposed that reproducibility of results can be improved by using Coblentz factors, which show the seasonal fluctuation of UV energy in the range of 2900 Å - 3150 Å, proportionate to the total energy measured. By applying these factors, exposure periods can be based on the energy in the 2900 Å - 3150 Å range rather than on total radiation. This range is reportedly the most sensitive to seasonal fluctuations, and also the most important in actinic degradation. While outdoor exposure is a valuable route to the evaluation of the degradation caused by UV radiation and "weathering", the length of time it requires has made it imperative to develop accelerated laboratory tests for research. Laboratory studies also allow the use of controlled atmospheres so that the interdependence of radiation energy and specific environmental factors may be detected. The artificial light sources most commonly used in the laboratory have been the carbon-arc and the Xenon-arc lamp, for which standard tests have been developed. Considerable uncertainty remains regarding the possibility of correlating test results obtained by these techniques with those of outdoor exposure (Singleton and Cook, 1969; Tweedie et al., 1971). Although the Xenon-arc has been found to compare more closely with sunlight than the carbon-arc, results of laboratory tests generally may be considered only indicative of degradation encountered in outdoor use and must be interpreted with caution.

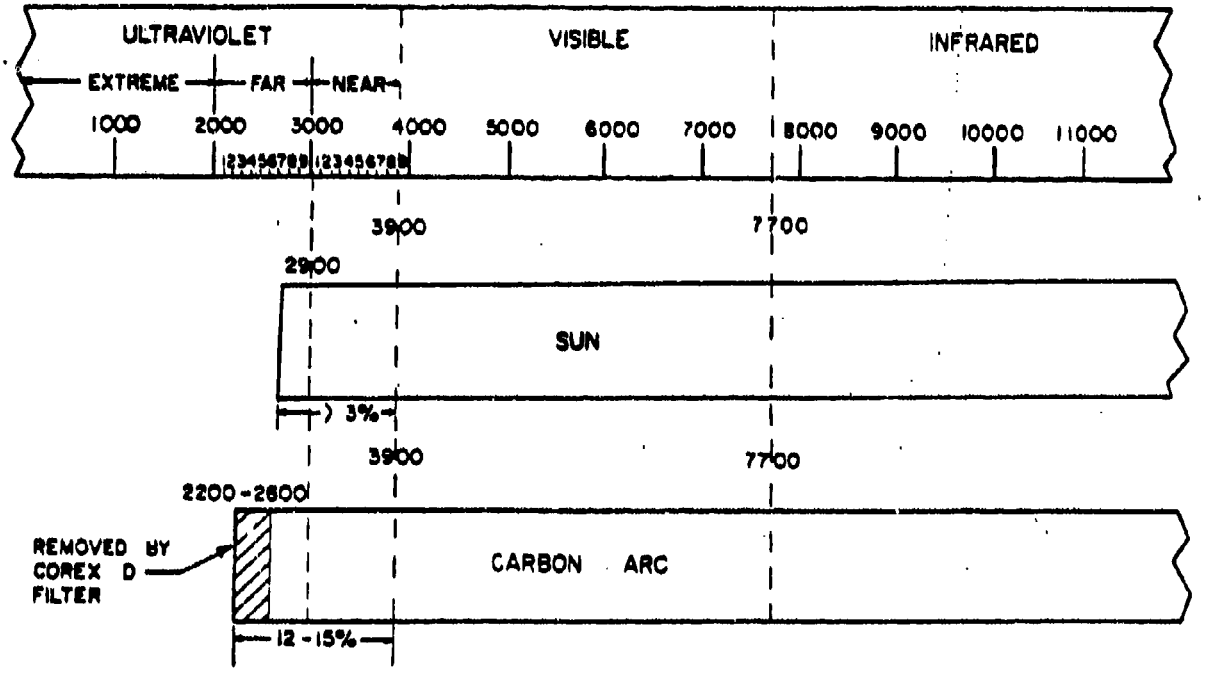

Spectral distribution in angstroms of sunlight at the earth's surface and the carbon arc [1]. Reprinted with the permission of John Wiley and Sons.

FIGURE 2-1. (STOWE ET AL., 1974)

For example, the effects of Xenon-arc radiation (Weather-Ometer), and of outdoor exposure behind window glass on the breaking strength, extension-to-break, and energy-to-break have been compared (Wall and Frank, 1971) for several nylon and polyester textile yarns containing titanium dioxide in varying amounts. Degradation of nylon yarns was found to be slower than that of polyester yarns in the Weather-Ometer tests, but the reverse was true in outdoor exposure tests. The differences observed were attributed to several factors, including temperature and humidity, differences between continuous laboratory exposure and normal daily cycles of light and dark, and differences in intensity distributions of the UV radiation of the arc as compared to sunlight. These results, confirmed in later studies (Lock and Frank 1973) provide but one illustration of the limitations of laboratory simulations of outdoor exposure which must be borne in mind in reviewing the results and discussion which follow.

2. The role of moisture (relative humidity) and of additives. The effects of relative humidity, of titanium dioxide content, and of UV stabilizers on the photodegradation of undyed nylon 6.6 and PET yarns exposed to Xenon-arc radiation, and to sunlight behind window glass have been studied for a broad spectrum of nylon and polyester yarns (Lock and Frank, 1973). Tensile properties of yarn examined in previous work (Wall and Frank, 1971), namely breaking strength, elongation at break, and energy to break were again employed as criteria for assessing the extent of yarn degradation. Selected results of this investigation are included in this report, because they are believed to be of considerable significance in the context of the problems of degradation in rope yarns. Table 2.1 (reproduced, in part, from p. 504 of the above reference) shows details of the commercial yarn samples used in the experimental study.

Some results have been compiled in Tables 2-2 and 2-3 for nylon and PET yarns respectively, in support of conclusions that may be summarized as follows:

(i) Rates of degradation of nylon and PET were seemingly in reverse order for exposure to Xenon-arc as opposed to sunlight behind glass (see also Wall and Frank, 1971).

Table 2-2

Yarn Variables (Lock and Frank, 1973)

Code	Yarn Description	Titanium Dioxide (TiO_2) content Percent	Polymer Additives (unspecified)
N_1	Nylon 66, Type 728 Tire Cord, 840 den., 140 fil - bright	----	Thermal Stabilizer
N_2	Nylon 66, 70 den., 34 fil - semidull	0.20	----
N_3	Nylon 66, 40 den., 13 fil, dull	2.00	----
N_4	Nylon 66, Type 288, 70 den. 34 fil, semidull	0.30	UV Stabilizer
N_5	Nylon 66, Type 685, 70 den. 34 fil, dull	2.00	UV Stabilizer (identical to N_4)
F_1	PET, Tire Cord, 901 den. 75 fil, bright	----	----
F_2	PET, 40 den., 24 fil, semidull	0.50	----
F_3	PET, 40 den., 24 fil, dull	2.00	----

Table 2-3

Percent Loss of Tensile Properties of Nylon Yarns

Exposure Conditions	% Loss in Breaking Strength					% Loss in Elongation to Break				
Xenon Arc % RH Hours	N_1	N_2	N_3	N_4	N_5	N_1	N_2	N_3	N_4	N_5
20 100	4.5	9.3	8.7	9.8	6.2	6.4	18.8	24.6	16.1	5.4
50 100	4.4	7.1	5.9	7.4	4.3	0.5	22.8	19.1	20.4	0.8
80 100	2.3	15.6	18.9	14.7	25.9	4.1	51.6	63.5	49.2	53.5
20 200	4.1	13.5	16.1	16.1	14.8	1.4	27.1	39.4	29.8	20.7
50 200	3.6	10.3	17.1	10.9	12.6	3.7	32.8	54.1	27.8	19.4
80 200	6.7	18.3	23.9	15.9	27.2	8.7	52.4	68.1	49.5	52.9
Sunlight Behind Glass										
Langleys (2900-3500 Å)										
500	7.6	21.3	38.4	18.4	21.2	1.4	55	70.8	31.1	32.2
1500	13.9	70.6	83.9	52.3	59.2	8.4	74.6	91.3	53.2	70.7
2500	24.7	85.6	89.5	73.7	77.8	18.8	92.3	97.1	73.9	83.6
3500	32.2	---	---	85.4	85.8	24.3	---	---	91.0	93.9

Table 2-4

Percent Loss of Tensile Properties of PET Yarns

Exposure Conditions		% Loss in Breaking Strength			% Loss in Elongation to Break		
Xenon Arc							
% RH	Hours	F_1	F_2	F_3	F_1	F_2	F_3
20	100	24.6	28.2	28.4	31.8	69.5	71.2
50	100	24.8	27.9	29.3	28.5	70.5	70.8
80	100	28.3	31.2	37.0	33.1	76.4	75.4
20	200	37.2	36.4	44.7	43.0	77.1	76.3
50	200	45.7	36.3	39.2	45.7	78.5	75.4
80	200	44.2	41.8	51.5	48.3	81.1	80.9
Sunlight Behind Glass							
Langleys (2900-3500 Å)							
500		1.6	7.0	25.1	0.7	27.6	67.8
1500		5.3	32.8	56.2	4.3	68.0	77.1
2500		12.3	41.1	73.1	8.0	74.5	86.0

(ii) Degradation on exposure to sunlight behind glass was accelerated by increasing TiO_2 content. Degradation of bright (N_1 and F_1) yarns was far less--but these yarns also had high denier per filament, and the results may be attributed to the absence of delustrant only if considered in conjunction with other comparisons (N_2 vs. N_3); F_2 vs. F_3).

(iii) Loss of tensile properties as a result of Xenon-arc exposure increased with increasing relative humidity. This effect was greater for nylon than for PET yarns. Elongation at break was affected by humidity more than breaking strength.

(iv) Loss in elongation at break was shown to be a more sensitive indication of degradation than breaking strength loss.

Comparative evaluation of degradation (loss in tensile strength, elongation, and energy to break) of undyed textile fibers exposed to natural sunlight, and to an atmosphere of controlled humidity (45% RH) in a light-fastness tester employing a 500 W mercury-tungsten fluorescent lamp (Shah and Srinivasan, 1975) showed that different fibers ranked in the same order on the basis of results obtained with the light-fastness tester and on the basis of results obtained upon exposure to natural sunlight. The effect of humidity on degradation of different yarns, including bright nylon 6, dull nylon 6 and delustered PET was subsequently investigated by this testing technique. Degradation was found to increase with increasing humidity in the atmosphere surrounding the sample for all fibers, but the magnitude of the effect of RH on loss of strength differed for different fibers. For example, the effect of humidity was negligible for PET. The rate of degradation was greater for delustered (dull) nylon 6 than for bright nylon 6 at all levels of humidity, suggesting that the delustrant acts as an accelerator in the actinic degradation of nylon 6 under the conditions used. Although experiments at different temperatures were not reported, the authors also suggest that temperature "has a greater influence on degradation in moist air than in dry air", in accordance with earlier hypotheses

that different mechanisms are involved in the photosensitized degradation of textile fibers in dry and moist air.

3. Oxygen and environmental contaminants. The role of oxygen and of environmental contaminants in chemical degradation caused by exposure to UV radiation has been investigated extensively in conjunction with studies of the mechanism of photochemical degradation for specific polymers. For example, comparisons of losses in tensile strength and in elongation for films and fibers irradiated in air, in vacuo, and in nitrogen have been presented and discussed in depth (Stephenson and Wilcox, 1963). The higher rate of degradation noted for all polymers when irradiated in oxygen as compared to nitrogen was explained on the basis of mechanisms proposed by earlier investigators. In the case of nylon 6.6 films and fibers, it was also found that the rate of degradation was greater for irradiation in nitrogen than in vacuo. This difference was attributed to the effect of pressure, and/or of trace amounts of oxygen present in the nitrogen. Irradiation in oxygen was found to cause more rapid deterioration of polyester film and fiber samples (MYLAR film and DACRON fiber) than irradiation in vacuo. A significant wavelength dependence of the rate of degradation was observed for DACRON fibers, but not for MYLAR film. Later studies of the chemical changes occurring in PET (MYLAR film) exposed to UV radiation (Marcotte et al., 1967) included consideration of "quantum yield for fractures" for PET irradiated in vacuo and in air, with tentative conclusions regarding the significance of observed differences, and the role of oxygen in the photochemical degradation of PET.

The effect of sulfur dioxide, a prototype environmental contaminant, has been studied for laboratory (Weather-Ometer) exposures of nylon 6.6 fibers (Zeronian et al., 1971, 1973). Selected aspects of this work will be discussed below in Section 3.4 (Degradation of polyamides). Two salient conclusions were that degradative effects of SO_2 on fiber surfaces require the combined presence of SO_2 and moisture, and that degradation occurring in nylon exposed to light, moisture, and air contaminated by SO_2 cannot be characterized as hydrolytic

(acid) degradation. A study of degradation of nylon 6.6 films of different morphologies in the presence of nitrogen dioxide, ozone, oxygen and near-UV radiation (>2900 Å) showed that the solvent and conditions used in the preparation of the films influenced the course of reaction (Jellinek and Chaudhuri, 1972). It was postulated that in some instances, degradation and chain scission on exposure to the degradative environments were inhibited by hydrogen bonding, or even by chemical reaction of the polymer with the solvent used for casting the film.

4. Photochemical degradation of polyamides. Most aspects of the photochemical degradation of polyamides are covered in reviews and textbooks on the photochemistry of commercial polymers. Reviews of the "photochemistry of commercial polyamides" (Allen and McKellar, 1978) and of "UV degradation of nylon 6.6" (Stowe et al., 1974) are valuable background documents for the summary of specific investigations and results presented in this section of the report. In addition, work summarized in selected publications on the photosensitized oxidation of polyamide fibers (e.g. Egerton, 1971) includes consideration of factors which influence degradation by near-UV and visible radiation, of the nature of chemical changes involved, and of methods which may improve photochemical stability.

The work of Moore (1963) on photochemical degradation of polyamides provides an important basis for subsequent investigations, and for discussion to date. The author examined the response of nylon films (6.6; 6.10; 10.6 and 6), of model N-alkyl amides, and of nylon 6.6 yarns, exposed to artificial light of different wavelengths, under different conditions of atmosphere and humidity, and to sunlight under glass for one year. In the context of the present report, the relationships between loss of strength and chemical changes observed for nylon yarns exposed to sunlight are of particular significance. The nylon yarns used in the experiments are shown in Table 2.5 and some analytical data obtained on exposed yarns are summarized in Table 2.6. Figure 2-2 reproduces Figs. 2, 3, and 4 from Moore's paper, which highlight the difference between bright and delustered yarns, and allow additional, albeit

Table 2.5

Experimental Nylon 6.6 Yarns Exposed to UV Light* (Moore, 1963)

60 denier bright, 20 filaments, no TiO_2;
Tenacity 324 g - Extensibility 15.0%

90 denier bright, 30 filaments, no TiO_2;
Tenacity 465 g - Extensibility 17.8%

90 denier delustered, 30 filaments, 1.6% TiO_2;
Tenacity 492 g - Extensibility 19.2%.

*Wavelength regions investigated by using quartz on Pyrex windows in the exposure cells, or by interpolating filters in the light beam.

Table 2.6

Chemical Analyses on Nylon 6.6 Yarn
(exposed to sunlight under glass for one year)
(Moore, 1963)

	Degraded Yarns	Control Yarn*
Carboxyl end groups (g equiv/10^6 g polymer)	117	82
Amine end groups (g equiv/10^6 g polymer)	20	39
Intrinsic viscosity (in 90% phenol-water)	0.54	0.82

*30 denier bright (no delustrant)

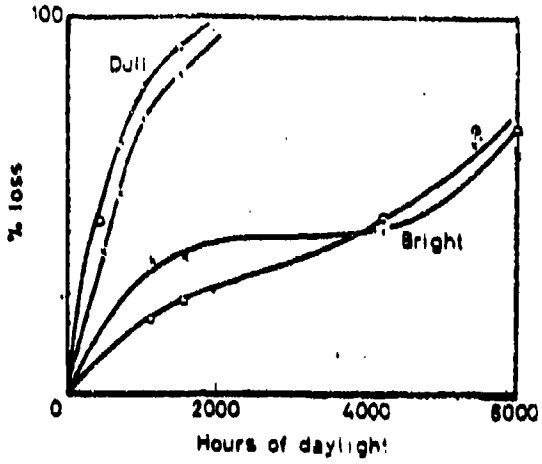

Variation of loss of tenacity and extensibility with exposure time for sunlight-degraded 6.6 nylon yarns (O tenacity; × extensibility)

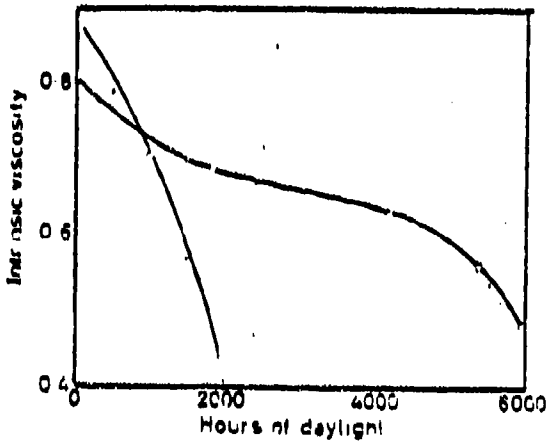

Variation of intrinsic viscosity in 90% phenol–water with exposure time for sunlight-degraded 6.6 nylon yarns (O bright; × delustred)

Volume of intrinsic viscosity with loss of tenacity (O bright; × delustred)

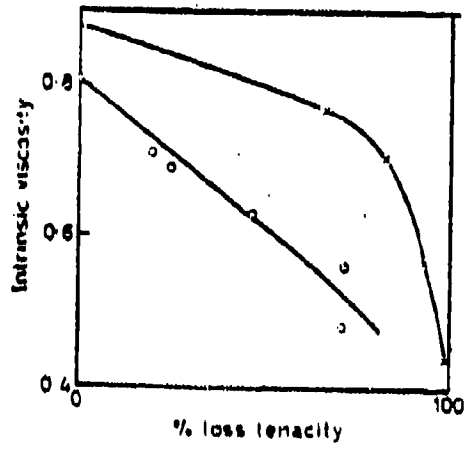

FIGURE 2-2. (MOORE, 1963)

speculative, conclusions concerning photochemical degradation of (bright) nylon yarns in rope. For example, the sharp rise in tenacity and extensibility loss after about 4000 hours of daylight suggest the possibility that sudden, near-catastrophic property changes may occur as a result of exposure in fibers on rope surfaces when the period of exposure to incident sunlight reaches a critical length.

A change in intrinsic viscosity of about 10%-15% corresponds to a tenacity loss of about 25%, suggesting that measurements of molecular weight may provide meaningful indications of the extent to which fiber mechanical properties are affected by photochemical reactions, in proportion to the duration of exposure.

On the basis of Moore's comprehensive investigation and convincing results, it would be tempting to assume that, at least for UV exposure and photochemical degradation, chemical analytical data adequately reflect the extent of strength losses and the probability of failure. However, it is essential to consider changes on the level of fiber structure, which, while not necessarily simultaneous with, or parallel to chemical degradation on a molecular level, are factors of great importance and may even be dominant in determining changes in fiber properties. The effects of structural changes on the properties of fibers exposed to UV light have been the subject of several investigations which, while more narrowly focused and perhaps less definitive than the work of Moore, nevertheless contribute significantly to our understanding of the problem.

The photodegradation of nylon 6 was studied by exposing fabric samples made from bright yarn in a Fadeometer (Carbon-arc), and in daylight under tropical atmospheric conditions, with and without treatment with a UV absorber (2,2' dihydroxy-4,4' dimethoxy-benzophenone), (Subramanian and Talele, 1973). Predictably, tensile strength and viscosity average molecular weight decreased with increasing exposure. Application of UV absorber to the fabric decreased the extent of degradation in subsequent exposure somewhat. Coupled with analytical data, these results were interpreted as showing that degradation resulted in random scission of C—N bonds in the polymer

chain. A free radical mechanism of degradation was postulated, leading to the formation of peroxides and, subsequently, two stages in the degradative process.

The effect of light, and of air contaminated with SO_2, with and without the presence of moisture, on surfaces of nylon 6.6 fibers, has been reported by Zeronian et al. (1971, 1973). The experimental approach for the assessment of degradation included chemical tests, scanning electron microscopy, differential thermal analysis (DTA), and measurements of tensile properties on fabric samples made from delustered nylon 6.6 spun yarns exposed to Xenon-arc radiation in a Weather-Ometer. Selected data are summarized in Table 2.7. It is evident that the presence of SO_2 increases the extent of degradation for a given exposure, both in the presence and in the absence of water spray. Scanning electron microscopy studies of exposed samples showed that, although the presence of SO_2 accelerates degradation, it does not alter the appearance of fiber surfaces (pitting and cavities) unless a water spray is used during the exposure cycle. Results obtained by DTA were interpreted as evidence of changes in microstructure resulting from exposure to light and air contaminated by SO_2, but the nature of these changes was not characterized.

The effect of UV radiation from a Carbon-arc source (Fadeometer) on the tensile behavior of air-dry and wet nylon fibers at defined levels of extension below rupture has been postulated to be of particular significance in the context of proposed photodegradation mechanisms involving both chain scission and crosslinking (Morton, 1973). Accordingly, observed changes in tensile moduli, stress decay and elastic recovery of samples irradiated for up to 100 hours were interpreted as reflecting the relative extents of scission and crosslinking reactions. However, in this author's discussion of results, there seems to be some confusion regarding the distinction between molecular and structural changes, and their effects.

The changes in fine structure and morphology of nylon 6.6 caused by near-UV radiation, have been examined in some depth

Table 2.7

Properties of Nylon 6.6 Fabric Exposed for 168 Hours*

Program Cycle	Exposure Conditions	Relative Breaking Load	Relative Extension	Relative Viscosity
Continuous light; no water spray	Control	1.00	1.00	51
	Light ^ air	0.87	0.83	--
	Light ^ air + 0.2 ppm SO_2	0.52	0.56	28.8
Two-hr. cycle of 102 min light, followed by 18 min of light and water spray	Control	1.00	1.00	----
	Light ^ air	0.61	0.58	27.0
	Light ^ air + 0.2 ppm SO_2	0.23	0.31	12.8

*Weather-Ometer : black panel temperature 68°C; RH = 42%

(Stowe et al., 1973; Fornes, et al., 1973). Near-UV radiation, found on the earth's surface, had been shown to be the most severely damaging to fiber properties (see Section 3.1 above; Singleton et al., 1965), but the work of Stowe et al. provides the first report of work specifically focused on the effects of UV radiation on fiber morphology. Measurements of viscosity, density, acid dye take-up, wideline nuclear magnetic resonance (NMR), and differential scanning calorimetry (DSC) were employed to assess structural changes caused by radiation exposure in a dry oxygen atmosphere for a commercial, delustered nylon 6.6 yarn (630 den, 104 filament) from which the spin finish was removed. Anionic dyeing was sensitive to small changes in fiber structure, and detected UV effects at low exposure times. Wideline NMR detected changes only after 240 hours' exposure. Results of density, viscosity, and DSC measurements provided support for and were consistent with the results of dyeing and NMR experiments.

The overall results of the study confirmed that photo-oxidation at low energy levels causes chain scission and reduction in molecular weight primarily in the amorphous regions of the fiber. No measurable crosslinking occurred under the conditions studied. Increased density and percent crystallinity, in conjunction with reduction of dye diffusion rate, and other data, showed that there was a measurable increase in molecular order on prolonged UV exposure: The explanation suggested was that newly free chain ends resulting from photo-oxidative cleavage of polymer chains in the amorphous regions of the fiber could relax into a crystalline configuration.

Norwithstanding the numerous investigations on the mechanisms and effects of photochemical degradation in polyamides, considerable uncertainty remains regarding concurring chain scission and crosslinking reactions in irradiated nylon fibers. This problem was discussed in a recent publication (Yano and Murayama, 1980) on the photodegradation of nylon 6, reporting on changes in the dynamic mechanical properties of nylon 6 film irradiated with spectrally dispersed UV light.

Increases in the modulus of elasticity and in density on irradiation with light below 300 nm were attributed to cross-linking, and a kinetic analysis of photodegradation of nylon 6 entailing simultaneous occurrence of chain scission and cross-linking is presented in this work.

Another aspect of the photodegradation of nylon, namely interactive effects of material composition, exposure conditions, and chemical change on the fracture morphology of yarns exposed to light (Hearle and Lomas, 1977) has been studied on semi-dull nylon 66 monofil exposed to sunlight behind glass, for periods of time ranging from 2 days to 24 weeks. Large changes in apparent fracture morphology were accompanied by remarkably small losses in breaking load and breaking extension of the fiber, even after 24 weeks' exposure. As part of this study, similar results were obtained on samples of high tenacity bright multifilament yarn exposed to sunlight in Florida for 2 and 3 months, although the appearance of the fractured filaments (which did not contain delustrant) was significantly different in this case. The effect of TiO_2 on fracture morphology, and mechanism of failure in light-degraded filaments, is discussed at some length in conjunction with the experimental observations made by the authors, and by other investigators.

5. Photochemical degradation of polyester (PET). The detrimental effects of exposure to UV radiation on mechanical properties are, as a first approximation, less pronounced for polyester (PET) than for polyamide (nylon 6.6 and nylon 6) fibers. This is illustrated, for example, by some results obtained in the evaluation of photochemical degradation of different yarns (Shah and Srinivasan, 1975, 1978) reproduced in Figs. 2-3 and 2-4. Because of the large number of experimental variables, and the uncertainties involved in generalization, the comparisons shown are to be considered merely indicative of approximate ranking. Perhaps for historical reasons, the literature on photochemical degradation and weathering of polyester fibers "per se" is less extensive than on polyamides, and although numerous reports have been published on various aspects of the degradation of the polymer by UV light, the

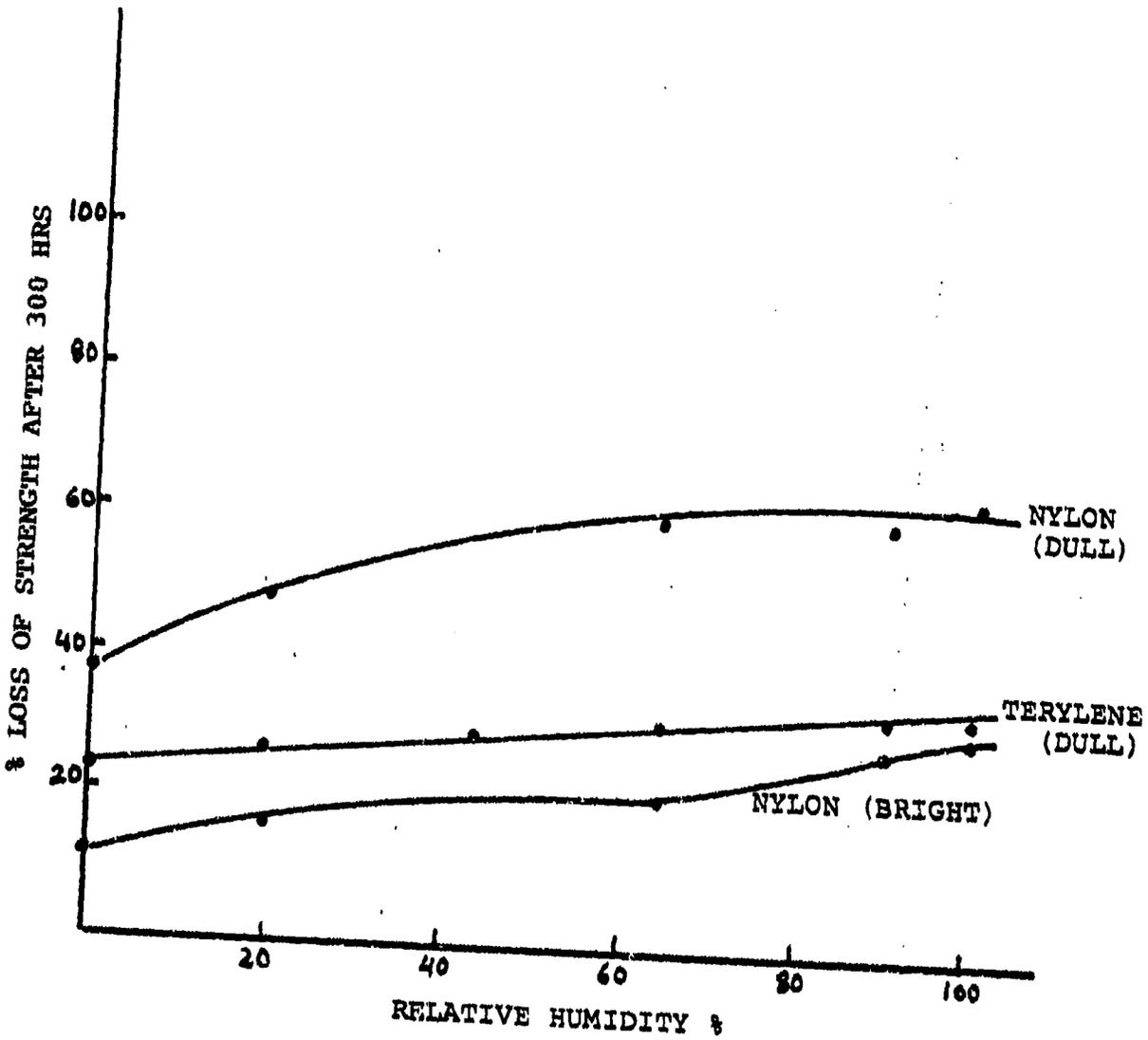

FIGURE 2-3
RELATION BETWEEN % RH AND % LOSS IN STRENGTH AFTER 300 HRS' EXPOSURE IN LIGHT-FASTNESS TESTER (SHAH & SRINIVASAN, 1978)

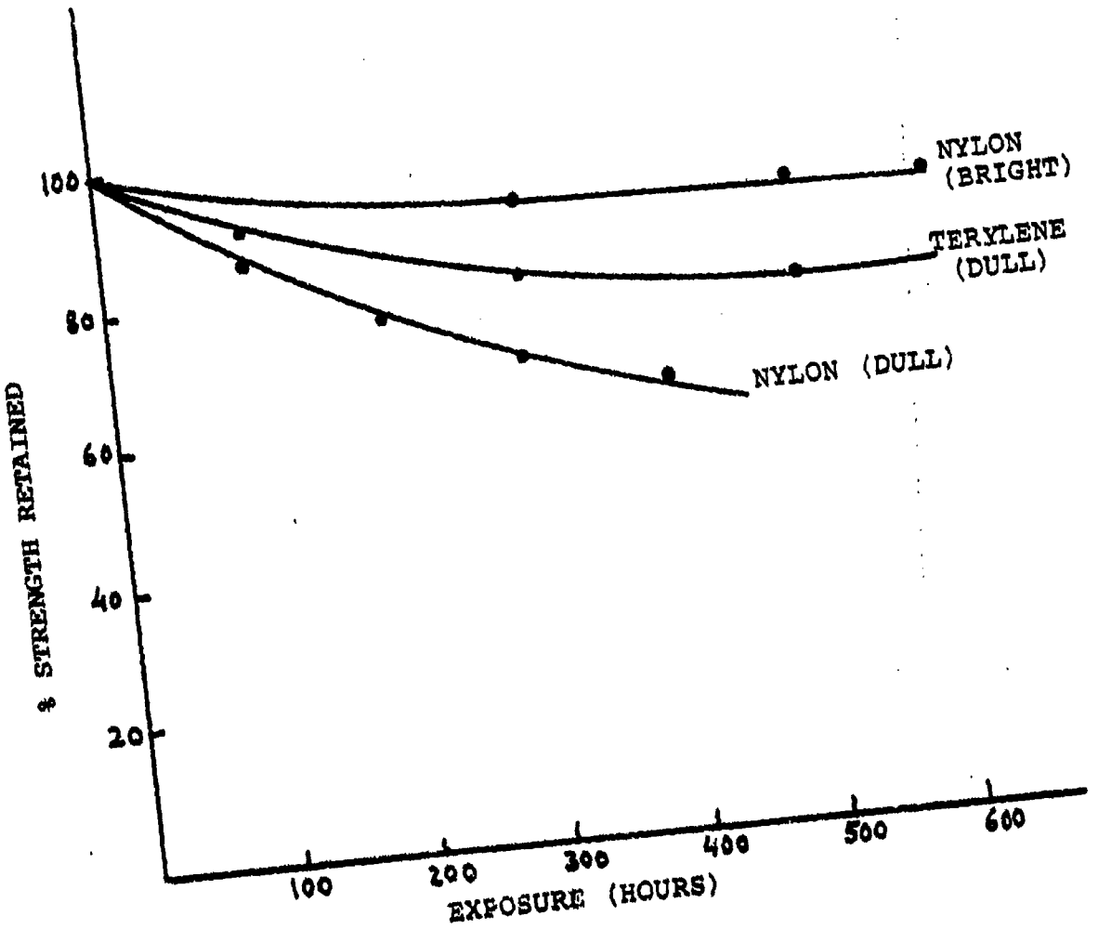

FIGURE 2-4

RELATION BETWEEN PERCENTAGE RETAINED STRENGTH AND DURATION OF SUNLIGHT EXPOSURE (SHAH & SRINIVASAN, 1975)

investigations have been primarily focused on the mechanism of photochemical degradation, and on specific techniques employed to detect and characterize the chemical reactions occurring as a result of UV exposure.

The effects of environment (oxygen, nitrogen and vacuum), and of the wavelength of incident light on tensile properties have been examined for DACRON fibers and for MYLAR films (Stephenson and Wilcox, 1963) in a study designed primarily to establish the ratio of scission to crosslinking reactions in irradiated PET. Under the conditions used, fibers deteriorated at the same rate as films, and "orientation of the (PET) fibers seemed to be unaffected by UV irradiation". A later study of the photolysis of PET (Marcotte et al., 1967), was also directed at the characterization of chemical changes occurring when PET film was exposed in vacuo to monochromatic light of specified wavelengths.

The effect of photochemical degradation on properties was one of the objectives of work reported in a series of four papers (Day and Wiles, 1972, I, II, III; Blais, Day and Wiles 1973, IV) which cover several aspects of the problem and are relevant to the subject matter of this report. The work reported in these publications was carried out on commercial PET films, varying the conditions of exposure, wavelength and environment.

In the first series of experiments (Day and Wiles, 1972[I]), film samples were exposed in a (Carbon-arc) Fadeometer and in a (Xenon-arc) Weather-Ometer in order to compare the effect of different spectral distributions calculated for these two light sources on the tensile properties of irradiated film samples and on molecular weight. The effect of 1000 hours' irradiation on the number-average molecular weight of three film samples is shown in Table 2.8. The greater decrease in $\bar{M}_n$ observed for Xenon-arc irradiation is consistent with the greater strength losses observed, and with other data. In the second paper of this series (Day and Wiles, 1972 [II]), the effect of wavelength and environment on the decomposition process of a PET film containing no UV stabilizer was studied in greater detail. The light source was a high-pressure mercury arc in which the

Table 2.8

Changes in m.wt. for PET Films
Exposed to Light

Film Number	Initial $\bar{M}_n$	Xenon-Arc Final $\bar{M}_n$	Carbon-Arc Final $\bar{M}_n$
1	17,500	13,800	16,900
2	18,800	12,300	16,200
3	19,700	13,200	16,500

wavelength range was varied by the use of appropriate filters. The effect of irradiation wavelength on the properties measured showed that the cut-off wavelength of the filter plays an important part in the rate and nature of the photodegradation. A strong correlation was observed between tensile strength and surface deterioration measured by infrared (ATR) and fluorescence techniques. This was attributed to fracture propagation from the surface when tension is applied to the polymer. It was concluded that the critical wavelength in photochemical degradation of PET corresponds to about 310 nm, with radiation at shorter wavelengths resulting in rapid deterioration of physical properties as a result of major photochemical change in the surface, but not the bulk, of the polymer film.

Subsequent work on vacuum photolysis, and photo-oxidation of PET film (Day and Wiles, 1972[III]) exposed to light of predetermined wavelengths was designed to provide additional data in support of the mechanism of photochemical decomposition of PET postulated on the basis of the prior work. The surface changes observed (Day and Wiles, 1972[II]) were examined further in concluding work (Blais et al., 1973) in which preferential surface photodegradation was confirmed by several analytical techniques for PET film exposed to UV light in a Xenon-arc Weather-Ometer, even though conventional electron microscopy revealed little change in the appearance of irradiated film. The conclusion of this work was that UV-induced photochemical deterioration of PET films leads to extensive surface degradation even under moderate irradiation. On prolonged exposure, progressive deterioration of the interior is evident. Selected chemical data of a PET film front surface (d_p = 0.17μ) as a function of irradiation time are summarized in Table 2.9 (Blais et al., 1973, p. 1900). It is evident that photochemical reactions occurring in the surface layers cause chain scission and drastic decreases in molecular weight. The author also concludes that "the mechanical properties of the deteriorated surface are grossly different from those of the interior", but the evidence in support of this statement is to be found only in the appearance of transverse fracture

surfaces (SEM) in which the side exposed to radiation is granular and "suggestive of brittle failure".

Table 2.9

Chemical Change in PET Film as a Function of Irradiation Time

Irradiation time, hours	0	66	191	555	956
——COOH groups x 10^6 equiv g^{-1}	41.4	219.9	481.2	700.3	722.9
Repeat units/polymer chain	103	22	10	6	6

6. Photostabilization. The photostabilization of a light-sensitive commercial polymer (e.g. polyamides) involves the retardation or elimination of photochemical processes that occur during degradation. It has been recently proposed that photostabilization may be attained by four general mechanisms which have been designated as:

(Allen and McKellar, 1978):

(1) Light screening--the light capable of initiating photodegradation is "screened" by incorporating additives of high reflectance into the polymer (e.g. ZnO, MgO, $CaCO_3$, iron oxides, chromium oxides, etc.).

(2) Light absorption--the stabilizer (UV absorber) prevents light from reaching the photoactive species in the polymer by absorbing it and dissipating it by some rapid process of internal conversion. Effective UV absorbers are those which have high absorbance in the wavelength range which is most harmful to the polymer (e.g. 2-hydroxy-benzophenones and 2-hydroxybenzo-triazoles are widely used for polyamides).

(3) Excited-state quenching--the stabilizer deactivates the photoactive species by one or more energy-transfer processes before chemical reactions leading to polymer degradation are initiated (e.g. complex chelates of transition metals, usually Nickel).

(4) Radical scavenging--inhibition of the chain propagation processes that occur during oxidation of the polymer is obtained by adding radical scavengers (peroxy, alkoxy or

alkyl radical involved in oxidation). Examples of radical scavengers (antioxidants) are phosphites, thio-dipropionate esters, dialkyl dithiocarbamates. In many cases, antioxidants are used in combination with UV absorbers to provide more efficient protection.

Many examples of specific compounds reported to be effective photostabilizers can be found in the patent literature, and in several reviews and textbooks. A critical evaluation of their relative merits, and limitations, would require an in-depth study of the technical literature on the subject. A recent book (Ranby and Rabek, 1975) may provide an appropriate starting point for this study.

OXIDATIVE AND THERMO-OXIDATIVE DEGRADATION

The role of oxidative reactions in the photochemical degradation of nylon and polyester has been discussed in the preceding section. Other aspects of oxidative degradation, pertaining to effects of oxygen in conjunction with water, and with elevated temperature, are briefly reviewed below, including some reported results on the effect of thermal exposure in air, and in moist air, on physico-chemical properties of fibers.

The experimental protocols of reported investigations differ considerably, and specific references have been selected primarily for their potential relevance to the subject matter of the present report. Oxidative degradation of rope in use may result, for example, from changes in supramolecular structure and increased accessibility, from increased sorption of oxygen on surfaces "eroded" or altered by chemical degradation and/or by mechanical wear, or from diffusion of oxygen into water surrounding the fibers in the rope structure during actual use.

A study of "wet oxidation" of undrawn nylon 66 (Mikolajewski et al., 1964) was carried out on rope yarns from sources characterized as follows:

(A) yarns from new undrawn ropes of 2-inch circumference (and yarns from unserviceable returned ropes of the same construction),

(B) new undrawn singles yarn as used for (A),

(C) material dating from 1956 in the form of undrawn ropes of 2-1/2-inch circumference,

(D) drawn nylon cordage complying with British Aircraft Materials Specification.

The properties of the materials are summarized in Table 2.10

Table 2.10

Properties of Plied Nylon Yarns from New Ropes

	(A)	(B)	(C)	(D)
No. of filaments (approx.)	200	10	136	360
Count, tex (g/Km length)	209	9.8	445	130
Breaking strength (Kg)	2.2	----	3.6	5.6
Tenacity g/tex	10.6	----	8.2	43.8
Breaking extension %	234	267	579	----
Delustrant (anatase TiO_2) %	0.3	----	0.04	0.3
Filament diameter (μ)	35	----	----	10

Results of experiments on yarn (A), immersed in distilled water at temperatures ranging from 20°C to 100°C, showed that the rate of degradation evidenced by changes in tenacity increased with increasing temperature, but was lower at 100°C than at any temperature between 40°C and 90°C, possibly as a result of "greatly reduced oxygen pressure at the boil". The rate of degradation of all the samples in water was increased by replacing air with oxygen, or water with H_2O_2 solution, particularly in the presence of iron salts. Drawing of the yarn (A) by 200% decreased the rate of degradation in water at 60°C, and drawn yarn (D) suffered no significant strength loss after 100 days' immersion in water at 60°C. The absorption of oxygen by nylon immersed in distilled water at 60°C from air and from an atmosphere of oxygen was measured experimentally, and by plotting rate of oxygen uptake vs. absorption of oxygen, and extrapolating to zero rate, a maximum oxygen uptake of about 30 moles by 10^4g of nylon from both air and oxygen was calculated.

The results obtained when nylon 6.6 and nylon 6 yarns were exposed in air, nitrogen and vacuum to temperatures ranging from 136°C to 215°C for periods of 5 min to 17.5 hours have been reported (Valko and Chiklis, 1965). In one aspect of this

work, the role of air in the heat degradation process was assessed by exposing yarn samples to 168°C for 90 minutes in air, and in a stream of preheated oxygen-free nitrogen. The loss of strength, which was 33% in air and 2% in nitrogen, was interpreted as showing that thermal degradation in air is essentially oxidative in nature. Other aspects of the investigation included experiments on the effects of thermal exposure on molecular weight, acid sorption, and end group. It was also established that exposure to heat reduced the equilibrium moisture content of the yarn (at 65% RH, 70°F), independently of the presence or absence of oxygen or of antioxidant in the fiber. This change was interpreted as reflecting secondary crystallization "in a broad sense".

The response of nylon 6.6 fibers to oxygenated water at 80°C was investigated in depth (Vachon et al, 1965; 1968). The initial observation of deep crevices in surfaces of undrawn nylon 66 fibers treated with oxygenated water at 80°C (1965) motivated a study of the extent of chemical degradation as a function of time for drawn and undrawn nylon 66 filaments exposed to oxygenated aqueous systems under controlled conditions (1968). Measurements of viscosity--average molecular weight, end groups, oxygen absorption, density revealed a significant effect of pH on the chemical and structural changes observed (maximum rate of degradation at pH 8.3), and a tentative mechanism, including pH dependence, for the auto-oxidation of nylon was postulated on the basis of these results.

Lisitsyn et al. (1971) studied the changes in fiber tensile strength, elongation, and cyclic bending strength, under conditions of accelerated ageing, and also the temperature dependence of thermo-oxidative processes before and after aqueous heat treatment for Capron polyamide (nylon 6) tire yarn which had been processed in various manners. It was shown in this work that the rate of change in properties is slower for fibers subjected to aqueous heat treatment in the stressed state, and that a boiling water treatment inhibits changes in morphological structure of the fibers during the thermo-oxidative degradation

process. Results were discussed in the context of the relationship of structural development in the fiber to the effects of thermo-oxidative degradation. The effect of temperature on morphological structure was characterized by measuring the swelling and dissolution time of 1 mm-long pieces of fiber in a 23.5% solution of H_2SO_4 (observed in a light microscope).

Although prolonged exposure of the entire rope to elevated temperature is not likely to be encountered in use, it is appropriate to consider the occurrence of localized temperature rise in some sections of the rope, and thus the possibility of thermal and/or thermo-oxidative degradation events occurring in isolated sites within the rope over a period of time.

IMMERSION IN WATER AND AQUEOUS SOLUTIONS

Many aspects of the response of fibers to water and to aqueous solutions are important determinants of properties. In the case of water in fibers, equilibrium moisture regain and equilibrium swelling, which depend on the molecular and microstructural features of the particular polymer, govern the water content, and the fiber properties under specified conditions of exposure (relative humidity) or immersion. In the case of aqueous solutions of compounds (e.g. acids, oxidizing agents, salts, etc.) which can initiate, accelerate, or cause chemical degradation reactions, penetration of the aqueous solution, and interaction of the solute with the polymer substrate will also have significant effects, and in some instances, control degradative reactions in the heterogeneous system comprising fiber and solution, reflected in changes in fiber properties under the conditions of immersion. The results of selected studies of these effects, believed to be relevant to the investigation of rope deterioration in use, are discussed below with reference to the general concepts of (1) water-polymer interactions (swelling), (2) heterogeneous degradation in aqueous systems, and (3) chemical degradative stress cracking in aqueous solutions.

1. Water-polymer interactions (swelling). The effect of the presence of water in fibers, both at equilibrium regain level and completely wet out, on the T_g, and the significance of the

"wet T_g" of fibers have been discussed in conjunction with a review of methods for measuring T_g that are particularly adaptable to fibers in the dry and/or in the wet state (Fuzek, 1980). The equilibrium moisture content of fibers (70°F, 65% RH) was shown to lower the T_g for many fibers, and further reductions in T_g were shown to occur when the fiber was allowed to wet out in water until equilibrium saturation was reached. Some data are shown in Table 2.11 below.

Table 2.11

T_g for Wet, Conditioned and Dry Fibers

Fiber	T_g °C			% Water in Wet Fiber	% Moisture Regain
	Conditioned (75°F 65%RH)	Dry (Calcd)	Wet (24 hrs in water)		(70°F 65% RH)
Polyester (PET)	71	73	57	6.8	0.4
Nylon 6.6	40	59	29	6.1	4.2

The lowered T_g has significant effects on fiber properties, and some of these relationships have been studied and interpreted in detail over many years. For example, the plasticizing effect of water vapor and its relationship to the dynamic mechanical properties of nylon 66 monofilaments has been investigated over a wide humidity range at 9°C, 35°C, and 60°C (Quistwater and Dunell, 1958; 1959). Results showed dispersion of mechanical properties with change in humidity at each temperature.

More recently, the influence of water molecules on molecular motion in wet commercial nylon 6.6 fibers at room temperature has been examined by pulsed NMR techniques (Smith, 1976). Based on a chain-folded model of semicrystalline fiber morphology, the behavior observed was explained in terms of mobilization of amorphous chain segments above the T_g, and of the ability of these segments to be plasticized by water molecules.

The Proceedings of a symposium on "Water in Polymers" (Rowland, Editor, 1980) include a paper on water in nylon 66 film (Starkweather, 1980) in which evidence is presented in

support of the concept that the water first absorbed and most tightly bound is hydrogen-bonded to the oxygen atoms of amide groups in the amorphous regions, and that "clustering" of water then begins.

The effect of water on dimensional changes in polymer substrates has been the subject of countless investigations. Illustrative reports are summarized below.

An interesting study of the variation in length of "suddenly moistened" polyamide fibers has been carried out for fibers of various thickness at temperatures of 20°C to 80°C (Kunzman, 1961). The change in length was found to be delayed as compared to water absorption, and the delay was theoretically considered as a relaxation process.

Dimensional changes in unoriented nylon 6 film on absorption and desorption of water have been studied as a function of time and amount of absorbed water (Inoue and Hoshino, 1976). The behavior was found to be similar to that previously reported for nylon 6 fiber (Kunzman, 1961; Takagi and Hattori, 1965) and the authors concluded that there is no essential difference in the mechanism of swelling for fibers and films made from a specific polymer. A theoretical analysis was based on assumption that the modulus of the polymer is determined only by the instantaneous concentration of absorbed water. This analysis gave good agreement with experimental results, and showed that the characteristic swelling behavior of unoriented nylon 6 film arises from instantaneous relaxation of the polymer molecules, without time lag between water absorption and polymer expansion. The effect of molecular orientation on dimensional changes caused by swelling in nylon 6 films of different degrees of orientation and comparable crystallinity was studied in a subsequent investigation (Inoue and Hoshino, 1977) which is perhaps of more direct interest with regard to the swelling behavior of fibers. On the basis of the results of this later work, it was concluded that the degree of linear swelling in water is determined by the distance between crystallites, which depends on molecular orientation, such that swelling is greater in the orientation direction than in the direction perpendicular to it.

Measurements of longitudinal swelling in water for commercially available, drawn nylon 6.6 filaments (and fabrics) before and after heat setting treatments, and the effects of longitudinal swelling on the stresses developed during drying of moist specimens have also been reported (Shishoo, 1977). Dimensional changes in multifilament nylon 6.6 yarn (taken from fabric) after wetting, drying and conditioning, are shown below in Table 2.12.

Table 2.12

Change in Length (% of Original Length) Nylon 6.6 Yarn from Fabric

Specimen	Wetting	Drying at 12% RH, 30°C	Conditioning at 65% RH, 20°C
Not set	+1.37	-0.3	+0.43
Washed and dried at 150°C	+2.15	0	+0.97
Heat set (slight tension)	+3.35	+0.25	+1.64
Heat set (no tension)	+5.70	+1.74	+3.92

Measurements of stress changes during drying on specimens held at constant length showed an initial stress decay, followed by a sharp rise in stress due to deswelling of filaments. The increase in stress was largest for specimens heat-set without tension, and the level of stress recovery during drying was dependent on the magnitude of the reversible longitudinal swelling due to wetting (see Table 2.12, first column).

The effect of water at various temperatures on fatigue was studied in conjunction with a comparison of the effects of adverse environments on tensile and fatigue properties of nylon 6.6 fibers (Hearle and Wong, 1977). A comparison of median fatigue life of nylon 6.6 in tap water and in air under different conditions of testing (shown in Table 2.13) demonstrates the extent to which water reduces the fatigue life of nylon 6.6 fibers--presumably by reducing intermolecular cohesion and allowing slippage of adjacent molecules past one another.

An extensive study of the effect of moisture on fatigue crack propagation in injection-molded plaques of nylon 6.6

Table 2.13

Effect of Water on Median Fatigue Life of Nylon 6.6 Fibers

Median Life (cycles)

Mass of applied weight (g) / Strain Amplitude %		5.8	8.3	9.6
In air	13.6	31,090	19,855	9,181
	22.1	8,832	4,740	4,430
	28.4	4,424	2,151	1,290
In water	13.6	14,400	7,330	5,009
	22.1	2,351	1,123	1,008
	28.4	1,720	800	671

(Bretz et al., 1980) led to several major conclusions concerning fatigue mechanisms. The results of this investigation showed that fatigue crack growth rates in nylon 66 are very sensitive to moisture content in the range from ≤0.2 wt % ("dry") to 8.5 wt % (saturated). A twenty-five-fold variation was found to exist between the fastest and the slowest rate. (The authors warned, however, that the fatigue response as a function of water content is strongly dependent on the test method.)

The effect of absorbed water on the dielectric constant and on the density of polyesters (including PET) has been studied (Ito and Kobayashi, 1980), primarily for the purpose of providing data for the design of electric insulation materials. It was clearly established in this work that even the very small amounts of water absorbed by hydrophobic polyesters have significant effects on the physical and electrical properties of the materials.

2. Heterogeneous chemical degradation reactions in aqueous media. The subject of chemical degradation in heterogeneous systems, when the polymer or fiber is immersed in an aqueous solution of compounds which may induce, catalyze or accelerate degradation reactions, is obviously broad and complex: Suffice it to mention hydrolytic scission of polymer chains, pH effects in oxidative degradation, and sorption of gaseous contaminants from the environment by moist polymer as potential causes of degradation. For fibrous substrates exposed in the presence of water to chemical substances commonly encountered in use, the range of probable exposures is limited, and there are several reports of interest in the technical literature.

An investigation of degradation of undrawn nylon 66 under "wet or humid conditions" at temperatures between 50°C and 90°C (Mikolajewski et al., 1964) included, for example, the results summarized in Table 2.14 in conjunction with experiments on oxidative degradation for the rope yarns described in Table 2.10 and discussed earlier in this report. There are some interesting anomalies in the results, including the profound effect of relative humidity at 60°C, and the difference in effect between saturated NaCℓ and 1% NaCℓ. These are acknowledged by the authors: However, the objective of the work was primarily to study the mechanism of oxidative degradation of nylon in the presence of water, and only limited data were presented on

Table 2.14

% Tenacity Retention of Nylon 66 Yarns after Immersion in Aqueous Media

Yarn Source (Rf. Table 4-I)	Temperature °C	Environment	% of Original Tenacity after Immersion (days)			
			5	20	50	100
(A) (Rope)	20°	Water	98	95	50	95
	20°	3% H_2O_2	95	95	--	95
	60°	Air (10% RH)	100	100	--	100
	60°	Air (80% RH)	80	55	--	--
	60°	Saturated NaCℓ	100	100	100	100
	60°	1% NaCℓ	100	55	40	--
	60°	Water	--	30	10	--
	60°	Oxygen in water	50	--	--	--
	60°	3% H_2O_2	80	0	--	--
(B) (Bobbin undrawn)	60°	Water	25	0	--	--
(C) (Rope, undrawn)	60°	Water	100	100	100	100
	60°	1% $FeCℓ_3$	65	60	50	--
(D) (Cordage, drawn)	60°	Water	100	100	100	100
	60°	1% $FeCℓ_3$	90	55	--	--

effects of aqueous solutions other than H_2O_2.

The kinetics of specific degradation reactions, including hydrolysis, of semidull nylon 6 fibers in heterogeneous medium at 40°C to 60°C has been investigated (Bhattacharya and Lokhande, 1976). Predictably, the rate of hydrolysis was shown to be strongly dependent on the temperature of the aqueous acid medium (5% HCℓ). Hydrolytic attack at a given temperature was found to be initially rapid, and slower as the reaction proceeded. The two distinct rates, and apparent activation energies for the hydrolytic cleavage reaction were interpreted by the authors as reflecting attack in "weakly hydrogen-bonded", and in "strongly hydrogen-bonded" regions of the fiber.

A different aspect of the effect of aqueous acid on polyamide fibers was studied (Hearle and Wong, 1977) by evaluating the mechanical properties of nylon 6.6 fibers immersed in different liquid environments. The reduction of fatigue life at low pH, and the loss of breaking strength for fibers immersed in 1,0 normal HCℓ for one hour prior to testing, are consistent with the rapid rate of hydrolytic degradation of polyamides in acid media reported by other investigators.

3. Chemical degradative stress cracking in aqueous solution. A specific aspect of the effect of degradative aqueous environment on fibers which is of importance in the context of this report is chemical stress cracking--a fracture phenomenon in which the material in contact with a chemical environment develops cracks at a stress level which is lower than its short-time fracture strength. It has been suggested (e.g. Sweet and Bell, 1978) that chemical stress cracking may be termed "environmental", "solvent", or "oxidative", depending on whether the crack-promoting agent produces no apparent change in the polymer substrate, or solvates and swells it, or reacts with it. According to these definitions, aqueous solutions of salts and of non-reactive compounds may cause environmental stress cracking in fibers, and selected investigations pertaining to this phenomenon in nylon and polyester are discussed below.

The work of Dunn and Sanson (1969, 1970) established by

infrared (IR) and by nuclear magnetic resonance (NMR) methods, that among the many salts which in aqueous solutions were found to promote cracking in nylons, some are bound directly to the carboxyl oxygen in the polymer (classified as Type I; e.g. zinc chloride), while others complex normally with a hydroxylic solvent molecule (classified as Type II; e.g. lithium chloride). It was postulated by the authors that Type I salts plasticize the polymer matrix by diffusion, lower the yield strength and, as a consequence, induce stress cracking, while solutions of Type II salts can dissolve polyamides, and cause stress cracking through solvation. It was also proposed by Dunn and Sansom that zinc chloride, the most active halide in promoting stress cracking of nylon, is a Type I salt. However, subsequent work on the stress cracking of nylons by zinc chloride solutions (Reimschussel and Kim, 1978) presented convincing evidence that solutions of this halide have solvent action on polyamides, and that a close relationship exists between the solvent action of zinc chloride solutions on nylons and its effect on stress cracking. In the context of these results, stress cracking of nylons in zinc chloride solutions would thus be classified as "solvent stress cracking". Furthermore, it was shown that stress cracking of nylon in zinc chloride solutions is accelerated by the presence of low molecular weight components, and retarded by orientation of the polymer--thus related to other events in chemical degradation, and to fine structure.

The fracture morphology of nylon 6.6 and nylon 6 plastic specimens, strained in the presence of salt solutions under many different conditions of testing was examined in detail (Burford and Williams, 1979), with the objective of formulating a generalized mechanism of craze formation and breakdown. Tensile testing, and scanning electron microscopy studies in (1 Molar) aqueous solutions of $ZnCl_2$, $CoCl_2$, LiI, LiBr and $Mg(ClO_4)_2$ revealed differences in activity for the systems investigated, but essentially the same morphological features for different salts, solvents and initial water content of the polymer. In a subsequent paper, the same investigators (Burford and Williams, 1979) referred to the environmental stress cracking phenomena

caused by inorganic salt solutions in nylons as an example of "failure of hydrogen-bonded polymers in the presence of agents capable of disrupting that bonding", and addressed the problems of polymer-salt interactions, associated with the transport of ions during fracture. They concluded that the morphology of fracture of nylon crazed in the presence of different salts is consistent with a generalized mechanism, but exhibits differences that may be attributed to salt solution mobility.

Chemical stress cracking in polyester (PET) fibers has been recently studied (Sweet and Bell, 1978) for commercial undrawn and drawn PET yarns (containing 0.2% TiO_2) exposed to 40% aqueous methylamine solution. While this system is only peripherally related to environments which may be encountered by PET fiber rope in use, it is of interest to note that the observed behavior was similar to that of other stress-cracking systems, and that cracking during degradation occurred only when the fiber encountered internally or externally applied stress above a critical level. Visible surface cracking did not occur until the chemical degradation reached a level which caused measurable weight loss. Crack density increased with increasing draw ratio, because of residual stresses created by higher molecular orientation. Irregularities in cracking patterns were attributed to variations in the stress distribution and structure within the oriented fibers.

ASSESSMENT OF CHEMICAL DEGRADATION IN FIBERS

The multitude of factors which may cause chemical degradation of fibers in use is evident from the discussion of selected causative environmental variables in the preceding sections of this report. The reactions, the changes in molecular structure, and their effects on microstructure, physical properties and mechanical response of exposed fibers and fiber assemblies present an overwhelming array of questions and problems. These can be investigated experimentally only by defining specific objectives, and by designing the conditions of exposure and testing in the laboratory with awareness of inherent limitations in the interpretation of results, and in the formulation of generalizations and conclusions based on them.

With these considerations in mind, the selection of methods and analytical techniques for the evaluation of chemical degradation in fibers from used ropes, presents enormous difficulties, and a critical scrutiny of the literature, such as given in the present report, can offer only tentative guidelines. An attempt is made here to identify some chemical methods which have been employed effectively in many applied research investigations on nylon and polyester, for the purpose of establishing correlations between the extent of chemical degradation encountered under specified conditions of exposure, and observed effects on polymer properties. In concert with scanning electron microscopy, and with the evaluation of changes in mechanical properties, these chemical techniques have provided considerable insight into the effects of environmental variables on molecular and structural changes in fibers, and into the dominant mechanisms of chemical degradation for polyamides and polyesters. Advanced techniques of instrumental analysis have also been used for the detection and characterization of chemical changes, and for a quantitative estimation of degradation products. The methods of major interest in the context of this discussion include (1) determinations of changes in molecular weight averages, and in the concentration of specific functional groups as indicative of degradation on a molecular level and (2) measurements of moisture regain, swelling and dye diffusion as criteria for the assessment of structural changes.

1. Molecular weight averages and functional groups. Changes in molecular weight averages of polymers exposed to degradative environment provide prima facie evidence of chain scission. When crosslinking of polymer chains occurs concurrently with cleavage of bonds in the macromolecule, the interpretation of observed changes in molecular weight averages becomes complex. Identification and quantitative analysis of specific functional groups must then be combined with molecular weight measurements for characterizing the chemical species present in the polymer at a given time. For the case of nylon or polyester fibers in rope, the mode of exposure is such that crosslinking reactions are not probable, and the determination

of molecular weight differences between exposed and unexposed fibers may be of value. Comparisons might be made, for example, for new fibers, and those taken from rope after extended use, or for fibers located in exposed (e.g. surface yarns) and protected (e.g. inner core yarns) parts of used rope, or for fibers exposed to controlled degradative environments in the laboratory according to suitable experimental design. Molecular weight averages reported in the literature for studies of chemical degradation of polyamides and polyesters have been most frequently derived from viscosity data (e.g. ASTM D-2857-70 [Reapproved 1977]; $[\bar{M}_v]$; test method for dilute solution viscosity of polymers). For a given polymer-solvent combination, the intrinsic viscosity is proportional to m. wt., and the average viscosity molecular weight $[\bar{M}_v]$ may be calculated by using the Mark-Houwink equation,

$$[\eta] = KM^a$$

where $[\eta]$ is the intrinsic viscosity, and K,a are constants.

Precise and reproducible number-average ($\bar{M}_n$) and weight-average ($\bar{M}_w$) molecular weight values can be obtained by Gel Permeation Chromatography (GPC) techniques (Maley, 1965; Yau et al., 1979). The value of the polydispersity index ($\bar{M}_w/\bar{M}_n$) is, furthermore, an important measure of the broadness of molecular weight distribution, because weight average ($\bar{M}_w$) and number average ($\bar{M}_n$) are each influenced by an opposite end of the molecular weight population in the polymer--namely, by the concentration of high m. wt. ($\bar{M}_w$) and of low m. wt. ($\bar{M}_n$) species respectively.

Illustrative examples of molecular weight changes reported for experimental investigations of chemical degradation of nylons and of polyesters exposed to various environments are briefly reviewed below.

The effect of oxidative environments on intrinsic viscosity was studied for drawn and undrawn nylon 6.6 filaments exposed to oxygen-water systems at 80° (Vachon, 1968). The decrease in viscosity, and hence molecular weight, as a function of time was dependent on pH; at any given pH, the rate of degradation determined from intrinsic viscosity measurements was greater

for undrawn filaments.

The relationship of decreases in intrinsic viscosity and in molecular weight calculated from it ($\bar{M}_v$) for nylon 66 yarns exposed to ultraviolet radiation in the laboratory at 52°C is shown in Figs. 2.5 and 2.6 (Stowe et al., 1973). In this work, values for intrinsic viscosity were obtained in 90% formic acid at 30°C, using the ASTM method D-2857-70 cited above, and calculated (assuming that no crosslinking or branching occurred) from the equation:

$$\bar{M}_v = K[\eta]^a$$

with values of $K = 1.3 \times 10^4$; and $a = 1.39$.

The changes in number-average molecular weight with irradiation time for exposure of a commercial PET (MYLAR) film to Xenon-arc and carbon-arc sources were calculated from intrinsic viscosity values (measured at 25° in o-chlorophenol) using the equation:

$$[\eta] = 1.7 \times 10^{-4} \bar{M}_n^{0.83}$$

(Day and Wiles, 1972). Results are shown in Fig. 2.7. The data are significant in that they reflect the magnitude of molecular weight changes that may be termed modest, and severe, in the case of exposure to carbon-arc and Xenon-arc respectively. Changes produced in the viscosity average molecular weight ($\bar{M}_v$) have been measured, and results have been compared with those obtained in ESR (electron spin resonance) spectra, to determine the extent of bond rupture occurring during tensile deformation of nylon and polypropylene polymer samples, including nylon 6 industrial quality yarn, and nylon 66 yarn (Stoeckel et al., 1978). It was shown that the amount of irreversible bond rupture occurring during tensile deformation could be estimated from changes in m. wt. In highly oriented nylon 6 fibers, the amount of chain rupture can account for 10% to 100% of the irreversible work of tensile deformation. In annealed or undrawn polymers, this fraction is considerably smaller. The molecular mechanism of deformation and fracture of oriented fibers was further explored in studies of chain rupture during

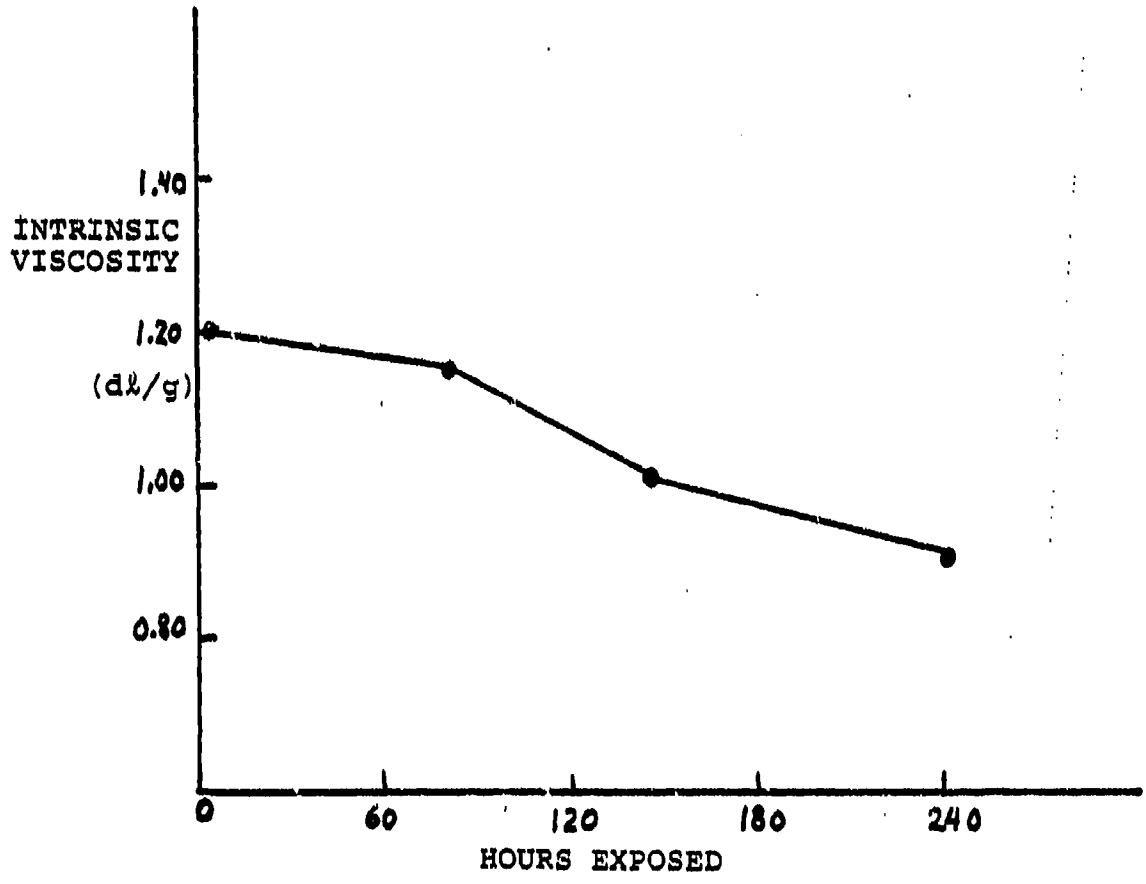

FIGURE 2.5
DECREASE IN INTRINSIC VICSOSITY WITH TIME OF LIGHT EXPOSURE (STOWE ET AL., 1973)--
Nylon 6.6 Yarn

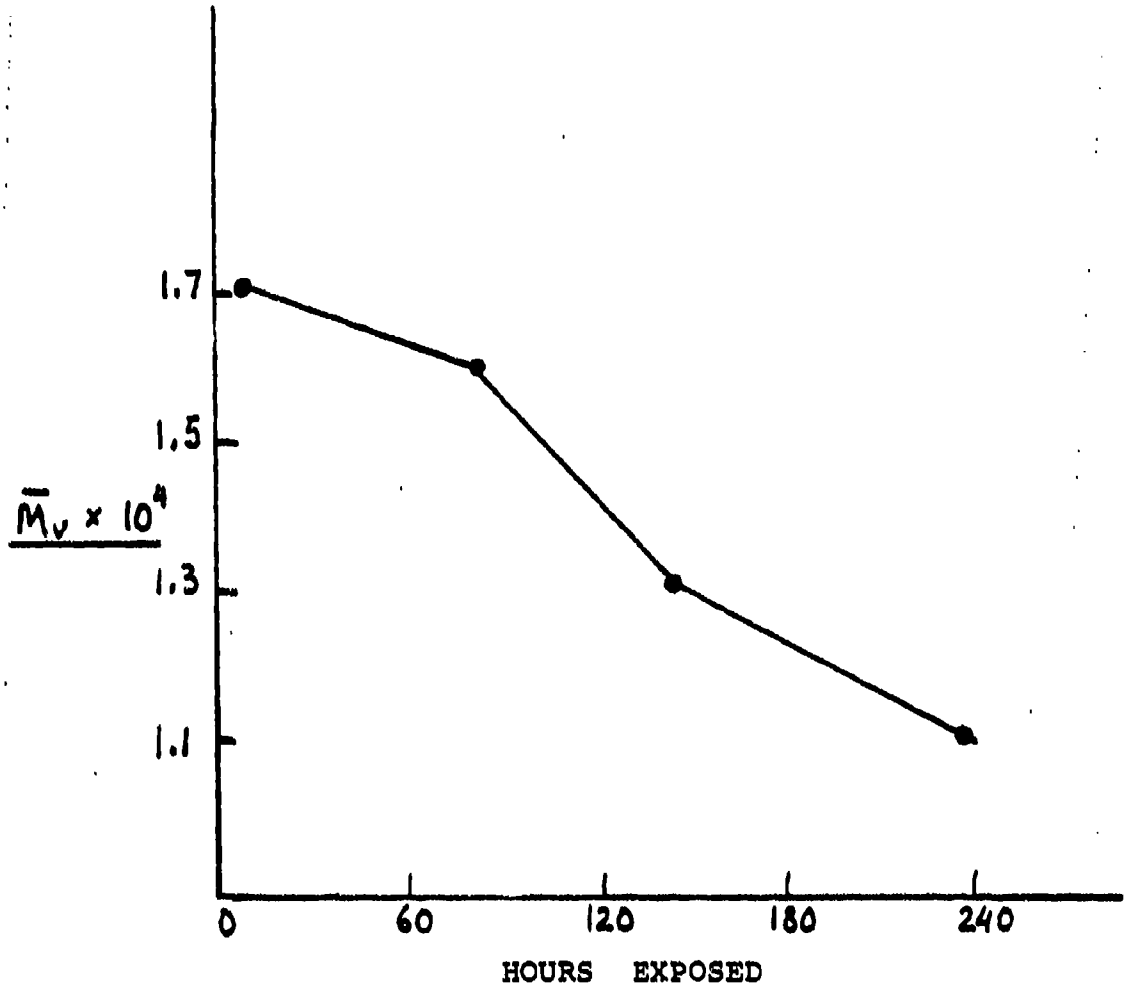

FIGURE 2.6
DECREASE IN MOLECULAR WEIGHT WITH
TIME OF LIGHT EXPOSURE
(STOWE ET AL., 1973)

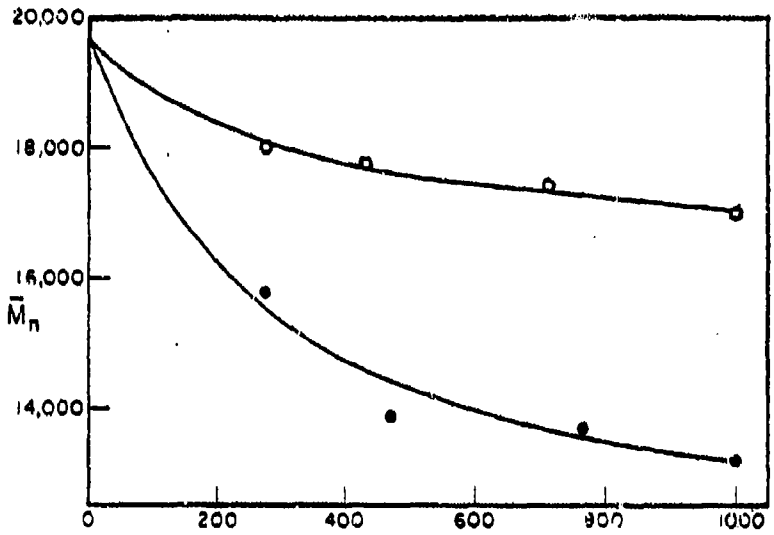

Variation in number-average molecular weight with irradiation time for: (O) carbon arc; (●) xenon arc.

(PET Film)

FIGURE 2.7 (DAY AND WILES, 1972)

tensile deformation of nylon 6 fibers prepared for use as high strength cords in tires (number-average m. wt. 30,000; filament diameter 0.027; yarn composed of 136 filaments plied together with a slight twist, (Park et al., 1978). In this work, tensile stress-strain data and free radicals formed during bond rupture were simultaneously recorded. Determinations of concurrent changes in molecular weight were, however, not made.

In work on the mechanisms of chemical degradation, the analysis of functional groups by chemical and by instrumental methods has included titration of end groups (COOH and NH_2), infrared spectra showing changes in bands for functional groups (e.g. amide) in the chain, and specialized techniques for the detection of intermediates and reaction products in postulated degradation reactions. The reader is referred to references cited in previous sections of this report for details on some of these techniques.

2. Moisture regain, swelling and dye diffusion. The absorption of moisture in fibers has important effects on fiber properties: it causes swelling, which alters the dimensions of the fibers, and this, in turn, affects the size, shape, stiffness and permeability of yarns. Mechanical and frictional properties are changed; cycles of wetting and drying may lead to permanent set; and the moisture content of the material is a major factor in determining its electrical properties. In an application such as rope, where exposure to high humidities and wet environments is certain, moisture response is thus of critical importance. The mechanisms of moisture absorption in fibers, and the theories associated with them will not be discussed here, but some broad generalizations concerning the principal variables that affect equilibrium absorption (moisture regain/moisture content), rate of absorption, and swelling in fibers exposed to high relative humidity and to water are summarized below.

The presence of hydrophilic groups in the polymer molecule, and, for a given polymer, the ratio of crystalline to non-crystalline material and intermolecular bonding are primary factors in determining moisture sorption (Morton and Hearle, 1975, pp. 229-238). Water molecules cannot easily penetrate

regions in which polymer molecules are closely packed, with crystallites and hydrogen bonds providing strong intermolecular forces. The regions of the fiber accessible to water are limited to disordered or non-crystalline regions, and surfaces of crystallites. It follows that, for a specific fiber, the moisture regain at a given relative humidity is proportional to the amount of accessible (effectively non-crystalline) material present, and measurements of moisture regain (as well as density measurements) provide a method for estimating the ratio of crystalline to non-crystalline material, and for monitoring structural changes that may occur as a result of extensive chemical degradation in some environments. The swelling behavior of fibers is also of great significance. Variation of swelling with relative humidity generally follows the change of moisture regain (Morton and Hearle, 1975, pp. 223-228). For swelling of fibers in water, values reported in the literature have varied somewhat, depending on the experimental conditions, but, as in the case of regain, the degree of swelling in water is determined primarily by the presence of hydrophilic groups in the polymer, and by the structural features of the fiber. Changes in swelling behavior, in conjunction with moisture regain and density thus reflect structural changes in fibers exposed to degradative environments.

Indications of structural change may also be derived from measurements of dye diffusion behavior in fibers. The relationship between dye diffusion behavior and time-dependent mechanical properties (creep and stress-relaxation) which are controlled by the mobility of polymer chain segments has been studied in depth for commercial multifilament yarns made from nylon 6.6 and nylon 6 (Bell, 1968).

A pragmatic investigation of the effect of draw ratio on moisture sorption, density, dyeability and stress-strain behavior in nylon 6 monofilaments drawn in the laboratory at draw ratios of 1.0 to 4.21 has also been reported (Varma and Cameotra, 1973).

The value and the interpretation of results obtained in dye diffusion experiments, in concert with other techniques,

for the assessment of changes in fiber morphology upon exposure to a degradative environment, are perhaps best illustrated by a study of the effects of near-ultraviolet radiation on nylon 66 (Stowe et al., 1973). As mentioned, it was established in this work that anionic dyeing in nylon is sensitive to small changes in fiber structure, and can detect effects at low exposure time and low levels of degradation.

More recently, structural changes occurring within the microstructure of nylon 6 during drawing have been investigated by dye diffusion experiments (Sweet and Bell, 1976). Correlations of dye diffusion constants, loss modulus, and birefringence with draw-ratio effects were examined and discussed in the context of the roles of orientation, and "available" molecular mobility of the polymer chains at various stages of the drawing process.

SUMMARY/CONCLUSIONS AND RECOMMENDATIONS

Published papers on environmental degradation of fibers and films which have been reviewed and discussed in this report provide some valuable knowledge to guide the study of wear caused by environmental exposure of synthetic fiber in use. However, caution must be exercized in applying specific concepts based on literature data to the problem at hand, and some of the statements which follow are submitted in a tentative vein.

1. General conclusions

(1) Variables of materials' composition which determine the rate and extent of chemical degradation in a specified environment are the polymer (nylon 6.6, nylon 6, or polyethylene terephthalate), fiber additives (e.g. delustrants, UV inhibitors, antioxidants), and added components in the yarn (e.g. dyes, lubricants).

(2) The fiber structure (orientation and crystallinity) plays a major role in the interaction of environmental variables with the polymer substrate, and in the magnitude of degradative effects.

(3) Dimensions and geometry of the rope structure are important factors in that they determine the level of exposure of fibers in specific locations within the rope. Chemical

degradation of rope at any given time is thus inherently non-uniform, and, as a first approximation, more extensive in fibers located near the circumference (surface) of the rope structure.

(4) With reference to exposure of rope in use, the environmental factors which cause chemical degradation under some conditions are primarily untraviolet radiation, elevated temperature, oxygen, high humidity and water, and solutions of inorganic salts.

(5) Changes in chemical, physical and mechanical properties of fibers, yarns, and ropes under any exposure conditions may reflect effects of these factors operating individually, interactively, or sequentially.

(6) Changes resulting from chemical degradation occur in fibers and fiber assemblies on a molecular level, on the level of supramolecular structure and on a macroscopic level.

(7) Even for a specific material, characterized as to chemical structure, microstructure, composition and geometry, and for controlled conditions of exposure, simple relationships between specific causative factors and their effects on properties cannot be defined with precision. Thus, laboratory experiments have limited significance as simulations of realistic exposures in use.

(8) Change in any one chemical, physical, or mechanical property of fiber or yarn exposed to a specified degradative environment is not a sufficient criterion for the assessment of environmental degradation, nor for the prediction of effect on the performance of rope.

(9) Since exposure conditions in use cannot be altered or controlled, the value of this discussion and of recommendations based on it resides in (a) defining some criteria for detecting ongoing chemical degradative processes in rope during use, and (b) formulating research approaches for modifications of fibers and ropes which may retard chemical degradation during use.

2. Specific conclusions

(1) In the photochemical degradation of polymers, the

wavelength of ultraviolet radiation is an important consideration. Many laboratory studies on nylons (6 and 6.6) and on polyester (PET) have employed broad-band wave sources which include visible and far UV, as well as the near-UV light which is found in sunlight at the earth's surface.

(2) The photodegradation of polyamides and of polyesters may occur by a photolytic process, which results in both chain scission and crosslinking, or, in the presence of oxygen, it may occur by photosensitized oxidation processes in which chain scission predominates.

(3) Chain scission occurring as a result of photodegradation is reflected in decreased average molecular weight, and changes in the concentration of end groups. In the case of fibers, microstructural changes and changes in tensile strength, and elongation also result from UV exposure.

(4) In the presence of oxygen, titanium dioxide (delustrant) accelerates photodegradation of nylon fibers at some wavelengths (above 300 nm).

(5) Photochemical degradation can be retarded or inhibited by fiber additives which operate by one of several mechanisms. The identity of compounds used as UV stabilizers or as antioxidants in commercial fibers is not necessarily disclosed.

(6) Exposure of nylons to oxidative and thermo-oxidative environments has significant effects on properties and can be monitored by changes in average molecular weight and in fiber morphology.

(7) The changes that occur in fibers as a result of exposure to water vapor, by immersion in water, or by prolonged contact with salt solutions may accelerate degradative effects of other factors significantly.

(8) In environments in which moisture sorption and photo-oxidative processes play a significant role, nylon fibers are more vulnerable to chemical degradation than polyester fibers.

3. Recommendations

(1) For detection and characterization of the extent

and location of chemical degradation in used rope, determinations of molecular weight in fiber samples taken from carefully selected locations in the rope can provide valuable data. Comparative values for fibers taken from surfaces and from inner cores along the length of used rope "as received" should, in principle, be considered with values for fibers taken from new rope, and/or from new rope exposed to extreme conditions in the laboratory. However, the appropriate "new rope" samples may not be available, and the selection of "extreme conditions" realistically simulating exposure in long-term use is essentially impossible. Therefore, changes in molecular weight can be interpreted at this time only as evidence of chemical degradation occurring in some parts of the rope as a result of combined effects of environmental and mechanical factors.

(2) Molecular weight data on fibers taken from specific locations in used rope should be examined in conjunction with Scanning Electron Micrographs and measurements of mechanical properties on fibers in close proximity--in order to determine correlations that may exist between chemical changes, surface asperities, and strength for fibers in a given locus.

(3) Measurements of swelling in water and of dye diffusion should be made on fibers identified as having undergone chain scission, and on appropriate controls, for the purpose of characterizing microstructural changes associated with chemical degradation.

(4) For the formulation of approaches to improve resistance to chemical degradation in rope, it is essential to define the chemical composition of the material of interest (fiber and additives) and their processing history. The possibility of incorporating improved UV stabilizers and/or antioxidants in the fiber manufacturing process is primarily the task of the fiber producers. It is probable, however, that an in-depth study of the literature on compounds and mechanisms for retarding photochemical, thermal and oxidative degradation in the fibers used would suggest novel and potentially effective approaches to the application of protective agents to rope (e.g. by spraying), penetrating the outer layers of the structure which, in use, are more accessible to UV radiation, water,

oxygen, and contaminants.

(5) The application of coatings designed to provide barriers to the degradative environments may be effective, providing that the coatings can afford the desired protection without impairing the frictional and performance properties of the rope. The reported use of polyurethane coatings (McKenna, 1980) to improve the abrasion resistance of rope suggests that the processing technology is feasible. The development of viable and effective coating compositions and processes is a valid objective.

Great improvements in the performance and durability of synthetic fiber rope have been realized through research on rope materials (fibers) and design (size and construction) (W. Paul et al., 1980). It is suggested that additional strides may be made by new systematic studies of chemical degradation processes, and of chemical approaches to the protection of ropes in use.

REFERENCES

B.G. Achhammer, F.W. Reinhart, G.M. Kline, J. Res. Natnl. Bureau of Standards 46(5), 391-421 (1951), and J. Appl. Chem. (London) 1, 301-320 (1951), Mechanism of Degradation of Polyamides.

N.S. Allen and J.F. McKellar, J. Pol. Sci.-Macromolecular Reviews 13, 241-281 (1978), The Photochemistry of Commercial Polyamides.

J.P. Bell, J. Appl. Pol. Sci. 12, 627-738 (1968), Relation between Nylon Fiber Mechanical Properties and Dye Diffusion Behavior.

N. Bhattacharya and H.T. Lokhande, J. Appl. Pol. Sci. 20, 873-889 (1976), Kinetics of Hydrolysis, Acetylation and Deamination reactions on Polyamide Fibers in Heterogeneous Medium.

P. Blais, M. Day, and D.M. Wiles, J. Appl. Pol. Sci. 17, 1895-1907 (1973), Photochemical Degradation of PET. IV. Surface Changes.

P.E. Bretz, R.W. Hertzberg, J.A. Manson and A. Ramirez in "Water in Polymers" (S. Rowland, Editor), ACS Symposium Series No. 127 (1980), pp. 531-553, Effect of Moisture on Fatigue Crack Propagation in Nylon 66.

R.P. Burford, and D.R.G. Williams, Journal Mat. Sci. 14, 2872-2880 (1979), The Morphology and Mechanism of Crack Propagation in Nylons in the Presence of Inorganic Salts.

R.P. Burford and D.R.G. Williams, Journal Mat.Sci. 14, 2881-2886 (1979), The Influence of Salt Type in the Environmental Fracture of Nylon.

M. Day and D.M. Wiles, J. Appl. Pol. Sci. 16, 175-189 (1972), Photochemical Degradation of PET. I. Irradiation with the Xenon and Carbon Arc.

M. Day and D.M. Wiles, J. Appl. Pol. Sci. 16, 191-202 (1972), Photochemical Degradation of PET. II. Effect of Wavelength and Environment on the Decomposition Process.

M. Day and D.M. Wiles, J. Appl. Pol. Sci. 16, 203-215 (1972), Photochemical Degradation of PET. III. Decomposition Products and Reaction Mechanism.

P. Dunn and G.F. Sansom, J. Appl. Pol. Sci. 13, 1641-1655 (1969), The Stress Cracking of Polyamides by Metal Sales. I. Metal Halides.

P. Dunn and G.F. Sansom, J. Appl. Pol. Sci. 13, 1657-1672 (1969), The Stress Cracking of Polyamides by Metal Salts. II. Mechanism of Cracking.

P. Dunn and G.F. Sansom, J. Appl. Pol. Sci. 13, 1673-1688 (1969), The Stress Cracking of Polyamides by Metal Salts. III. Metal Thiocyanates.

P. Dunn and G.F. Sansom, J. Appl. Pol. Sci. 14, 1800-1806 (1970), The Stress Cracking of Polyamides by Metal Salts. IV. Metal Nitrates.

G.S. Egerton, Faserforschung und Textiltechnik 22(2), 86-94 (1971), Photosensitized Oxidation of Polyamide Fibers.

F. Figucia and R.D. Wells, U.S. Army Natick Laboratories, Technical Report 68-45-CM, Series TS-156 (March 1968), Strength Losses in Nylon Parachute Materials with Time, Exposure and Uses.

R.E. Fornes, R.D. Gilbert, B.S. Stowe, G.P. Cheek, Tex. Res. J. 43, 714-715 (1973), Photodegradation of Nylon 66 Exposed to Near-UV Radiation.

J.F. Fuzek in "Water in Polymers" (S. Rowland, Editor), ACS Symposium, Series No. 127 (1980), pp. 515-530, Glass Transition Temperature of Wet Fibers.

Hawkins and Tipson Ltd: Polyester and Nylon Rope, "Background Document" on ICI/UV exposure trials, unpublished results (personal communication) (received in 1981).

J.W.S. Hearle and B.S. Wong, J. Tex. Inst. 68, 127-132 (1977), The Effects of Air, Water, Hydrochloric Acid and Other Environments on the Fatigue of Nylon 6.6 Fibers.

J.W.S. Hearle and B. Lomas, J. Appl. Pol. Sci. 21, 1103-1128 (1977), The Fracture of Nylon 66 Yarns Which Have Been Exposed to Light.

H.M. Heuvel and K.C.J.B. Lind, J. Pol. Sci. Part A-2-8, 401-410 (1970), ESR Study of the Initial Reaction of the Photodegradation of Nylon 6.

K. Inoue and S. Hoshino, J. Pol. Sci., Polymer Physics ed. 14, 1513-1526 (1976), Swelling of Nylon 6 Film due to Water Sorption.

K. Inoue and S. Hoshino, J. Pol. Sci.--Polymer Physics ed. 15, 1363-1378 (1977), Effect of Molecular Orientation on the Swelling of Nylon 6 (film).

E. Ito and Y. Kobayashi, J. Appl. Pol. Sci. 25, 2145-2157 (1980), Effects of Absorbed Water on Physical Properties of Polyesters.

H.H.G. Jellinek and A.K. Chandhuri, J. Pol. Sci. Part A-1 10, 1773-1788 (1972), Inhibited Degradation of Nylon 66 in Presence of Nitrogen Dioxide, Ozone, Air, and Near-UV Radiation.

S. Kaufmann, Faserforschung und Textiltechnik 22(3), 120-129 (1971), Physical Problems in the Effect of UV and Visible Radiation on Synthetic Fibers.

G. Kunzman, Faserforsch u. Textiltech. 12(2), 61-66 (1961), Time Dependent Length Changes of Moistened Polyamide Fibers.

A.P. Lisitsyn, V.Y. Efremov, T.N. Kashina, N.V. Mikhailov, Fiber Chemistry 3, 343-347 (1971), Effect of Hot Water Treatment on Thermo-Oxidative Degradation of Polycaproamide Fibers, and 3, 593-597 (1971), Morphological Structure of Polycaproamide Fiber Thermo-Oxidative Degradation (translated from Khimicheskie Volokna No. 4 and No. 6 [1971]).

L.M. Lock and G.C. Frank. Tex. Res. J. 43, 502-512 (1973), A Study of Some Factors Affecting the Photodegradation of Textile Yarns. Part II. Nylon 6.6 and PET Yarns.

L.E. Maley, J. Polymer Sci. Part C, No. 8, 253-268 (1965), Application of Gel Permeation Chromatography to High and Low Molecular Weight Polymers.

F.B. Marcotte, D. Campbell, J.A. Cleaveland, D.T. Turner, J. Pol. Sci. Part A-1-5, 481-501 (1967), Photolysis of Polyethylene Terephthalate.

E. Mikolajewski, J.E. Swallow, M.W. Webb, J. Appl. Pol. Sci. 8, 2067-2093 (1964), Wet Oxidation of Undrawn Nylon 66 and Model Amides.

R.F. Moore, Polymer 4, 493-513 (1963), The Photochemical Degradation of Polyamides and Related Model N-Alkylamides.

M.I. Morton, Tex. Res. J. 43, 385-393 (1973), Below-break Tensile Behavior of Irradiated Nylon.

W.E. Morton and J.W.S. Hearle, Physical Properties of Textile Fibers, Second Edition, The Textile Institute and Butterworth Co., Manchester, Great Britain, 1975.

H.A. McKenna, A.I. ch. E. Symposium Series 76, No. 194, pp. 127-132 (1980), Polyurethane Coated Fiber Ropes for Mooring Systems.

J.B. Park, K.L. Devries, W.O. Statton, J. Macromol. Sci.--Phys. B15(2), 205-227 (1978), Chain Rupture During Tensile Deformation of Nylon 6 Fibers.

W. Paul, S.S. Weidenbaum, K.R. Bitting, P.F. Hartman, A. I. ch. E. Symposium Series 76 , No. 194, pp. 98-106 (1980), Systems Design and Testing of Ropes for Ocean Engineering Applications.

R.H. Petus and R.H. Still in Applied Fiber Science, Vol. 2, F. Happey, Editor, Academic Press (1979), Chapter 10, Some Aspects of the Degradation Behavior of Polymers Used in Textile Applications, pp. 376-390 (Polyamides), pp. 355-376 (Polyester).

J.M.R. Quistwater and B.A. Dunell, J. Pol. Sci. 28, 309-318 (1958) and J. Appl. Pol. Sci. 1(3), 267-271 (1959), Dynamic Mechanical Properties of Nylon 66 and the Plasticizing Effect of Water Vapor on Nylon.

B. Ranby, J.F. Rabek, Photo-Oxidation, Photodegradation and Photostabilization of Polymers, Wiley-Interscience, New York (1975).

A.C. Reimschuessel and Y.J. Kim, Journal Mat. Sci. 13, 243-252 (1978), Stress Cracking of Nylon Induced by Zinc Chloride Solutions.

S. Rowland, Editor, ACS Symposium Series No. 127 (1980), "Water in Polymers".

C.D. Shah and R. Srinivasan, J. Tex. Inst. 66, 249-254 (1975), A Study of Light Damage to Undyed Textile Yarns Under a Fading Lamp at Fixed Humidity.

C.D. Shah and R. Srinivasan, J. Tex. Inst. 69, 151-156 (1978), The Effect of Humidity on the Phototendering of Undyed Fibers.

R. Shishoo, Tex. Res. J. 47, 5-9 (1977), Longitudinal Swelling in Water of Heat Treated Nylon 66 Yarns and Fabrics.

R.W. Singleton, R.K. Kunkel and S. Sprague, Tex. Res. J. 35, 228-237 (1965), Factors Influencing the Evaluation of Actinic Degradation of Fibers.

R.W. Singleton and P.A.C. Cook, Tex. Res. J. 39, 45-49 (1969), Factors Influencing the Evaluation of Actinic Degradation of Fibers. Part II. Refinement of Techniques for Measuring Degradation in Weathering.

E.G. Smith, Polymer 17, 761-767 (1976), Pulsed NMR Studies of Molecular Motion in Wet Nylon 6.6 Fibers.

H.W. Starkweather in "Water in Polymers" (S. Rowland, Editor), ACS Symposium Series No. 127 (1980), pp. 433-440, Water in Nylon.

C. V. Stephenson and W.S. Wilcox, J. Pol. Sci. Part A 1, 2741-2752 (1963), Ultraviolet Irradiation of Plastics, IV. Further Studies of Environmental Effects on Films and Fibers.

T.M. Stoeckel, J. Blasius, B. Crist, J. Pol. Sci.--Polymer Physics 16, 485-500 (1978), Chain Rupture and Tensile Deformation of Polymers.

B.S. Stowe and V.S. Salvin - R.E. Fornes and R.D. Gilbert, Tex. Res. J. 43, 704-715 (1973), The Effect of Near-UV Radiation on the Morphology of Nylon 6.6.

B.S. Stowe, R.E. Fornes, R.D. Gilbert, Polymer-Plast. Technol. Eng. 3(2), 159-197 (1974), UV Degradation of Nylon 6.6.

R.V.R. Subramanian and T.V. Talele, Tex. Res. J. 42, 207-214 (1972), Photodegradation of Nylon 6.

G.E. Sweet and J.P. Bell, Tex. Res. J. 46, 447-452 (1976), Relations Between Dye Diffusion and Fiber Structure in Nylon 6.

G.E. Sweet and J.P. Bell, J. Pol. Sci.-Polymer Physics 16, 2057-2077 (1978), Chemical Degradative Stress Cracking of PET Fibers.

Y. Takagi and H. Hattori, J. Appl. Pol. Sci. 9, 2177-2187 (1965), Studies on the Drawing of Polyamide Fibers. IV. Effect of Drawing on the Degree of Longitudinal Swelling.

A.S. Tweedie, M.T. Mitton and P.Z. Sturgeon, Textile Chemist and Colorist 1, 22-35 (1971), How Reliable are Artificial Light Sources for Predicting Degradation of Textiles by Daylight?

R.N. Vachon, L. Rebenfeld, H.S. Taylor, Tex. Res. J. 35, 473-474 (1965), and 38, 716-728 (1968), Oxidative Degradation of Nylon 66 Filaments.

V.G. Valk, G. Heidemann, S. Dugal, H. Krüssmann, Angew. Makromolekulare Chemie 10, 135-142 (No. 144) (1970), Reactivity of N-vicinal Methylene Group in Polyamides.

E.I. Valko and C.K. Chiklis, J. Appl. Pol. Sci. 9, 2855-2877 (1965), Effect of Thermal Exposure on the Physico-Chemical Properties of Polyamides.

D.S. Varma and S.S. Cameotra, Tex. Res. J. 43, 745-747 (1973), Effect of Draw Ratio on Moisture Sorption, Dyeability and Mechanical Properties of Cold Drawn Nylon 6 Filament.

M.J. Wall and G.C. Frank, Tex. Res. J. 41, 32-38 (1971), A Study of the Spectral Distribution of Sun-sky and Xenon-arc Radiation in Relation to Degradation of Some Textile Yarns.

S. Yano and M. Murayama, J. Appl. Pol. Sci. 25, 433-447 (1980), Effect of Photodegradation on Dynamic Mechanical Properties of Nylon 6.

W.W. Yau, J.J. Kirkland, D.D. Bly, Modern Size-Exclusion Liquid Chromatography, J. Wiley, 1979, pp. 390-394.

S.H. Zeronian, K.W. Alger, S.T. Omaye, Tex. Res. J. 41, 184-185 (1971) and 43, 228-237 (1973), Effect of Sulfur Dioxide on the

Chemical and Physical Properties of Nylon 6.6.

S.H.Zeronian in Surface Characteristics of Fibers and Textiles. Part I. M.J.Schick, Editor, M. Dekker, 1975, Chapter 9, 365-386, Effect of Photochemical and Environmental Degradation on the Surface Properties of Textile Fibers.

LIST OF FIGURES

2.1 Spectral Distribution at the Earth's Surface and the Carbon-arc.

2.2 Variation of Loss of Tenacity, Extensibility and Intrinsic Viscosity with Exposure Time for Nylon 6.6 Yarns.

2.3 Relation between % RH and % Loss in Strength after 100 Hours' Exposure (light fastness tester) for Different Yarns.

2.4 Relation between % Retained Strength and Duration of Exposure (sunlight).

2.5 Decrease in Intrinsic Viscosity of Nylon 6.6 Yarns with Time of Exposure to light.

2.6 Decrease in Molecular Weight of Nylon 6.6 Yarns with Time of Exposure to Light.

2.7 Decrease in Molecular Weight with Irradiation Time for PET Film.

LIST OF TABLES

2.1 Approximate range of % strength retained in exposure trials.

2.2 Yarn variables (Lock and Frank, 1973).

2.3 Percent loss of tensile properties of nylon yarns (UV exposure).

2.4 Percent loss of tensile properties of PET yarns (UV exposure).

2.5 Experimental nylon 6.6 yarns exposed to UV light (Moore, 1963).

2.6 Chemical analyses of nylon 6.6 yarn exposed to sunlight (Moore, 1963).

2.7 Properties of nylon 6.6 fabric exposed to light for 168 hours.

2.8 Changes in number average m. wt. for PET films exposed to light.

2.9 Chemical change in PET film as a function of irradiation time.

2.10 Properties of nylon rope yarns (Mikolajewski et al., 1964).

2.11 T_g for wet, conditioned and dry fibers.

2.12 Change in length of nylon 6.6 yarns in wetting/drying.

2.13 Effect of water on median fatigue life of nylon 6.6 fibers.

2.14 % Tenacity retention of nylon 6.6 yarns after immersion in aqueous solutions.

LIST OF TABLES

2.1 Approximate Range of % Strength Retained in Exposure Trials.

2.2 Yarn Variables.

2.3 Percent Loss of Tensile Properties of Nylon Yarns (UV Exposure).

2.4 Percent Loss of Tensile Properties of PET Yarns (UV Exposure).

2.5 Experimental Nylon 6.6 Yarns Exposed to UV Light.

2.6 Chemical Analyses of Nylon 6.6 Yarn Exposed to Sunlight.

2.7 Properties of Nylon 6.6 Fabric Exposed to Light for 168 Hours.

2.8 Changes in Number Average m. wt. for PET Films Exposed to Light.

2.9 Chemical Change in PET Film as a Function of Irradiation Time.

2.10 Properties of Nylon Rope Yarns.

2.11 T_g for Wet, Conditioned and Dry Fibers.

2.12 Change in Length of Nylon 6.6 Yarns in Wetting/Drying.

2.13 Effect of Water on Median Fatigue Life of Nylon 6.6 Fibers.

2.14 Percent Tenacity Retention of Nylon 6.6 Yarns after Immersion in Aqueous Solutions.

3. PATHOLOGICAL STUDY OF WORN ROPES

INTRODUCTION

A critical examination has been conducted on worn synthetic fiber ropes selected by Navy and Coast Guard representatives. Samples studied to date include two basic rope structures: 3-strand twisted and double braided, as well as three polymer fibers: nylon 6, nylon 66 and polyester. Specimens of new ropes have also been obtained to permit identification of base levels of fiber properties and geometries. The identification of the lines received is provided in Table 3.1a and 3.1b.

These ropes have been studied as to their structural composition and geometry. Tests and analyses conducted thus far include stress-strain measurements of fibers and yarns identified as to structural location within each rope, as well as observation both by optical microscopy and by scanning electron microscopy of fibers and yarns as extracted from the rope. In addition, fractography studies have been made of selected fibers after completion of stress-strain measurements.

Gel permeation chromatography has been employed to determine relative differences in molecular weight distributions between exposed surface filaments and essentially protected filaments in the strand core. Differential scanning calorimetry has been undertaken to detect changes in fine structure which may occur between exposed vs. protected fibers. Filament shrinkage (dry vs. wet) has also been measured as an indication of fine structural changes which may have occurred during rope usage.

STRUCTURAL COMPOSITION OF USED ROPES

Each of the ropes identified in Tables 3.1a and 3.1b has been analyzed as to its structural composition. Results of these studies are provided in Tables 3.2a through 3.2d and show the number of "textile singles" yarns (as furnished by the fiber producer) and twisted together in a "rope" yarn, the number of rope yarns which constitute the basic plied yarn, and the number of said plied yarns in a single twisted strand. Local twists and approximate diameters are also furnished for each structural level. Fibers numbers and denier are included as well.

Since much of the mechanical and chemical testing discussed in the following sections differentiates among samples taken from various locations of the twisted strand, it is important to specify the distribution of plied yarns in various layers of each strand considered. These observations are reported in Table 3.3 for each of the 3-strand ropes listed in Tables 3.1 and 3.2. Specimens #3 and #5 are double braided ropes, hence do not appear in this table.

As can be seen in Tables 3.2a through 3.2d, most of the 3-strand twisted ropes have similar structural arrangements,

in particular, the (approximately) 9-inch circumference ropes. Yet, there are differences worth noting. The base yarn furnished by the fiber producer is either an 840/140 (denier/filaments) or a 1260/210 (denier/filaments) with 6 deniers per filament. The first twisting of the "textile" yarn to form the "rope" yarn incorporates from 12 to 18 textile singles yarns, and in a few cases, even as many as 24 singles. The plied yarn is always composed of 3 rope yarns, however, because of the indicated differences in rope yarn deniers, the plied yarns may differ significantly in denier. Most of the 9-inch ropes have plied yarns of about 45,000 denier, but ropes #8 and #4 have a plied yarn denier of about 90,000; rope #4 is unique in having some rope yarns at 20,000 denier, others at 30,000 to be subsequently 3-plied. And, clearly, the denier (size) of the plied yarns used in the 9-inch rope dictates the number of plied yarns used to form the final strand, about 125 in most cases, but, as expected, fewer in the case of #8 and #4. Again, rope #4 is unique, showing the use of smaller rope yarns (20,000 denier) in the core section of its strands and of larger plied yarns (≈90,000 denier) in the peripheral locations of each strand.

The double braided constructions listed in the Tables 3.2b and 3.2c (ropes #3 and #5) are approximately of the same size, yet they differ significantly in structural composition, employing different base textile yarns, different structural arrangements in the first twisting and in subsequent plying, different plied yarn structure in braid core vs. cover and different braid constructions. Since these two worn braided structures have been analyzed, other worn double braids have been received, but tests on the latter have been limited thus far.

The discussions which follow concerning fiber properties in the 3-strand twisted ropes require identification of specific locations within the rope. Tables 3.2 and 3.3 provide only partial location designations, i.e. indicating radial position of a given plied yarn within the basic rope strand. It remains to furnish additional designation of plied yarn location relative to the total rope structure, as can be seen in Fig. 3.1. Here, 6 idealized successive sections of the rope are provided, showing clockwise rotary motions of each strand about the rope axis accompanied by counterclockwise motion of the given 3-plied yarn about the given strand axis, marked with an "X". Only 6 sections are shown out of the 12 (or 13) required for a complete turn of twist of strand "X" about the rope axis, but during this interval, the designated 3-plied yarn lying on the strand surface is seen, at the outset, in the outer rope position (to be later designated as the "soft" position, then, in the succeeding sections, it moves to the rope center (or "hard" position), and, finally in 6 sections, back to the rope surface. Clearly in this idealized rope, the plied yarn radial motion relative to the rope structure takes place at a frequency twice that of the strand around the base rope.

It is recognized that actual strand sections in a real

3-strand twisted rope will not appear circular, but rather elliptical because of strand obliquity, as well as laterally compressed because of interstrand pressures. Further, the key subcomponents of each strand, namely the plied yarns, do not maintain trilobal cross sections (as shown for the plied yarn in Fig. 3.1). Rather, they assume varied shapes depending on the strand layer in which they reside. The cross sectional variations found in the plied yarns of rope #2 are shown in Fig. 3.2. Particular note should be made of the numerous acute angles appearing around the periphery of the cross sections shown, for in the actual plied yarn these regions can behave as relatively sharp ridges over which the "rope yarn" (lying in the plied yarn) must bend. More will be said of this phenomenon of lateral distortions due to local pressures.

TENSILE PROPERTIES OF FIBERS AND YARNS

An extensive study has been conducted of the distribution of fiber and yarn tensile properties in worn ropes. The purpose of the exercise was first, to provide empirical data on local rope deterioration during marine usage, and second, to furnish the basis for formulating a realistic model of ropes in service to be used in subsequent applied mechanics studies.

It is fully expected that deterioration of fibers and yarns in worn ropes will be highest at the outer surface of the rope which is subjected to maximum wear and abrasion, as well as to maximum photochemical exposure. Yarns located in central portions should, accordingly, manifest less deterioration from any of these causes. At the same time, any given yarn which, during twisting around the strand, migrates from outer to inner zones of the rope, as indicated in Fig. 3.1, can be expected to vary in the extent of local deterioration along its length.

Techniques for measurement of stress-strain behavior of fibers and yarns are well established in the textile testing art for new and relatively uniform materials. However, in dealing with worn and highly variable materials, one encounters numerous difficulties in conducting valid tests. These include undesirable stress concentrations at the clamping jaw, or at the fiber-test tab interface, which lead to artificially low tensile strength values. On the other hand, if stress concentrations are minimized by means of a frictional letdown of tensile forces along the fiber (e.g. in the case of a capstan jaw) or by a mild shear force letdown of fiber tension by means of embedment in a soft elastomeric matrix, then the resulting fiber extension within the jaw will tend to vitiate the reading of fiber extension between the jaws.

During the testing of new uniform filament specimens, the stress concentration in the clamping jaw can be eased by use of elastomeric linings and the specimen can be lengthened to the point where filament elongation within the jaw is negligible compared to that of the free specimen within the jaws. And

in the testing of heavier yarns on capstan clamping devices, the specimen length can likewise be increased so as to reduce the relative contribution of yarn elongation in the capstan. Or, it is possible to test load-elongation behavior of yarns with different gauge lengths. The data can then be cross plotted as elongation vs. gauge length at various loads to permit extrapolation to zero gauge length and the resultant extrapolated elongations provide an extensional correction factor at each load.

In the case at hand, there was a need to utilize quite short gauge lengths, of the order of 0.5 inches, to permit measurement of local filament strengths across a particular cross section of the rope. Likewise, it was necessary to employ short gauge lengths to allow for continuous sampling of a filament along an extended length, equivalent to a period of twist or of migration within the strand structure. For such tests it was found useful to prepare two test tabs (of cardboard) for each filament specimen and to lay them flat, separated at their inner edges by 0.5 inches. The filament was laid across the tabs and taped thereto along its inner portion. A drop of epoxy glue was placed at the end of the filament at the outer edge of the tab, and after setting, the tab was then gripped in the Instron jaw. This procedure was employed successfully, with 80% of test breaks occurring in the 0.5-inch span between the tabs. However, filament extension under the tape was observed, hence valid measurement of filament strain was precluded.

Short Span Tensile Tests Across Strand Section

The 0.5-inch test span was employed for various worn ropes in measurements of local filament breaking strength in the plied yarn from the surface layer of the strand, when that plied yarn, in one instance, was in outer region of the rope and in the other instance, in the inner region of the rope. Tests were also conducted on filaments from plied yarns in the first subsurface layer of the strand, at two locations outside the rope and inside the rope.

These outer and inner regions are designated as the "soft zone" and the "hard zone", respectively, due to the fact that the surface layer of the strand located in the central region of the rope is often compressed and "welded" to such an extent that the plied yarn feels hard to the touch, with low lateral compressibility and high bending rigidity. In contrast, the same plied yarn, when it twists into the outer zone of the rope, is soft and flexible.

A geometric representation of a 3-strand rope is provided in Fig. 3.3 and shows the location of the plied yarn in the surface layer of the strand in the outer (soft) region of the rope. The inclination angle between the plied yarn axis and the rope axis is minimum in this zone. The same plied yarn,

when it twists around to the center of the rope (as shown to the left in dotted lines) is designated as "hard" and is seen to possess a maximum inclination angle to the rope axis.

On the right side of Fig. 3.3, the diagram indicates removal of the top strand, exposing the upper (outer) surface of bottom strands. One portion of this exposed surface is designated as the "usually" clean inside of the rope, relatively yellow or cream colored. Adjacent to it is somewhat grayish surface, with considerable fuzz, presumably representing frictional damage. Either of these two exposed zones is termed a "hard" spot in the classification of data which follows.

In Table 3.4 there are listed the tensile strength values for filaments removed from the surface plied yarns (in both soft and hard spots), from the first sublayer plied yarns, and from core plied yarns. Each value of tensile strength cited represents the average of 10 tests on filaments taken from that location in a given cross section. The ratios of tensile strength "A" and "B" were determined for the same filament as it moved from hard to soft zones. The average of ten such ratios determined for 10 surface yarn filaments is shown in Ratio "B" in Table 3.4 and for the 10 first subsurface yarns, as Ratio "A". (It is seen that the average of such ratios does not equal the ratio of the averages.)

Clearly, the comparison of strength losses from rope to rope varying in age and in usage as shown in Table 3.1 would benefit from the availability of rope filaments of the same age, though unused. But, in the absence of such controls, it was deemed advisable to substitute the core yarns of each rope as the standard for comparisons. Thus, the tensile data of Table 3.4 were normalized relative to the core yarns and are presented in Table 3.5 and plotted in Fig. 3.4. Here, we see, as expected, a significant reduction in filament strength in the surface layers of the strand when passing through the "soft" outer rope zones. It must be noted that the filaments selected from the outermost portions of the strand were often so weakened as to preclude removal of a suitable test specimen, or they were already ruptured. It follows that the filament population tested was in effect filtered to exclude very weak or even zero strength specimens. Thus it may be expected that yarn tests, rather than fiber tests would show even greater reductions in strength in the surface plied yarns in the exposed "soft" zone than is shown in Fig. 3.4. It is further noted that the standard deviation tensile data are highest for the surface "soft" yarns.

These test data are in keeping with expectations, but the behavior of the tensile data for the strand surface yarns in the "hard" zone at the rope center was not. It is seen that some of the rope specimens show no significant differences between core fiber strengths and the strength of surface yarn

fibers taken from the "hard, protected" zone, but several ropes manifest a 10% to 30% strength loss in the outer plied yarn layer in the central hard zone. This strength loss is attributed to internal abrasion during cyclic tensioning and rope bending and the presence of such abrasion is verified in discussions on microscopy studies to follow.

Short Span Tensile Tests Along Strand Length

Another series of short span (0.5-inch) tests was conducted on three of the ropes studied in this program. In this phase, successive 2-inch lengths were selected from five single filaments in a given plied yarn and were tensioned as indicated above, with a 0.5-inch span. The breaking strength values at each lengthwise location were then averaged and plotted as shown in Figs. 3.5, 3.6 and 3.7 for rope specimens #2, #4 and #9. The former two ropes are approximately 9 inches in diameter, while #9 is about 6 inches.

The data of these figures show a consistent reduction in filament strength from the core position to the layers of the outer strand. In rope #2 the strength of the surface fibers tested lies a full 20 gf below the core fiber strength, while the fibers from the first sublayer fall about 5 gf below the core fibers. (The numerous damage areas in the surface yarns made the successive location testing of their fibers impractical and so the figures contain the surface fiber averages without reference to location along the yarn.) In rope #4, the surface yarn fibers manifest approximately a 50% drop in strength from the core fiber values, while the first and second sublayer fibers show a loss of 5 to 10 (gf), depending on location.

The extent of variation of strength along the core fibers was unexpected, although it may be accounted for through occasional radial migration. The persistent rise and fall of strength of the first and second sublayers of rope #4, cycling every 4 inches, corresponds to the 4-inch period during which each plied yarn twists from the protected side of the strand to its exposed side. And, obviously, there is a region of heavier damage observed in the first sublayer between the 8- and 12-inch location.

The data for rope #2 (Fig. 3.5) shows an unusually parallel strength variation for the core and the first sublayer fibers, but there is no explanation for this observation. Finally, the data for rope #9 suggest that periodic damage was incurred in the first sublayer, but did not penetrate to the second sublayer which evidenced a very uniform fiber strength.

Long Span Tensile Tests

The possible contribution of local damage to periodic weakening of the fibers in the surface layer and in successive layers below the surface was the subject of another phase of the pathological study. In this case, the test span of

individual filaments was increased to 8 inches, corresponding to the period of rotation of the strand in the rope, measured along the strand axis. This also corresponded to the 8-inch period for rotation of a surface plied yarn around the strand, measured along the plied yarn axis. In this study phase tensile strength was again measured for each filament, but, in addition, note was taken of the location of the filament break within the span. A few test spans were taken at 12 inches.

The data for such tests conducted on all ten of the worn ropes available are reported in Figs. 3.8 to 3.17. In these figures each point plotted is for a single break at a single location--in that averaging of lengthwise locations would be meaningless. However, strength averages are calculated for each plied yarn layer tested and these averages are plotted in Fig. 3.18. It is noted that the averages plotted in Fig. 3.18 are generally lower than those plotted in Figs. 3.4 through 3.7, and listed in Table 3.4. This reflects the effect of the 8 to 12-inch gauge length of Fig. 3.18 based on the tensile data of Figs. 3.8 through 3.17 vs. the 0.5-inch span reported on in Figs. 3.4 through 3.17.

The data of Figs. 3.8 through 3.17 are of particular interest. In general, the core fibers of the 3-strand ropes manifest fairly constant values of tensile strength and fiber rupture locations are spread uniformly along the 8 to 12-inch span. Tensile values tend to drop somewhat in layers closer to the surface and rupture locations are no longer uniformly spread along the 8 to 12-inch span. At the surface, and in some cases at the first subsurface layer, the average tensile value decreases, the spread of breaking strengths increases markedly and the location markings congregate, indicating either highly concentrated damage (as in rope #1E in Fig. 3.8, or rope #4 in Fig. 3.11, or #7 in Fig. 3.14) or periodic damage (as in rope #2, Fig. 3.9, or rope #9, Fig. 3.16).

The use of the bar chart format provides another view of the distribution of weak spot locations in the 8 to 12-inch filament test span. An illustration of this format is given in Fig. 3.19 which shows the percentage of breaks occurring at various locations along a test span. Figure 3.19a contains the graphing of the core filament data, 3.19b the first subsurface data, and 3.19c the surface filament results. The periodic grouping is negligible in the core, modest in the sublayer and striking in the surface layer.

Test data for the short span tensile strengths did not include specimens from the two double braided lines of the worn rope series. However, the long span tests did include rope #3 (nylon) and rope #5 (PET) whose background and construction are cited in Tables 3.1a, 3.2b and 3.2c. The tensile strengths of filaments selected from inner and outer yarns of the braided cores and the braided covers for ropes #3 and #5 are plotted in Figs. 3.10 and 3.12, respectively.

Rupture locations are also indicated.

It is seen that filaments taken from the inside of the core plied yarns in both ropes have higher strengths than those from the outside of the core plied yarns and display a more uniform spread of rupture locations (Fig. 3.12a and b). The distinct rupture location groupings for the outside filaments of the core for ropes #3 and #5 (Figs.3.10b and 3.12b) reflect the likelihood of internal abrasion between the core outer surface and the cover inner surface.

Similarly, the outside filaments of the plied yarns used in the covers of ropes #3 and #5 show reduced strength vs. the inside filaments. The outside filaments likewise show pronounced groupings of the rupture locations. These periodic rupture groupings reflect the presence of local damage, but it is not possible from these data to separate that which occurs from cover to core abrasion vs. that from abrasion of cover to external objects and surfaces. The unexpectedly higher level of filament strength in the cover of rope #5 vs. its core is attributable to its higher cover filament denier (8 dpf in cover vs. 6 dpf in core, as seen in Table 3.2c).

A summary table of long span tensile tests for all ten worn ropes is provided in Table 3.6. These strength values represent the averages of about 30 filaments for each location as plotted in Figs. 3.8-3.17. It should be noted that filaments selected from plied yarns located at the core of the 3-strand ropes in general manifest tensile strengths ranging from 50 gf to 55 gf. The filament strength averages fall as their location is closer to the rope surface, with some loss of strength observable in the first sublayer (or plied yarns) in the strand. Significant strength loss is noted in all surface filaments accompanied by an increase in filament variability, as expected.

Rope #8 which was manufactured in 1979, shows a higher filament strength in the core (62.4 gf) than the other 3-strand ropes despite the fact that its filament denier is 6 dpf, as in all other 3-strand ropes except for rope #10. The latter shows a core filament average strength of 102 gf (the highest observed in all long span filament tests), but this can be attributed to its 13 dpf (see Table 3.2a) and its late date of manufacture (1979).

It is also worth noting that rope #8 showed the least loss in strength of its surface fibers of all 3-strand ropes, no doubt due to its younger age and to less service--with designation of "good" general condition. Ropes #9 and #10, the only 6-inch ropes in the group, manifested maximum strength drop in their surface filaments vs. core filaments--in the order of 60% loss. Rope #10 was designated as being in fair condition. The only other rope so designated in "fair" condition was #4, a 9-inch rope which lost 55% filament

strength in its surface vs. core locations. The remainder of the 9-inch ropes appeared to lose less surface filament strength than #4, although the differences are not always statistically significant.

The values posted for the double braided ropes are as expected, although it should be remembered that the cover yarn filaments in rope #5 are 8 dpf vs. 6 dpf in the core. This is reflected in the average strength values. Finally, it is worth considering the fact that the surface filaments exposed on the outside of the braided ropes, in general, evidence higher strength than those on the outside of the 3-strand ropes, the highest strength of all outside filaments occurring in double braided rope #5. The limited number of double braided ropes studied precludes generalization of these observations.

A final experiment corresponding to the 8-inch span filament tests was undertaken on one rope, #2, as follows. The specimen was first tested under standard conditions, as before, but upon completion of each break, a second test was conducted on the larger of the two broken filament segments. This procedure was undertaken for surface layer filaments and for core filaments of rope #2. Results of these tests are shown in Fig. 3.20 where the value of the second break is plotted against that of the first break, with the dotted line showing the case of equal second vs. first breaks.

The clustering near the dotted line of the data points for the core filaments indicates their second values to be close to the first values. The much higher second values for the surface filaments shown indicates that their first break was indeed the weakest point, by a significant magnitude. These results are consistent with those reported in Figs. 3.5, 3.9 and 3.19, but give added insight into the distribution of wear damage in the fibers of worn ropes.

Summary of Tensile Results

The purpose of these studies of the tensile properties of fibers and yarns taken from worn ropes has been to provide empirical data on local rope deterioration during marine usage and to furnish the basis for formulating a realistic model of ropes in service to be used in subsequent applied mechanics studies. Both short span (0.5-in) and long span (8-in to 12-in) tensile tests were conducted.

The short span tests were used to probe the extent and distribution of tensile loss over the cross section of the rope at a given location along its length. Short span tests were again employed to determine the distribution of residual filament strength along the lengths of selected yarns in a full twist period in the rope structure. Such tests were conducted at various locations over the rope cross section. Long span tests were then carried out to identify the distribution and severity

of weak spots along 8-in to 12-in yarn lengths extracted from inner and outer sections of the rope. And in one case, repeat tests were made on already tested filament lengths to identify a second weak spot.

The data indicate that core fibers of the 3-strand ropes manifest fairly constant values of tensile strength along their length and fiber rupture locations were spread uniformly along the 8-in to 12-in lengths. Tensile rupture locations in layers closer to the strand surface are no longer uniformly spread along the filament lengths. At the surface, and in some cases at the first sublayer of the strand, the average tensile value decreases significantly, the spread of breaking strength increases markedly and the failure locations tend to congregate. Such groupings can reflect either highly concentrated damage due to local external wear, or periodic damage indicating more uniform external deterioration condition interacting with the periodic geometric availability of the yarns at the rope surface.

In double braided ropes, filaments taken from the inside of plied yarns of the rope core manifest higher strengths than those from the surface layers of the same yarns. The inner zone fibers also display a more uniform spread of rupture locations. Distinct rupture location groupings for the outer zone filaments of the rope core yarns reflect the likelihood of internal rope abrasion between outer surface fibers of the core and the inner surface of the cover braid.

Evidence of the role of internal rope abrasion is also seen in the data from short span tests taken over the cross section of some 3-strand ropes. In particular, filaments extracted from the closely packed "hard" spots in the surface and subsurface strand layers (at rope center locations) show strength reductions, which in some cases, are significant. Microscopic examination confirms that internal abrasion is a contribution to these reductions.

The goal of these first year mechanical pathological studies has been reached to a reasonable extent and sufficient data are now at hand to enhance further studies of rope mechanics. It is expected that some limited studies of filament damage distribution will be continued, particularly in the case of rope samples for which more precise wear and exposure histories are available.

MOLECULAR WEIGHT STUDIES OF FIBERS FROM WORN ROPES

Reduction in mechanical strength of rope fibers can occur as a result of numerous factors, by mechanical attrition (through cyclic loads, external and internal abrasion, bending fatigue, friction, excessive tensions, crushing, and even fish bites) or by chemical attack due to immersion in clean or contaminated sea water, to gassous contaminants in air (e.g. SO_2), to heat and to oxygen (air) either singly or in combination with other variables, or by photochemical degradation (due to ultraviolet radiation). To provide a suitable background for studies of chemical degradation leading to reductions in mechanical properties of synthetic fibers, a thorough study was undertaken of the literature on environmental degradation of nylon and polyester. A critical evaluation of this literature undertaken in the context of Ocean Engineering applications of rope has been presented in the previous section of this report.

In considering the assessment of chemical degradation in fibers, an attempt was made to identify certain chemical methods which have been employed effectively in investigations on the two principal fibers of this rope study--for the purpose "of establishing correlations between the extent of chemical degradation encountered under specific conditions of exposure and observed effects on polymer properties". These chemical methods, in concert with scanning electron microscopy and with evaluation of changes in mechanical properties, have "provided considerable insight into the effects of environmental variables on molecular structural changes in fibers, and into the dominant mechanisms of chemical degradation for polyamides and polyesters".

The major methods of interest in the context of an applied research study of this nature are stated to include: (1) determination of changes in molecular weight averages and in the concentration of specific functional groups as indicative of degradation on a molecular level and (2) measurements of moisture regain, swelling and dye diffusion as criteria for assessment of structural change.

The effort directed toward determination of chemical degradation in the ten worn ropes listed in Table 3.1 was limited. Some initial tests to ascertain the extent of bond scission occurring in fibers taken from surface and core yarns of two ropes, #2 and #4, were undertaken. The initial method chosen was via viscosity measurements using concentrated sulphuric acid as solvent for the nylon. Preliminary data showed slight, but insignificantly higher molecular weight for the core fibers vs. surface fibers.

It was then decided to use Gel Permeation Chromotography (GPC) for determination of molecular weight changes, a method capable of providing precise and reproducible number-average ($\overline{M}_n$) and weight-average ($\overline{M}_w$) molecular weight values, as well

as a measure of polydispersity index relating to the broadness of the molecular weight distribution. Samples of unused rope of comparable age and similar filaments were not available for use as controls in these tests. Accordingly, it was decided to use the GPC values for the core fibers of the strand as a control "stand-in". And fiber specimens were then selected from various locations in the worn ropes for the GPC evaluation of molecular weight parameters.

The purpose of these measurements was to establish whether there is prima facie evidence of chemical degradation (chain scission) for fibers in regions of apparent maximum wear, in which visual and microscopic observation and testing of mechanical properties suggest that extensive degradation may have occured in use. Ropes from which samples were taken are listed in Table 3.1a and 3.1b, but excluded the two double braided ropes #3 and #5, and the 3-strand rope, #6.

The sampling scheme for the GPC measurements is shown schematically in Fig. 3.21, augmented by Fig. 3.3. Fiber specimens were taken from three locations in the exposed zone of the rope: from the outer fibers of the strand surface yarn, from the under fibers of the surface yarn, and from the first sublayer yarn. Specimens were also taken from three locations in the protected zone of the rope: from the strand core, from the first sublayer yarn at the rope inside, and from the strand surface yarn at the rope center (also called the hard zones).

The GPC measurements were undertaken in two groups with HFIP as the common solvent, but different standards were used for comparison in the two groups. In the case of ropes #1, #2, and #4, the standard was polystyrene; for the remainder of the measurements, a nylon 66 standard was employed. In the case of ropes #7 and #8, specimens were taken at locations as indicated in Fig. 3.21, but at two positions along the rope. In the case of all other ropes, specimens were selected over the rope cross section at a single position. In addition to these tests on worn ropes, samples were taken from two new ropes, a 6-inch and a 1/4-inch, 3-strand ropes of nylon 66. GPC was measured in the as-received condition, and in the case of the 1/4-inch rope, after 400 hours' exposure in a carbon-arc weatherometer.

The results for number average molecular weight of all worn specimens are shown in Table 3.7, for weight averages molecular weights in Table 3.8, and for polydispersity in Table 3.9. It is immediately evident that the molecular weight values for the measurements based on the polystyrene standard differ from those based on the nylon 66 standard. To permit ready comparison between molecular weight measurements for filaments in the exposed zones vs. the protected zones, the number average results have been normalized relative to the filaments in the strand core, much as was done for the mechanical property comparisons in Table 3.5 and Fig. 3.4. These "core" normalized molecular weight data are listed in Table 3.10 and are plotted in Fig. 3.22.

For some samples, the maximum differences in number average molecular weight between outer surface fibers and core or inner surface fibers are seen to exceed the reported margin of error for GPC analysis (±5%), while for others, the differences are within the 5% margin. In particular, it is noted in Table 3.10 that in all six of the older rope samples, (manufactured in 1972, or before) the molecular weight ($\bar{M}_n$) of the exposed surface fibers is more than 5% below that of the core fibers and for five of these six, the differences range from 10% to 17%. On the other hand, the difference of $\bar{M}_n$ between exposed surface and core fibers for the newer (worn) ropes (#8, 1978, and #10, 1979) is of the order of 3% to 6%, sometimes in reverse of expectation.

Reference to Table 3.7 indicates that the reproducibility of the $\bar{M}_n$ values in the most protected region of different ropes, is well within the experimental error for GPC measurements, the range being of the order of ±2.5% of the mean for the strand core fibers of each comparison-standard set. In addition, it was noted that the two samples taken from the new 3-strand nylon 66 rope had an average $\bar{M}_n$ of 48.3×10^3 while the 400-hour weatherometer exposed samples averaged 45.3×10^3, both falling within the error range of 45.7×10^3, the average $\bar{M}_n$ value for core fibers of the pre-1973 worn ropes.

Finally, it is seen in Table 3.9 that while the differences in polydispersity between the outside exposed fibers and the inside protected fibers are of doubtful significance when individually considered, there is a pattern of maximum polydispersity in the outside exposed fibers for all six specimens from ropes #7 to #10 inclusive (using the nylon 66 standard). Ropes #1, #2 and #4 for which the GPC standard was polystyrene displaced negligible differences in polydispersity between outermost filaments and core filaments.

It should be noted that the decrease in molecular weight for fibers near the rope surface is less than that reported in many laboratory studies of environmental degradation on polymers and fibers of comparable structure. This raises the question as to whether these results can be used as a basis for stating that chain scission was a key factor in degradation of the ropes examined. Such uncertainty is to an extent reinforced when one views the highly diffuse graphical correlation of "core" normalized data for $\bar{M}_n$ vs. core normalized data for filament breaking strength, as presented in Fig. 3.23.

Many reasons can be suggested for this weak correlation between molecular chain scission vs. tensile strength in filaments taken from selected locations across the worn ropes:

- If molecular weight decrease is taken as a criterion of chemical degradation in nylon filaments, the available evidence indicates that chemical change is probably not the

dominant factor over the entire cross section of the used ropes examined. Thus, a large portion of the data in Fig. 3.23 merely reflects sampling and test method variability.

- Despite the considerable age of the worn ropes studied, it is possible that the extent of weather exposure of the specimens analyzed was limited and the significant UV deterioration observed in other studies was simply lacking in the specimens at hand.

- The sampling techniques of extracting fibers from the surface layer of the worn ropes may inadvertently have included numbers of protected, undegraded filaments along with exposed, degraded filaments. Thus, the surface layer results might have represented an averaging of degraded and relatively undegraded specimens and, accordingly, the outer surface vs. core $\bar{M}_n$ differences may have been suppressed.

- Chain scission which is in evidence for certain samples is likely concentrated in the stress bearing molecular chains in the amorphous regions of their fiber structure, hence could have significant effect on residual fiber tenacity without a corresponding effect on number average molecular weights.

- Such selective chain scission would be expected to have a more significant influence on filament energy to rupture, or on subsequent abrasion resistance than on simple ultimate strength. If this is the case, then filaments subjected simultaneously or sequentially to UV degradation (or other forms of chemical degradation), plus abrasion and/or cyclic tensioning, would be expected to undergo far greater losses in mechanical properties than in the case of UV exposure by itself, or abrasion by itself.

In light of the scatter evidenced in the normalized $\bar{M}_n$ data (Figs. 3.22 and 3.23), statements concerning the role of chain scission in deterioration of marine ropes must be formulated with specific limitations. Further work on this subject is clearly necessary. Nonetheless, certain conclusions can be drawn on the basis of the evidence collected to date:

- Use of strand-core fiber $\bar{M}_n$ data as a basis for normalized comparisons of changes in number average molecular weights is a valid procedure. This follows from the observation that differences in $\bar{M}_n$ values for strand core fibers of

ropes varying in age from 3 to 16 years are well within the range of experimental error about their mean. Similarly, the average M_n for the one new nylon 66 rope tested is not significantly greater than the mean $\overline{M}_n$ of the core fibers of the older, worn ropes.

- Fibers taken from the outermost surface of worn ropes, 10 years or older, manifested significant reductions in number average molecular weights as compared to strand core fibers from corresponding ropes.

- Fibers taken from the outermost surface of worn ropes 3 and 4 years old did not evidence significant reductions in $\overline{M}_n$ as compared to strand core fibers from corresponding ropes.

- Consistently significant reductions in $\overline{M}_n$ are not observed in fibers taken from the underpart of the exposed surface yarns and from the first subsurface layers.

- On the basis of published results for the correlation between effect of UV exposure on $\overline{M}_n$ and on tensile strength, it is concluded that chain scission is an important component in the deterioration of outermost fibers in the marine ropes. (It has been suggested that the per cent loss in $\overline{M}_n$ due to UV exposure may be multiplied 2.5 times to provide an estimate of the corresponding loss in tensile strength.)

- The fact that measured losses in tensile strength exceed the losses thus estimated in 5 out of 6 of the "old" ropes, would suggest that chemical scission is not the sole factor in deterioration of the outermost fibers. Mechanical action must contribute the remaining damage, as is evidenced in Scanning Electron Microscopy studies.

- The absence of control specimens and the lack of detailed information on actual exposure (UV, immersion and mechanical) of each rope precludes the generalization of conclusions in a form more useful for marine applications. Further chemical tests are warranted based on other techniques as cited in the literature survey of Section 2.

DIFFERENTIAL SCANNING CALORIMETRIC MEASUREMENTS (DSC)

Differential scanning calorimetric (DSC) measurements were carried out on core fibers of all the ten worn ropes. The purpose of these tests was to determine the melting behavior of the

crystalline regions of the filaments of various ages. In addition, a new 1/4-inch nylon 66 rope was so tested.

The DSC measurements were performed on a Perkin-Elmer DSC-2 unit, using a small amount of rope filaments in a crimped aluminum pan. The calorimetric sensitivity of the DSC scan was 5 and 10 mcal/sec-inch and a heating rate of 20°C/min was chosen in order to obtain a well defined melting point. DSC measurements were run twice for each rope and all 22 original DSC thermograms are presented in Fig. 3.24.

The thermograms clearly show that the melting occurs over a broad temperature range. It is well known that the melting of fiber filaments is not as simple a process as the melting of perfect polymer crystals and the exact melting point of each crystalline region depends both on its size and on its degree of perfection. Accordingly, the values of melting temperature in these particular measurements were taken to be the point of melting of the highest melting crystallites, i.e. the point of disappearance of the last traces of crystallinity.

The melting temperatures determined in this manner are listed in Table 3.11. Here it is noted that rope #4 shows a melting temperature from 215°C-225°C, the range for melting of nylon 6 crystals. The PET sample of rope #5 exhibits a slightly higher temperature (262°C) than the remaining worn ropes, which range from 255°C-260°C, corresponding to the melting temperature of nylon 66. The new 1/4-inch nylon rope #11 is seen to melt at 265°C-267°C, possibly reflecting the effect of its different heat treatment.

It is noted that samples from ropes #2, #4, #7, #8 and #11 exhibit double melting endotherms in the DSC thermograms, these are no doubt caused by crystallites of different sizes and/or degrees of perfection and depend to some extent upon the thermal history of the rope specimens.

In conclusion, it is noted that the DSC data confirms the presence of one nylon 6 specimen among the worn ropes and one PET, the remainder being nylon 66. Additional information furnished reflects on differences in crystal structure, a subject which may be studied further in the coming year.

EFFECT OF WATER IMMERSION OF FIBER PROPERTIES

While molecular weight studies have not shown a significant difference to exist between $\bar{M}_n$ of new rope fibers and strand core fibers of worn ropes, a question remains as to the extent established that mechanical properties of a given fiber (i.e. with a fixed $\bar{M}_n$) can be altered by variations in original spinning speeds, in draw ratio, in heat stabilization, and in both dry and wet shrinkage. The focus of this section is on the effect of water immersion on mechanical properties.

Since no data were available on the original stress-strain properties of filaments from the worn ropes, it was deemed

advisable to obtain a limited amount of base line data on the effect of water immersion on properties of new filaments presently used on rope manufacture. Accordingly, a sample of new nylon 66 yarn, of 1260 denier and 210 filaments (6 dpf), was obtained and subjected to a variety of immersion and shrinkage tests and to subsequent tensile testing. In addition, samples of polyester (16-mil diameter) and nylon 66 (20-mil diameter) monofilaments were subjected to creep tests in air and/or in water.

The results of the nylon 66 monofilament tests are shown in Table 3.12 and indicate that the nylon specimens subjected to creep tests in air up to 40 hours (at a load equal to 40% of the dry breaking strength) do not lose strength when dry tested after creep; they do, however, lose up to about 15% in elongation to break after 40 hours of creep. In wet creep tests at 20% and 40% creep loads (i.e. per cent of breaking strength), the monofilaments show subsequent strength reductions of up to 15%, but significant increases in elongation to rupture. Merely soaking the monofil in water led to such shrinkage that in subsequent tensile testing the ratio of treated elongation to rupture to the original elongation to rupture was 217%. After creep tests in water, the elongation ratios of treated to original specimens were about 150%.

To compare the behavior of nylon vs. PET monofilaments, samples were subjected to dry creep tests under loads equivalent to 40% of their UTS. No reductions in subsequent tensile test values were observed and but significant decreases were recorded in elongations to rupture as per Table 3.13.

The results of tests on new nylon 66 filaments of six immersed for 50 hours in sea water (actually from Boston Harbor) are shown in Fig. 3.25. The filaments were first suspended in a sea water bath with weights varying from 0, 0.5, 1.0, to 1.5 gf/den for 50 hours. They were then air dried and tensile tested. Changes in resulting breaking strengths and extensions are shown, indicating significant losses in both strength and elongation at the higher immersion loads.

Still another test sequence involved filaments taken from surface and from core locations of the rope #2 strand. Here, the filaments were tensile tested before and after a 20-min exposure to hot water (98°C) and the resulting data plotted in Fig. 3.26 show that strengths are reduced significantly due to the hot water immersion, and elongations to rupture are correspondingly increased. The interesting feature in Fig. 3.26 is the tendency for the breaking strength/elongation to rupture points to lie on one composite strength-strain curve for the "after hot water treatment" fibers. Further, the points for the core fibers clustered along the upper part of the composite strength-strain curve, while the points for the surface fibers lay along the lower segment of the curves. Finally, the clockwise shift of the composite strength/elongations curves, due to

the hot water treatment, is consistent with known shrinkage behavior of thermoplastic fibers.

Still another set of tests were undertaken to show the effect of commercial heat setting of rope on the mechanical properties of rope yarns. In this case, a 3-strand twisted 0.6-in. diameter nylon rope was obtained in its before and after heat setting conditions. The construction of the rope was such that each strand contained seven plied yarns (6 twisted about a seventh core plied yarn with each individual plied yarn containing 4 rope yarns). Tensile tests were carried out on 120-in gauge lengths of rope yarns extracted from both heat set and unset ropes. The results for four tests for each specimen at 2 in/min rate of extension, were averaged and plotted in Fig. 3.27, showing a significant clockwise rotation of the curve, reduction in strength, and increase in elongation to rupture. Similar tests conducted on the 4 ply yarns are reported in Fig. 3.28, showing a similar clockwise rotation of the stress-strain curve. A slight difference is seen during loading of the 4 ply yarn taken from the strand surface vs. that from the core. But the major difference occurring in the heat set plied yarns is in the sequential rupture which occurs in both surface and core yarns. In contrast, the untreated plied yarn ruptures in a single clean break. This behavioral difference reflects on the interaction between rope components which occurred during the 8% to 10% shrinkage during the steam motivated commercial setting process. Such interactions will be the subject of further study.

Shrinkage Properties of Filaments

In addition to obtaining tensile stress-strain properties so as to determine the effect of service life on filaments taken from various locations in worn ropes, it is useful to measure the dimensional stability of these same fibers. Dimensional stability of fibers subjected to heat in dry or wet conditions is affected by the degree of prior drawing or extension and on the level of subsequent heat setting; stability is also affected by prior strains or shrinkage incurred during use of the end product. Accordingly, filaments taken from the core, as well as from all layers of rope #2, were subjected to 20-minute shrinkage treatments, in one case, dry (i.e. lying tensionless in an oven at 130°C), and in the second case, wet (i.e. completely relaxed in water at 99°C). The results of these tests reported in Fig. 3.29 (with 5 or more tests per point), show considerable difference in shrinkage tests run dry vs. those run wet, the latter reflecting considerably higher levels ranging from 3% to 5.5%, the former ranging from 1% to 1.5%. While not much can be made of the variation of 1/2% in dry shrinkage between core and outside surface filaments, the boiloff shrinkage differences are worth noting, with core set shrinkage at about 5.5% and shrinkage values falling off to 3% in the surface filaments of rope 2D.

Since it is well known that small concentrations of phenol in water serve to swell nylon fibers and concommitantly to

accelerate shrinkage, wet shrinkage tests were also run at low phenol concentrations and at room temperature for filaments from ropes #2 and #4. The average of more than five tests showed shrinkages to be much higher in the core filaments and inner layers of rope #2 than for corresponding filaments from outer layers. Filaments from the inner layers of rope #4 likewise showed somewhat higher shrinkage values than those in the outer layers. But, due to differences in the fiber type of the two ropes, and in the actual phenol concentrations employed, these data cannot be compared on an absolute basis. Nonetheless, the observed differences between shrinkage of inner vs. outer fibers warrant further study.

Despite the fact that the shrinkage data furnished above are limited, they consistently show higher water boiloff and (cold) phenol shrinkages for filaments taken from core or near core positions in both ropes. This difference is one more piece of evidence of the effects of differences in mechanical history and in exposure to ambient conditions experienced by fibers in different locations of the rope.

MICROSCOPIC STUDIES

The extensive loss in mechanical properties measured in worn rope samples was accompanied by some evidence of chemical (or photochemical) damage as indicated in the GPC data. While molecular chain scission can account for some of the observed loss in filament strength, the overall weakening of the fibers at the rope surface undoubtedly had a strong mechanical component of deterioration. Optical and scanning electron microscopy was used to examine filaments drawn from various locations across the rope strand section as per Fig. 3.21. These locations were the same as had been selected for measurements of GPC and for determination of tensile properties. It was expected that photomicrographs of these specific fiber specimens would provide some insight on their observed mechanical and chemical properties.

In addition to microscopic examination of fibers extracted from the ropes, longitudinal views of the worn ropes were studied in an intact state, and with single strands removed. Also, plied yarns removed from various sections of the rope were embedded in polyester resin, microtomed and photomicrographed. In all, two to three photographic records were made of the surface (or cross sectional) appearance for each of the locations of interest in the ten ropes, thus creating a problem in presentation. Large collections of data can be averaged and statistically analyzed by accepted techniques, but the summarization of pictorial evidence must be dealt with on a more subjective basis.

It was decided to present the microscopic evidence according to the following (arbitrary) list of phenomena or mechanisms:

(1) lateral distortion of plied yarn bundles,

(2) compaction of fibers in plied yarns,

(3) creasing of fibers in distorted yarn bundles,

(4) "asperity" filament abrasion,

(5) filament-filament abrasion,

(6) filament-filament embossing and/or crushing,

(7) filament surface cracking,

(8) filament surface encrustation,

(9) filament rupture in situ,

(10) filament rupture in tensile test,

(11) surface etching of filament,

(12) filament splitting,

(13) free end disintegration.

Lateral Distortion and Compaction of Plied Yarn Bundles

In discussing the structural composition of used lines, we have presented the idealized geometry of the 3-strand rope in Fig. 3.1, adding the modifications of ellipticity due to strand obliquity and of lateral plied yarn distortion. The plied yarn profiles of Fig. 3.2 were traced from photomicrographs of embedded yarns in the early stages of the program.

As the tensile studies progressed, the appearance of periodic hard spots along the ply yarn at the rope center, suggested the need for cross sectional studies in well identified yarns both across and along the rope strand. Accordingly, plied yarns were carefully extracted from various locations of rope #4, embedded and sectioned. Longitudinal views of the same yarns were also photographed.

Figure 3.30 shows tracings of the plied yarn sections of the surface yarns of the strand from the "soft" outer zone of the rope and from the "hard" inner zone of the rope. Yarns from the first sublayer and from the second sublayer are also shown, again from soft and hard zones. Profile tracings have been used in this case, since the contrast in the photomicographs obtained was not sufficient to survive reproduction in this report.

Even though the sections of Fig. 3.30 are those of yarns removed from the compressive constraints of the 3-strand rope,

the differences in their profiles are striking. The strand surface yarn in the outer "soft" zone of the rope is relatively open with nearly round rope yarn sections. In contrast, the strand surface plied yarn in the inner "hard" zone of the rope is highly compressed and the component rope yarns are likewise compressed and distorted. Soft zone yarns in the first sublayer, then the second sublayer, are somewhat more compressed than those in the soft outer layer, but they still maintain their approximate symmetry, even though no longer round. In contrast, profiles of the plied yarn in the hard zones are drastically distorted, asymmetric and compacted, whether in the surface yarn or in the sublayers.

Filament-Filament Abrasion and Fiber Creasing

If the vertical in Fig. 3.30 is established as the radial direction, r, in the rope, then the horizontal can represent the tangential (hoop) direction, θ. Examination of the yarns profiled in Fig. 3.30 reveals the following:

- Compacted fibers in the hard zones, Fig. 3.31A and B, in contrast to loosely packed fibers in the soft zones, Fig. 3.32A and B.

- Frictional damage at sides of the plied yarn in the hard zones, particularly on the θ planes, i.e. between plied yarns in the same radial layer. (See Fig. 3.33A and B at low magnification and Fig. 3.34A and 3.34B at higher magnification.) Frictional damage is also seen between the rope yarns of a given plied yarn taken from a hard zone of the rope. It is noted that this type of filament damage extends but a few filaments deep at the θ face of the plied yarns, or between rope yarns within a given plied yarn.

- Filaments which twist around the rope yarns sketched in Fig. 3.30 must negotiate relatively sharp corners, hence may be subjected to sharp curvatures. There are no residual bends observed in fibers drawn from the "soft" zones of rope #4; residual bends or creases are observed in fibers extracted from the hard zones. Observed between crossed polarizing lenses in the microscope, these permanently bent fibers show numerous color changes representative of residual strains. Figure 3.35 provides an example of creased edges along the length of a plied yarn in a hard zone of rope #4.

Asperity Abrasion

The terminology asperity abrasion refers to active mechanical abrasion of the filaments located in the surface layer of the strand at the outermost portion of the rope. The asperity attack presumably occurs because of the roughness of surfaces

contacting the outer surface of the rope. Such contact occurs at bollards, cleats, capstans, winding drums, deck surfaces, etc., even against other portions of the same rope. The resultant filament damage often shows up as axial gouges along the fiber axis, as in Fig. 3.36A and B. Such direction attrition reflects the parallel orientation of rope surface fibers to rope axes and the most frequent direction of rope movement against guiding surfaces.

Other filaments taken from rope #7D are seen in Fig. 3.36C, D and E to be encrusted at their surfaces and subjected to severe gouging. Such gouging reveals the internal fibrillar structure of the filament and leads to subsequent cracking and/or splitting along the filament axis.

Free End Disintegration

A number of broken or free ends of surface filaments were gathered and examined under the Scanning Electron Microscope. Among these were samples such as shown in Fig. 3.37 which appeared as etched porous sponge-like structures, suggesting the presence of photochemical degradation such as reported for fibers exposed for Florida sunlight [1] or to 670 hours in light of a Xenon-arc lamp [2].

Figure 3.37A shows longitudinal views of two spongy structured fibers. Figure 3.37B shows a fiber end with spongy structure, with rounded end and with longitudinal cracks at the tip of the fiber. Figure 3.37C presents a fiber broken in rope usage and displays a major axial crack originating at the principal fracture surface. Transverse cracking is also in evidence, as well as the beginning of surface etching.

Still other examples of broken or free ends of surface filaments are shown in Fig. 3.37D, E and F for rope #8, which is fairly new (1978 date of manufacture). These free ends have suffered a variety of attacks prior to failure and after flattening, splitting, encrustation and cracking.

Finally, a few free ends from the relatively old rope #7 (1966) are shown in Fig. 3.37G and H. Here one notes the virtual disintegration of the filament tip by attrition, the extreme bending of the filament, and the local removal of pieces from the filament surface.

Surface Encrustation and Cracking

Fibers drawn from the surface layer of the strand in the exposed soft zone manifest much encrustation, some transverse cracking, and occasional lateral compression or crushing, as can be seen in Fig. 3.38A and B. These filaments from the 1972 rope #4 fail at low tensile loads with very little deformation, as evidenced by their truncated load-elongation curves and the absence of scallop-shaped crack openings. In contrast, filaments from the same strand surface in the protected, hard zone show

little evidence of encrustation or surface cracking, as seen in Fig. 3.39A and B. Their fracture surfaces contain the classical scallop-crack initiation and opening usually observed in new nylon fibers; their load-elongation curves show but slight truncation compared to that of filaments from the core of the strand. Axial gouging or filament-filament abrasion is in evidence at these hard spots, as has been discussed earlier and shown in Figs. 3.33 and 3.34.

Filaments from the layer of plied yarns just below the surface of the 1972 rope #4 display very little surface deposit when specimens are taken from the exposed soft zone, but even less when taken from the protected hard zone. See Figs. 3.40A and B and 3.41. Fracture surfaces of both sets of fibers contain the scallop-crack opening characteristic of a tensile failure in a virgin fiber. However, the hard zone fiber often shows abrasion damage along its lateral surface, as seen in Fig. 3.41. Despite such damage, there is not much reduction in filament tenacity or elongation to rupture for these few specimens tested (compared to the strand core filaments). A strand core filament is pictured in Fig. 3.42, showing a clean surface and a typical scallop-crack.

Filament to Filament Embossing and/or Crushing

Rope #2 is even older than rope #4, having been manufactured in 1966. Hence, its behavior as observed in the SEM is of interest. Two surface yarn filaments removed from the exposed zone are shown in Fig. 3.43, with considerable surface encrustation. They both fail in tension without evidence of crack "yawning". The filament of Fig. 3.43A further has experienced a distinct modification of its cross section, due either to earlier abrasive gouging, or to lateral compression. And its load-elongation curve is severely truncated. The filament of Fig. 3.43B appears likewise to be coated or encrusted, and its failure mode reflects bicomponent structure with significant differences in properties in filament core vs. sheath. Obviously, the first example is severely degraded, as indicated by its truncated load-elongation curve. The second example still retains a good part of its original strength and elongation.

Still another specimen from the exposed strand surface layer of rope #2 is pictured (Fig. 3.44A) in a highly compressed state, crushed as it were by a flat surface. This crushing has apparently caused a series of axial cracks at the filament surface, similar to that reported in the literature in lateral compression tests of PET and nylon 66 monofilaments [3]. Whether these longitudinal cracks traverse the inner sections of the filament is not known, since in the tensile test of this filament rupture took place at another location, at a level not far below the strength of the core filaments. In any case, it is noted that there is only limited encrustation on the filaments of Fig. 3.44. A more typical filament with considerable encrustation is shown in Fig. 3.45. This filament clearly fails in a brittle mode with severe truncation of its load elongation curve.

In the protected (hard) zone, filaments of the surface layer of rope #4 show negligible encrustation and there is little evidence of loss in strength or elongation to rupture (see Fig. 3.46). The scallop-crack formation is present in the fracture surface.

Filaments from the first strand sublayer of yarns in the exposed zone of rope #2 sometimes show considerable encrustation and disruption of internal structural cohesion (Fig. 3.47) with resulting loss in strength; on other occasions, they show less evidence of surface attack and retain unusually high filament mechanical properties (see Fig. 3.48).

Some filaments of the first sublayer in the protected zone on occasion are highly compressed and appear to develop a sheath core structure as seen in Fig. 3.49. The fracture surface of another such fiber (Fig. 3.50) shows the presence of two scallop-crack formations leading to a stepwise rupture with very little loss of strength or elongation.

Still other examples of excessive lateral compression of filaments were found in the strand core of rope #2, as shown in Figs. 3.51, 3.52, 3.53 and 3.54A. Significant losses in tensile strength and elongation follow. Another example of lateral compression and embossing accompanied by some fretting is shown in Fig. 3.54B for a filament removed from the surface of rope #8,--a fairly new line (1978). This is not to say that all core fibers were so affected, for it is seen in Fig. 3.55 that roundness, strength and elongation are often retained. The longitudinal crack starting up from the fracture surface is noteworthy in this specimen.

Sheath-Core Fracture Mode

Fractographic records have thus far indicated that fibers exposed at the surface of marine ropes will convert from a ductile mode of rupture with a yawning scallop-shell-shaped crack to a comparatively brittle mode of rupture with indication of a sheath core structure. Several examples are given here to focus on this phenomenon. In Figs. 3.56 and 3.57 are shown fractograph records for filaments extracted from the outer exposed surface of rope #7 and tested on the Instron. The sheath core structure is distinctly in evidence in these photographs. It is noted particularly in Fig. 3.56 that the edges of the sheath are curled inward as if due to snap-back buckling. This same figure shows evidence of rodlike cells in the core of the filament similar to those described for nylon specimens exposed to weather conditions [1]. As the most exposed fibers of the rope, these specimens also manifest surface pitting and encrustation characteristics of weather exposed fibers.

Similar behavior is noted in Fig. 3.58A for a surface filament of rope #1, which shows the sheath core behavior, surface cracking and crusting, as well as significant loss in strength and elongation. A similar phenomenon is seen in Fig. 3.58B, C, D

for a surface fiber of rope #2D.

In contrast, filaments from the first strand sublayer in the protected zone failed in Instron tensile tests in the usual ductile mode with scallop-crack development, as seen in Fig. 3.59. Note the uniqueness of these fractures in the double scallop-crack development, each originating from a different flaw point in the fiber. All these to be contrasted with the classical tensile fracture mode for a strand core filament of rope #7, shown in Fig. 3.60.

The switching from scallop-crack failure mode for protected fibers to flat mode or bicomponent mode for exposed fibers is underscored in the fractographs shown for filaments from ropes #10 and #9 in Figs. 3.61A and B and 3.62A and B, respectively.

Longitudinal Views of Worn Rope Strands

The photomicrographs provided in the earlier section have focused on the damage to and the appearance of individual filaments. While each filament has been identified as to its rope source and its position within the rope, it is difficult to relate the single fiber damage observed to that of surrounding fibers and yarns. This section considers the overall damage noted in specific regions of a few selected ropes. To assist in evaluating the appearance of the optical photomicrographs which follow, it is useful to provide a cross sectional map of the typical 3-strand rope.

In Fig. 3.63 several positions are designated in the rope cross section, one at the exposed surface layer of the strand "O" and four in the center of the rope. Position "O" has been identified in earlier photomicrographs and in Figs. 3.1 and 3.3. Position "C" is at the very rope center, while positions "A", "E" and "B" define the zone of contact between two strands. As it turns out, the zone AE is relatively clean, as noted in Fig. 3.3, yet it is frictionally damaged. The filaments shown in Fig. 3.34 reflect the presence of such "clean" friction. Zone EB is another frictional zone, but in a worn rope, it is usually contaminated with sand and dirt.

Several views are shown of ropes 4, 7 and 8 in the figures which follow: Fig. 3.64A shows a strand of rope 7 at position O, i.e. at the outermost exposed surface of the strand; Fig. 3.64B shows a similar view of rope 4. These positions are dirty, even though it is not apparent in the photographs, but abrasive wear is in evidence resulting in considerable fiber rupture.

Figure 3.65A shows a strand of rope 8 at position B. Note this region is not in contact with outside surfaces and the damage indicated is due to friction between the strands. Figure 3.65B shows a view of rope 7 straddling the position B. Its upper right quadrant manifests extensive damage, but little

contamination; the lower left quadrant indicates considerable contamination. Figure 3.65C shows rope 7 at the middle of zone EB. Frictional damage and contamination prevail.

At position E the strand surface converts in appearance from a frictionally damaged/contaminated zone on the EB side to a frictionally damaged/uncontaminated zone on the EA side. This is seen in Figs. 3.66A (rope 8 relatively new) and 3.66B (rope 7 relatively old). A view of the AE section is shown in Fig. 3.67A for rope 7. Finally, the relatively protected position C is shown in Fig. 3.68A for rope 8 and Fig. 3.68B for rope 7. The effectiveness of protection of its position is evident.

Summary of Microscopic Studies

In summary, the microscopic studies of the ten worn rope specimens have documented the various types of degradation which occur during marine usage of synthetic fiber lines. The appearance of filaments at the outermost location of the 3-strand twisted rope varies from strand to strand, sometimes manifesting an encrustation and coating or surface attack. Etching of some fibers leading to a porous spongy structure is seen. Surface gouging, abrasion, and/or filament crushing is frequently in evidence. In many cases, photomicrographs are accompanied by filament load-elongation curves, to permit a subjective correlation between the extent of filament-surface encrustation or other non-mechanical filament modifications and stress/strain behavior. Fractography studies show a marked conversion in surface-exposed filaments from the scallop-shaped crack-spreading failure of a new synthetic fiber to the cup and cone, sheath/core, longitudinal splitting and occasional brittle failure characteristic of chemically or photochemically degraded fibers.

It has also been demonstrated that filaments in relatively protected sections of the rope can undergo significant mechanical damage through friction and filament-filament abrasion. Depending on the location in the rope cross-section, this type of mechanical attrition can take place in some cases with little accompanying contamination. In other cases, the presence of sand, grit and, possibly, salt deposits adds to the intensity of mechanical attack.

Finally, it is seen that internal pressures within the rope center, i.e. between strands, can be so intense as to cause "welding" of parallel filaments adding locally to the bending rigidity of the rope and focusing frictional damage to fibers at the boundaries of the "welded" zones. Such pressures often result in lateral filament compression and in locations where filaments are not parallel, to embossing of undivided fibers. Such compression/embossing is sometimes accompanied by the opening of surface cracks in the filament and, in extreme cases, to significant reductions in filament strength.

Summary/Conclusions

The goal of the first year of pathological study of rope failure has been reached to a reasonable extent. Considerable data have been obtained of distributions of local damage of varying types throughout the structure of 3-strand synthetic fiber twisted ropes. It has been determined that filaments located in the outer rope surface are, as expected, most vulnerable to chemical/photochemical attack, to surface encrustation, to abrasion, gouging, and crushing.

Filaments located on the outer surface of each strand may be degraded by a number of mechanisms, depending on their position in the total rope structure. Those appearing at the outer rope surface are, of course, the most vulnerable, as indicated, but other filaments on the strand surface, i.e. those at inner rope positions also undergo marked deterioration during rope use. This is not likely to have a photochemical element, but it has a variety of mechanical manifestations, including wear and frictional attrition due to relative motions between strands, compression and flattening and local embossing. Some such inner rope zones appear to suffer minimum damage, in particular at the very center of the rope. Other inner rope zones, particularly at the position of maximum compression between strands, receive a surprising amount of mechanical abuse, as documented in this section of the report. Depending on its specific location in the inter-strand contact zone, a filament may be subjected to compression and to frictional wear with or without the presence of abrasive contaminants.

The effect of lateral pressures occurring at layers below the surface of each strand and at the strand core has also been studied. Here it is found that compression and relative motion between plied yarns of the same strand also lead to mechanical attrition of the filaments, sometimes in the presence of abrasive contaminant, depending on the depth of the layer considered, but often without.

The changes in properties of the synthetic filaments during marine rope use (mostly for mooring lines) have been charted across the sections of ten ropes furnished by Navy and Coast Guard staff. Changes along yarn lengths have also been measured as the yarn migrates through the strand and the rope structure. The goal of determining these distributions is to establish the mechanisms of rope deterioration and also to provide a realistic foundation for modelling the rope structure and estimating its residual life under conditions of high load usage. A number of these same rope specimens have been prepared for full load tensile tests at the Coast Guard Research Laboratories in Groton.

There is some evidence presented in this section to indicate the occurrence of fine structural changes in filaments from worn ropes. This is not unexpected, but considerably more pathological work is essential to establish such changes and to

determine their effect on subsequent constitutive behavior of the filaments involved.

Future Plans

Further pathological work on 3-strand worn ropes is not, at this time, deemed desirable unless unique specimens with well defined use and exposure histories become available. Absence of definitive information on use history is a distinct drawback in the studies conducted to date.

The double braided lines which are in widespread use in marine applications warrant considerably more pathological study in the coming year. For there were only two such ropes in the current lot, one of nylon, the other of polyester. Effort will be made to obtain additional double braided specimens with definitive use histories and, if possible, of different fiber compositions.

In the absence of equally aged, but unused specimens to serve as controls for the various analyses here reported, filaments extracted from the relatively protected strand cores have been employed as a basis of comparisons. This was only rational procedure which could be adopted for specimens drawn from such a variety of sources and ranging in age from 2 to 15 years. It is anticipated that unused controls will be obtained in future studies, although controlled exposures may have to be conducted in order to achieve this goal.

The mechanical, chemical and physical techniques described in this section will be applied in further studies of the pathology of rope deterioration. In addition, other chemical techniques described in Section 2 will be employed. Greater emphasis will be given to earlier portions of the stress-strain behavior of filaments selected from worn ropes. Finally, effort will be made to determine the residual abrasion life and/or fatigue life of yarns or fibers from worn ropes of known histories.

3. REFERENCES

3.1 Hearle, J.W.S. and Lomas, B., The Fracture of Nylon 66 Yarns Which Have Been Exposed to Light, J. Appl. Polym. Sci. 21, 1103-1128 (1977).

3.2 Batra, Subhash K. and Nuruzzaman, Syed, Elastic-Inelastic Behavior of PET and Nylon 66 Monofilaments Under Lateral Compression, J. Poly. Sci, Polymer Physics Edition 13, 369-386 (1975).

3.3 Zeronian, S.H., The Effect of Light and Air Contaminated with Sulphur Dioxide on the Surface of Nylon 66 Fibers, TRJ 41, No. 2, 184-185 (1971).

LIST OF FIGURES

3.1 Twisting Geometry of 3-Strand Rope

3.2 Cross-Sectional Profiles of Plied Yarns from Different Strand Layers of Rope 2-D

3.3 Dissection Geometry of 3-Strand Twisted Rope

3.4 Fiber Strength in Strand Normalized to Core Fiber Strength

3.5 Fiber Strength Variation Along Yarn Axis--Rope 2-D

3.6 Fiber Strength Variation Along Yarn Axis--Rope 4-E

3.7 Fiber Strength Variation Along Yarn Axis--Rope 9-D

3.8 Distribution of Breaking Strengths Along Filaments Taken from Different Layers in Rope 1-E. (A) Core, (B) 2nd Sublayer, (C) 1st Sublayer, (D) Surface Layer

3.9 Distribution of Breaking Strengths Along Filaments Taken from Different Layers in Rope 2-D. (A) Core, (B) 1st Sublayer, (C) Surface Layer

3.10 Distribution of Breaking Strengths Along Filaments Taken from Different Layers in Rope 3-E. (A) Inside of the Core, (B) Outside of the Core, (C) Cover

3.11 Distribution of Breaking Strengths Along Filaments Taken from Different Layers in Rope 4-E. (A) Core, (B) Surface Layer

3.12 Distribution of Breaking Strengths Along Filaments Taken from Different Layers in Rope 5-E. (A) Inside of the Core, (B) Outside of the Core, (C) Inside of the Cover, (D) Outside of the Cover

3.13 Distribution of Breaking Strengths Along Filaments Taken from Different Layers in Rope 6-A. (A) Core, (B) 3rd Sublayer, (C) 1st Sublayer, (D) Surface Layer

3.14 Distribution of Breaking Strengths Along Filaments Taken from Different Layers in Rope 7-D. (A) Core, (B) 3rd Sublayer, (C) 1st Sublayer, (D) Surface Layer

3.15 Distribution of Breaking Strengths Along Filaments Taken from Different Layers in Rope 8-D. (A) Core, (B) 2nd Sublayer, (C) 1st Sublayer, (D) Surface Layer

3.16 Distribution of Breaking Strengths Along Filaments Taken from Different Layers in Rope 9-D. (A) Core, (B) 1st Sublayer, (C) Surface Sublayer

LIST OF FIGURES

3.17 Distribution of Breaking Strengths Along Filaments Taken from Different Layers in Rope 10-D. (A) Core, (B) 1st Sublayer, (C) Surface Layer

3.18 Average Breaking Strengths of Filaments Across the Strand

3.19a Distribution of Breaking Strengths Along Filaments of Core Yarns in Rope 2-D

3.19b Distribution of Breaking Strengths Along Filaments of the Sub-Surface Layer of Rope 2-D

3.19c Distribution of Breaking Strengths Along Filaments in Surface Yarns of Rope 2-D

3.20 Second vs. First Test Strengths, Rope 2-D

3.21 Locations of Filament Samples from 3-Strand Ropes

3.22 Local $\bar{M}_n$ Relative to that of Core

3.23 Relative $\bar{M}_n$ vs. Relative Strengths of Worn Ropes

3.24A,B,C,D,E,F DSC Thermograms

3.25 Properties of Nylon 66 after Sea Water Immersion for 50 Hours

3.26 Breaking Strengths and Elongation of Filaments of Rope 2-D Before and After Hot Water Treatment

3.27 Force-Elongation Curves of Heatset vs. Unheatset Single Yarn from German Rope

3.28 Force-Elongation Curves of Heatset vs. Unheatset 4-Ply Yarns from German Rope

3.29 Heat Shrinkage of Filaments from Various Locations in Rope 2-D

3.30 Cross Sectional Profiles of Plied Yarns, Rope #4

3.31 Longitudinal View of Hard Spot in Rope #4
(A) 50X; (B) 300X

3.32 Longitudinal View of Soft Spot in Rope #4
(A) 50X; (B) 300X

3.33 View of Abraded Face of Plied Yarn in Hard Spot, Rope #4
(A) 20X; (B) 50X

LIST OF FIGURES

3.34	Details of the Abraded Area in Hard Zone of Sample 4-E. (A) 300X; (B) 1,000X
3.35	Shows Creased Edges Along Length in Plied Yarn of Hard Zone, Rope #4
3.36A,B	Axial Gouges Along Surface Filaments Due to Asperity Abrasion
3.36C,D,E	Axial Gouges Along Surface Filaments Due to Asperity Abrasion
3.37A,B,C	Disintegrated Fiber Ends from Worn Ropes
3.37D,E	Disintegrated Fiber Ends from Worn Ropes
3.37F	Disintegrated Fiber Ends from Worn Ropes
3.37G	Disintegrated Fiber Ends from Worn Ropes
3.37H	Disintegrated Fiber Ends from Worn Ropes
3.38A	Surface Layer Fibers from the Exposed Zone of Rope #4 (1972)
3.38B	Surface Layer Fibers from the Exposed Zone of Rope #4 (1972)
3.39A	Surface Layer Fibers from the Protected Zone of Rope #4 (1972)
3.39B	Surface Layer Fibers from the Protected Zone of Rope #4 (1972)
3.40A	Subsurface Layer Fibers from the Exposed Zone of Rope #4 (1972)
3.40B	Subsurface Layer Fibers from the Exposed Zone of Rope #4 (1972)
3.41	Subsurface Layer Fibers from Protected Zone of Rope #4 (1972)
3.42	Filament from Core of Strand of Rope #4 (1972)
3.43A	Surface Layer Fibers from the Exposed Zone of Rope #2 (1966)
3.43B	Surface Layer Fibers from the Exposed Zone of Rope #2 (1966)
3.44A	Compressed Filament from Exposed Surface Layers of Rope #2 (1966)

LIST OF FIGURES

3.44B	Compressed Filament from Exposed Surface Layers of Rope #2 (1966)
3.45	Degraded Filament from Exposed Surface Layer of Rope #2 (1966)
3.46	Surface Layer Fiber from the Protected Zone of Rope #2 (1966)
3.47	Filament from First Sublayer in Exposed Zone of Rope #2 (1966)
3.48	Filament from First Sublayer in Exposed Zone of Rope #2 (1966)
3.49	Filament from First Sublayer in Protected Zone of Rope #2 (1966)
3.50	Filament from Strand Core of Rope #2 (1966)
3.51	Filament from Strand Core of Rope #2 (1966)
3.52	Filament from Strand Core of Rope #2 (1966)
3.53	Filament from Strand Core of Rope #2 (1966)
3.54A	Filament from Strand Core of Rope #2 (1966)
3.54B	Filament from Strand Surface at Center of Rope #8
3.55	Filament from Strand Core of Rope #2 (1966)
3.56	Filament from Exposed Strand Surface of Rope #7 (1966)
3.57	Filament from Exposed Strand Surface of Rope #7 (1966)
3.58A	Filament from Exposed Strand Surface of Rope #1 (1971)
3.58B,C,D	Filament from Exposed Surface of Rope #2 (1966)
3.59	Filament from Protected Strand Surface of Rope #1 (1971)
3.60	Filament from Strand Core of Rope #7 (1966)
3.61A	Filament from Exposed Strand Surface Layer from Rope #10
3.61B	Filament from Protected Strand Surface Layer from Rope #10

LIST OF FIGURES

3.62A	Filament from Exposed Strand Surface Layer from Rope #9
3.62B	Filament from Protected Strand Surface from Rope #9
3.63	Cross Section Map of 3-Strand Twisted Rope
3.64	Surface of Rope Strand at Position O A. Rope 7; B. Rope 4
3.65	Surface of Rope Strand A. Position B, Rope 8; B. Position B, Rope 7; C. Position EB, Rope 7
3.66	Surface of Rope Strand A. Position E, Rope 8; B. Position E, Rope 7
3.67	Surface of Rope Strand, Position AE, Rope 7
3.68	Surface of Rope Strand at Position C A. Rope 8; B. Rope 7

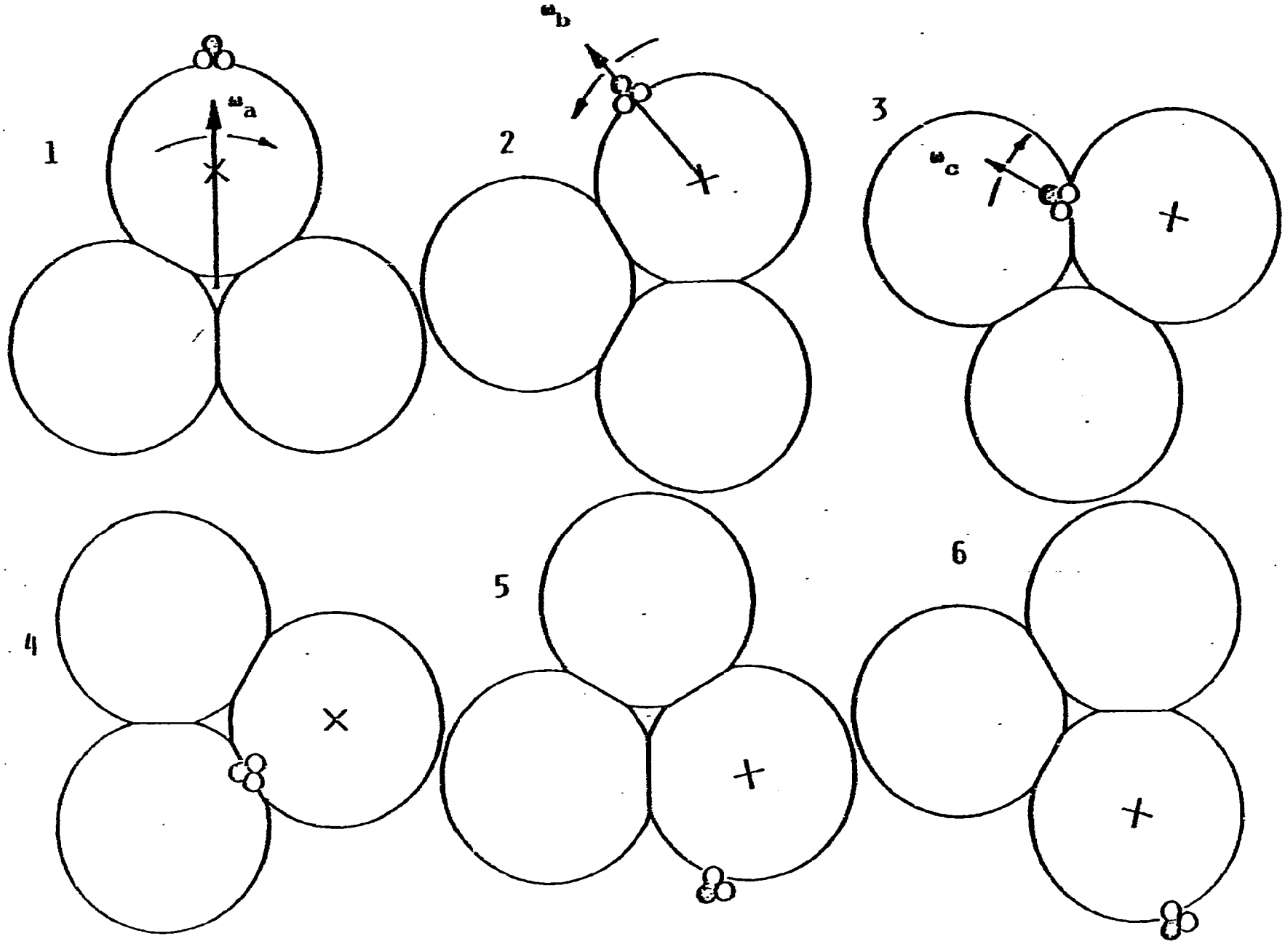

FIG. 3-1 TWISTING GEOMETRY OF 3-STRAND ROPE

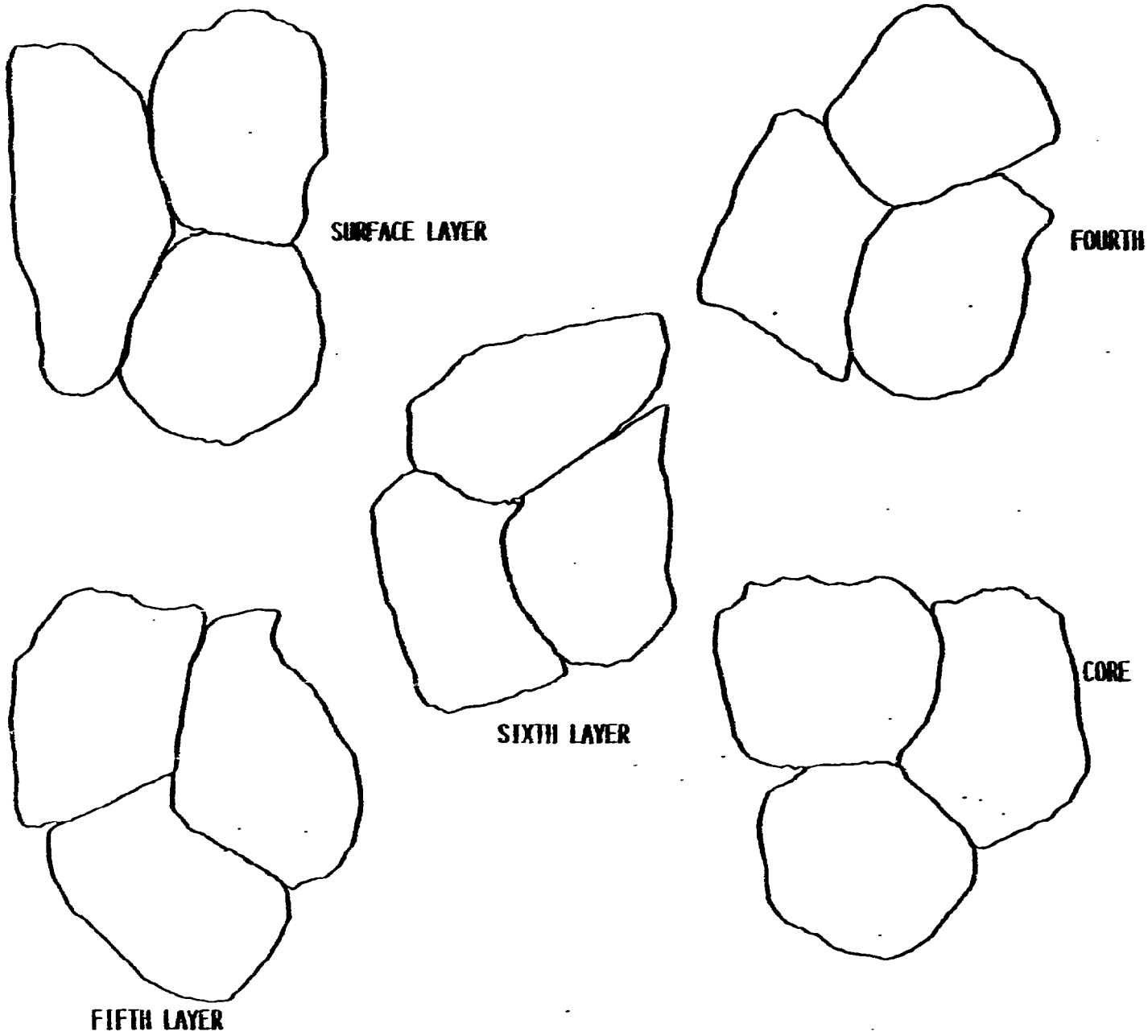

FIG. 3.2 CROSS-SECTIONAL PROFILES OF PLIED YARNS FROM DIFFERENT STRAND LAYERS OF ROPE 2-D

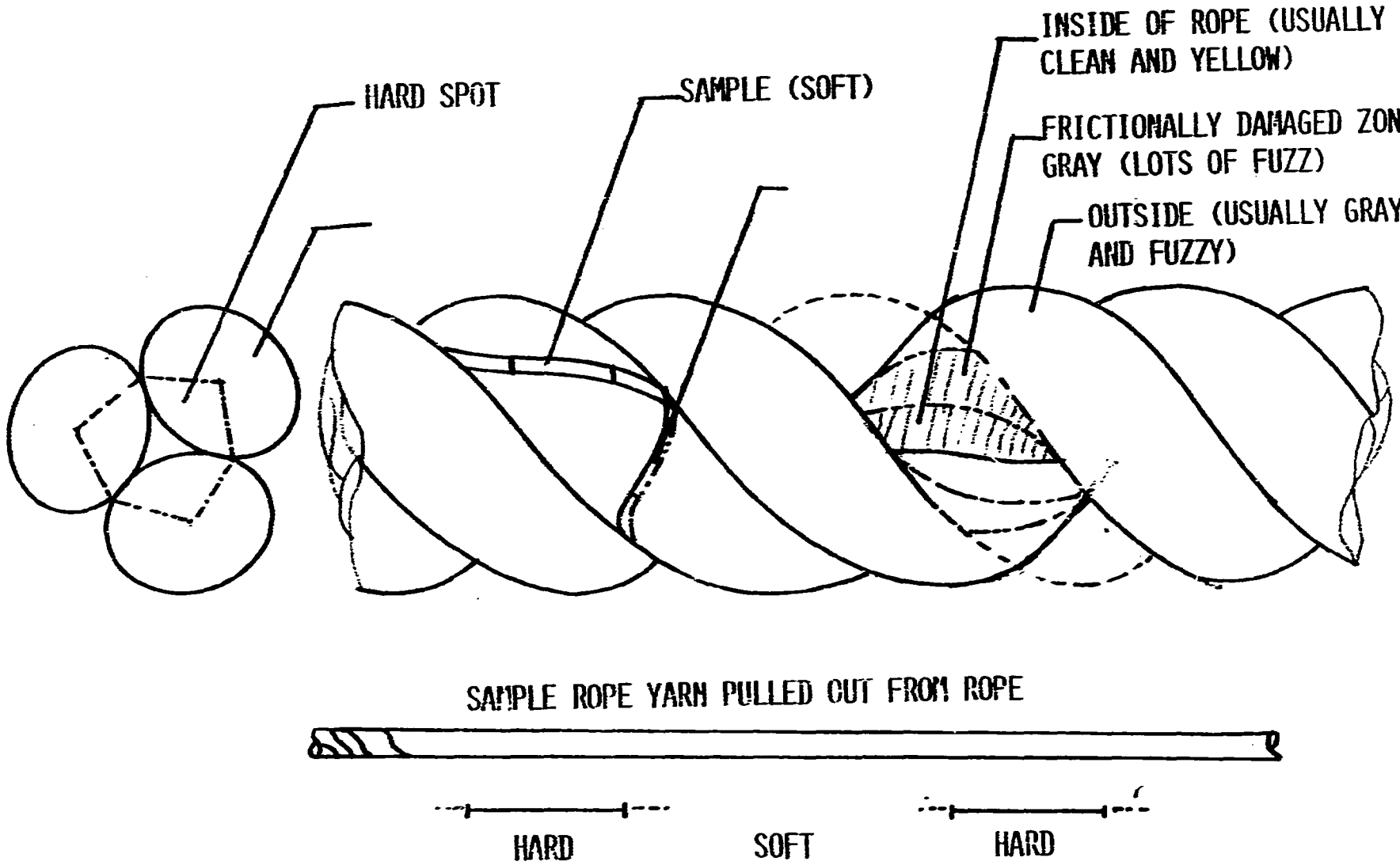

FIG. 3.3 DISSECTION GEOMETRY OF 3-STRAND TWISTED ROPE

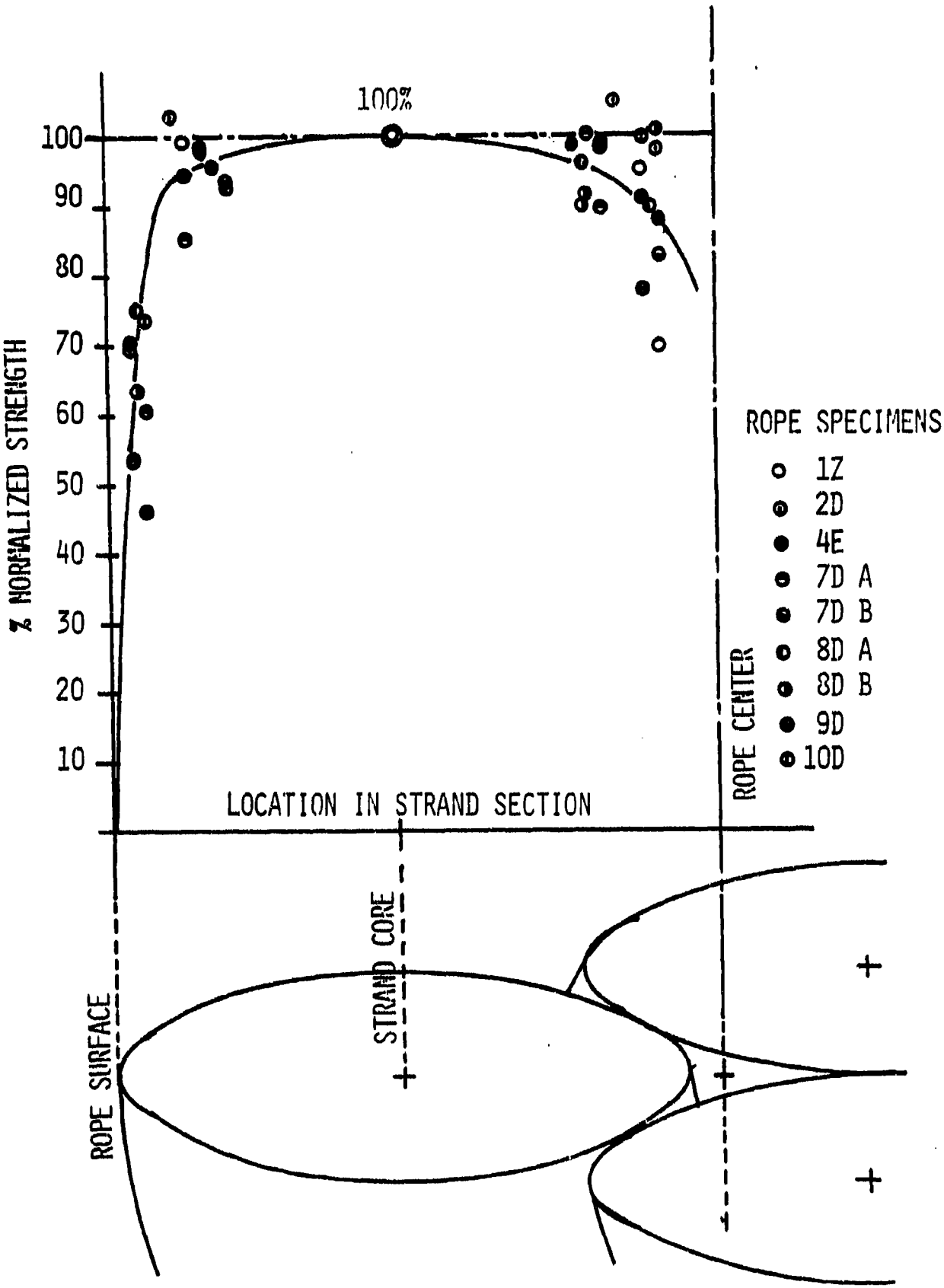

FIG. 3.4 FIBER STRENGTH IN STRAND NORMALIZED TO CORE FIBER STRENGTH

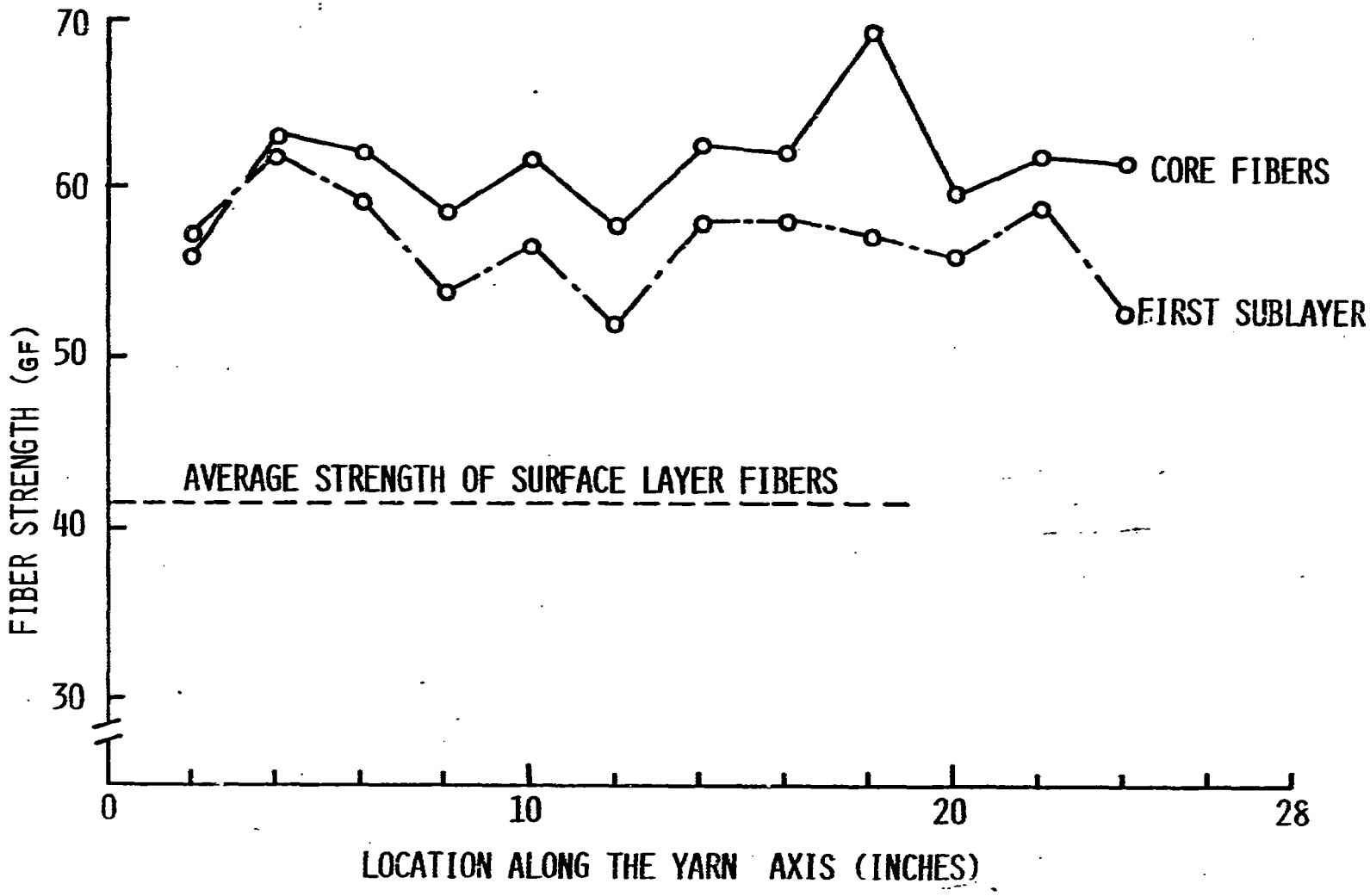

FIG. 3.5 FIBER STRENGTH VARIATION ALONG YARN AXIS -- ROPE 2-D

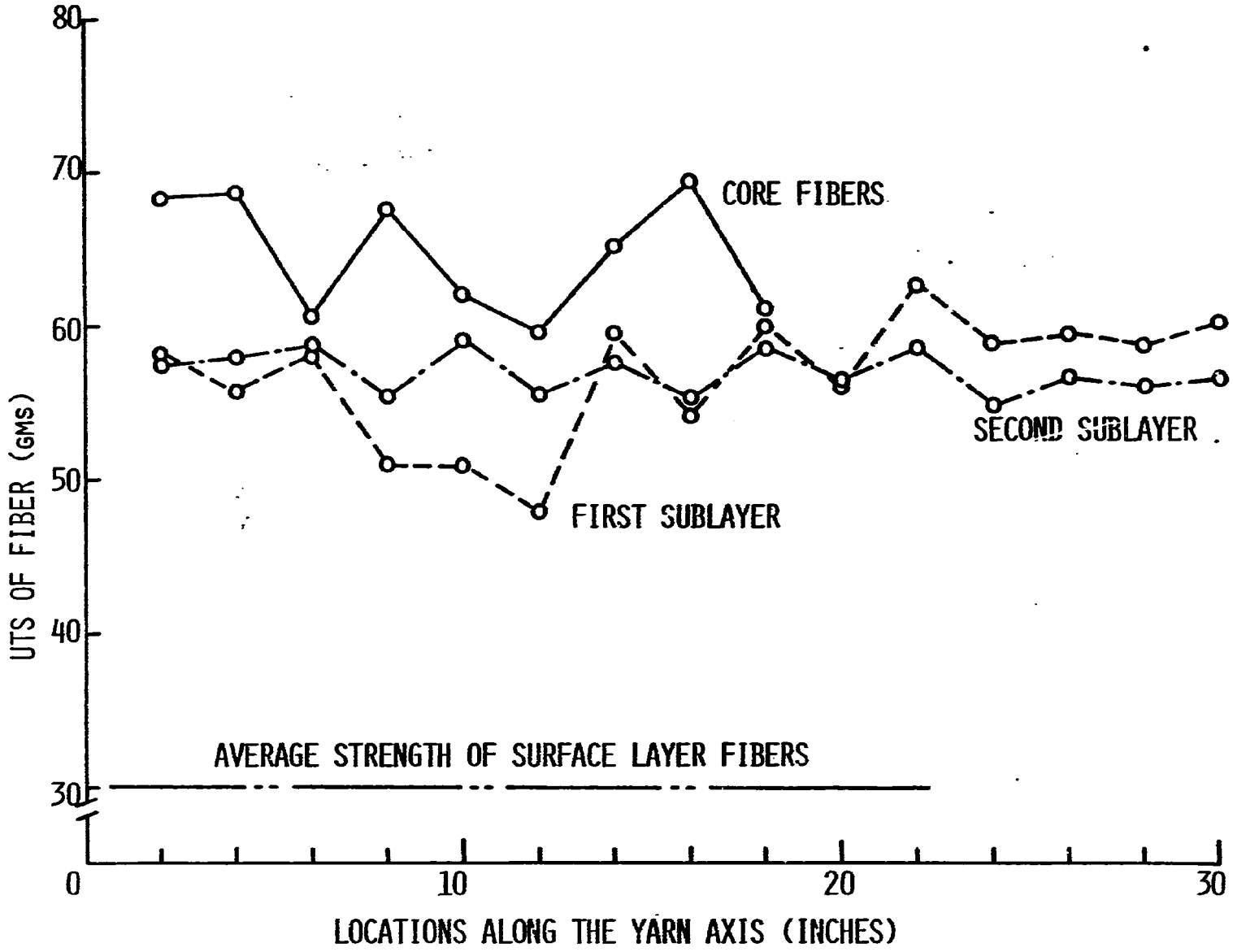

FIG. 3.6 FIBER STRENGTH VARIATION ALONG YARN AXIS -- ROPE 4-E

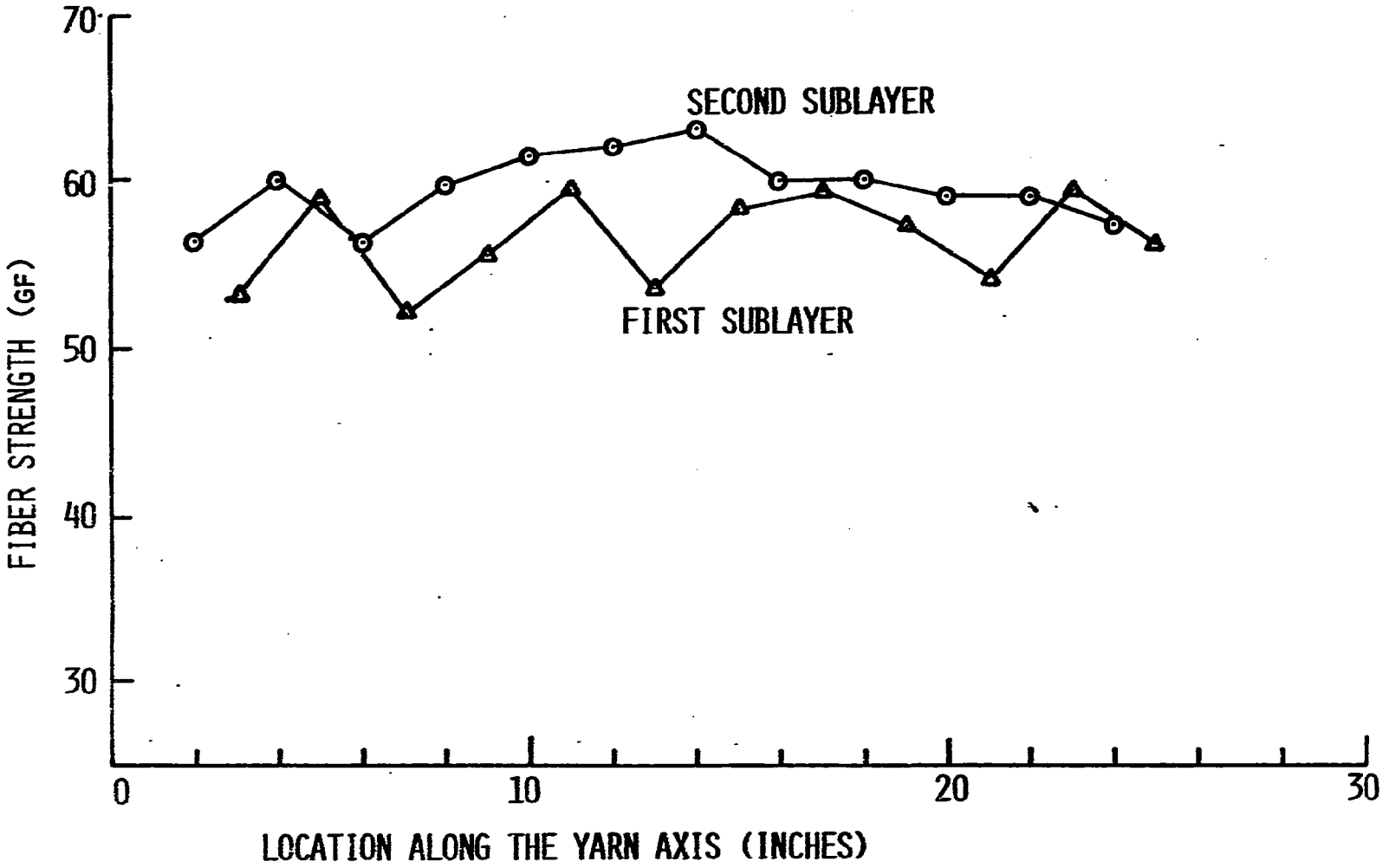

FIG. 3.7 FIBER STRENGTH VARIATION ALONG YARN AXIS -- ROPE 9-D

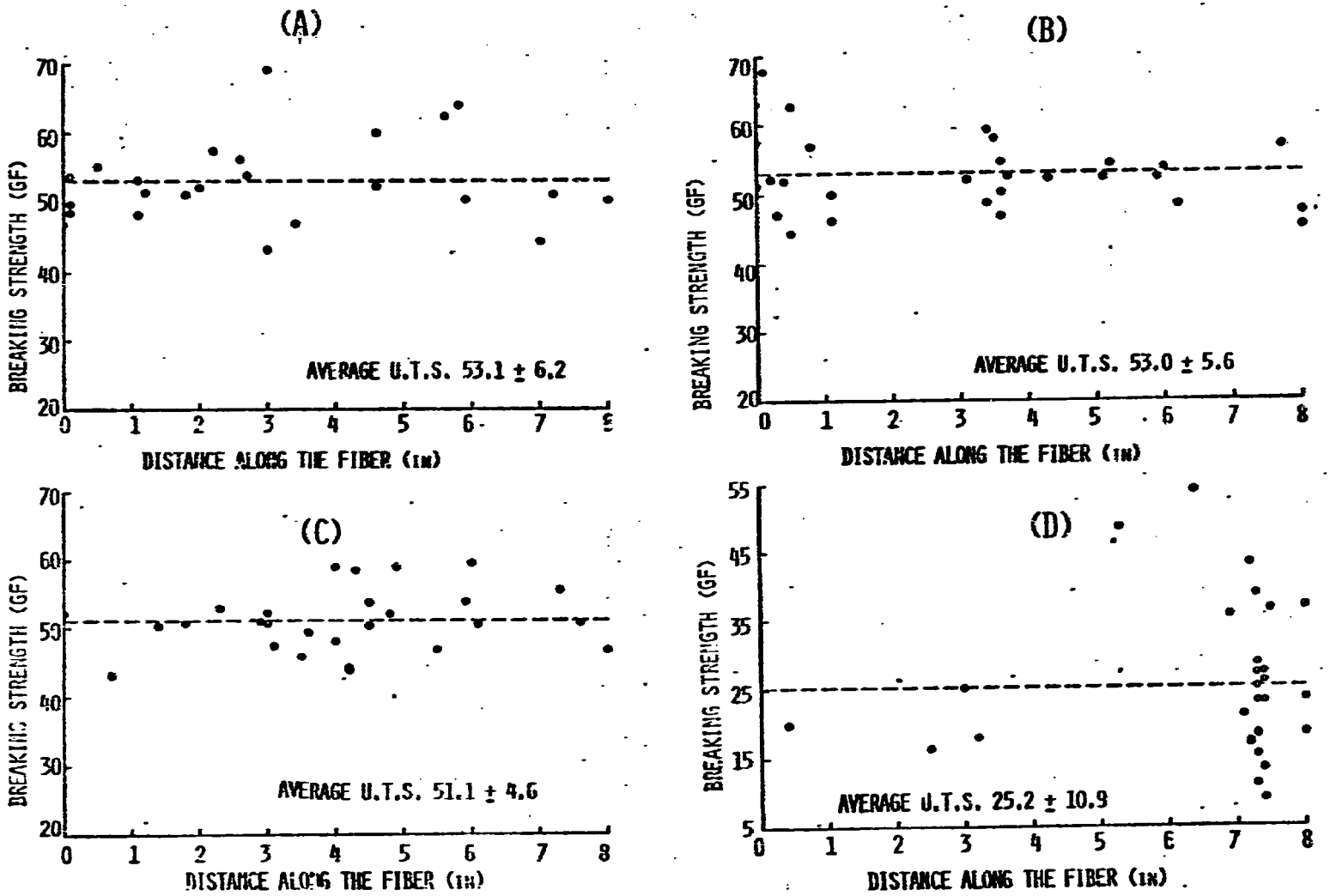

DISTRIBUTION OF BREAKING STRENGTHS ALONG FILAMENTS TAKEN FROM DIFFERENT LAYERS IN ROPE 1E. (A) CORE (B) 2ND SUBLAYER (C) 1ST SUBLAYER (D) SURFACE LAYER

FIGURE 3.8

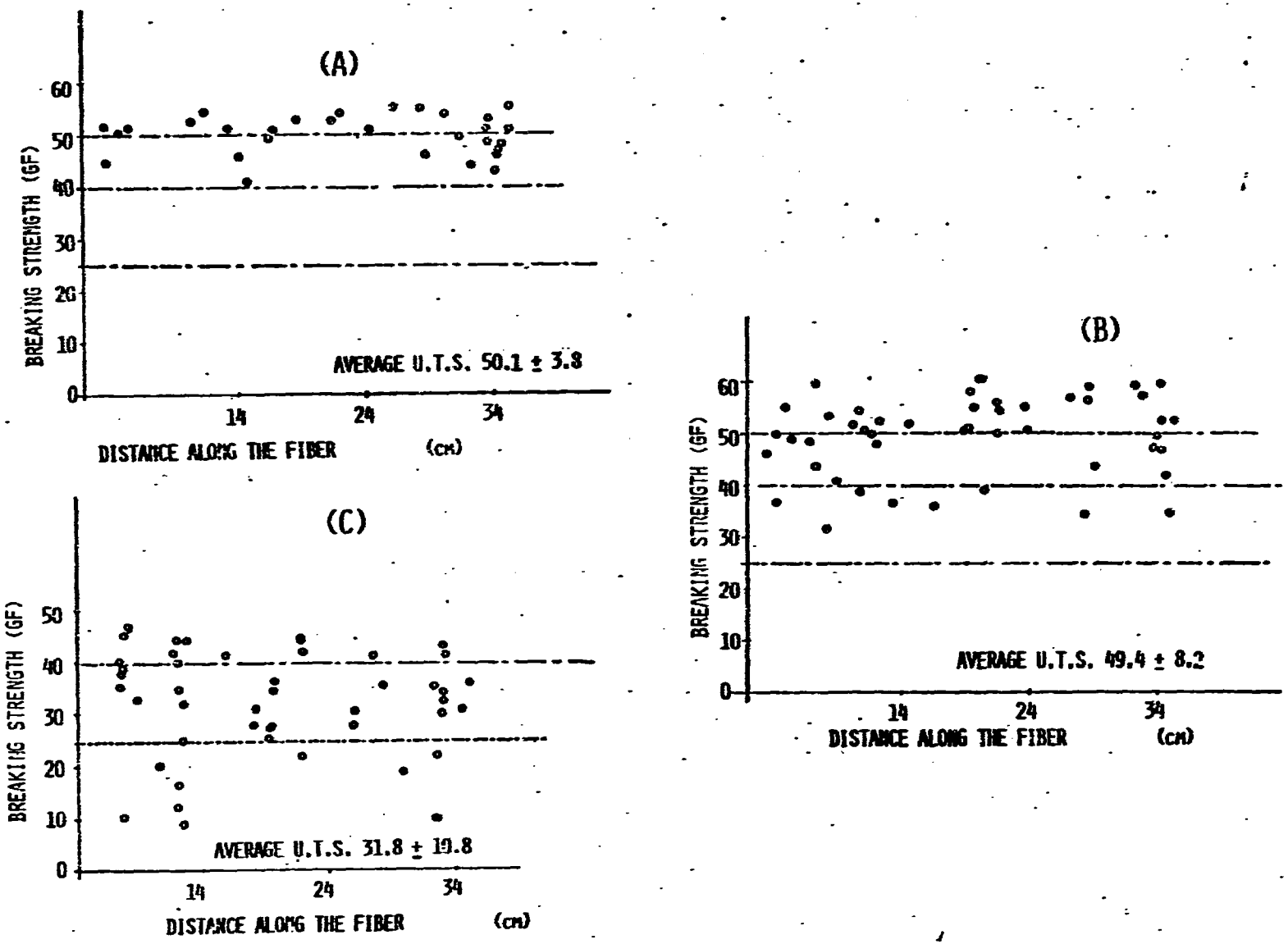

DISTRIBUTION OF BREAKING STRENGTHS ALONG FILAMENTS TAKEN FROM DIFFERENT LAYERS IN ROPE 2D. (A) CORE (B) 1ST SUBLAYER (C) SURFACE LAYER

FIGURE 3.9

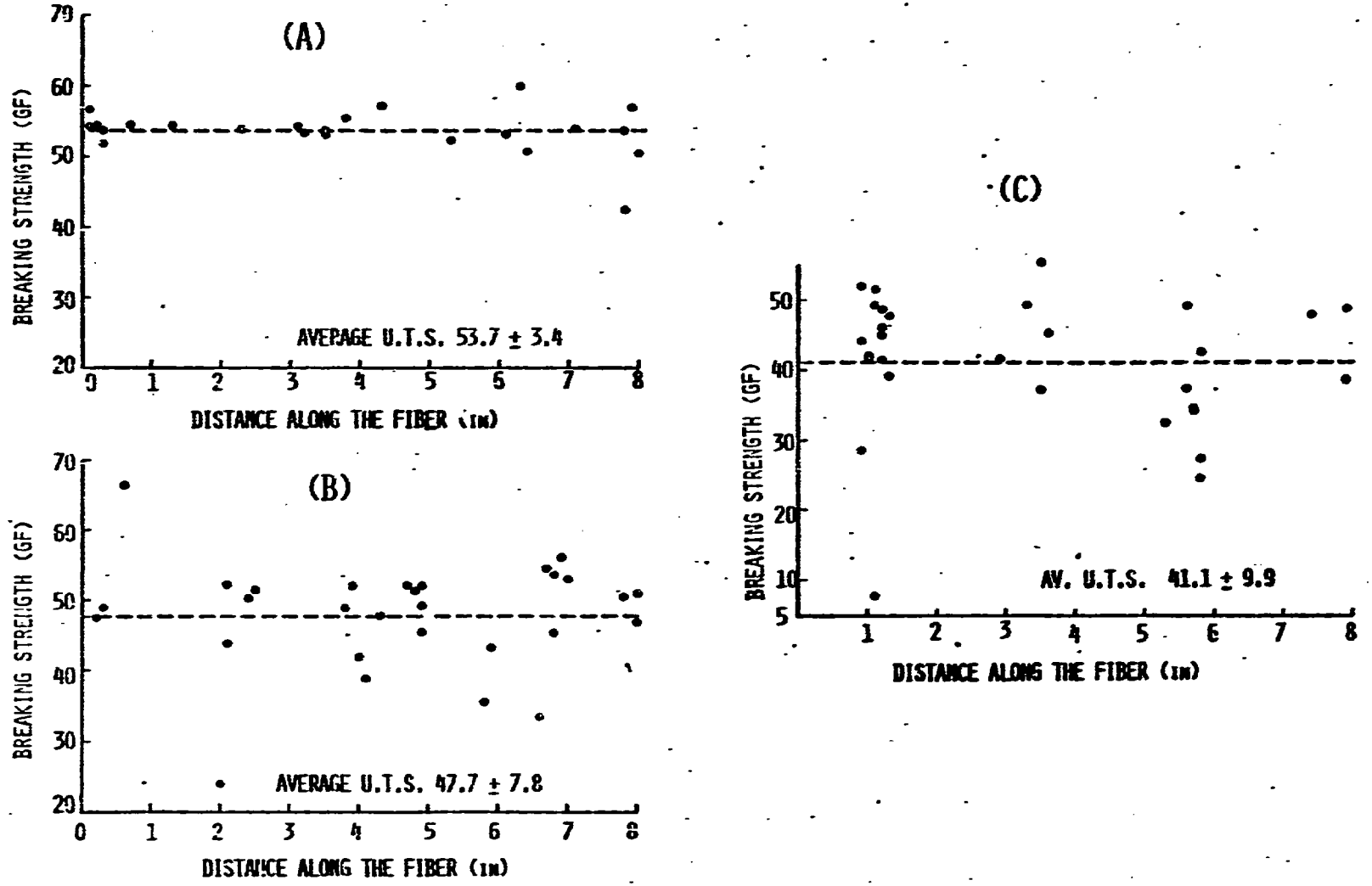

DISTRIBUTION OF BREAKING STRENGTHS ALONG FILAMENTS TAKEN FROM DIFFERENT LAYERS IN ROPE 3E. (A) INSIDE OF THE CORE (B) OUTSIDE OF THE CORE (C) COVER

FIGURE 3.10

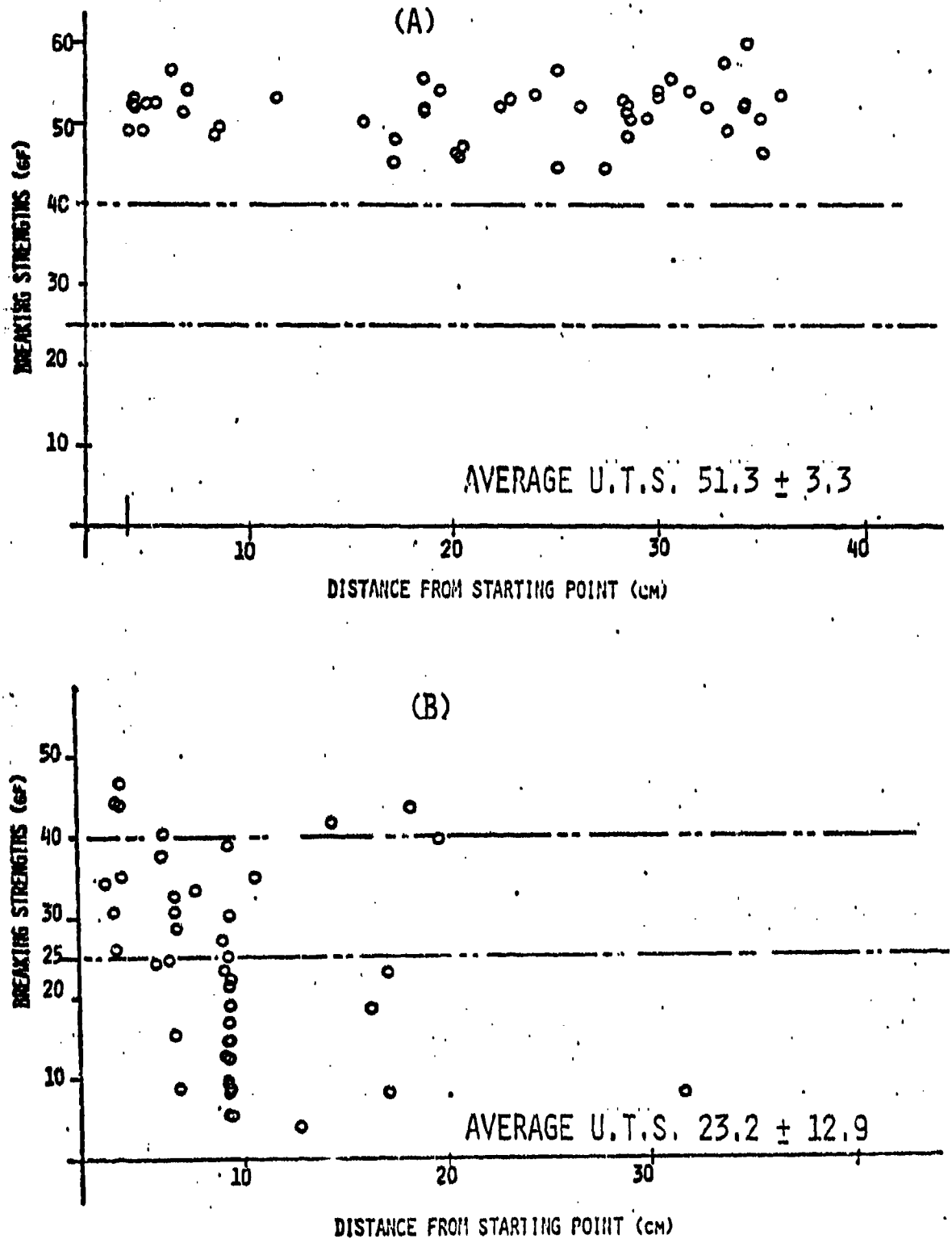

DISTRIBUTION OF BREAKING STRENGTHS ALONG FILAMENTS TAKEN FROM DIFFERENT LAYERS IN ROPE 4E. (A) CORE (B) SURFACE LAYER

FIGURE 3.11

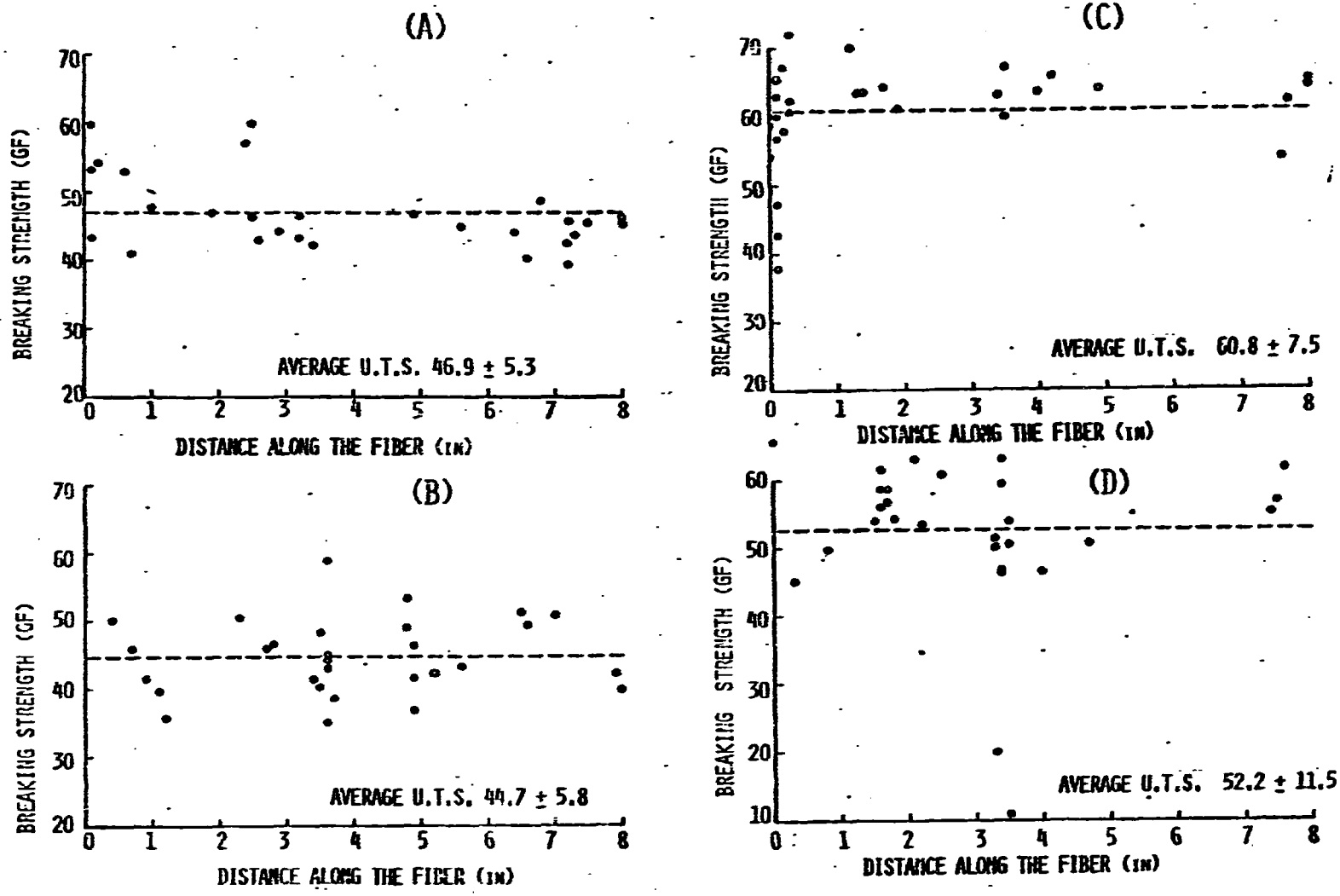

DISTRIBUTION OF BREAKING STRENGTHS ALONG FILAMENTS TAKEN FROM DIFFERENT LAYERS IN ROPE 5E. (A) INSIDE OF THE CORE (B) OUTSIDE OF THE CORE (C) INSIDE OF THE COVER (D) OUTSIDE OF THE COVER

FIGURE 3.12

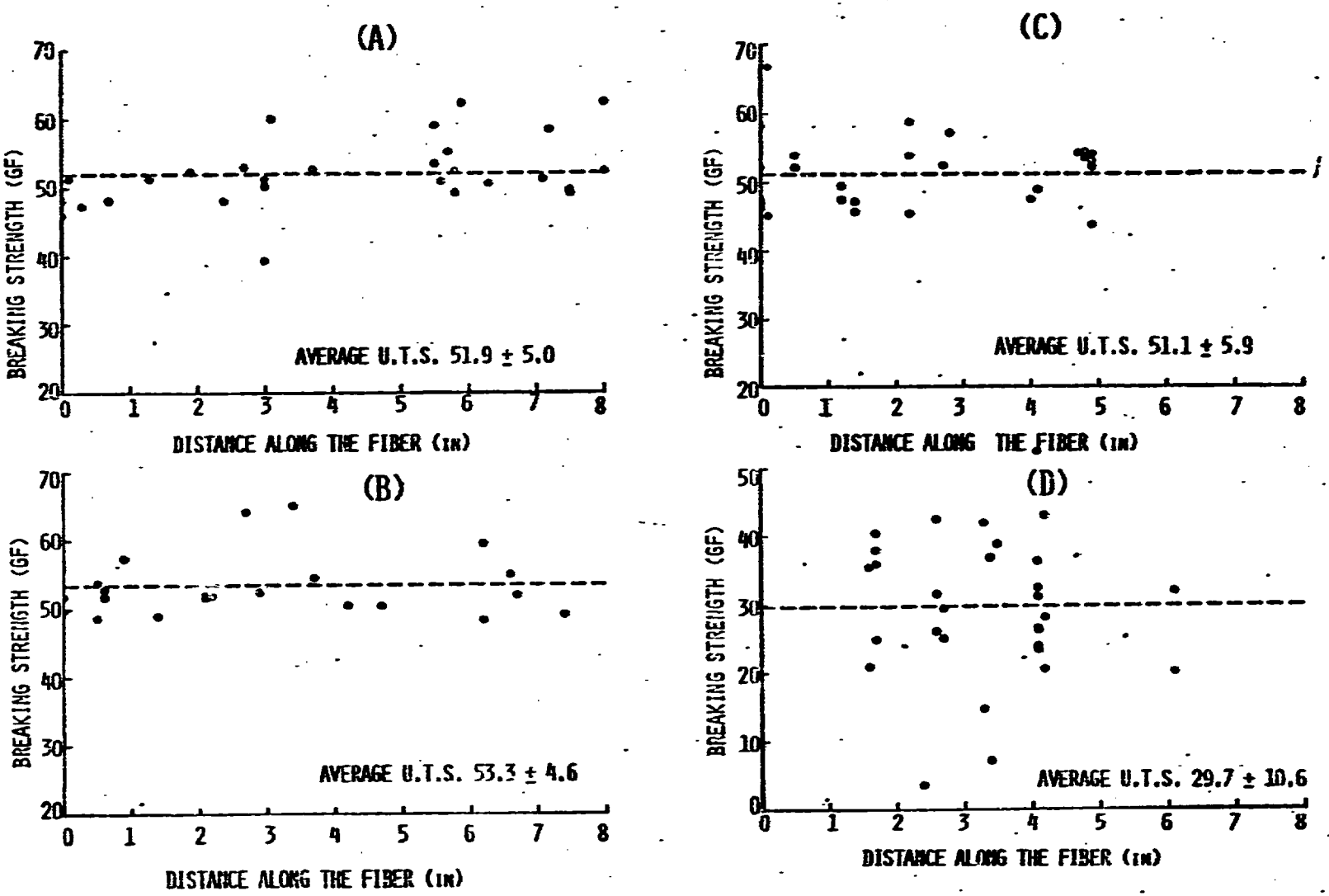

DISTRIBUTION OF BREAKING STRENGTHS ALONG FILAMENTS TAKEN FROM DIFFERENT LAYERS IN ROPE 6A, (A) CORE (B) 3RD SUBLAYER (C) 1ST SUBLAYER (D) SURFACE LAYER

FIGURE 3.13

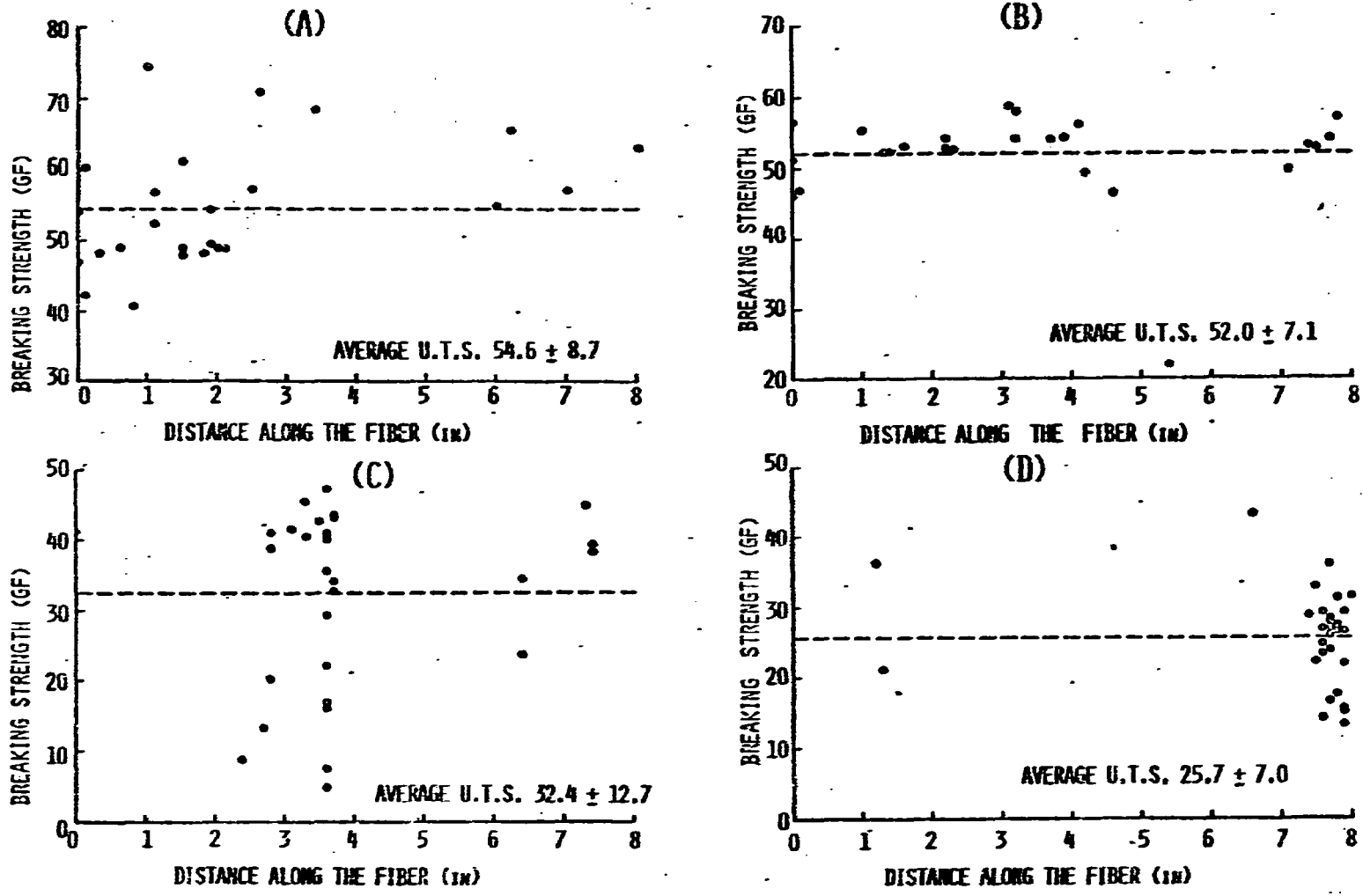

DISTRIBUTION OF BREAKING STRENGTHS ALONG FILAMENTS TAKEN FROM DIFFERENT LAYERS IN ROPE 7D.
(A) CORE (B) 3RD SUBLAYER (C) 1ST SUBLAYER (D) SURFACE LAYER

FIGURE 3.14

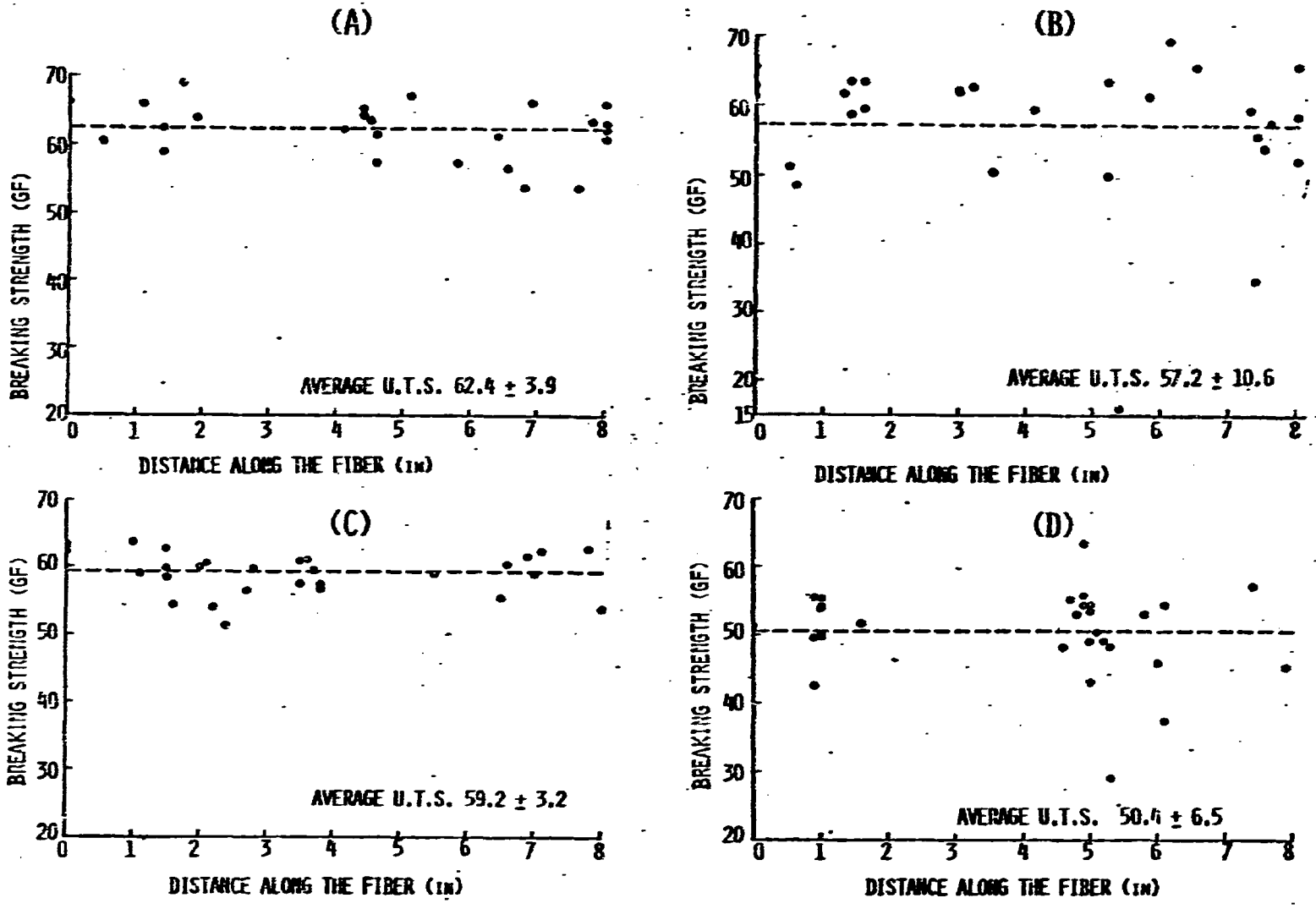

DISTRIBUTION OF BREAKING STRENGTHS ALONG FILAMENTS TAKEN FROM DIFFERENT LAYERS IN ROPE 8D. (A) CORE (B) 2ND SUBLAYER (C) 1ST SUBLAYER (D) SURFACE LAYER

FIGURE 3.15

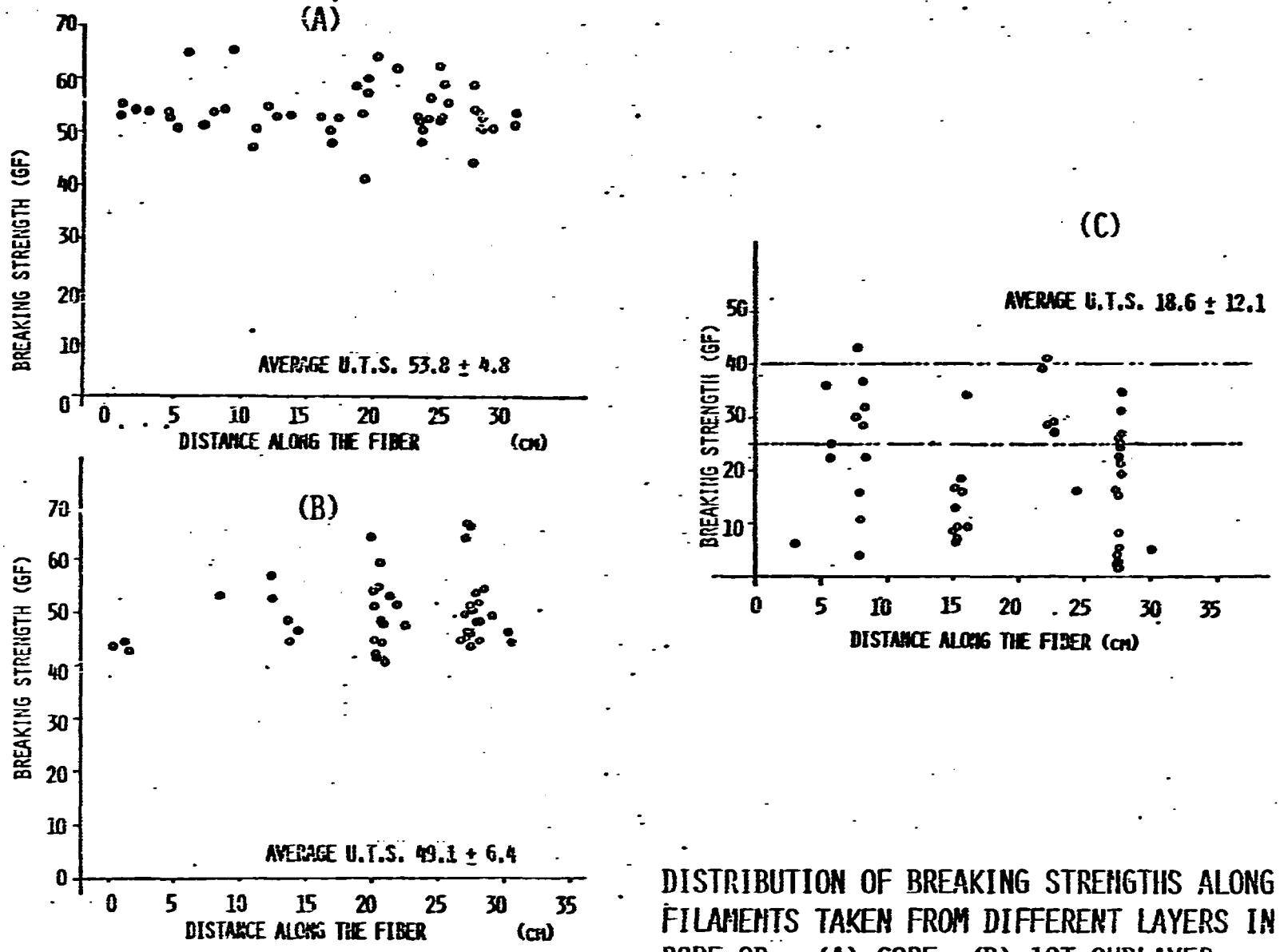

DISTRIBUTION OF BREAKING STRENGTHS ALONG FILAMENTS TAKEN FROM DIFFERENT LAYERS IN ROPE 9D. (A) CORE (B) 1ST SUBLAYER (C) SURFACE SUBLAYER

FIGURE 3-16

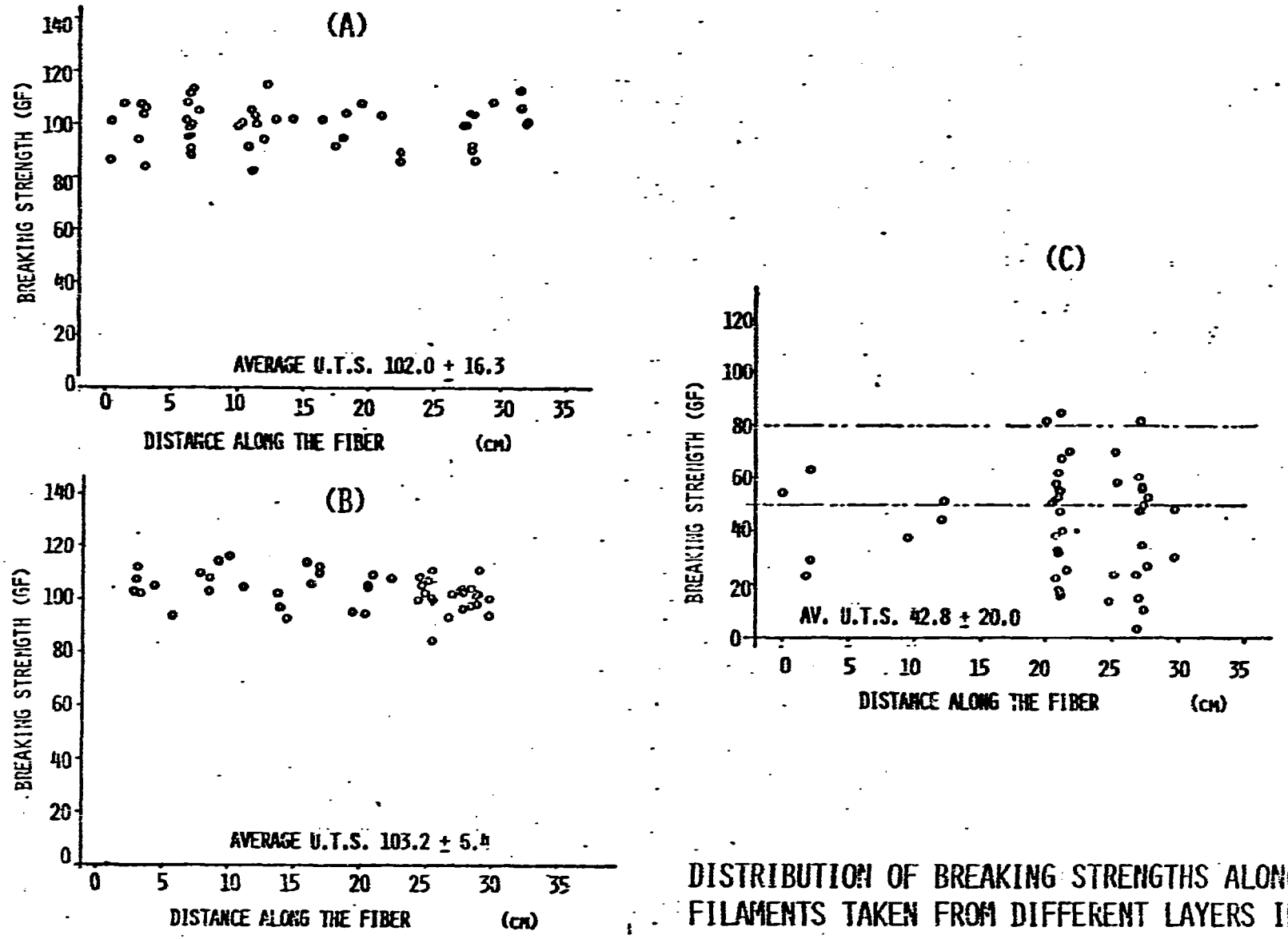

DISTRIBUTION OF BREAKING STRENGTHS ALONG FILAMENTS TAKEN FROM DIFFERENT LAYERS IN ROPE 10D. (A) CORE (B) 1ST SUBLAYER (C) SURFACE LAYER

FIGURE 3.17

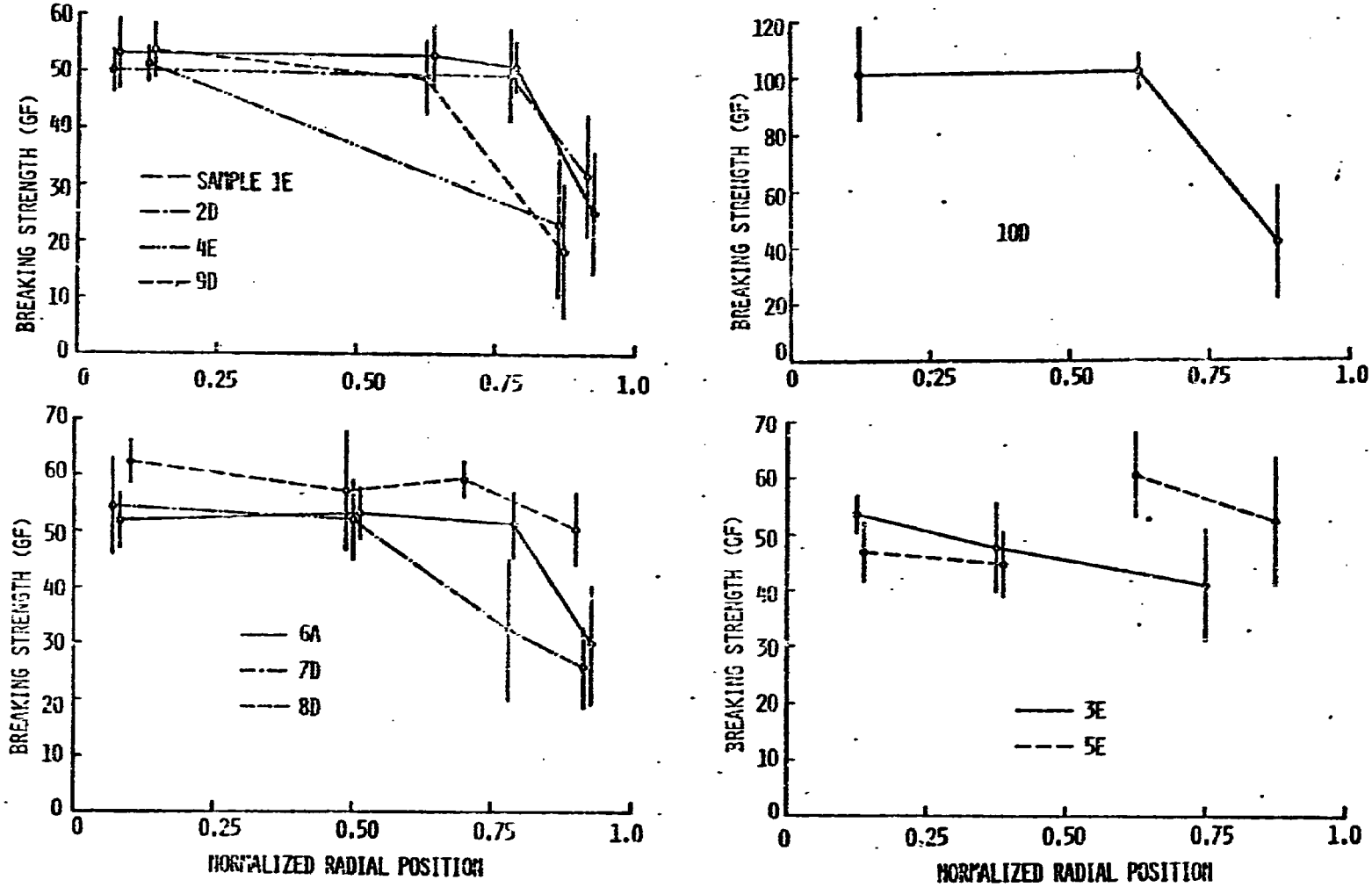

AVERAGE BREAKING STRENGTHS OF FILAMENTS ACROSS THE STRAND

FIGURE 3.18

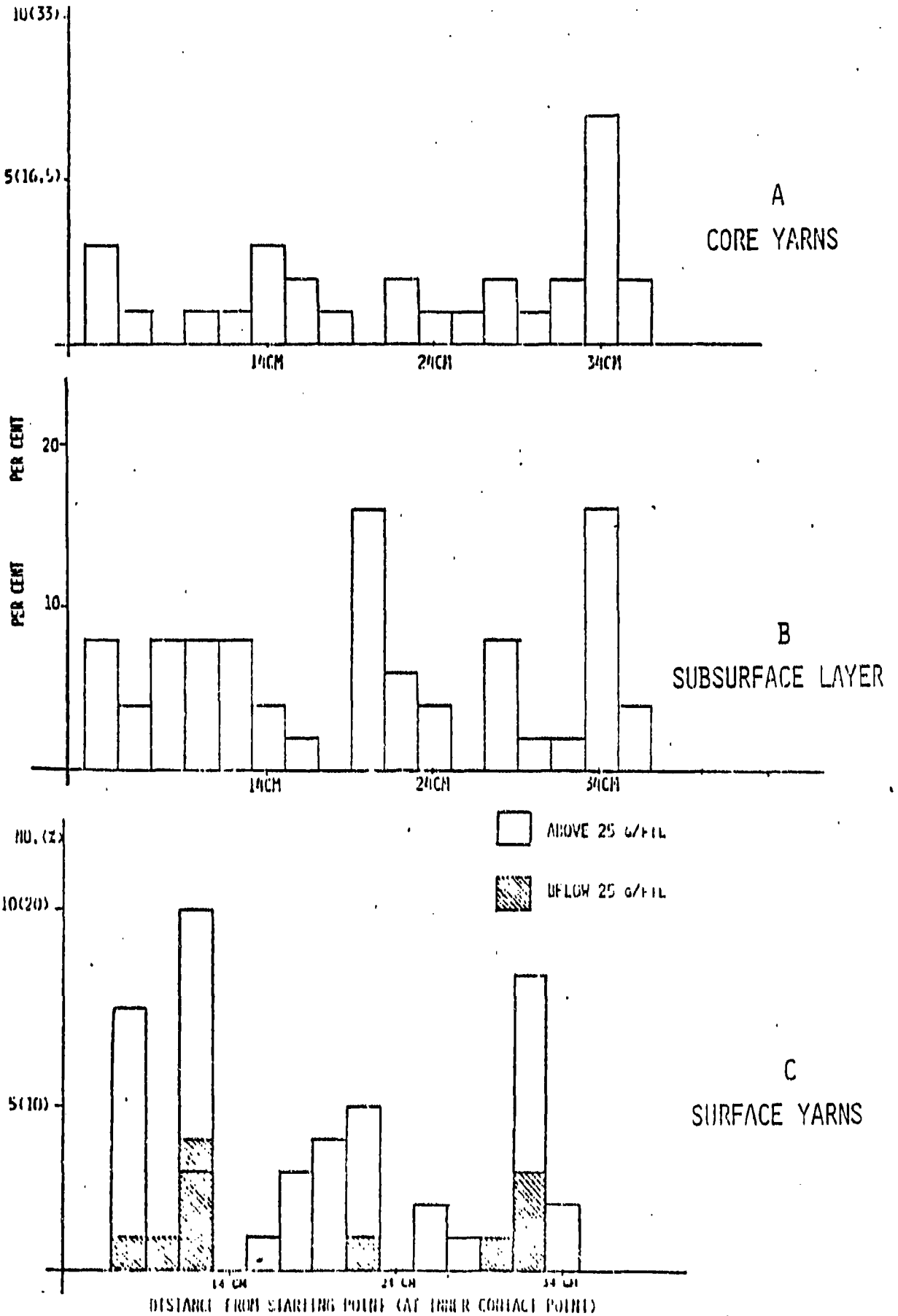

FIG. 3.19 DISTRIBUTION OF BREAKING POINTS ALONG FILAMENTS OF ROPE #2

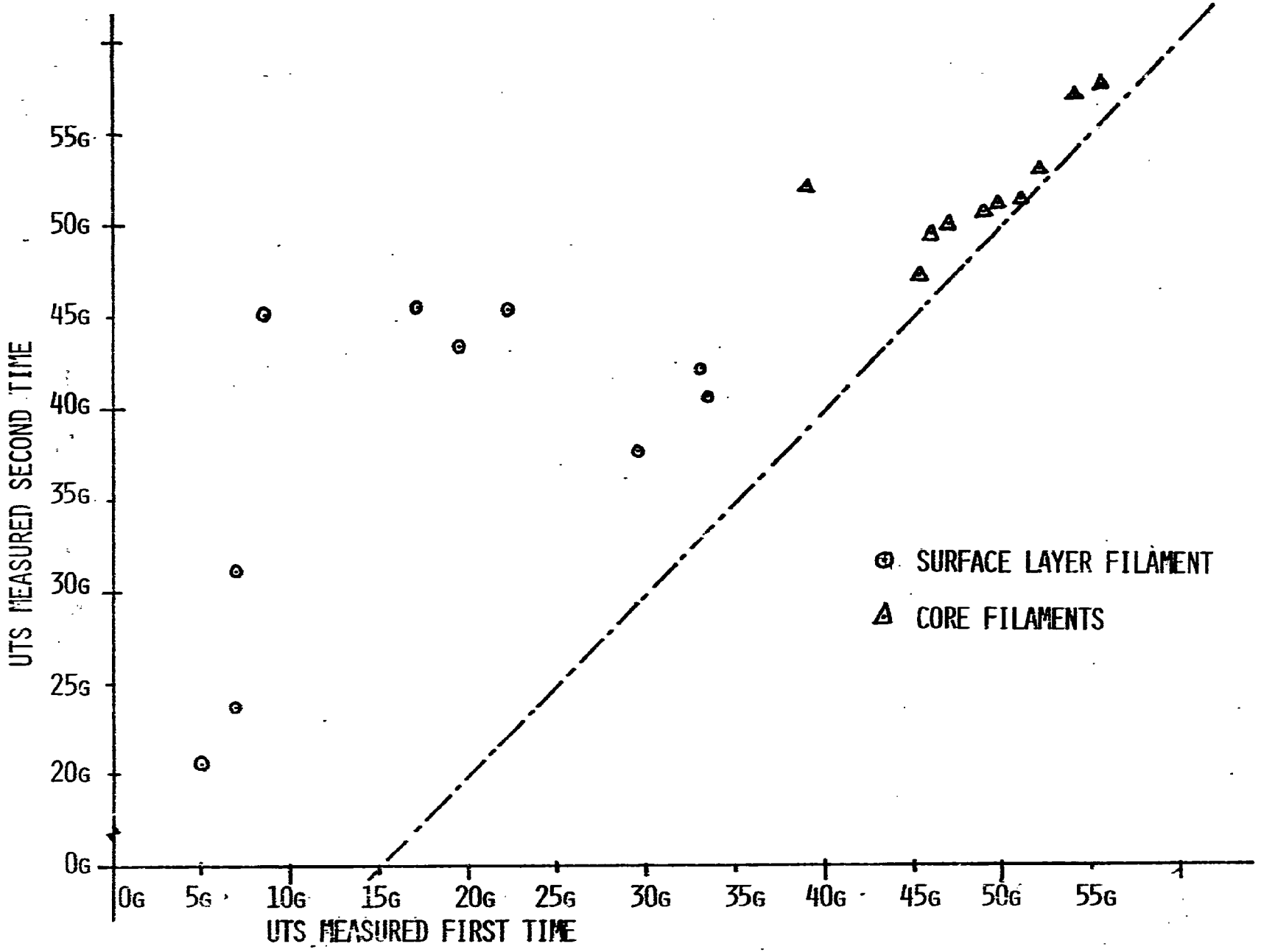

FIG. 3.20 SECOND VS. FIRST TEST STRENGTHS, ROPE 2-D

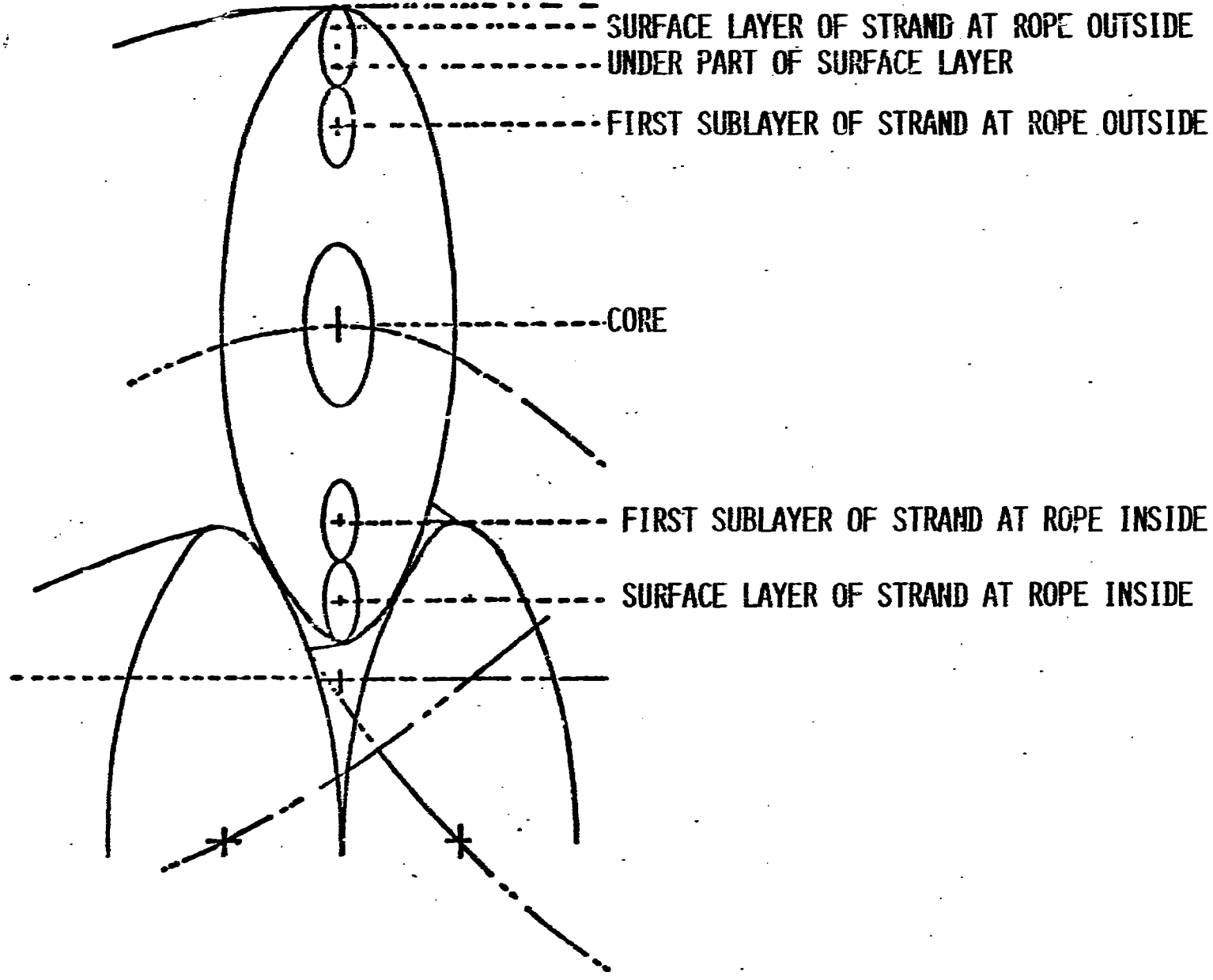

FIG. 3.21 LOCATIONS OF FILAMENT SAMPLES FROM 3-STRAND ROPES

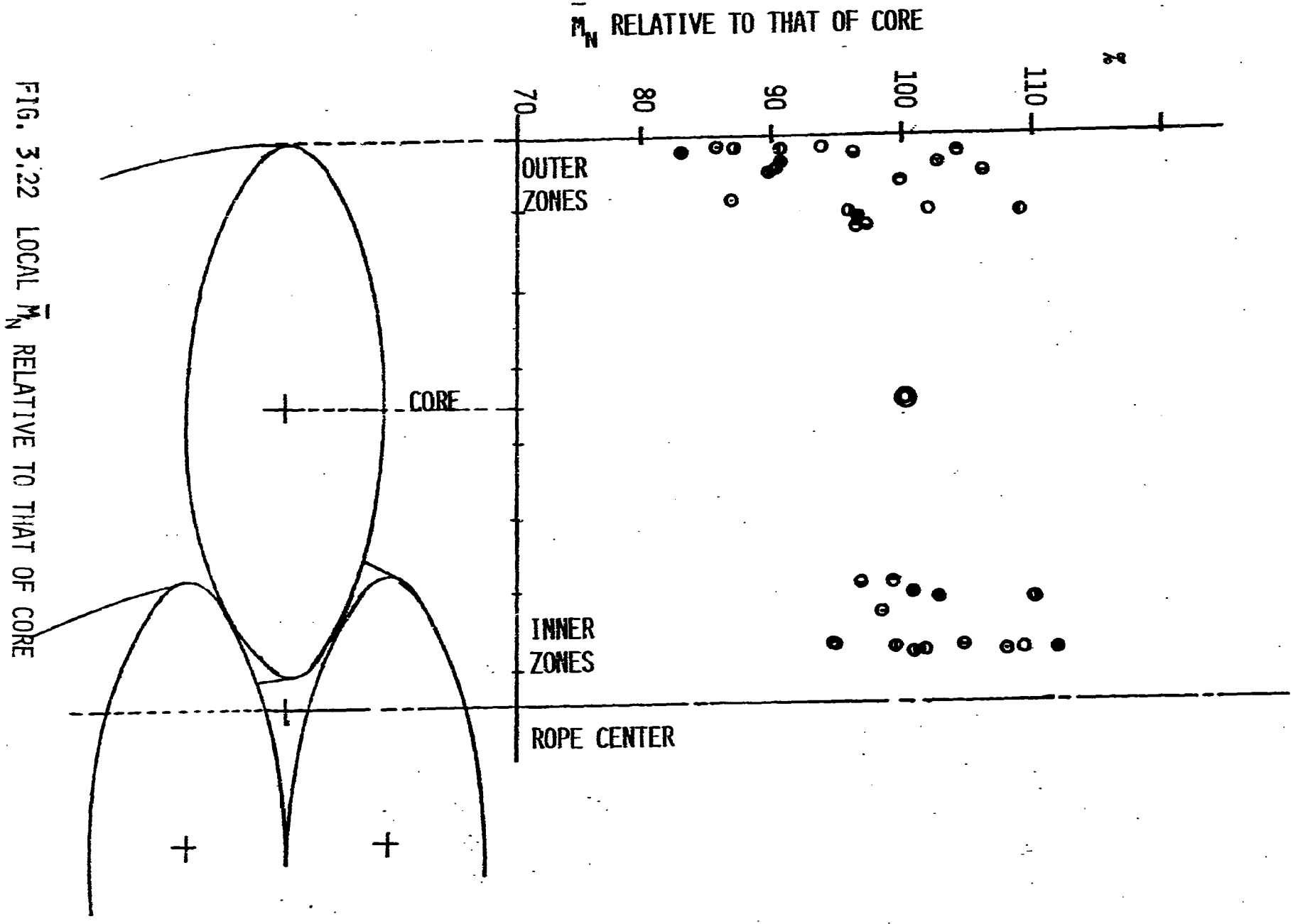

FIG. 3.22 LOCAL $\bar{M}_N$ RELATIVE TO THAT OF CORE

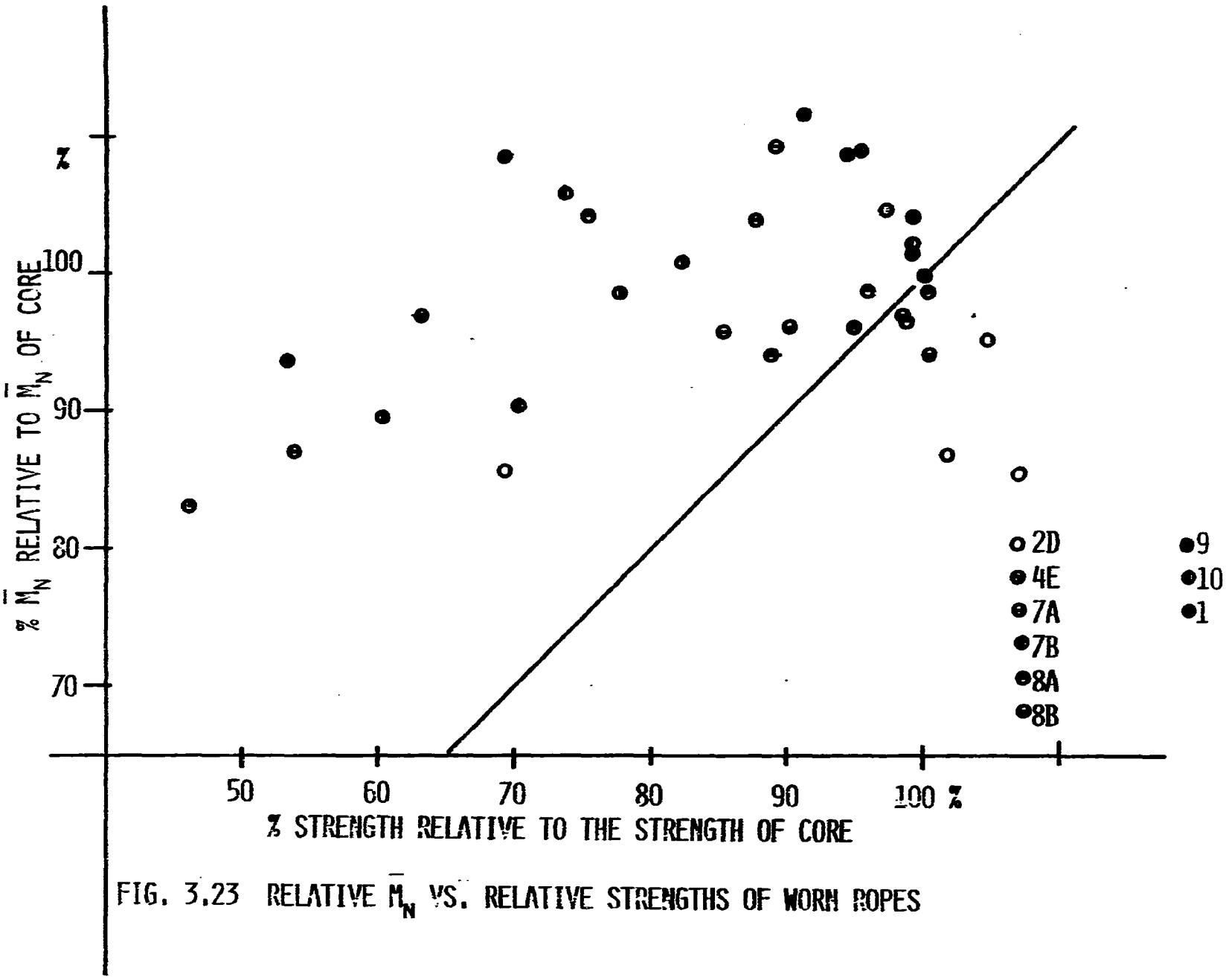

FIG. 3.23 RELATIVE $\bar{M}_N$ VS. RELATIVE STRENGTHS OF WORN ROPES

FIG. 3.24A DSC THERMOGRAMS

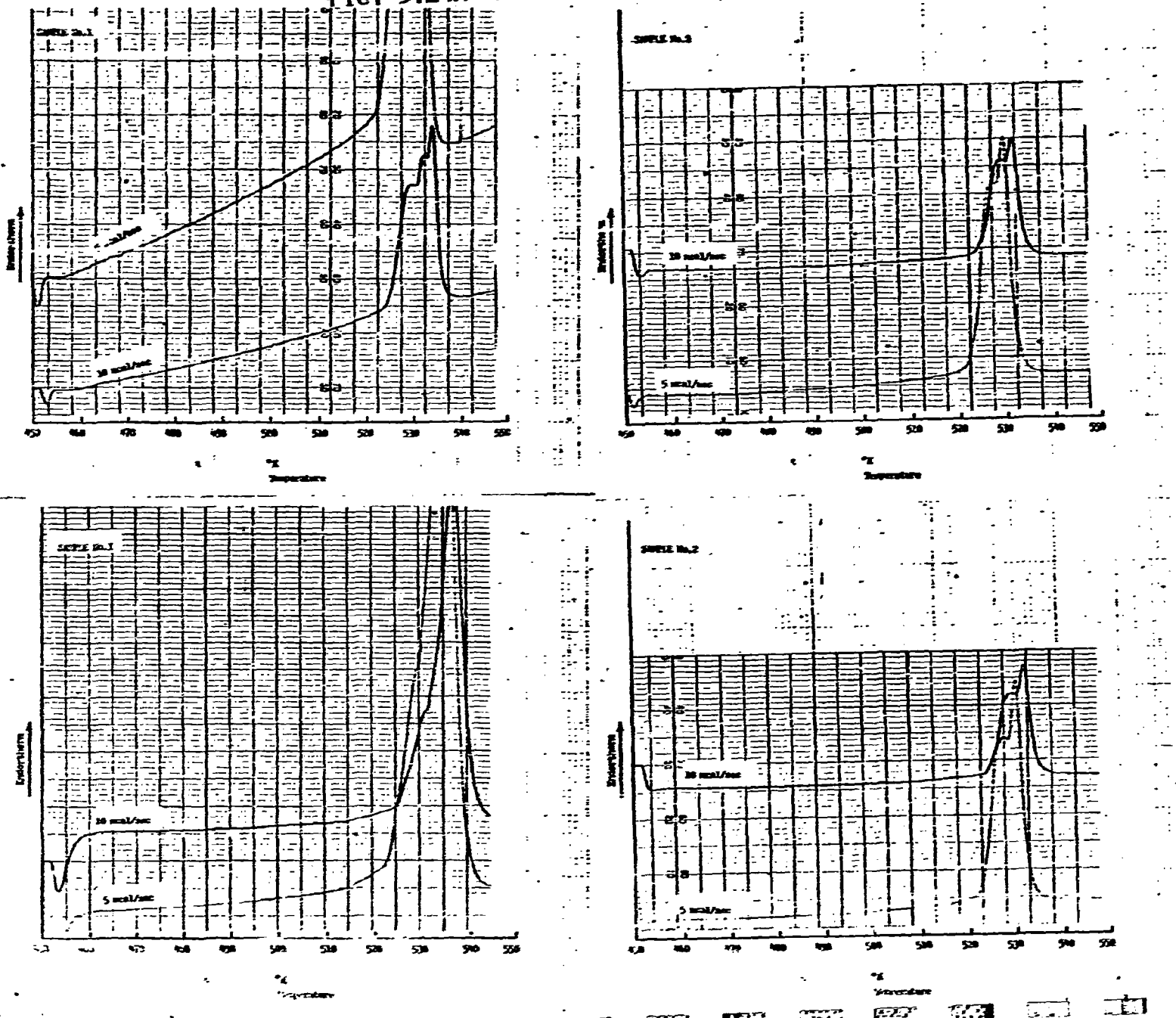

FIG. 3.24B DSC THERMOGRAMS

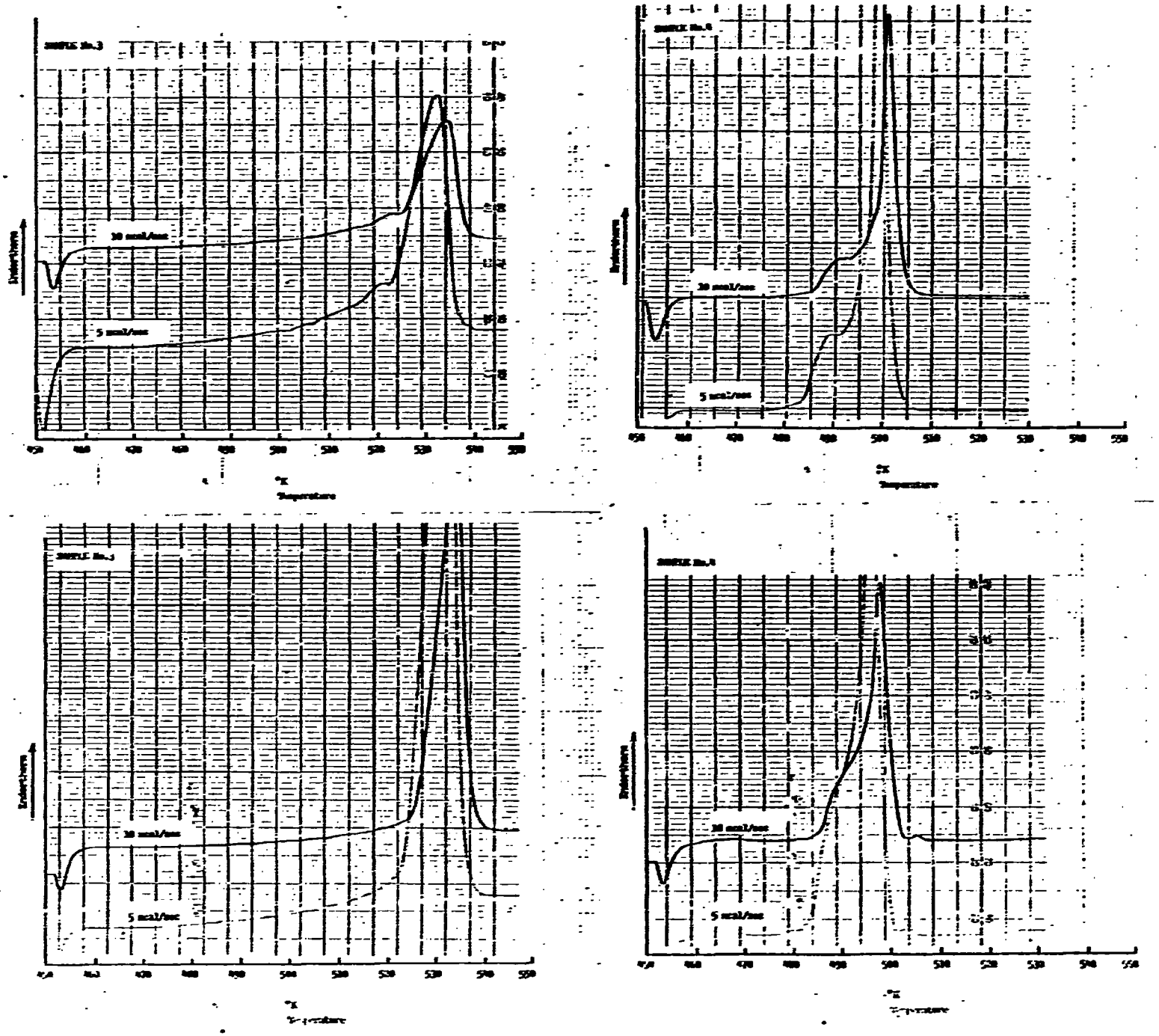

FIG. 3.24C DSC THERMOGRAMS

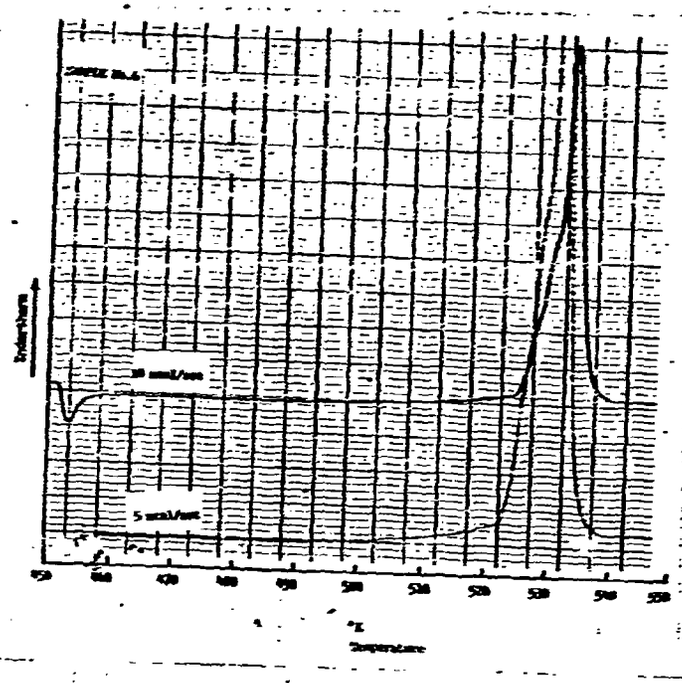

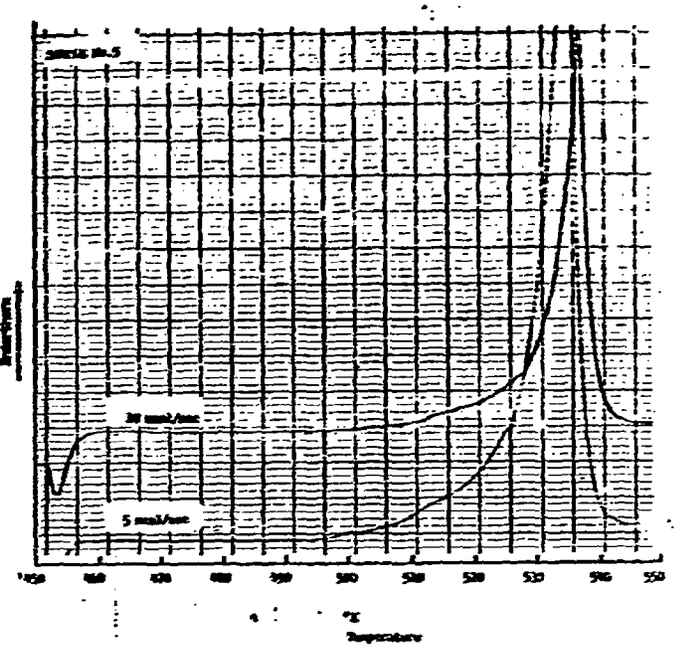

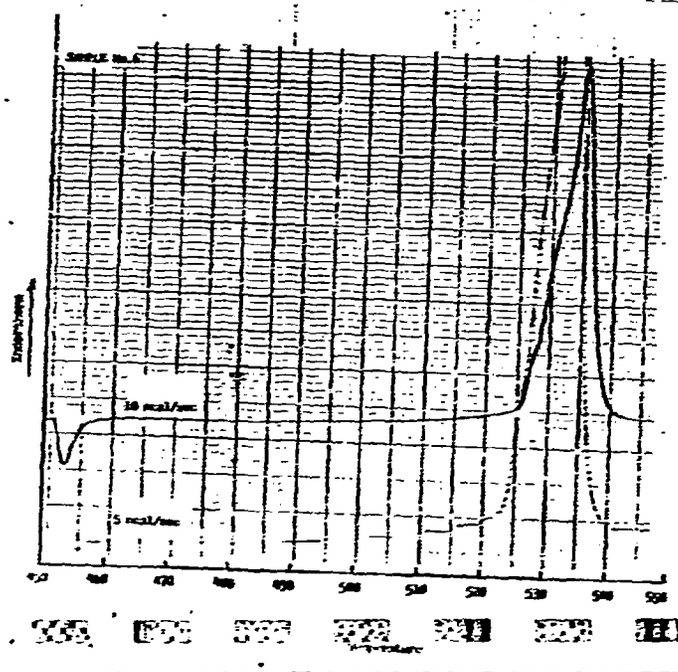

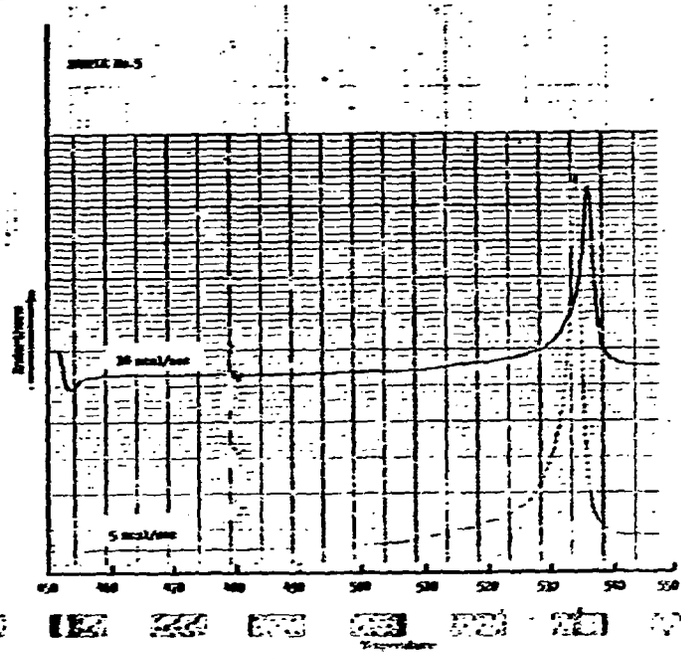

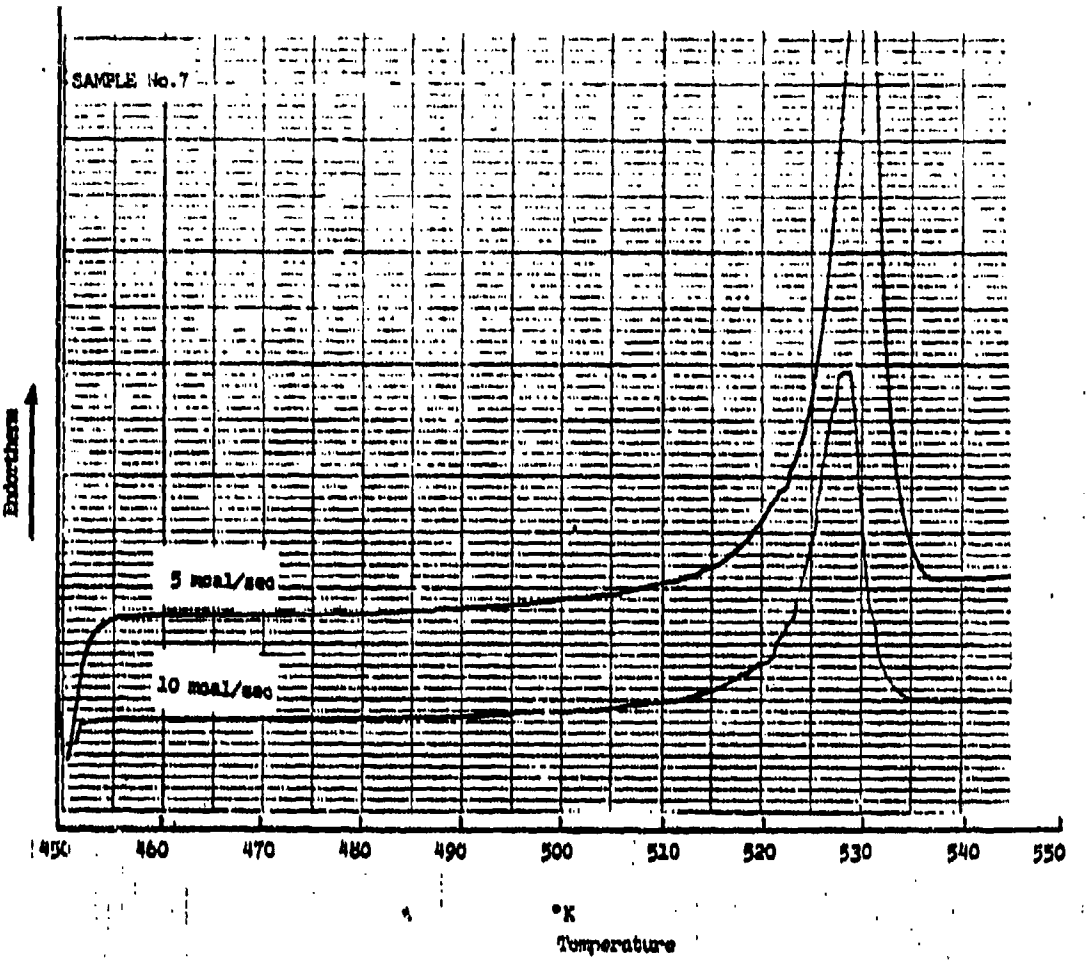

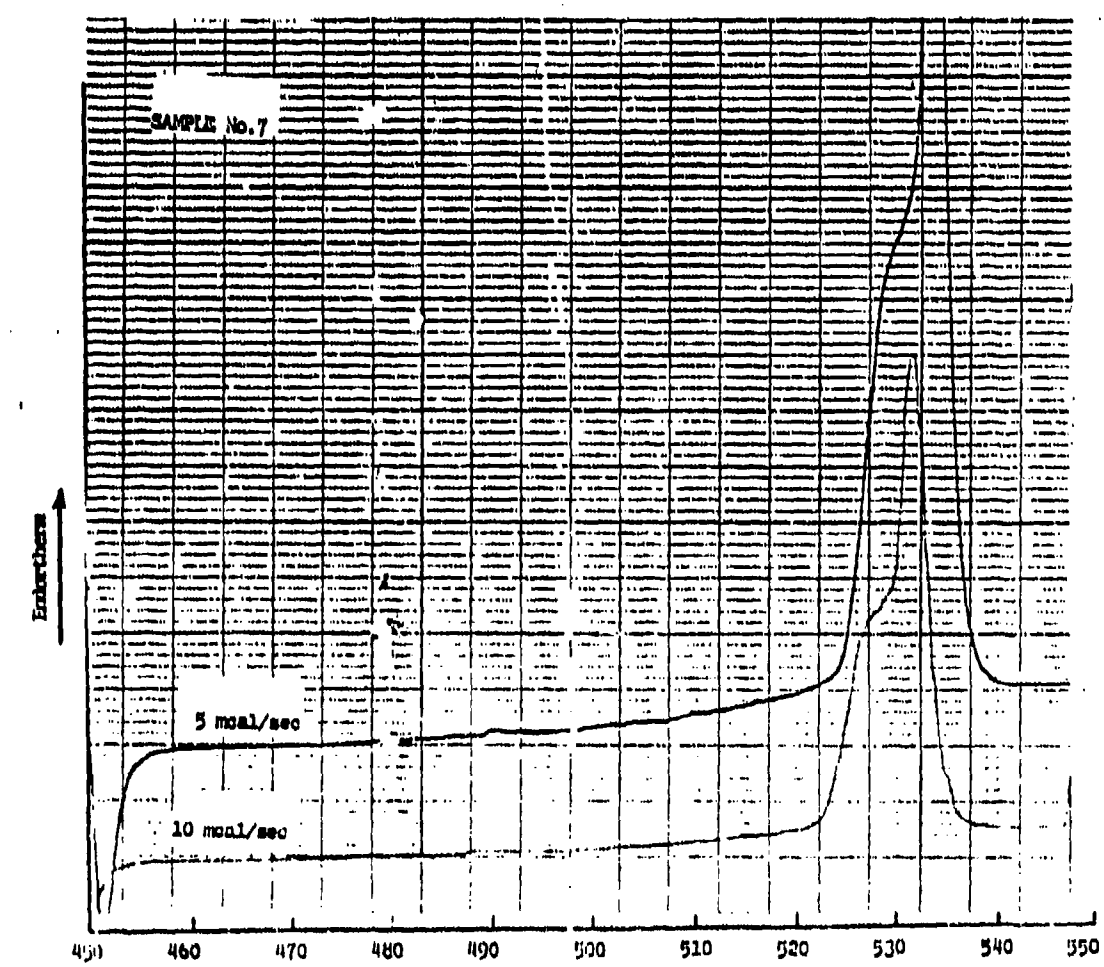

FIG. 3.24D DSC THERMOGRAMS

FIG. 3.24E DSC THERMOGRAMS

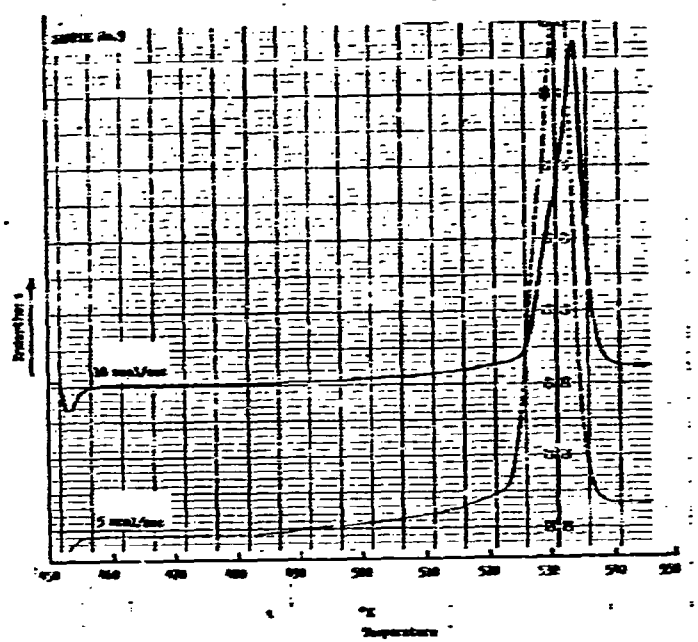

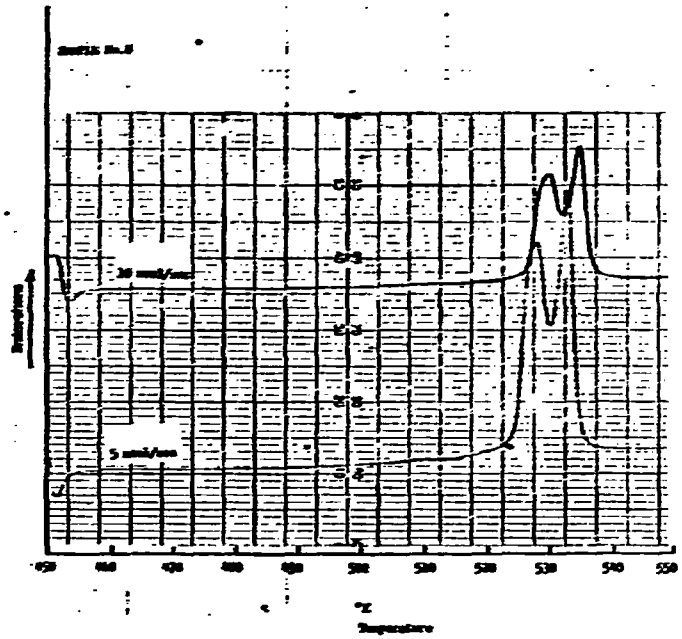

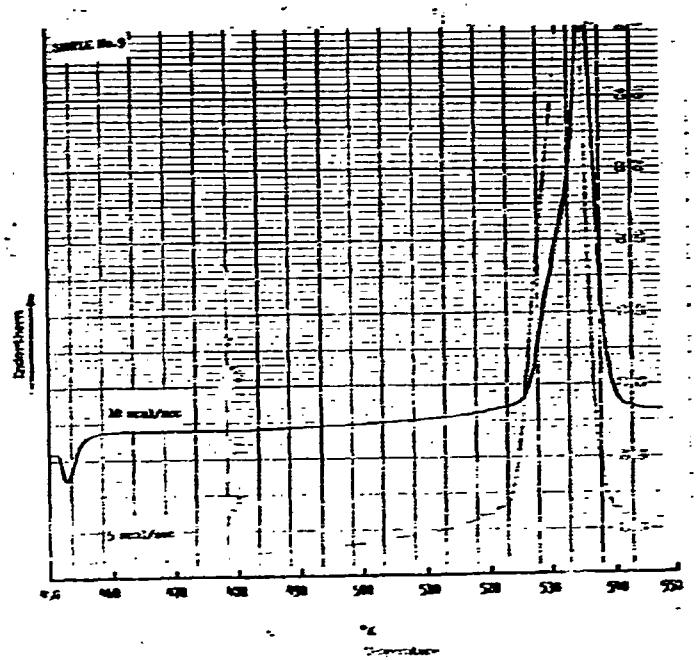

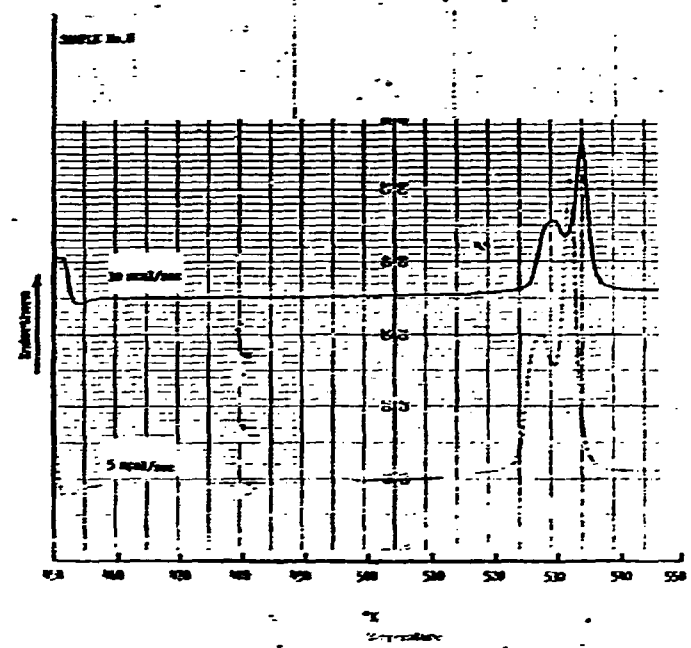

FIG. 3.24F DSC THERMOGRAMS

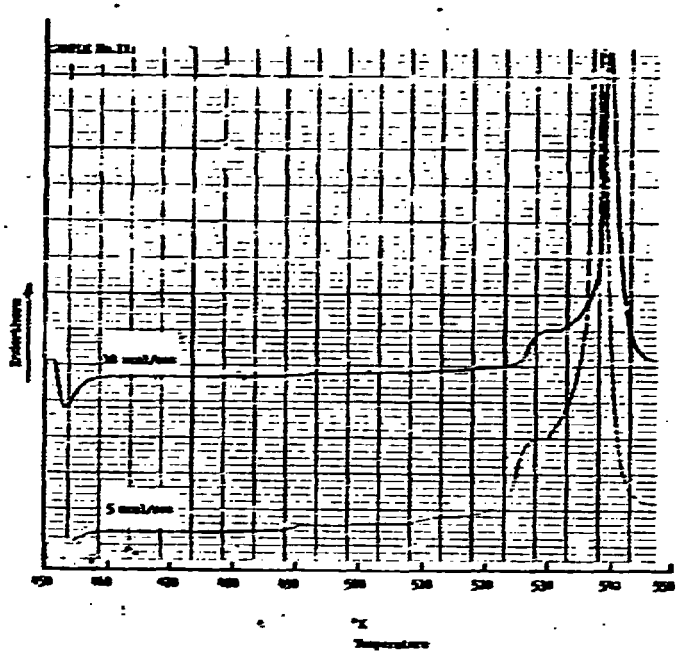

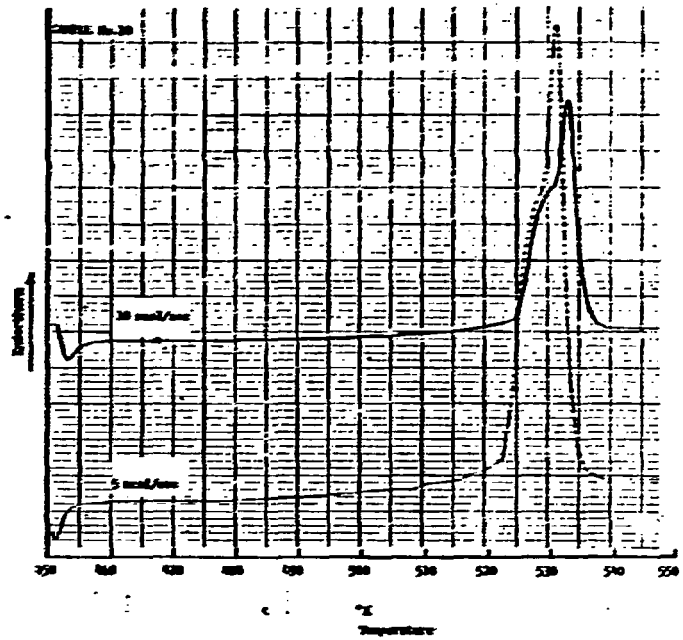

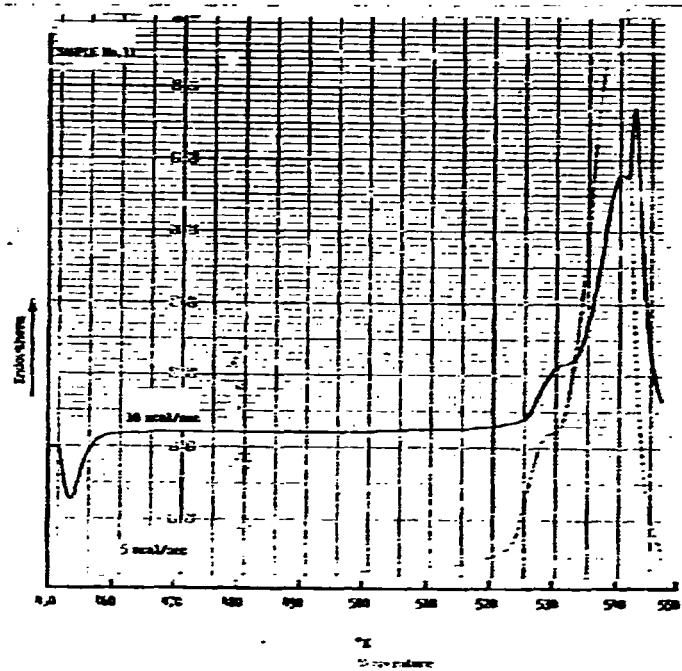

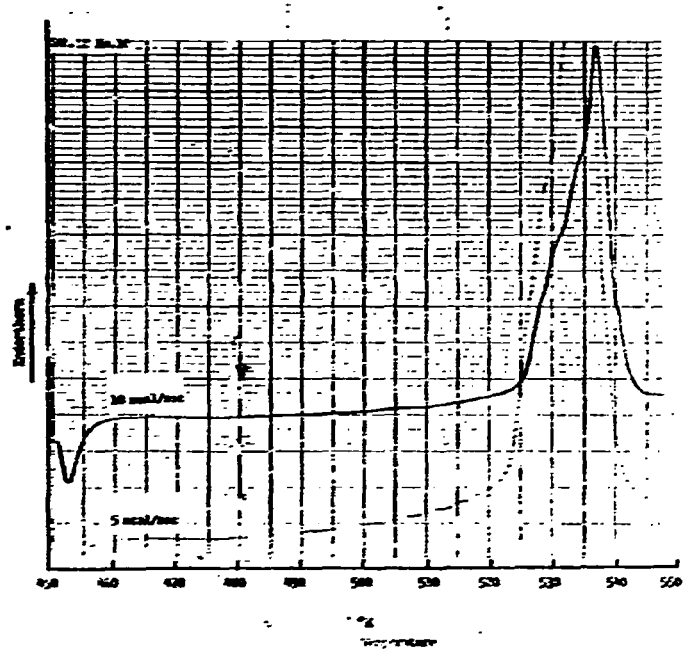

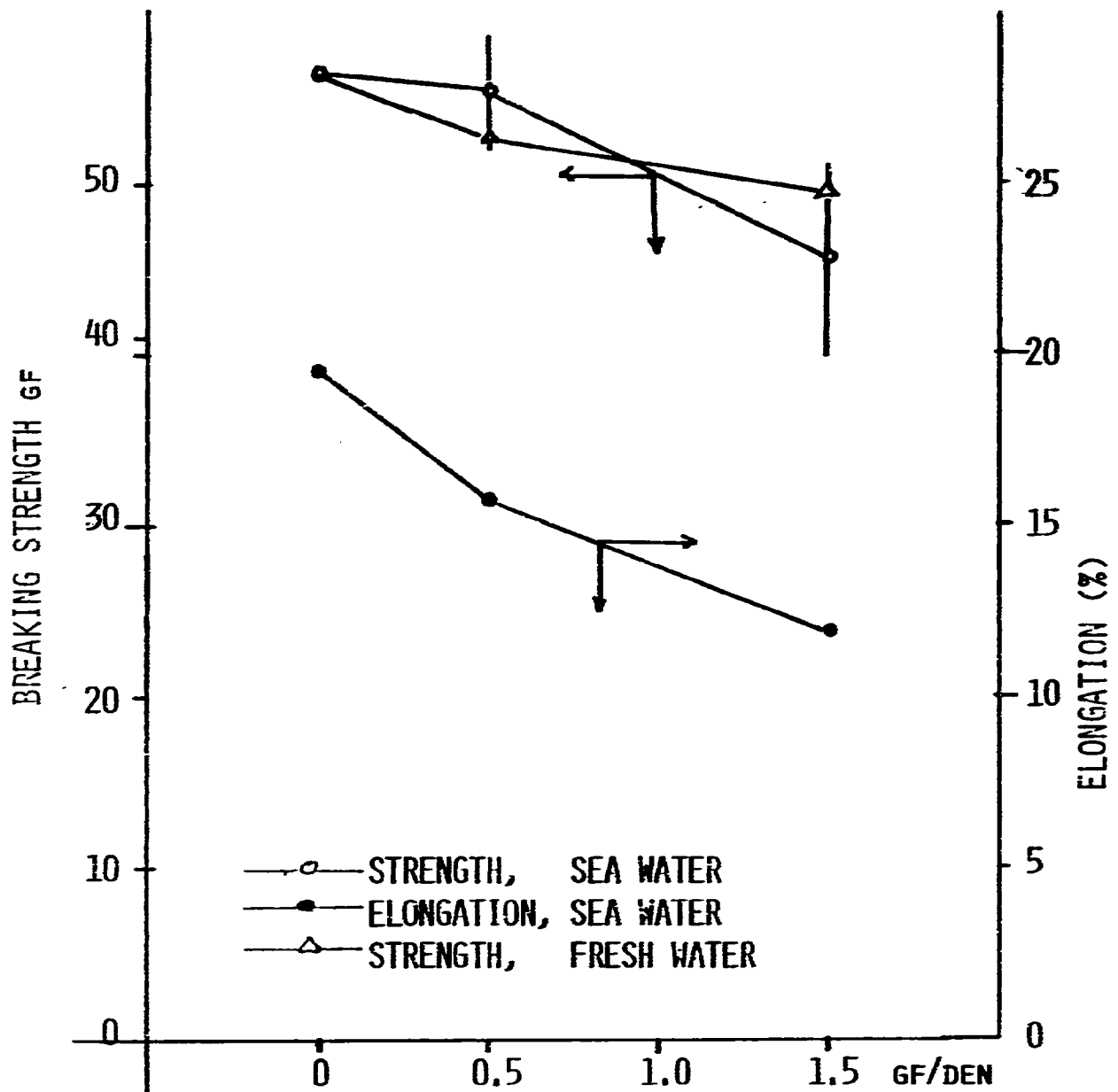

FIG. 3.25 PROPERTIES OF NYLON 66 AFTER SEA WATER IMMERSION FOR 50 HOURS

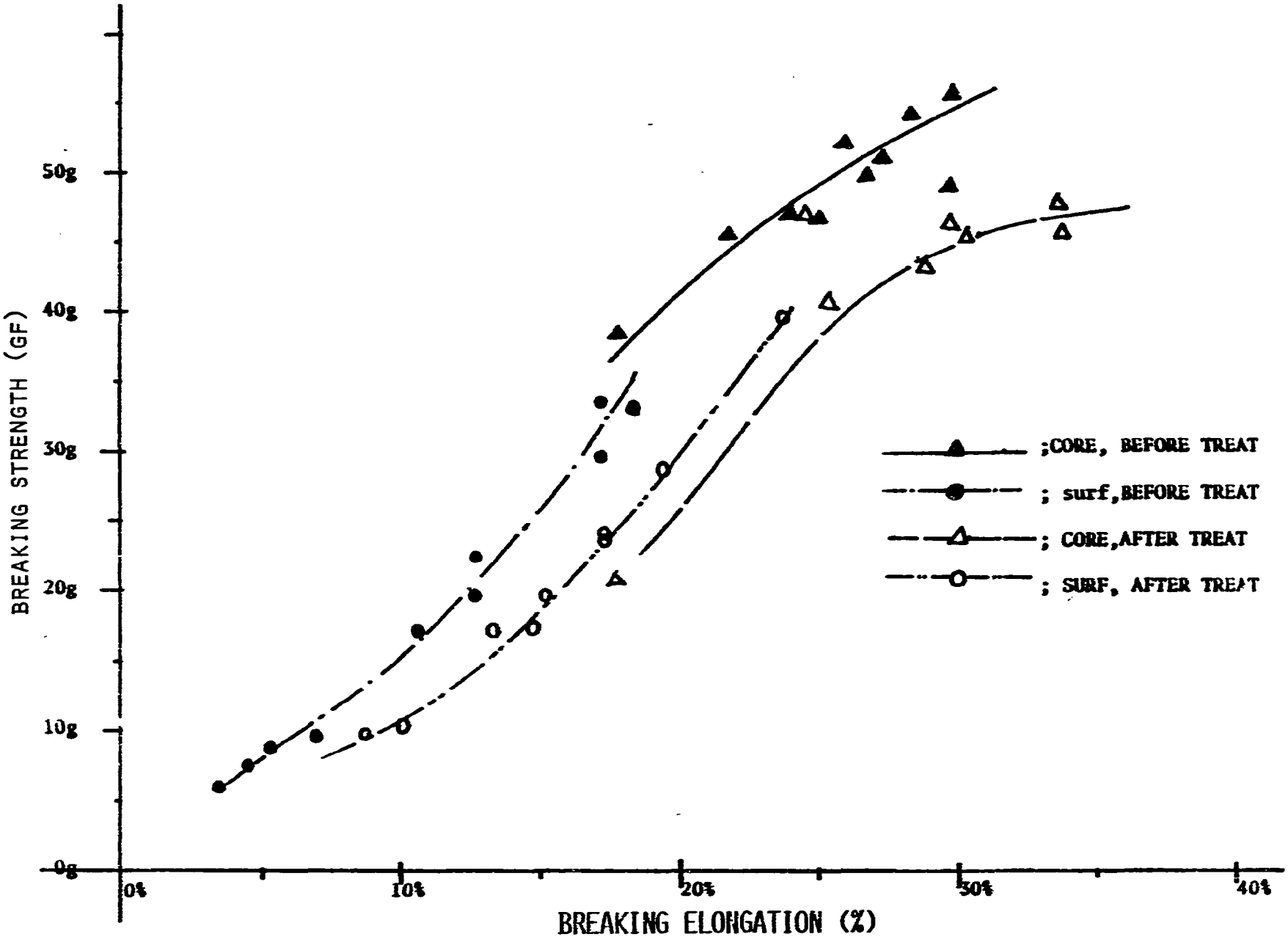

FIG. 3.26 BREAKING STRENGTHS AND ELONGATION OF FILAMENTS OF ROPE 2-D BEFORE AND AFTER HOT WATER TREATMENT

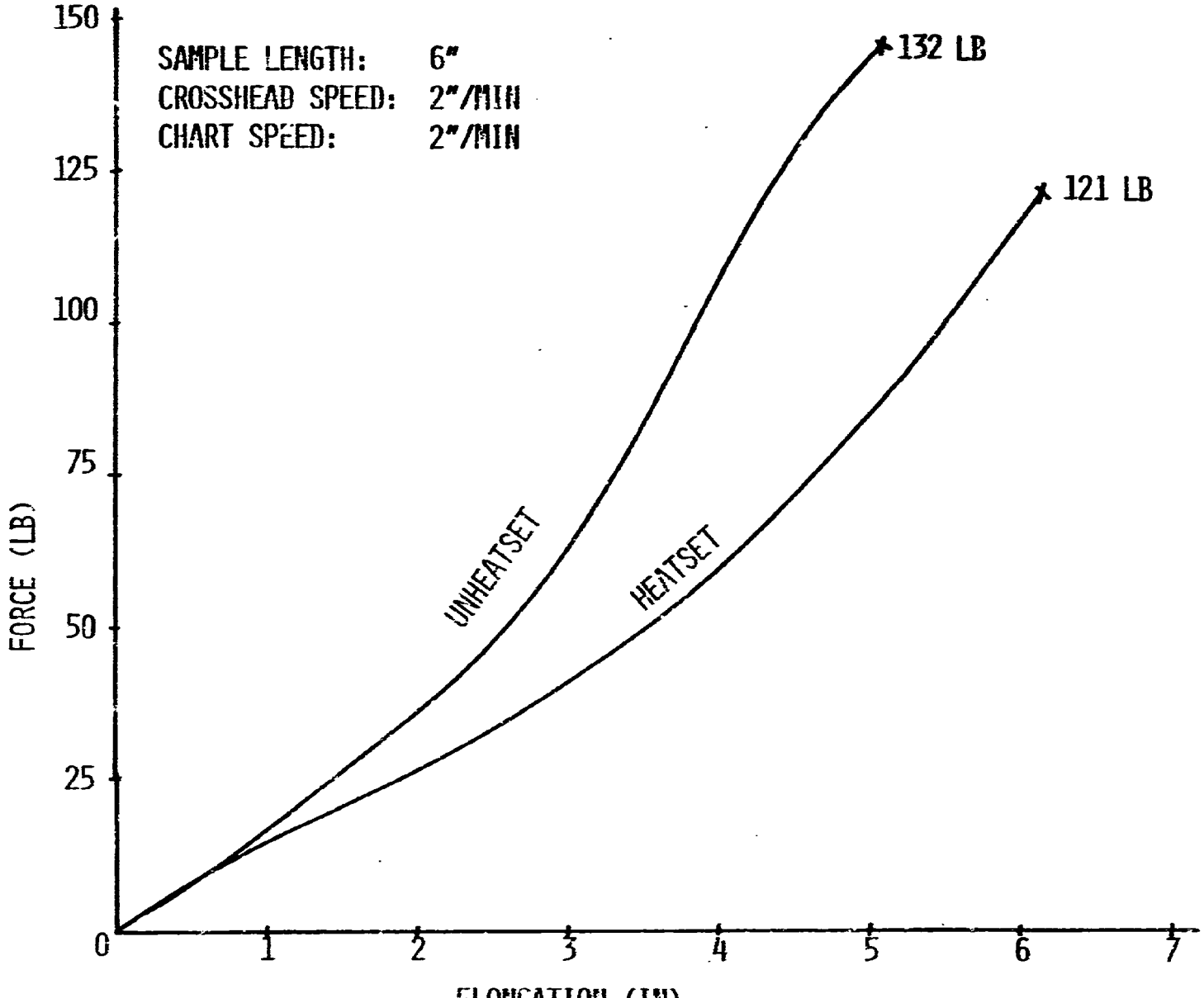

FIG. 3.27 FORCE-ELONGATION CURVES OF HEATSET VS. UNHEATSET SINGLE YARN FROM GERMAN ROPE

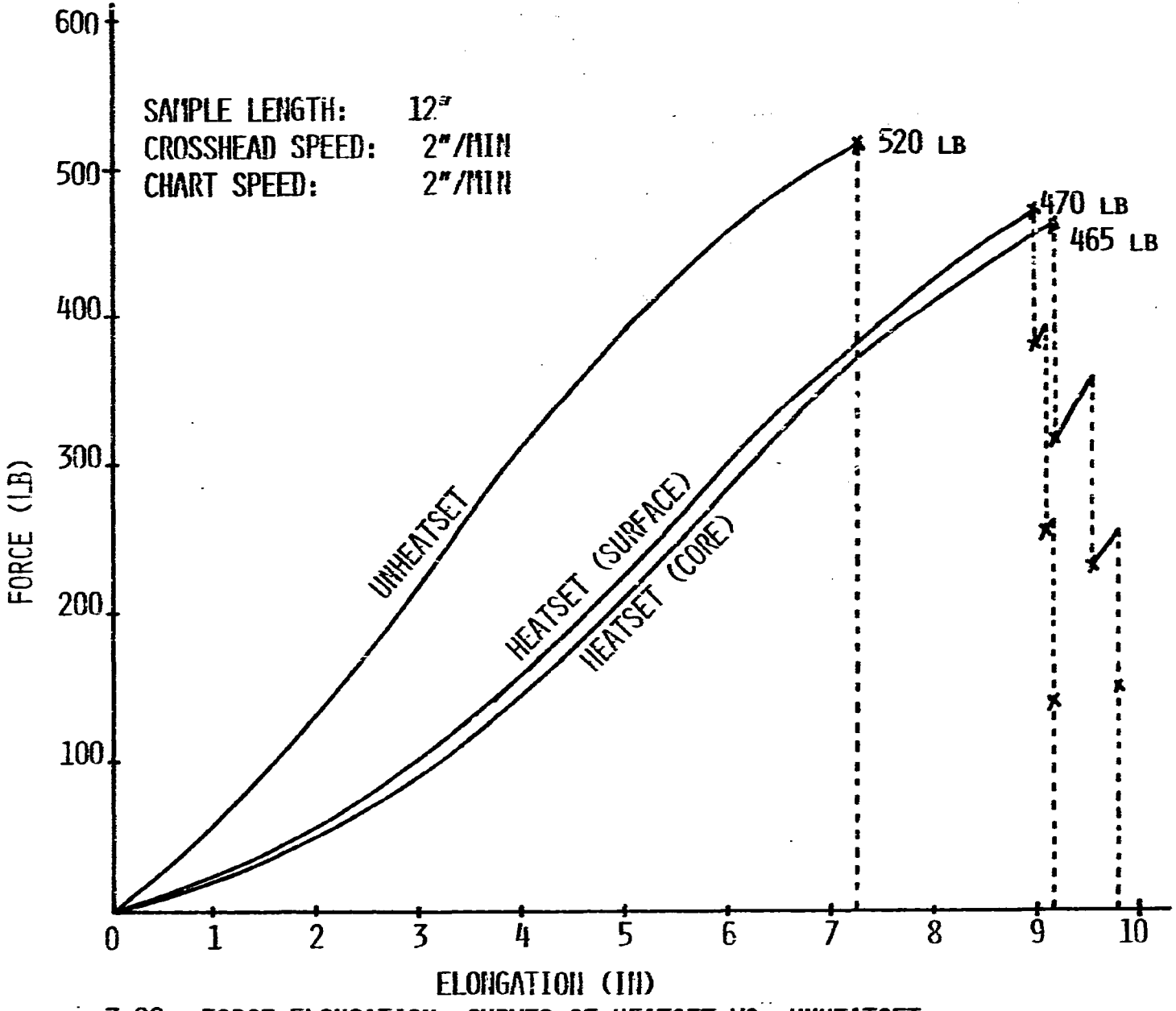

FIG. 3.28 FORCE-ELONGATION CURVES OF HEATSET VS. UNHEATSET 4-PLY YARNS FROM GERMAN ROPE

FIG. 3.29 HEAT SHRINKAGE OF FILAMENTS FROM VARIOUS LOCATIONS IN ROPE 2-D

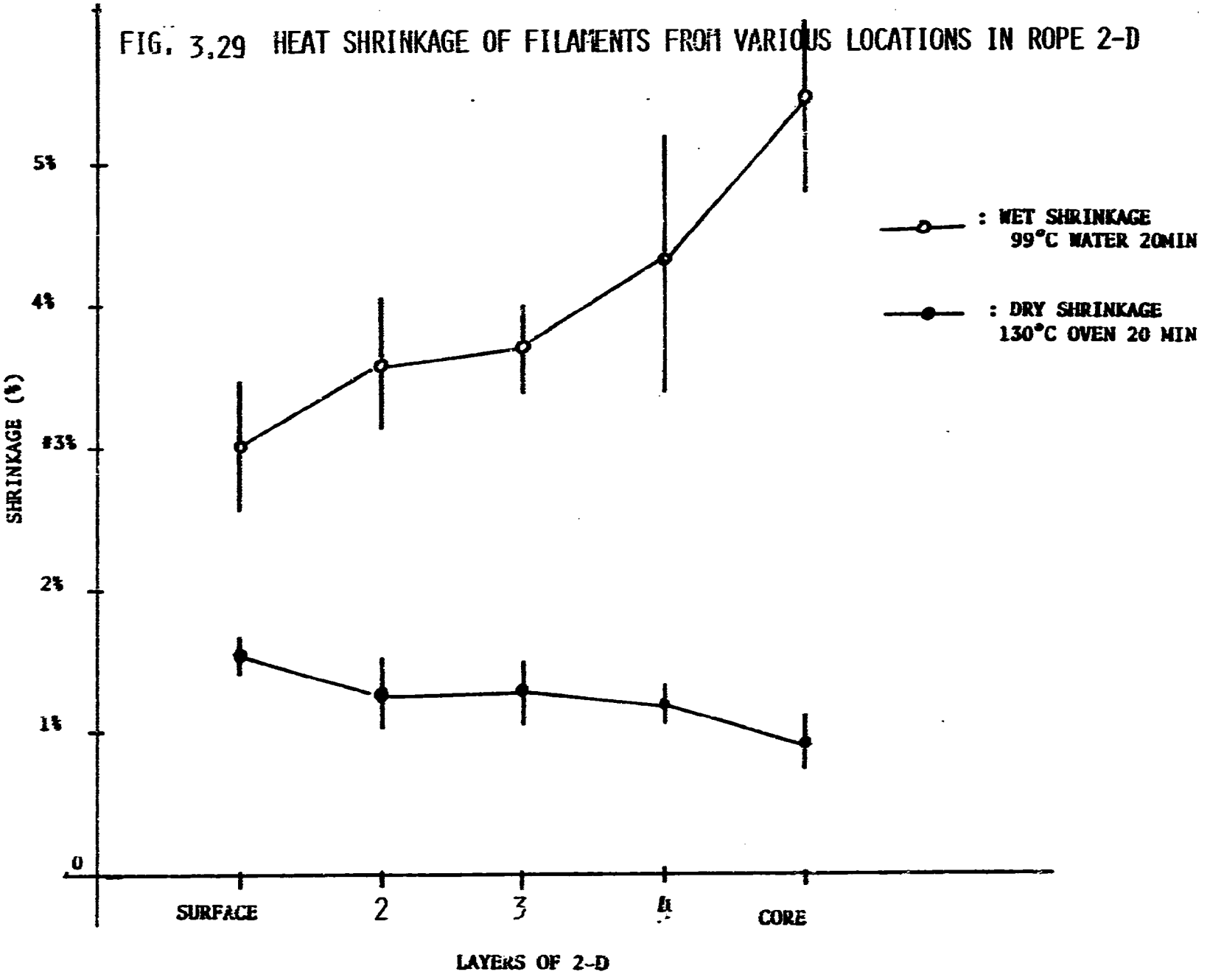

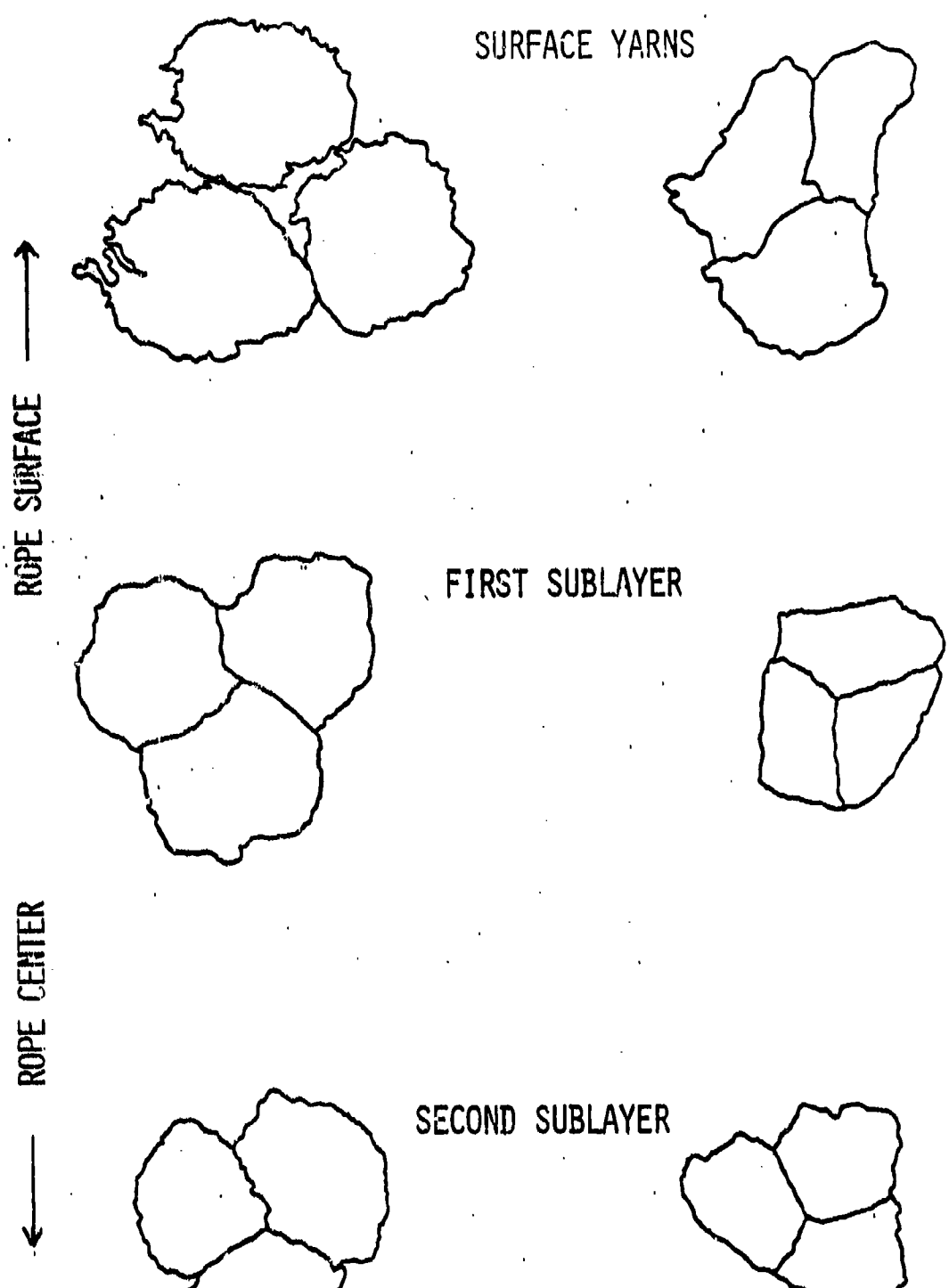

FIG. 3.30 CROSS SECTIONAL PROFILES OF PLIED YARNS, ROPE #4

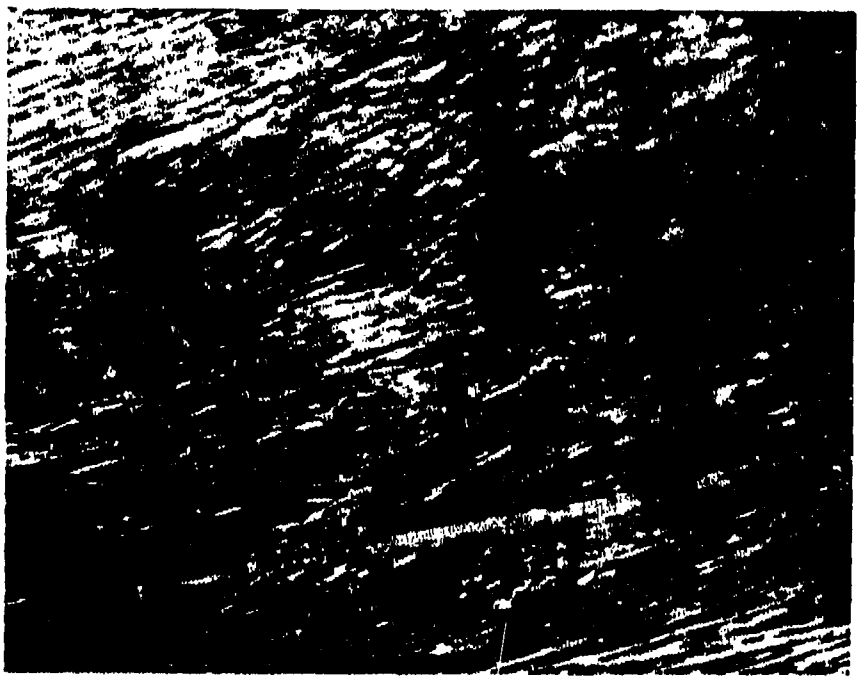

(A)

(B)

FIG. 3.31 LONGITUDINAL VIEW OF HARD SPOT IN ROPE #4
(A) 50X, (B) 300X

(A)

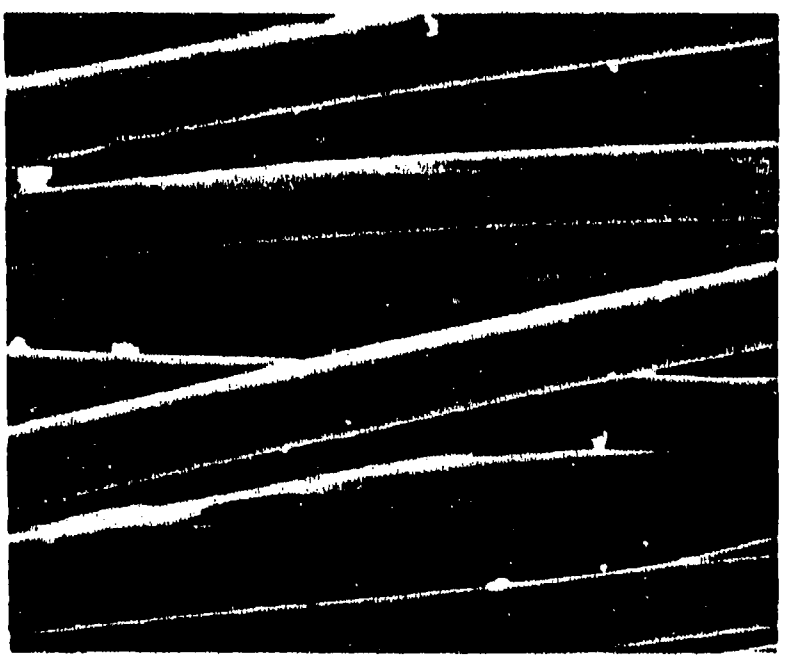

(B)

FIG. 3.32 LONGITUDINAL VIEW OF SOFT SPOT IN ROPE #4
(A) 50X, (B) 300X

(A)

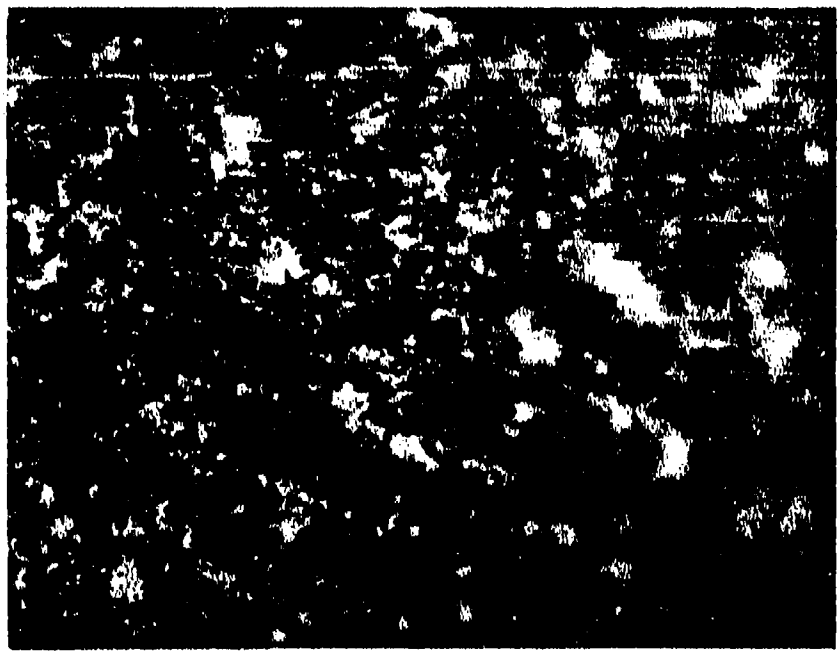

(B)

FIG. 3.33 VIEW OF ABRADED FACE OF PLIED YARN IN HARD SPOT, ROPE #4
(A) 20X; (B) 50X

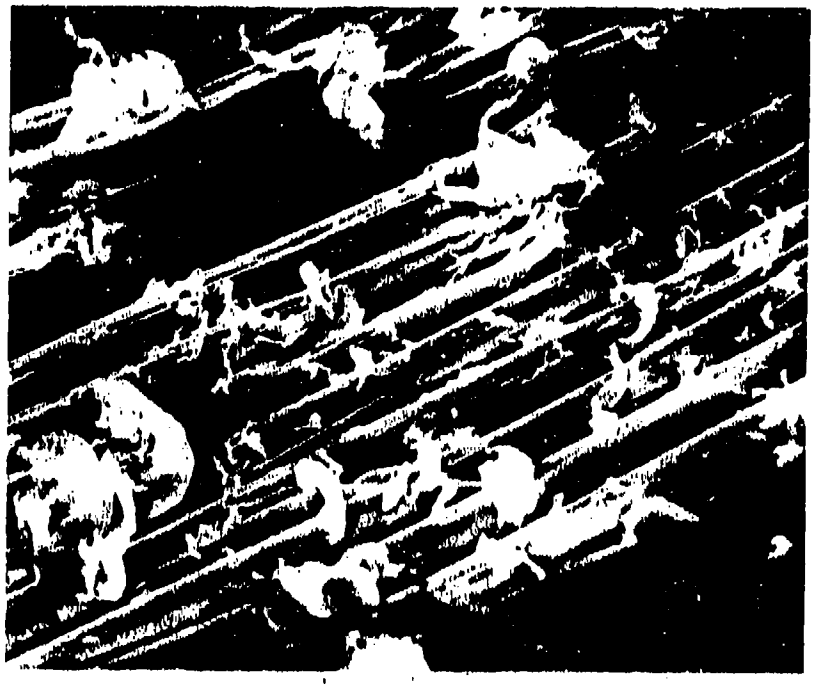

(A)

(B)

FIG. 3.34 DETAILS OF THE ABRADED AREA IN HARD ZONE OF SAMPLE 4-E, (A) 300X, (B) 1,000X

FIG. 3.35 SHOWS CREASED EDGES ALONG LENGTH IN PLIED YARN OF HARD ZONE ROPE #4

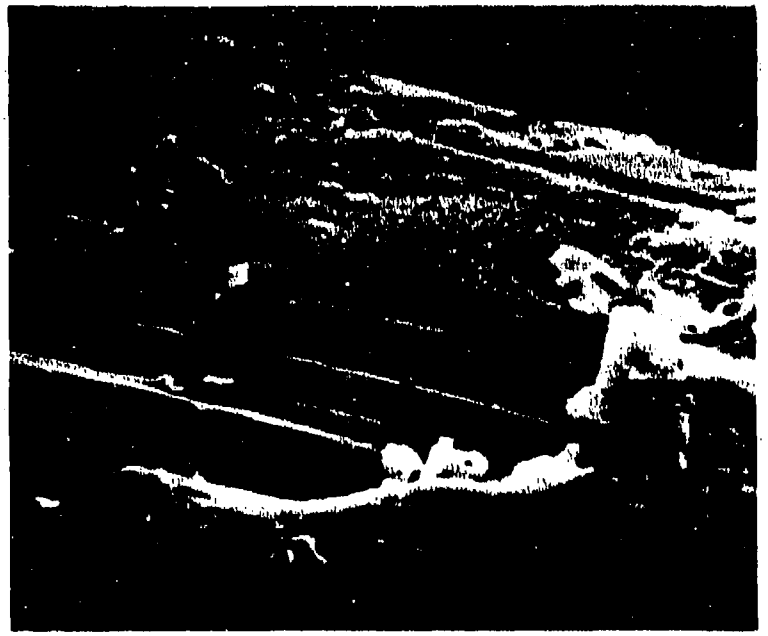

A

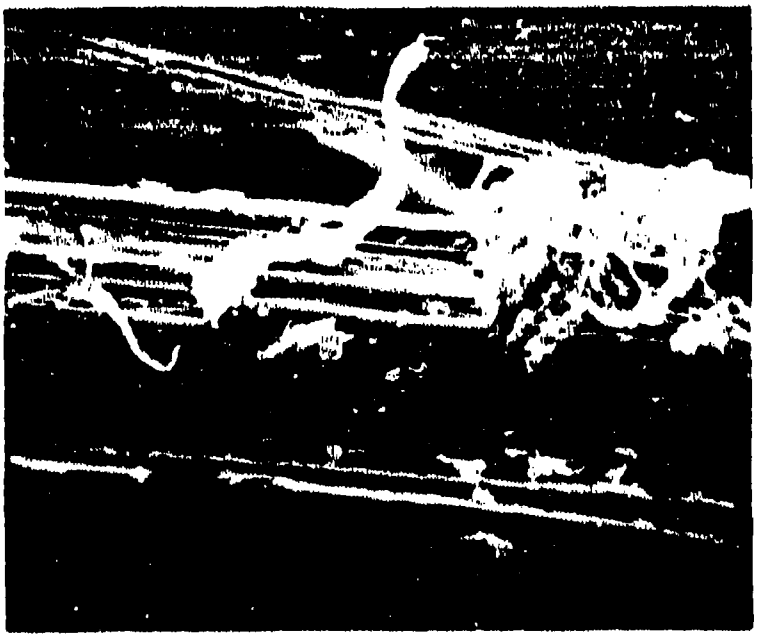

B

FIG. 3.36A, B AXIAL GOUGES ALONG SURFACE FILAMENTS DUE TO ASPERITY ABRASION

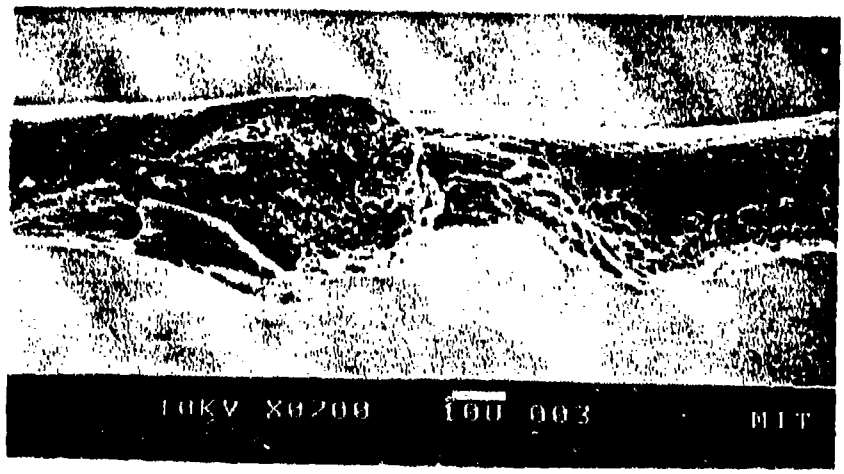

C

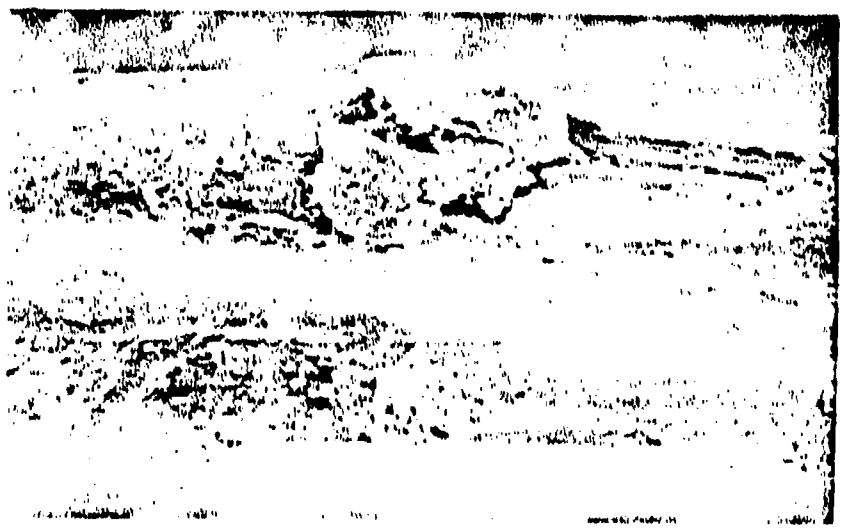

D

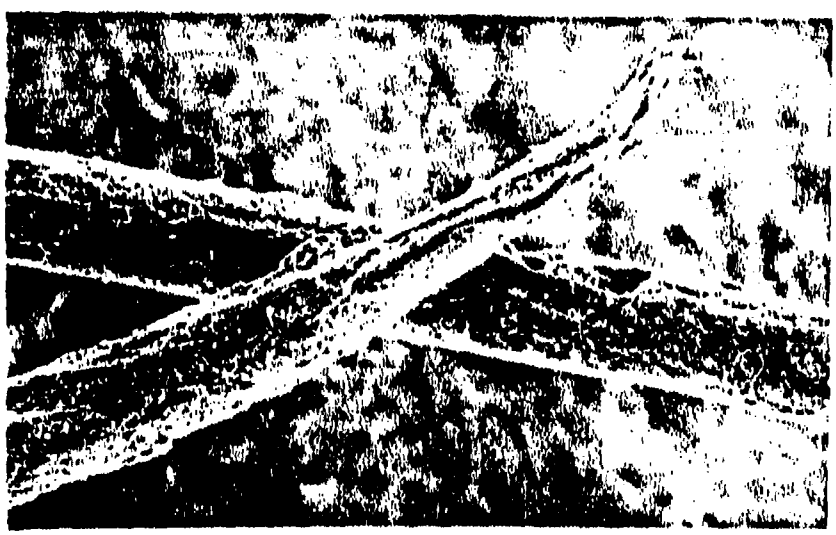

E

FIGURE 3.36C,D,E AXIAL GOUGES ALONG SURFACE FILAMENTS DUE TO ASPERITY ABRASION

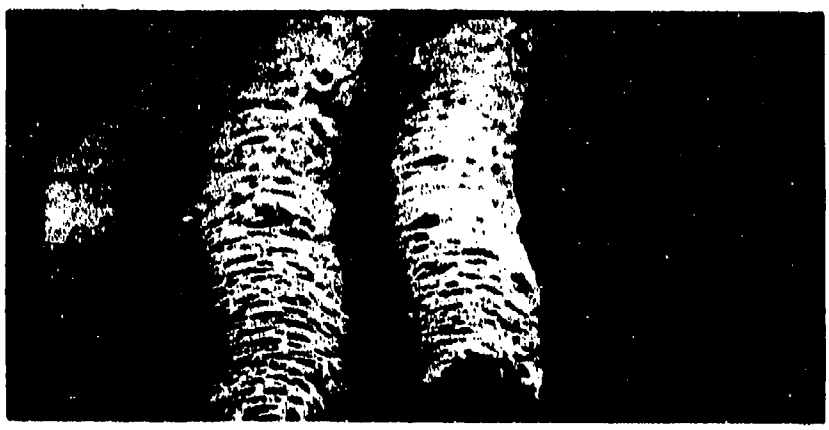

A

B

C

FIG. 3.37A,B,C DISINTEGRATED FIBER ENDS FROM WORN ROPES

D

E

FIG. 3.37D,E DISINTEGRATED FIBER ENDS FROM WORN ROPES

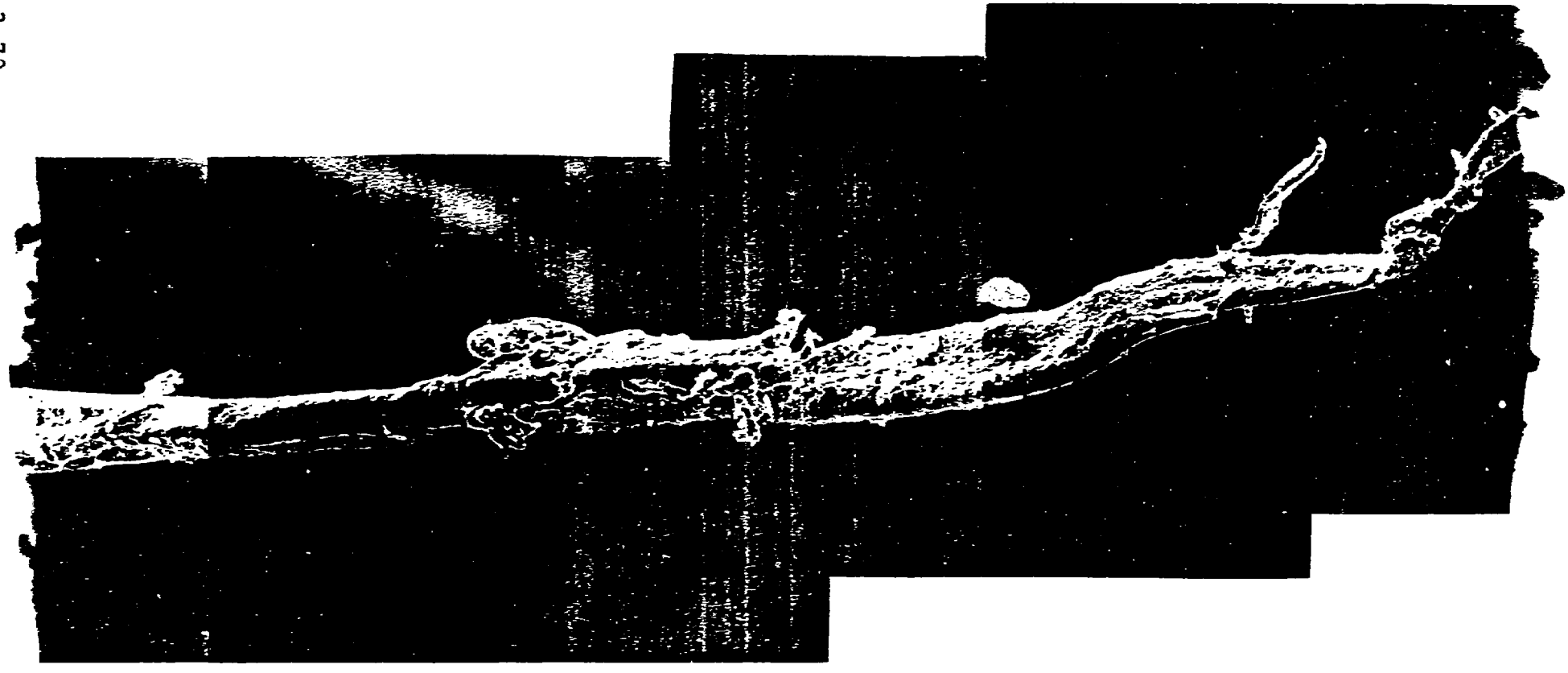

FIG. 3.37F DISINTEGRATED FIBER ENDS FROM WORN ROPES

G

FIG. 3.37G DISINTEGRATED FIBER ENDS FROM WORN ROPES

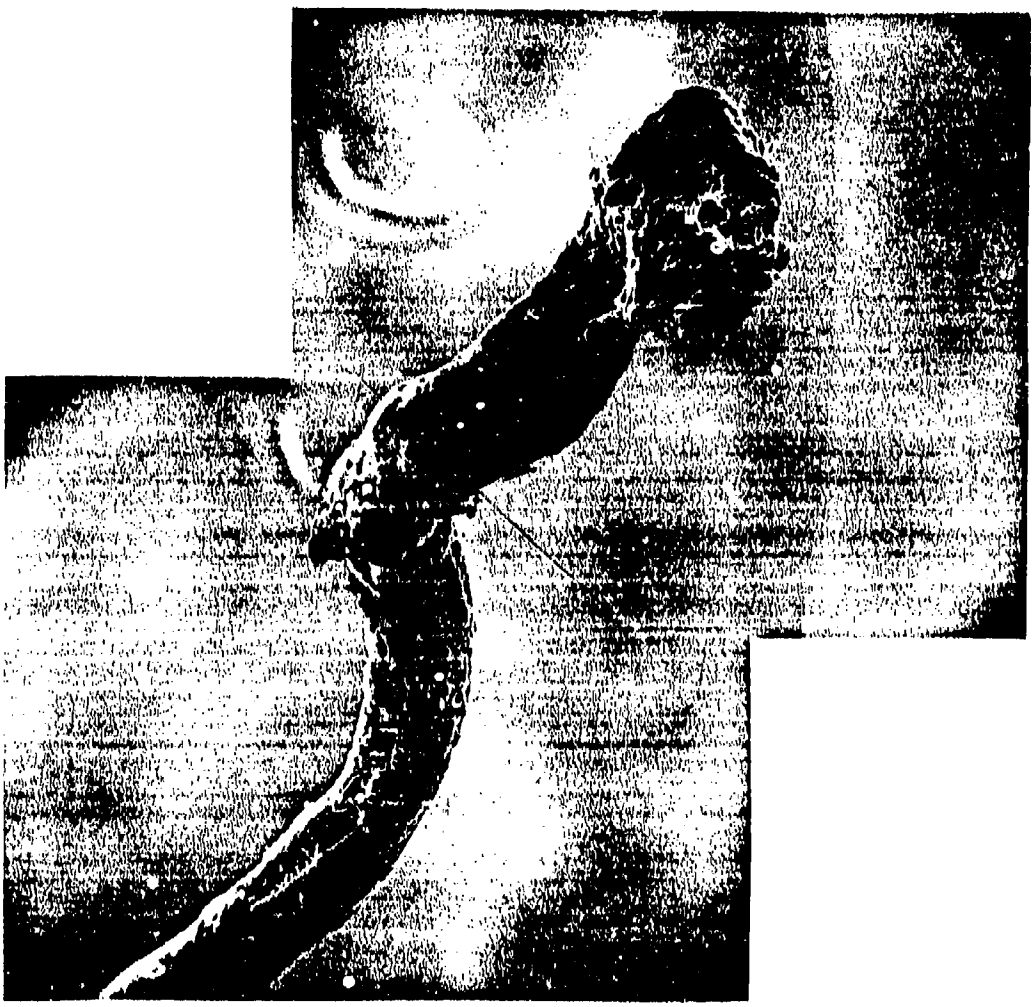

H

FIG. 3.37H DISINTEGRATED FIBER ENDS FROM WORN ROPES

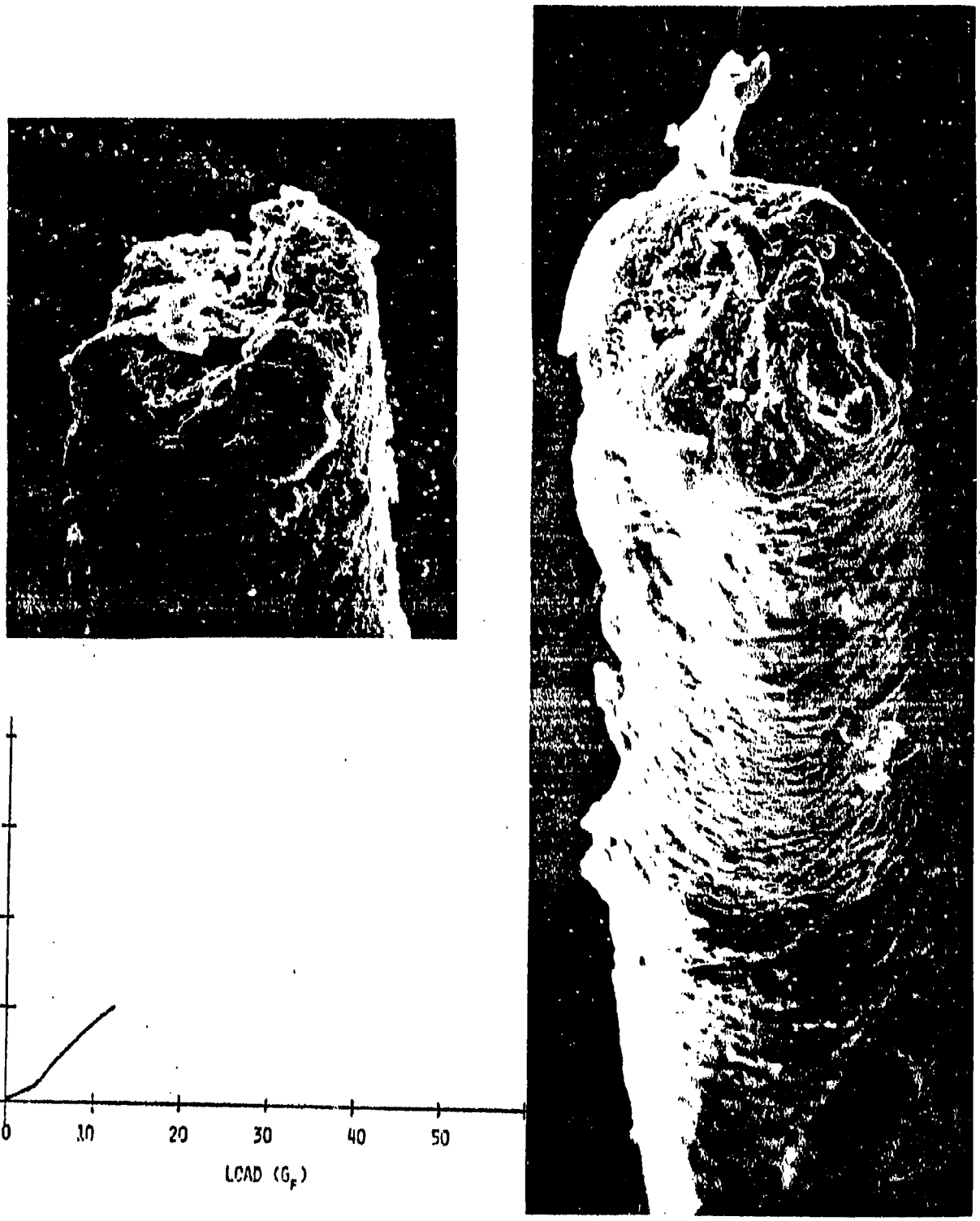

FIG. 3.38A SURFACE LAYER FIBERS FROM THE EXPOSED ZONE OF ROPE #4 (1972)

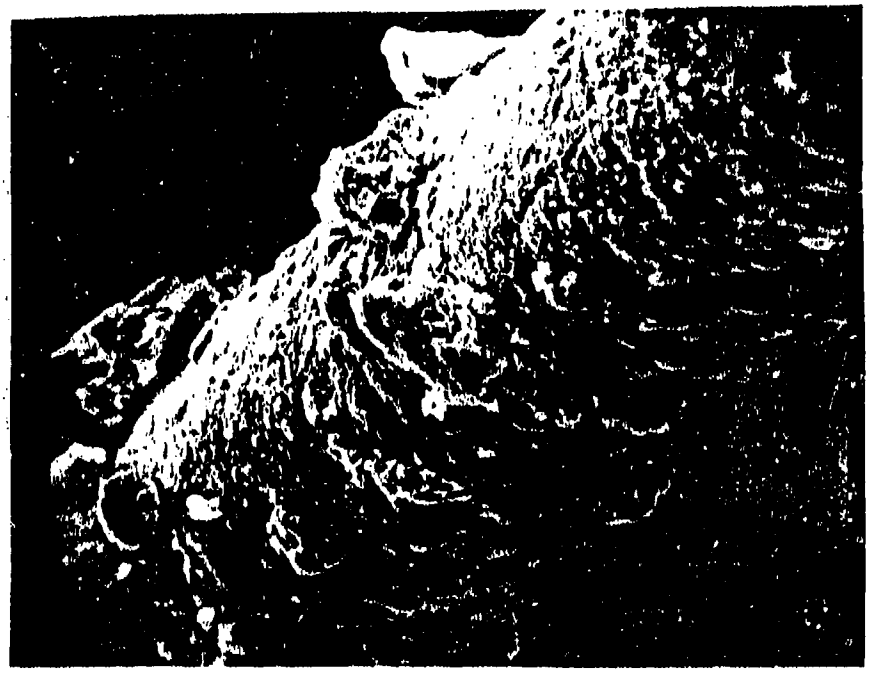

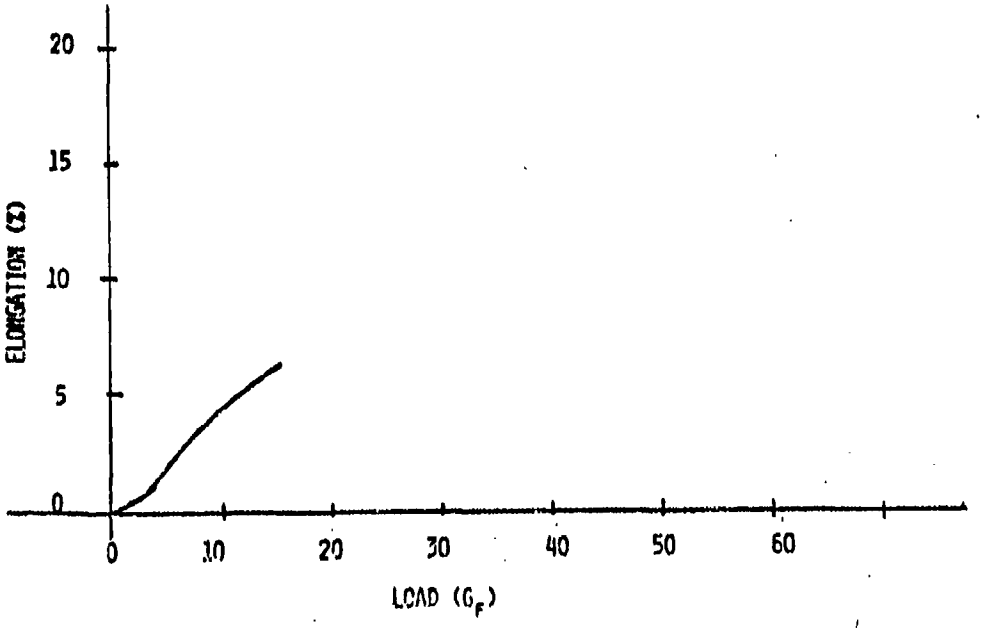

FIG. 3.38B SURFACE LAYER FIBERS FROM THE EXPOSED ZONE OF ROPE #4 (1972)

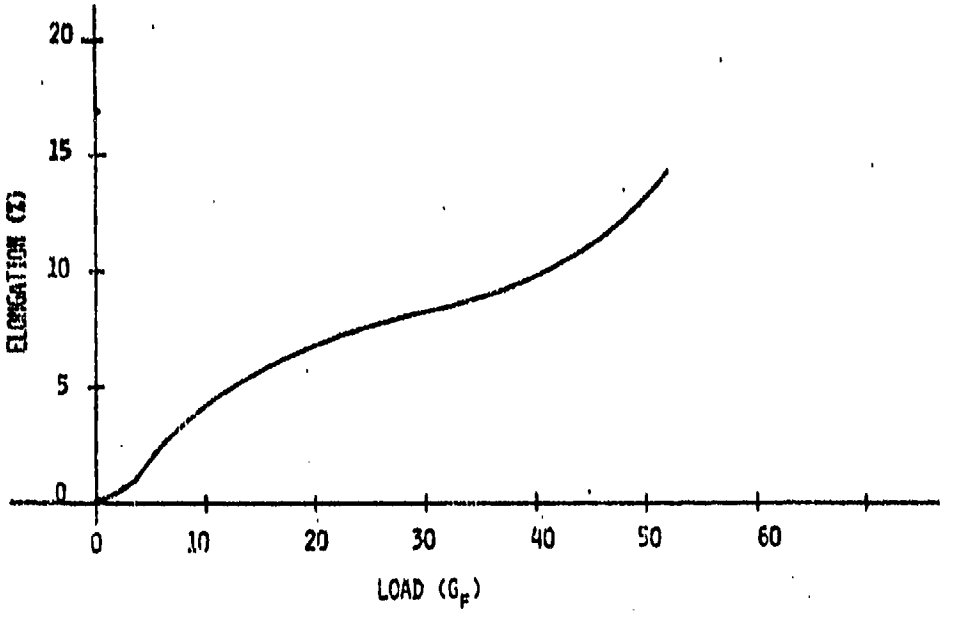

FIG. 3.39A SURFACE LAYER FIBERS FROM THE PROTECTED ZONE OF ROPE #4 (1972)

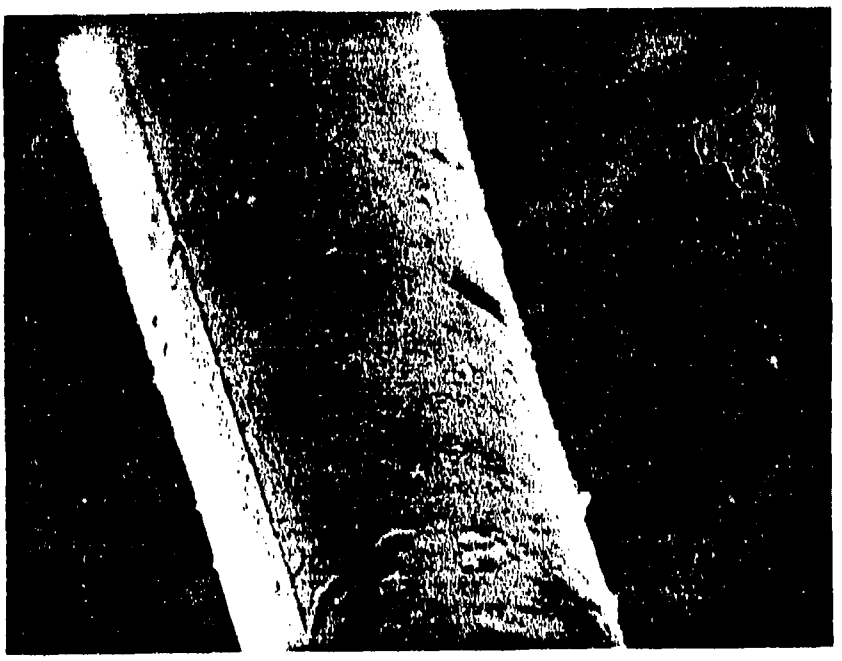

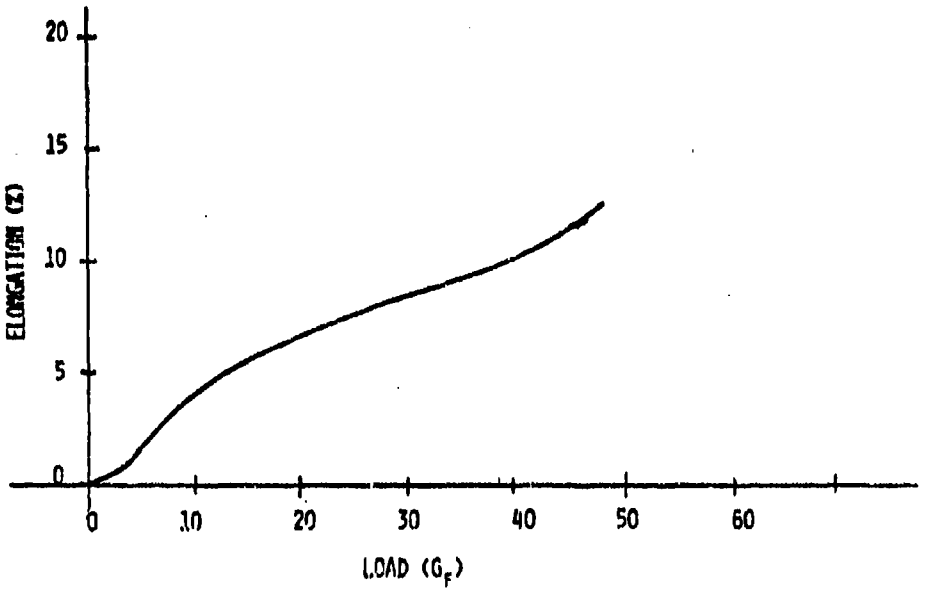

FIG. 3.39B SURFACE LAYER FIBERS FROM THE PROTECTED ZONE OF ROPE #4 (1972)

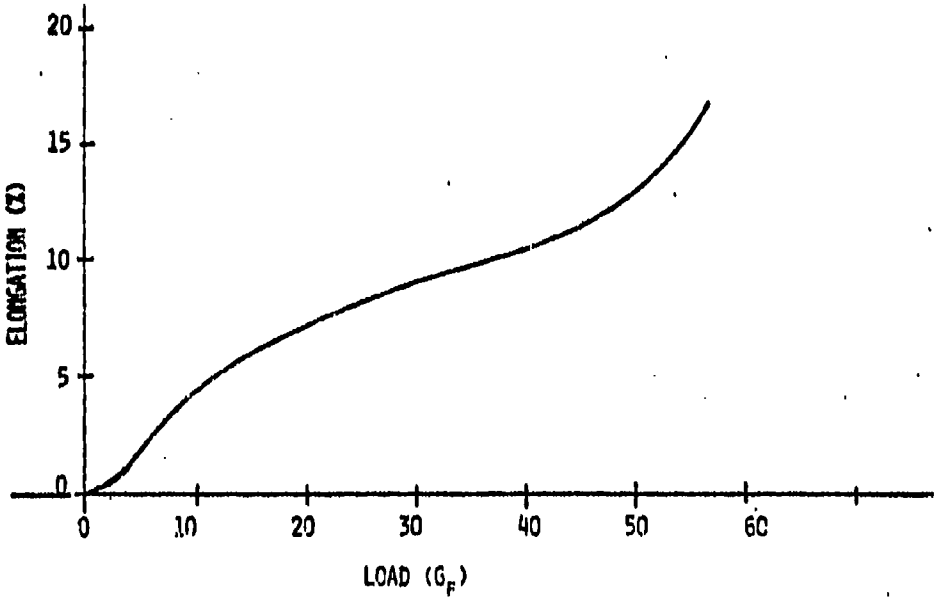

FIG. 3.40A SUBSURFACE LAYER FIBERS FROM THE EXPOSED ZONE OF ROPE #4 (1972)

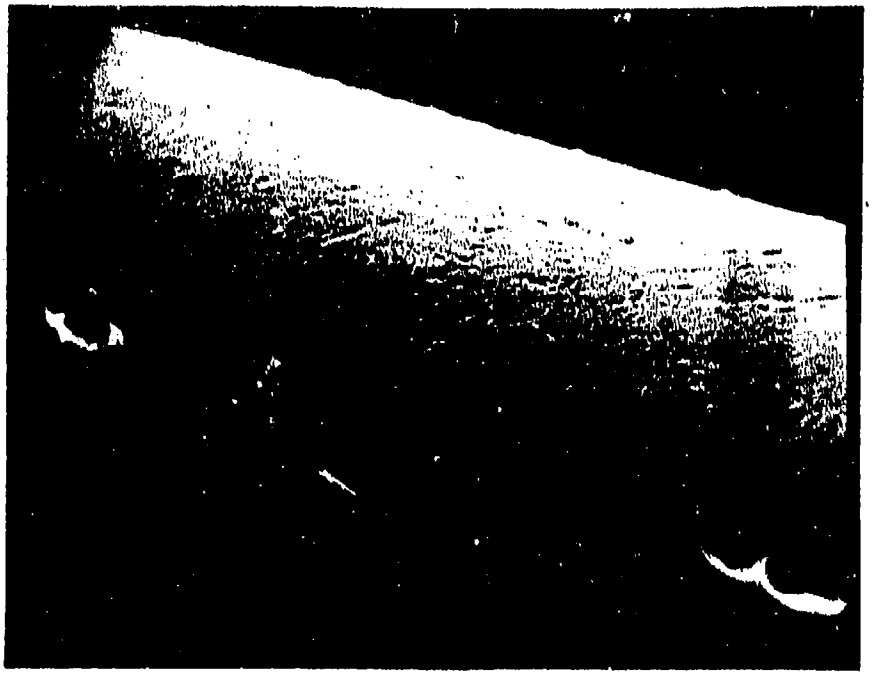

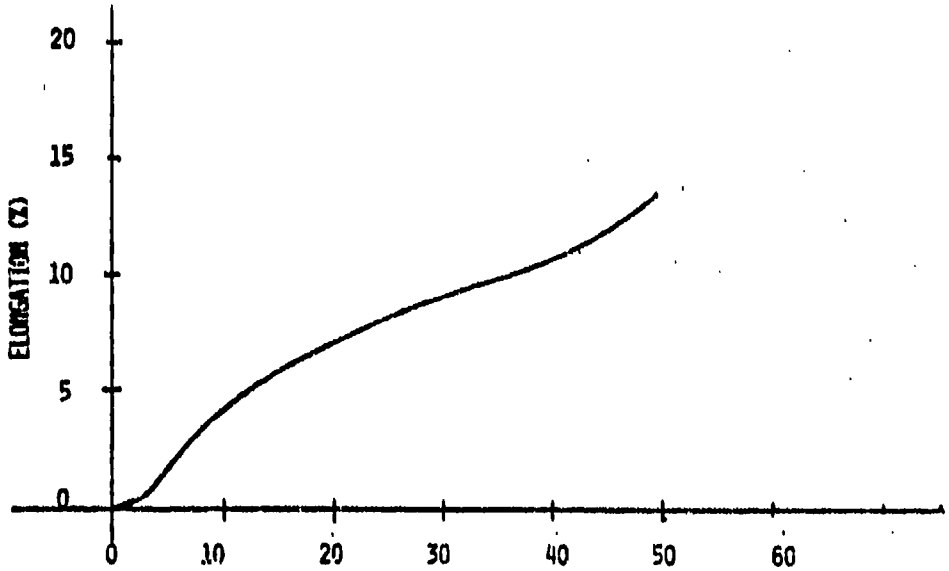

FIG. 3.40B SUBSURFACE LAYER FIBERS FROM THE EXPOSED ZONE OF ROPE #4 (1972)

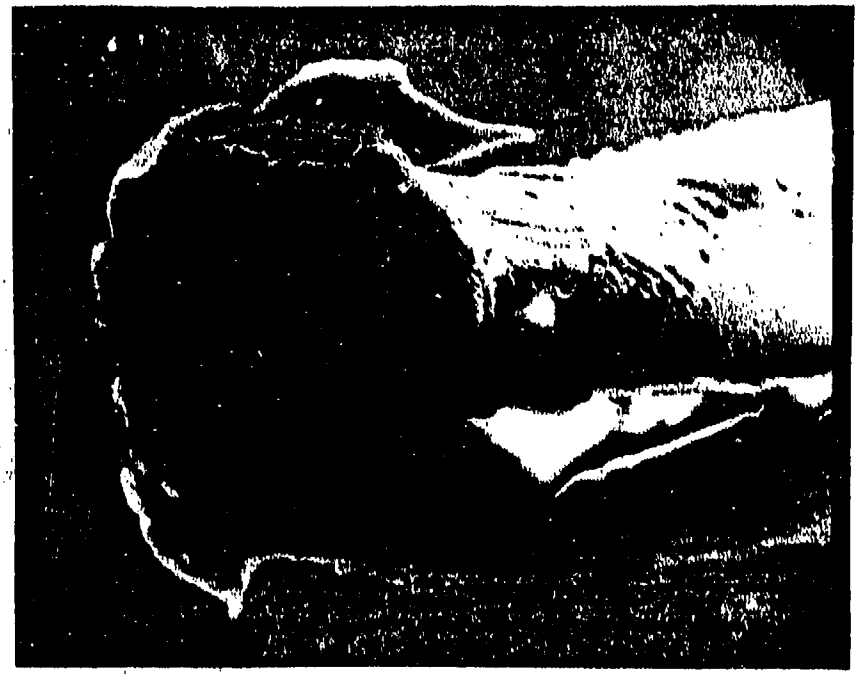

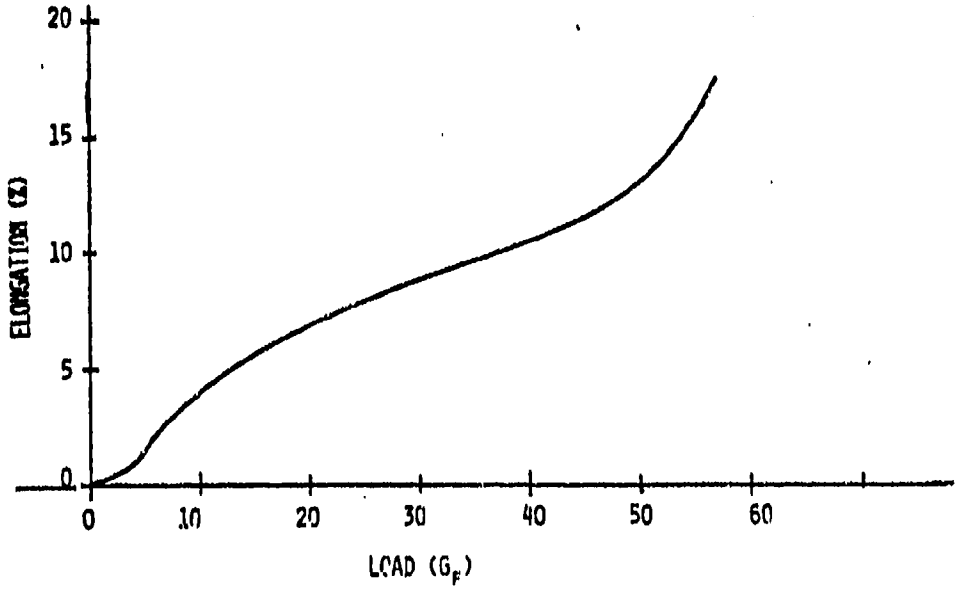

FIG. 3.41 SUBSURFACE LAYER FIBERS FROM PROTECTED ZONE OF ROPE #4 (1972)

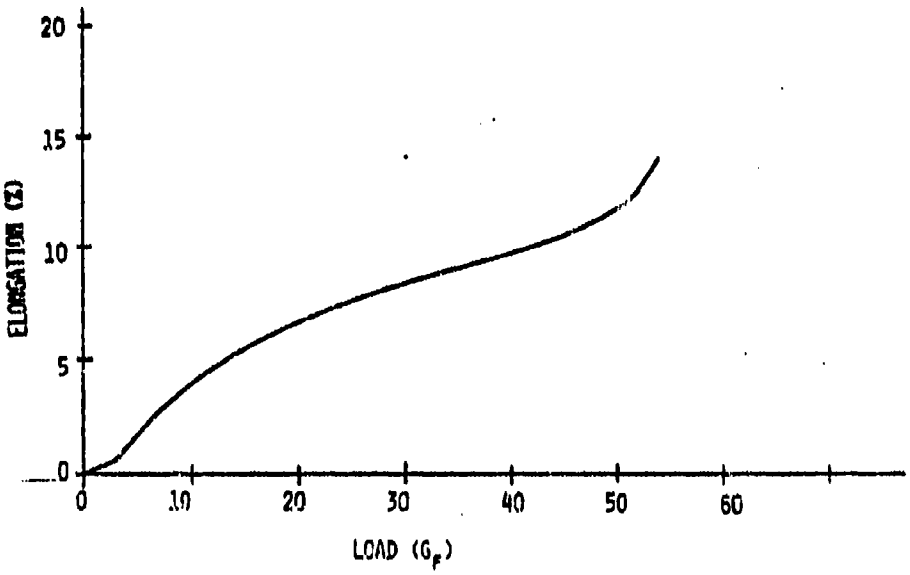

IG. 3.42 FILAMENT FROM CORE OF STRAND OF ROPE #4 (1972)

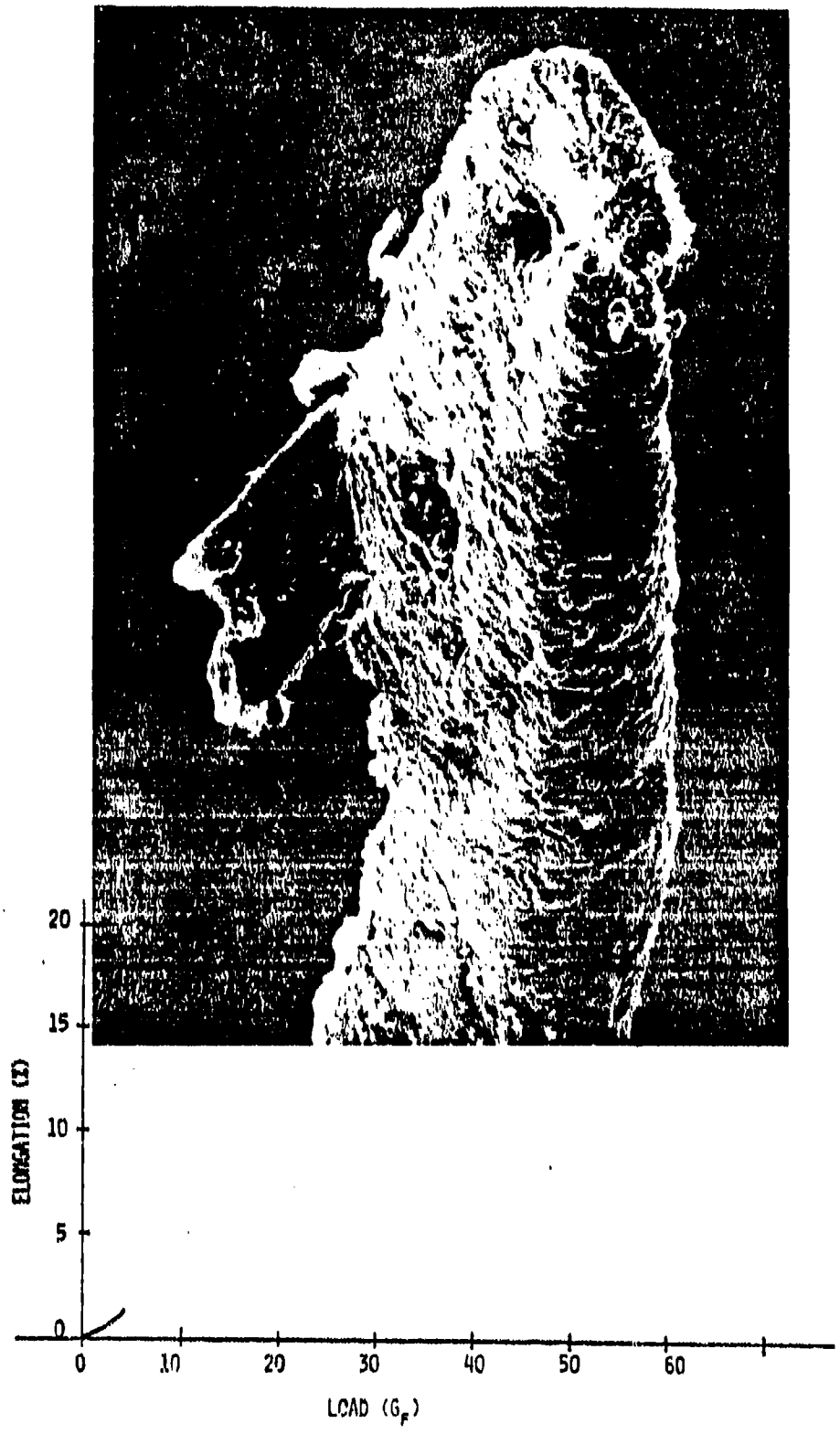

FIG. 3.43A SURFACE LAYER FIBERS FROM THE EXPOSED ZONE OF ROPE #2 (1966)

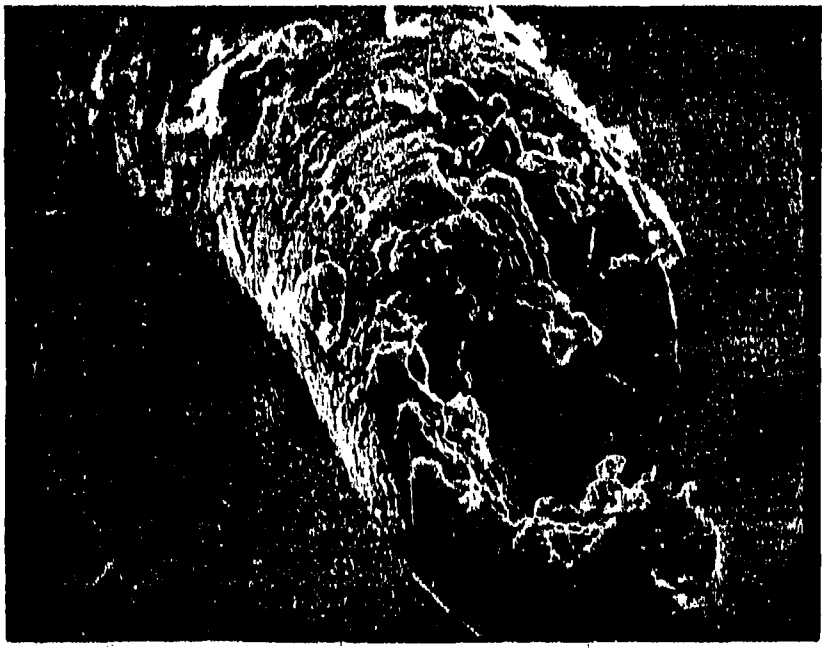

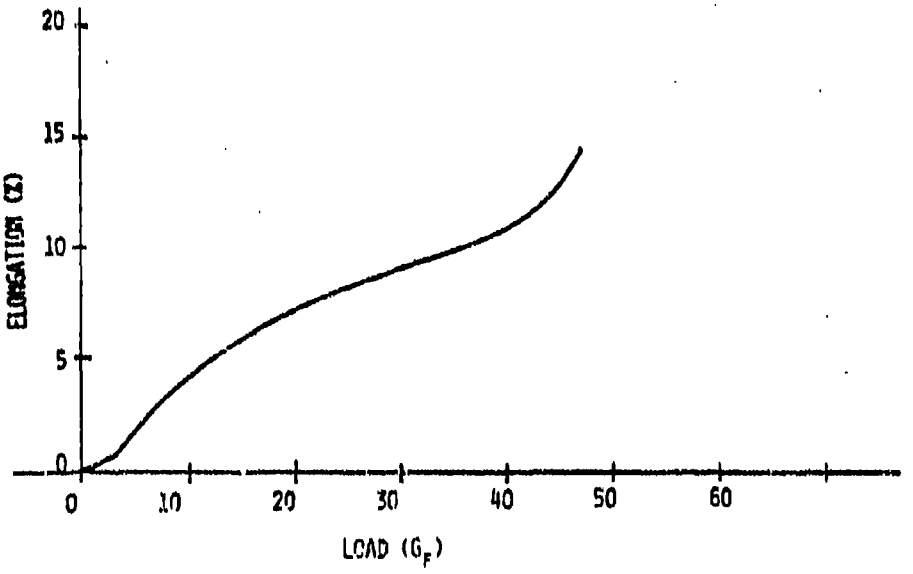

FIG. 3.43B SURFACE LAYER FIBERS FROM THE EXPOSED ZONE OF ROPE #2 (1966)

FIG. 3.44A COMPRESSED FILAMENT FROM EXPOSED SURFACE LAYERS OF ROPE #2 (1966)

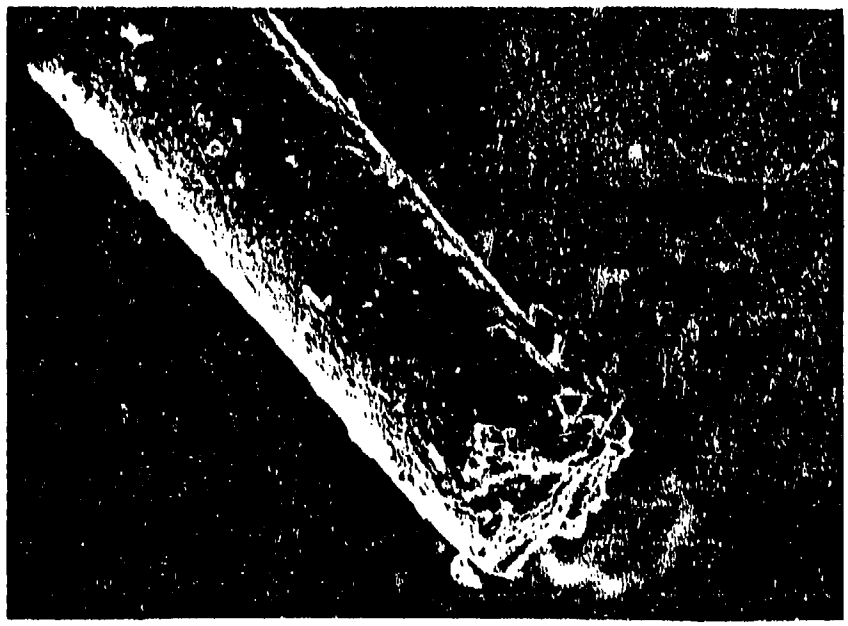

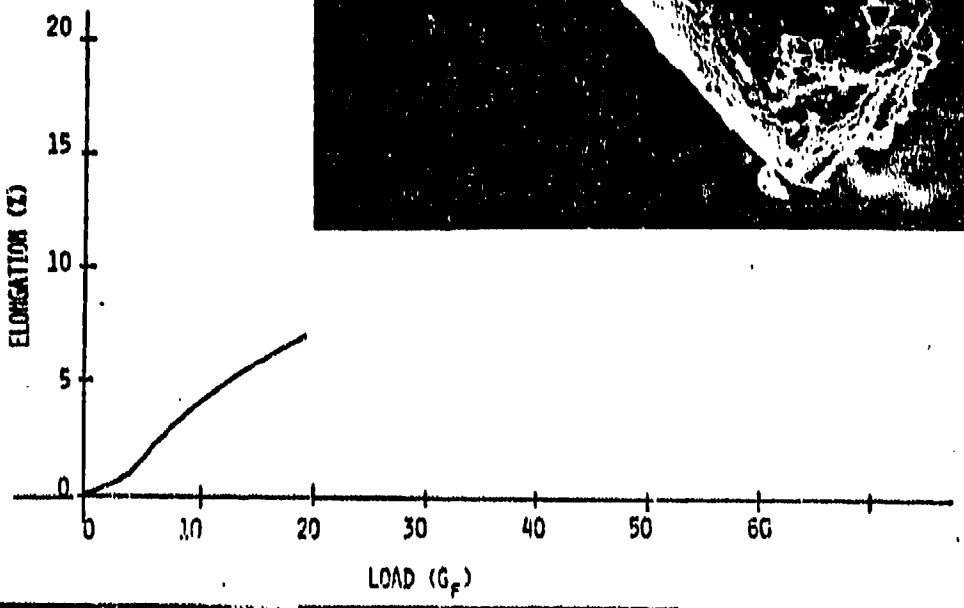

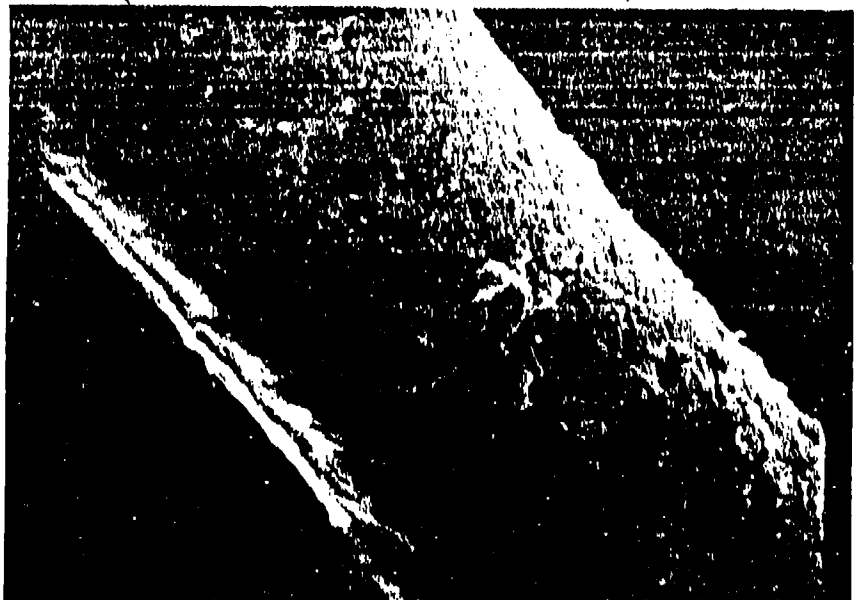

FIG. 3.45 DEGRADED FILAMENT FROM EXPOSED SURFACE LAYER OF ROPE #2 (1966)

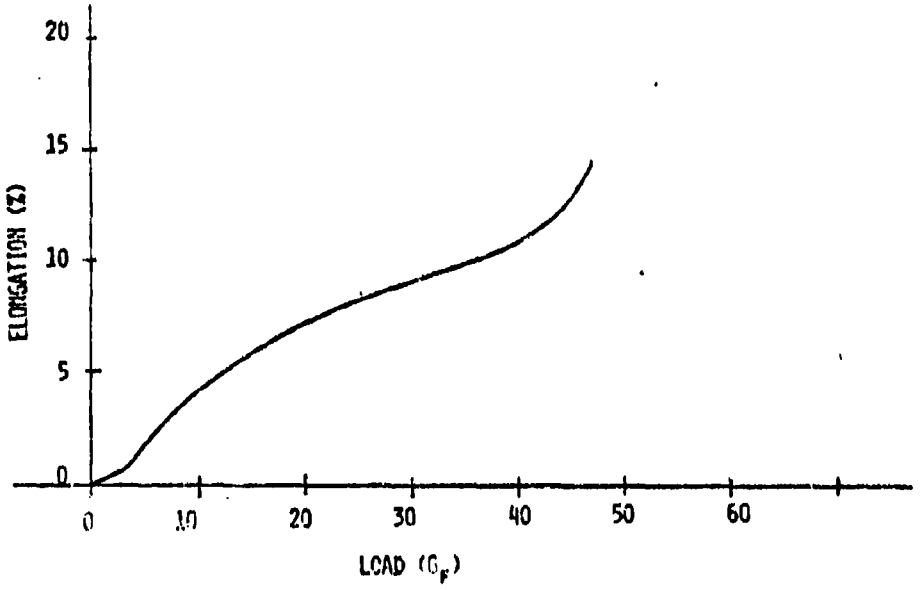

FIG. 3.44B COMPRESSED FILAMENT FROM EXPOSED SURFACE LAYERS OF ROPE #2 (1966)

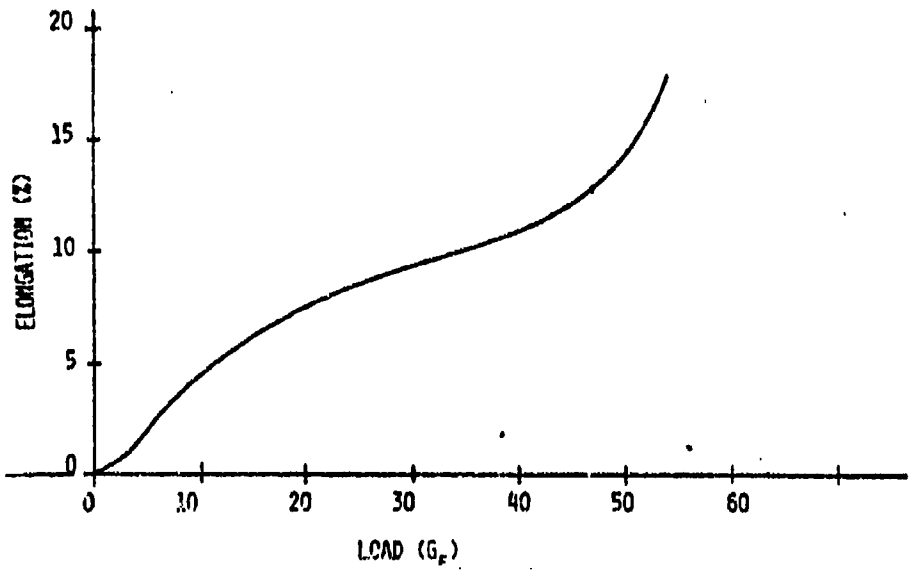

FIG. 3.46 SURFACE LAYER FIBER FROM THE PROTECTED ZONE OF ROPE #2 (1966)

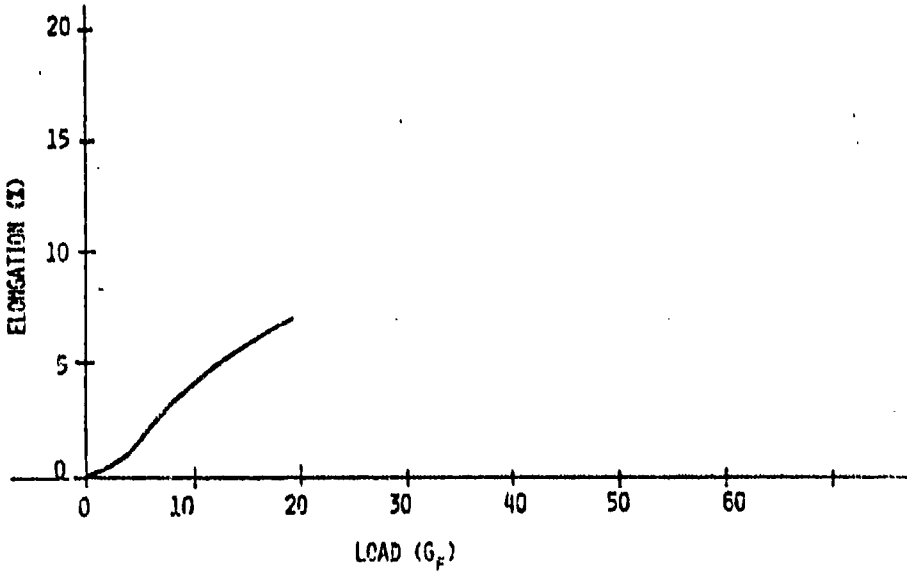

FIG. 3.47 FILAMENT FROM FIRST SUBLAYER IN EXPOSED ZONE OF ROPE #2 (1966)

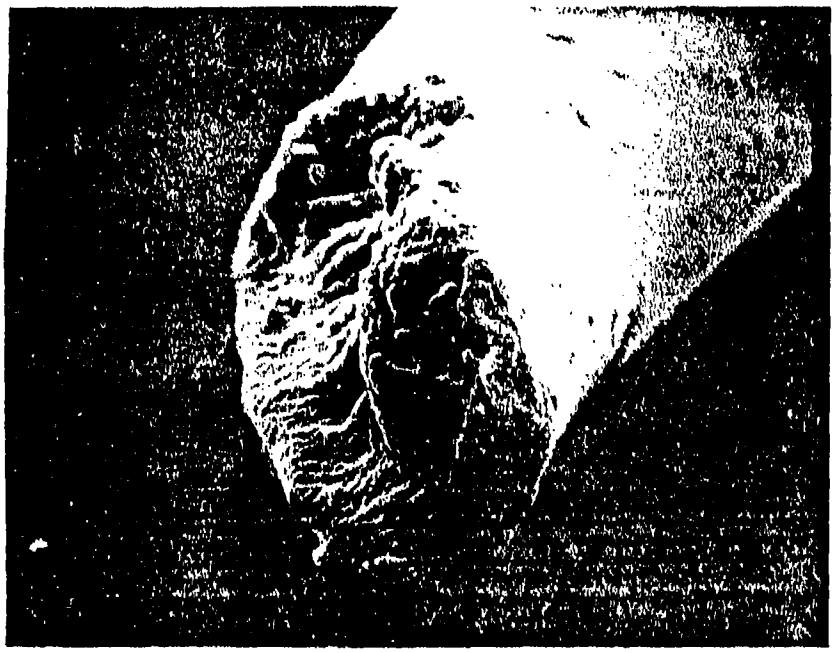

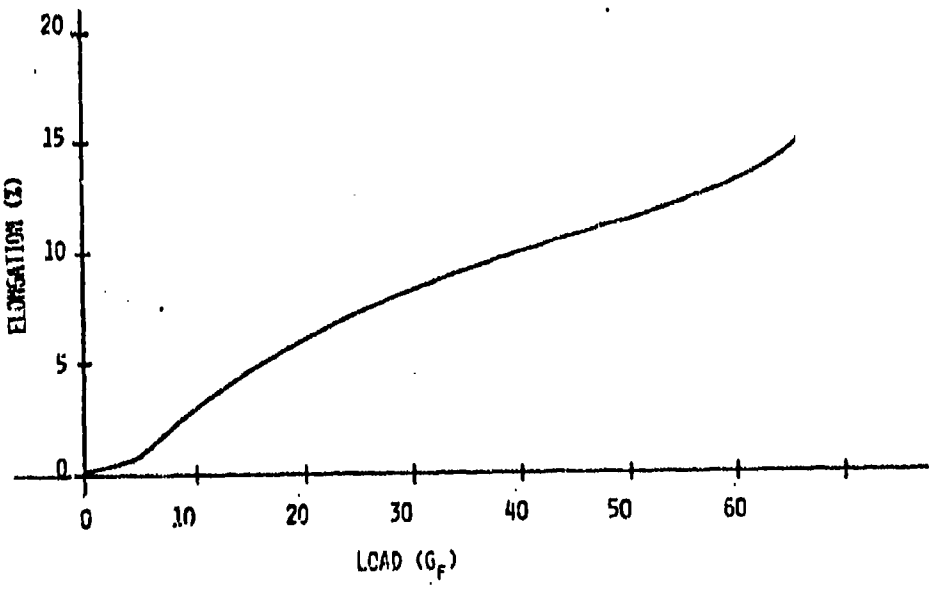

FIG. 3.48 FILAMENT FROM FIRST SUBLAYER IN EXPOSED ZONE OF ROPE #2 (1966)

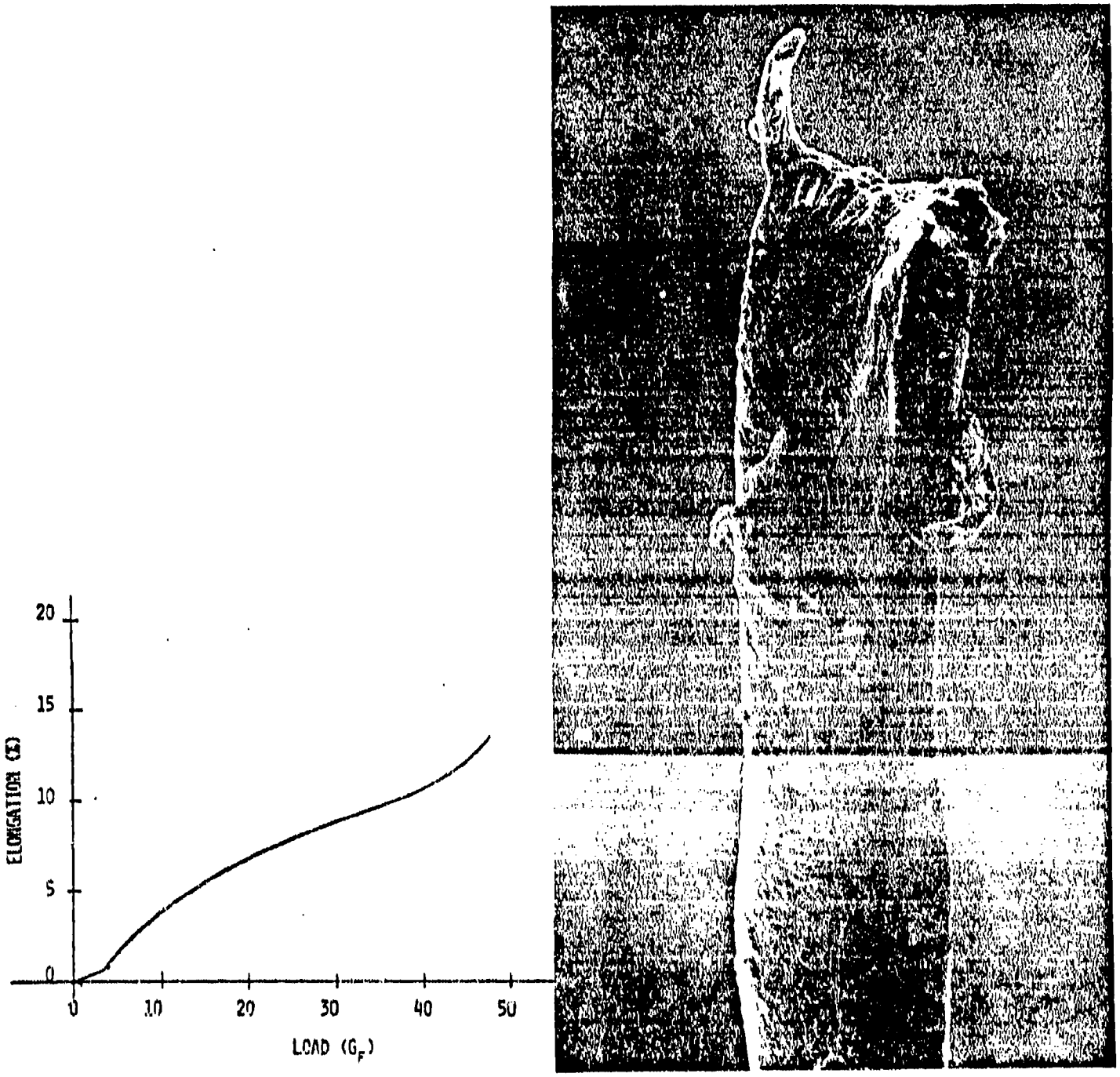

FIG. 3.49 FILAMENT FROM FIRST SUBLAYER IN PROTECTED ZONE OF ROPE #2 (1966)

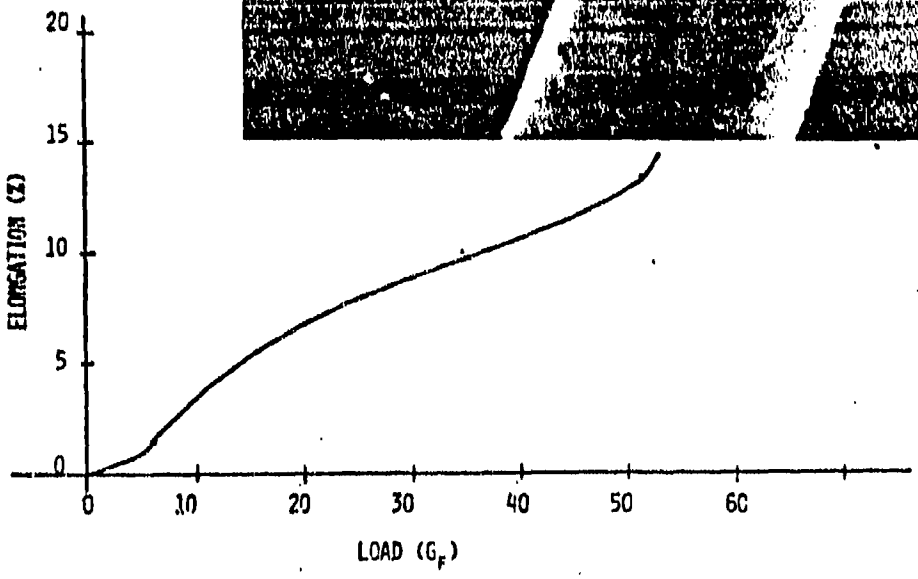

FIG. 3.50 FILAMENT FROM STRAND CORE OF ROPE #2 (1966)

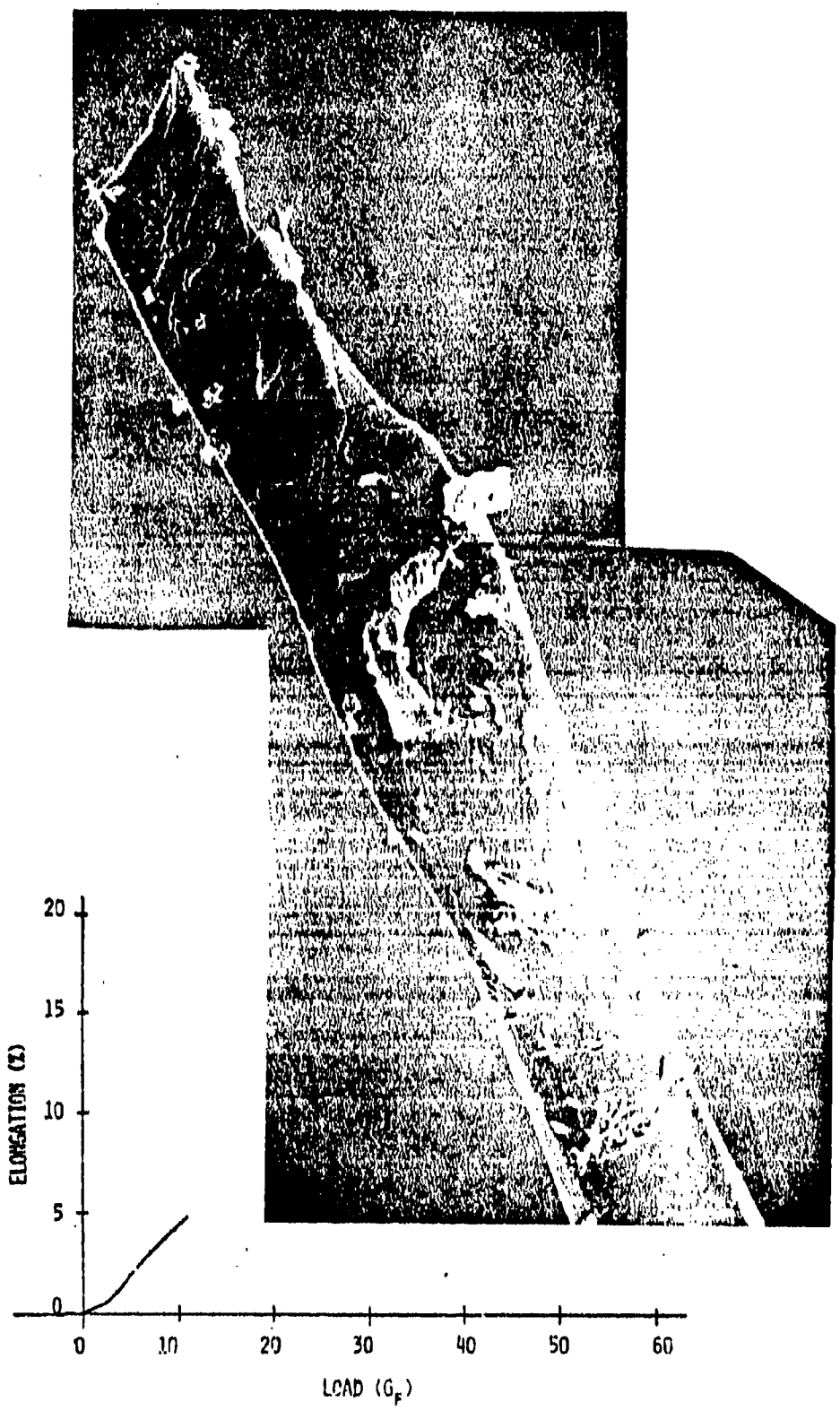

FIG. 3.51 FILAMENT FROM STRAND CORE OF ROPE #2 (1966)

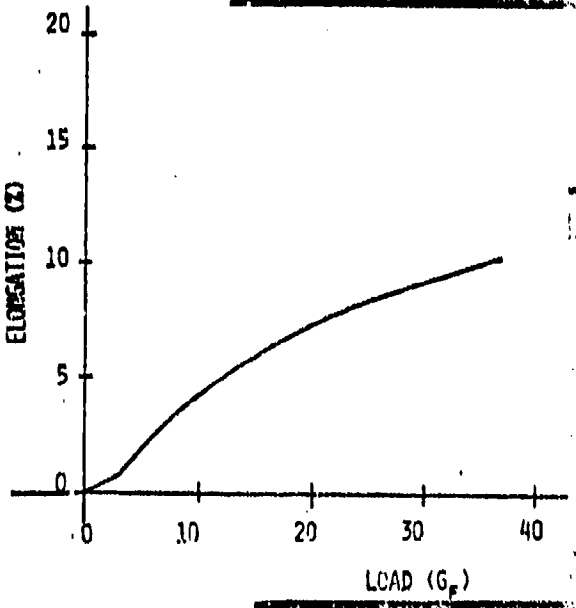

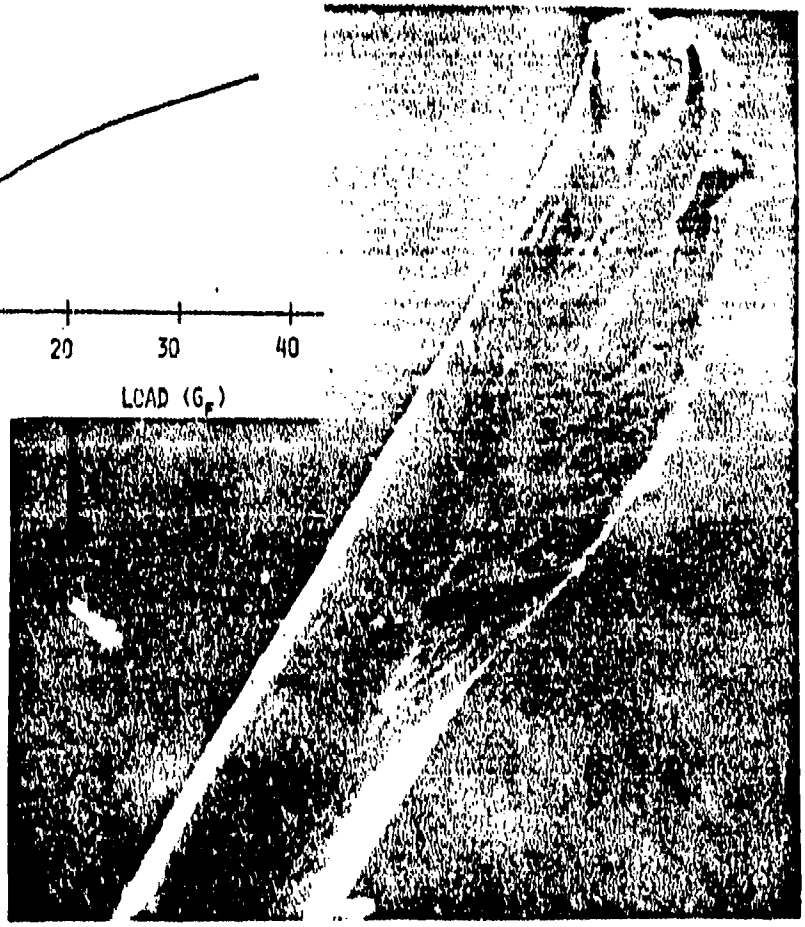

FIG. 3.52 FILAMENT FROM STRAND CORE OF ROPE #2 (1966)

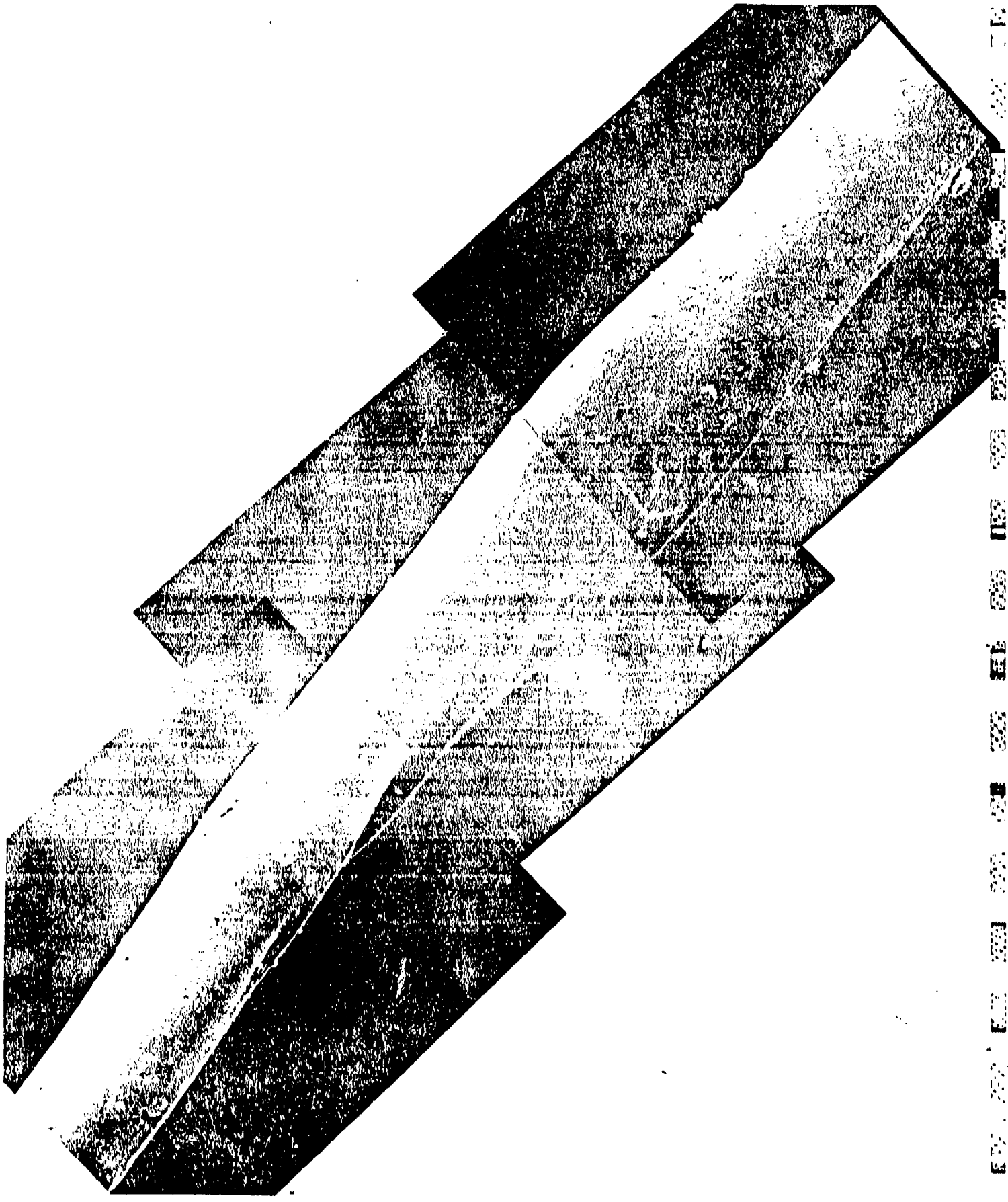

FIG. 3.53 FILAMENT FROM STRAND CORE OF ROPE #2 (1966)

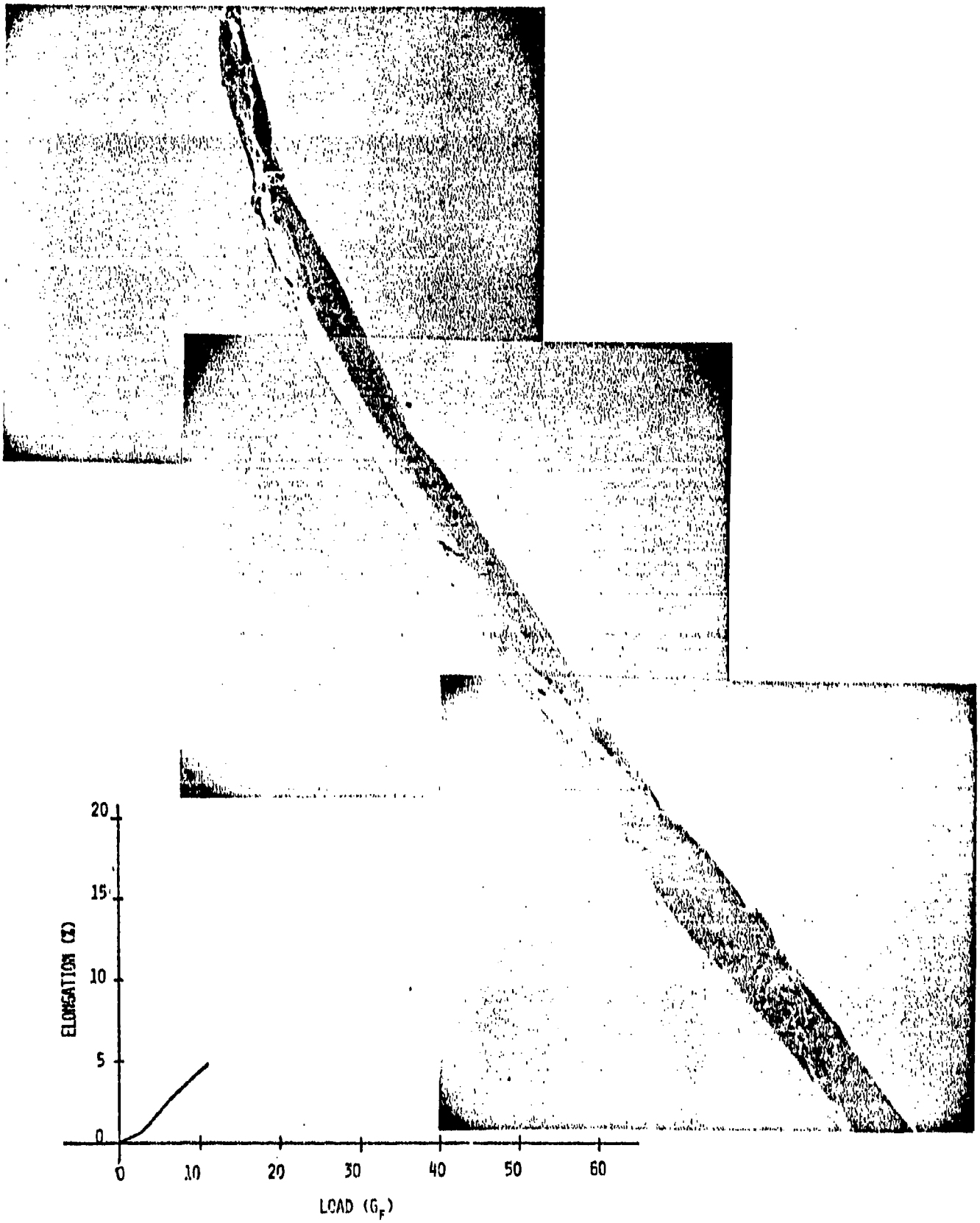

FIG. 3.54A FILAMENT FROM STRAND CORE OF ROPE #2 (1966)

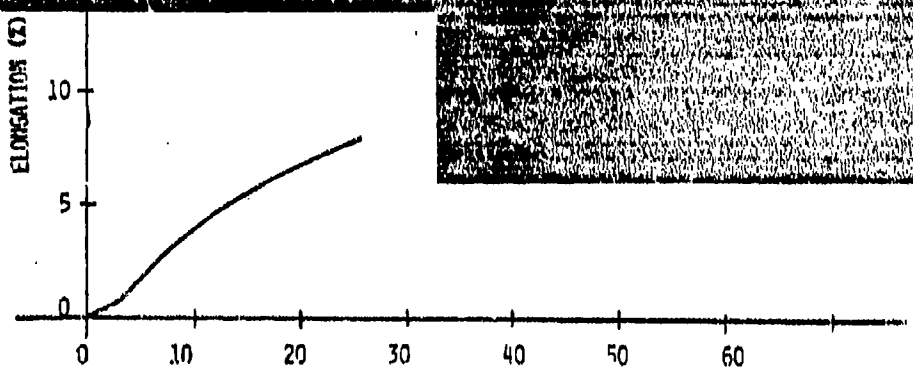

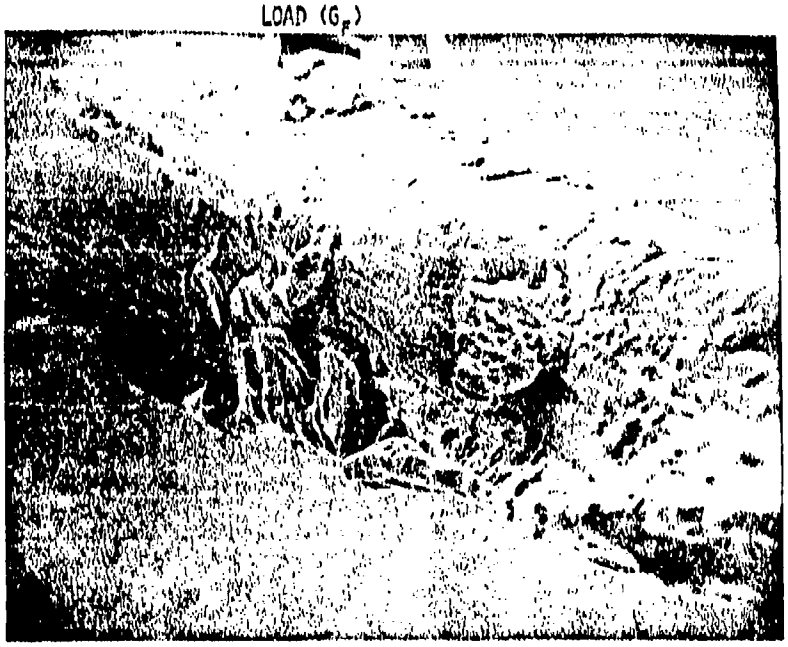

FIG. 3.54B FILAMENT FROM STRAND SURFACE AT CENTER OF ROPE #8

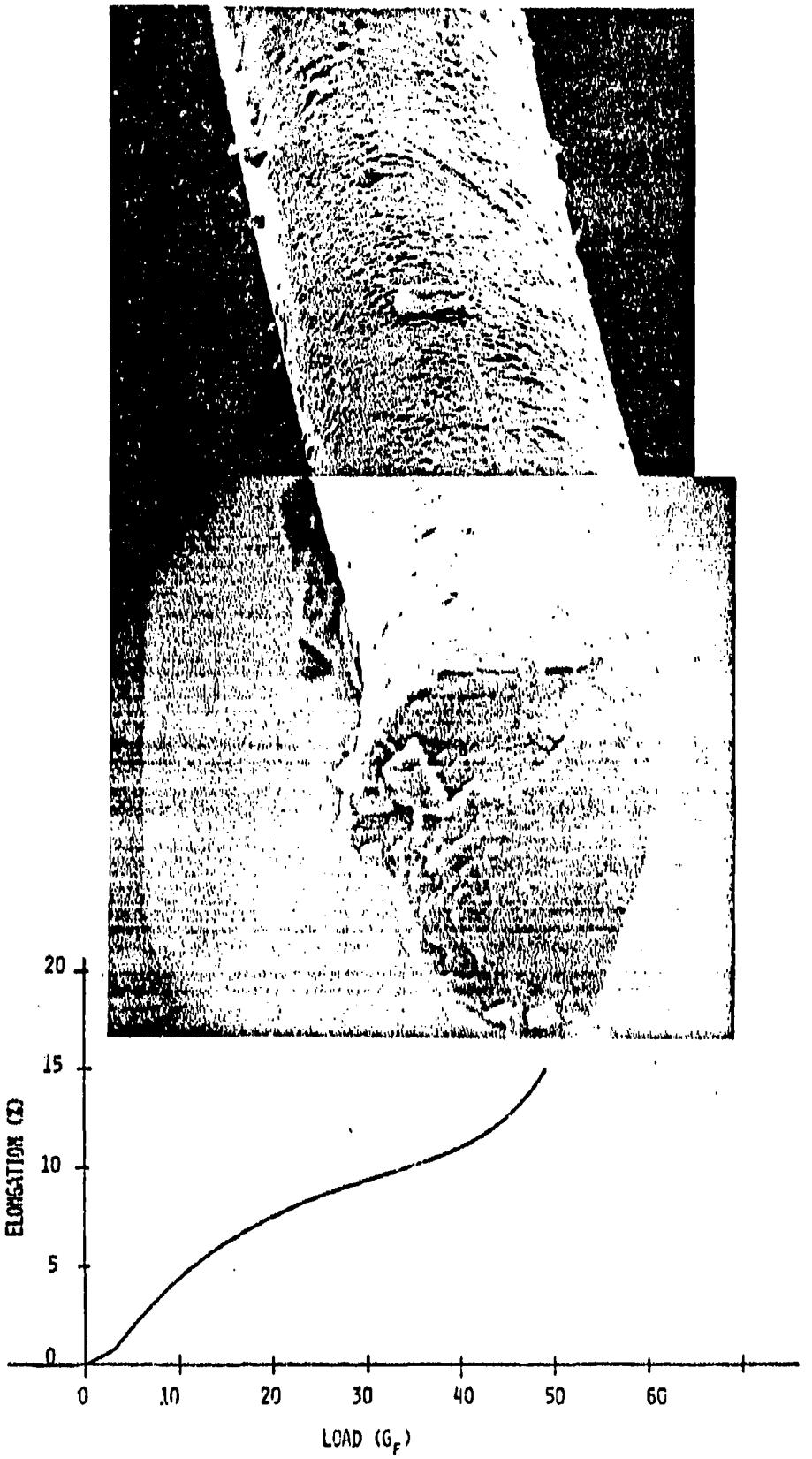

FIG. 3.55 FILAMENT FROM STRAND CORE OF ROPE #2 (1966)

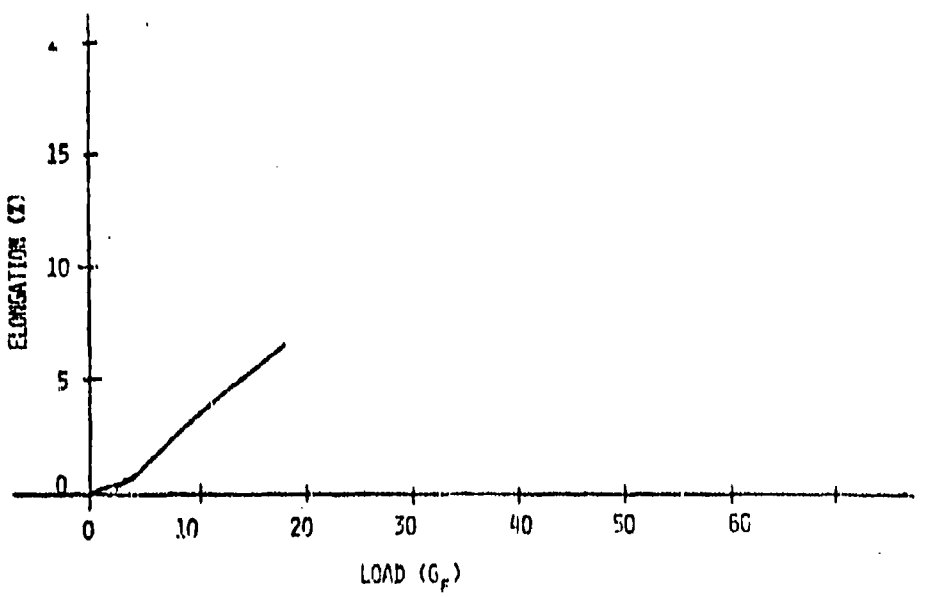

FIG. 3.56 FILAMENT FROM EXPOSED STRAND SURFACE OF ROPE #7 (1966)

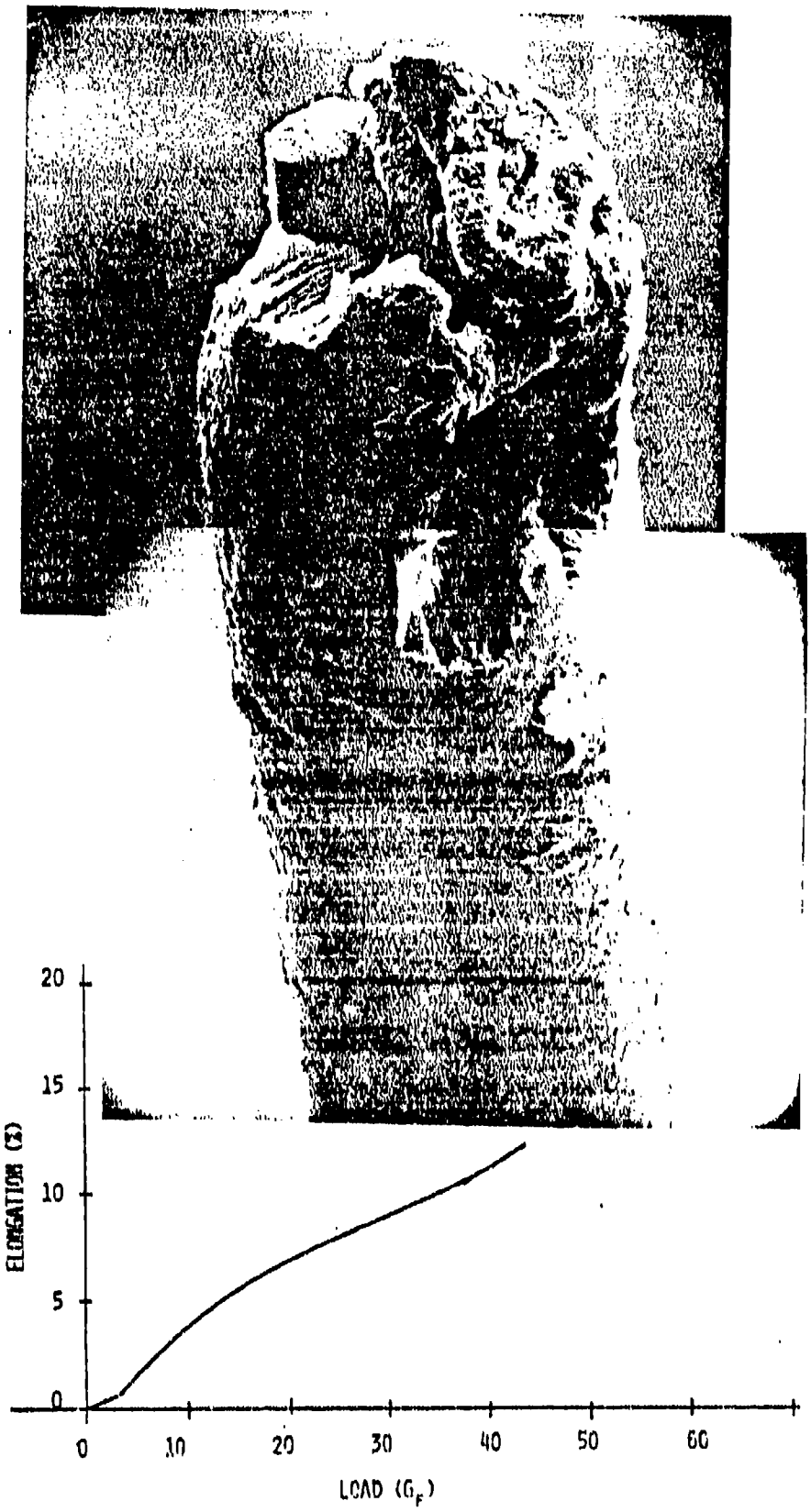

FIG. 3.57 FILAMENT FROM EXPOSED STRAND SURFACE OF ROPE #7 (1966)

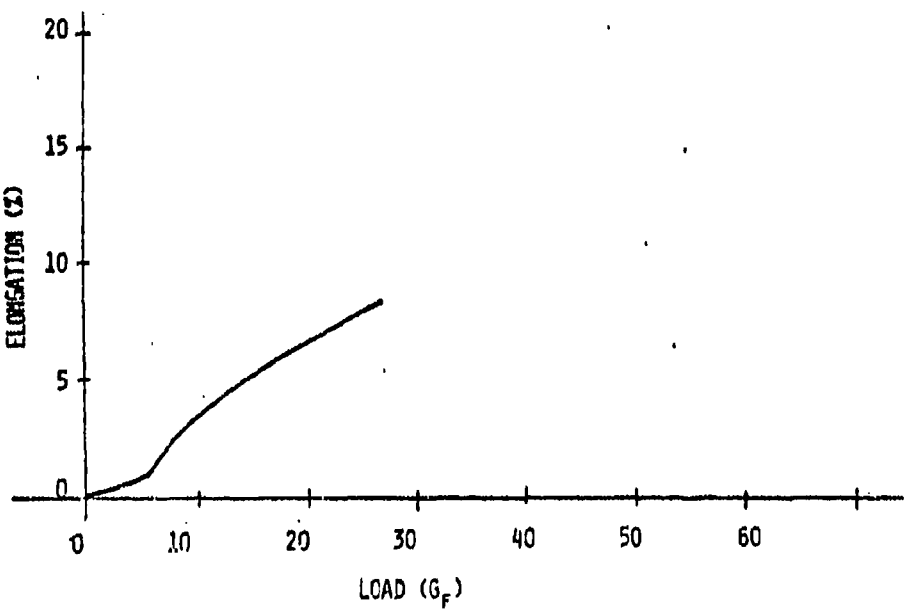

FIG. 3.58A FILAMENT FROM EXPOSED STRAND SURFACE OF ROPE #1 (1971)

B

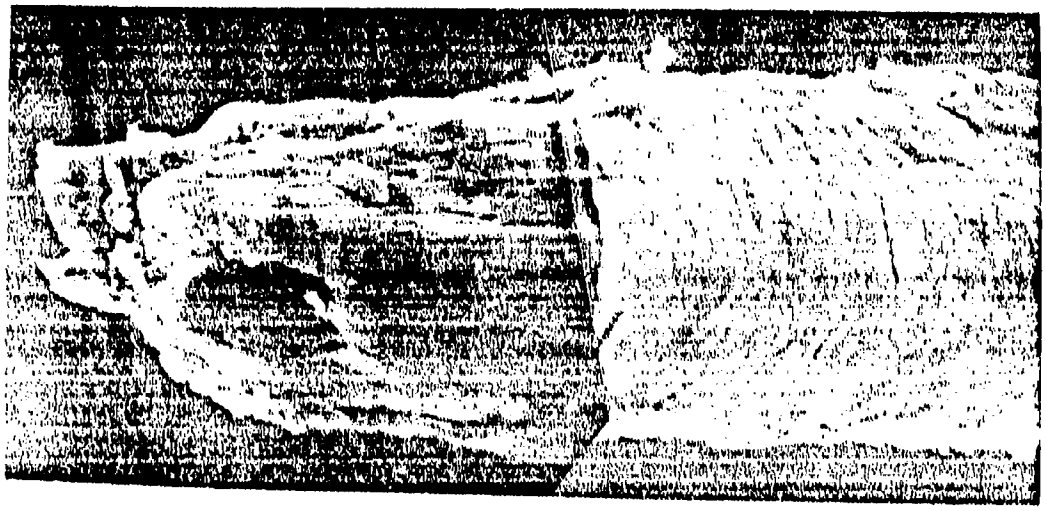

C

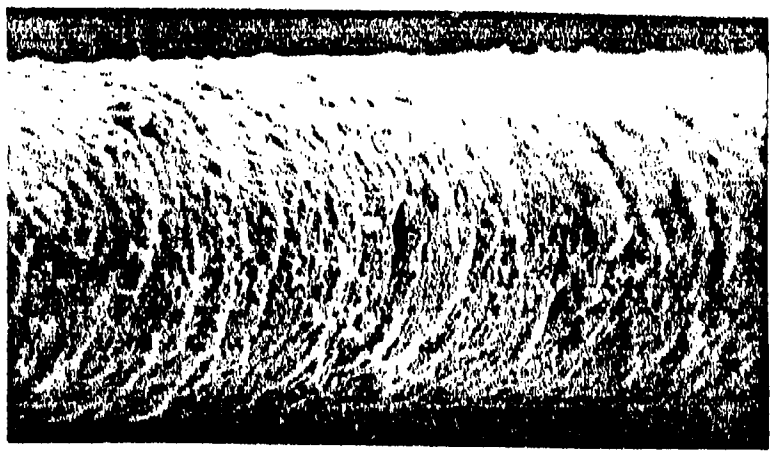

D

FIG. 3.58B,C,D FILAMENT FROM EXPOSED SURFACE OF ROPE #2 (1966)

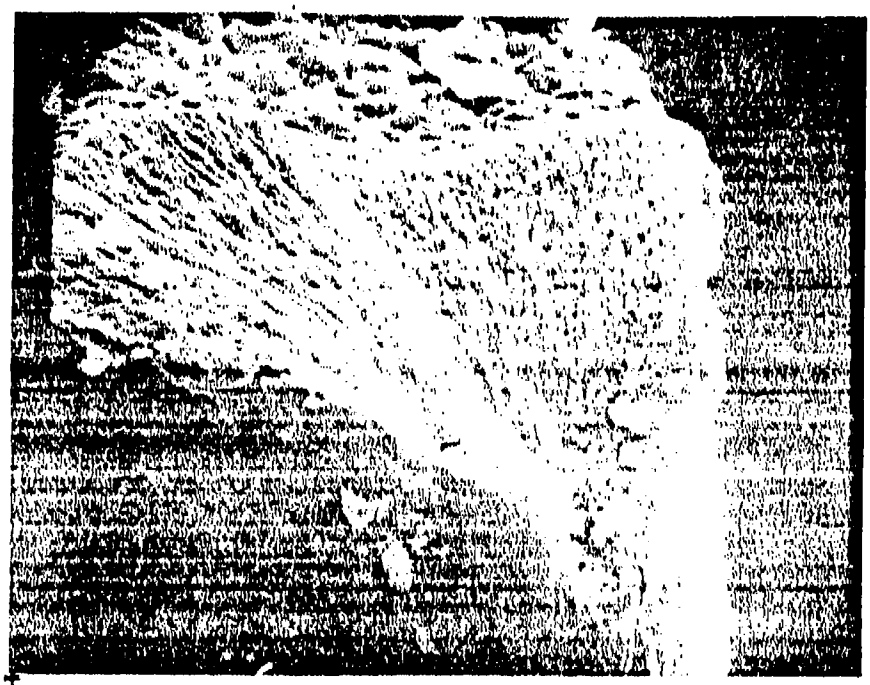

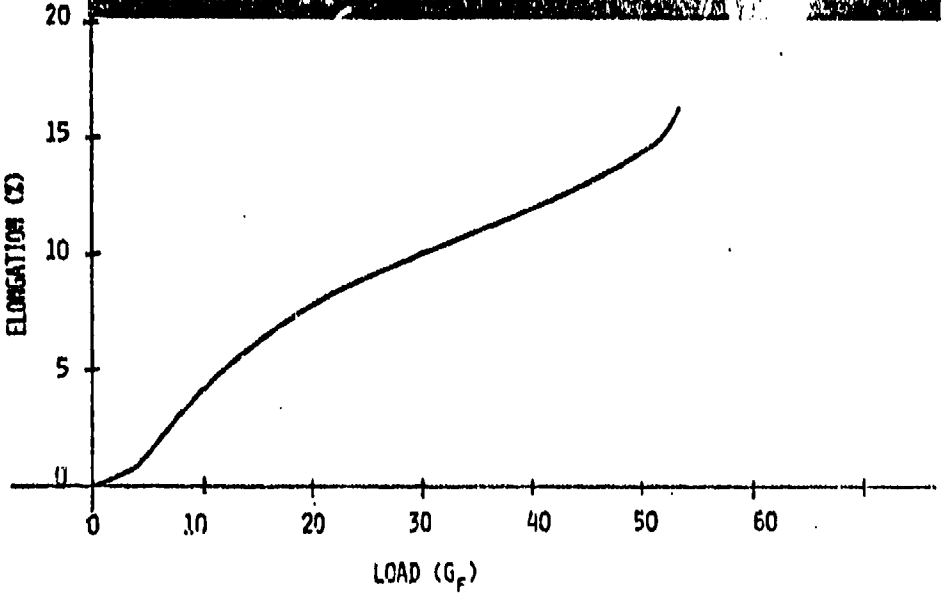

FIG. 3.59 FILAMENT FROM PROTECTED STRAND SURFACE OF ROPE #1 (1971)

FIG. 3.60 FILAMENT FROM STRAND CORE OF ROPE #7 (1966)

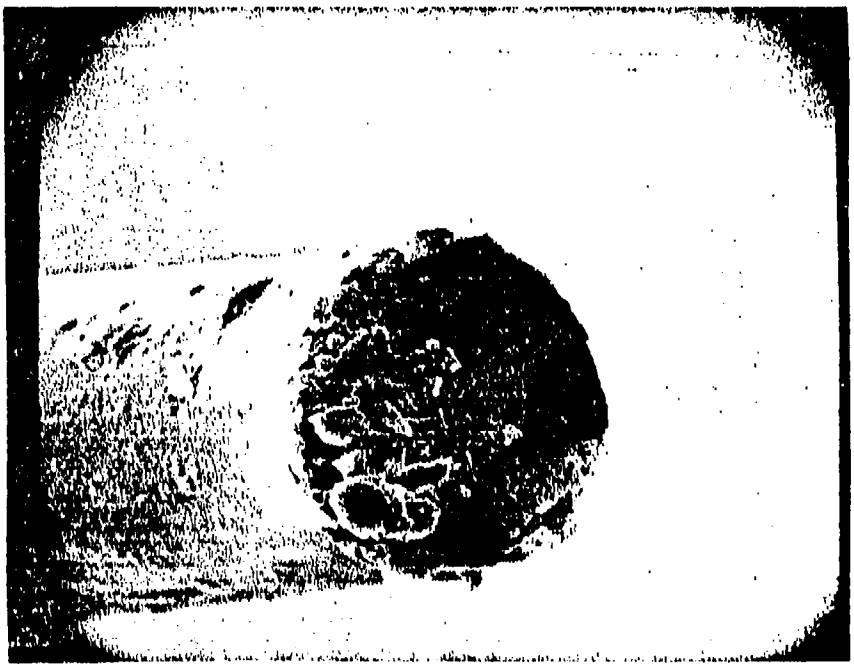

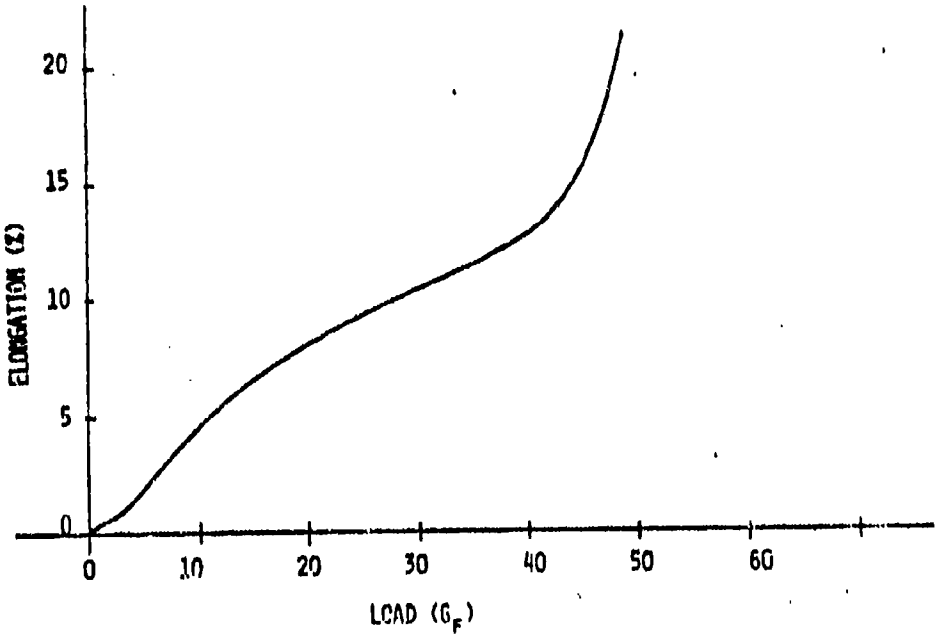

FIG. 3.61A FILAMENT FROM EXPOSED STRAND SURFACE LAYER FROM ROPE #10.

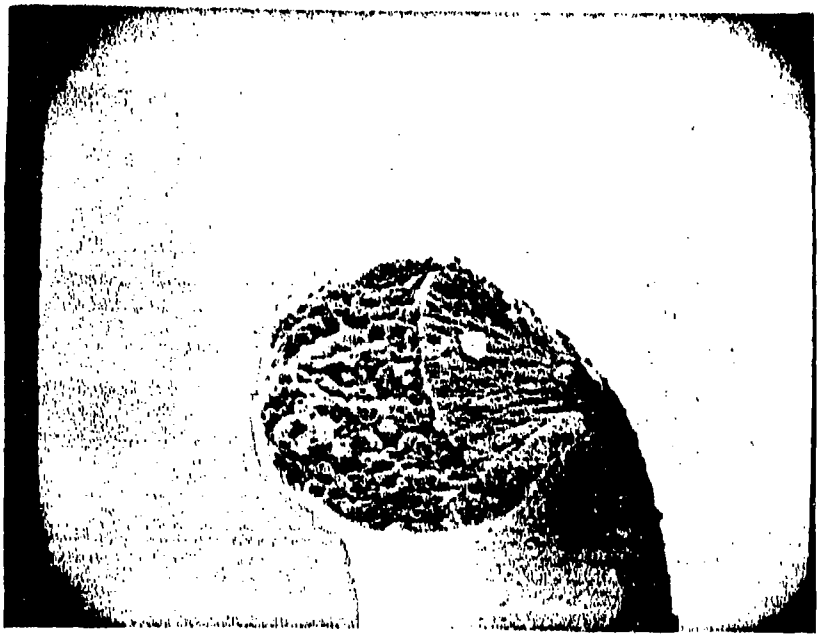

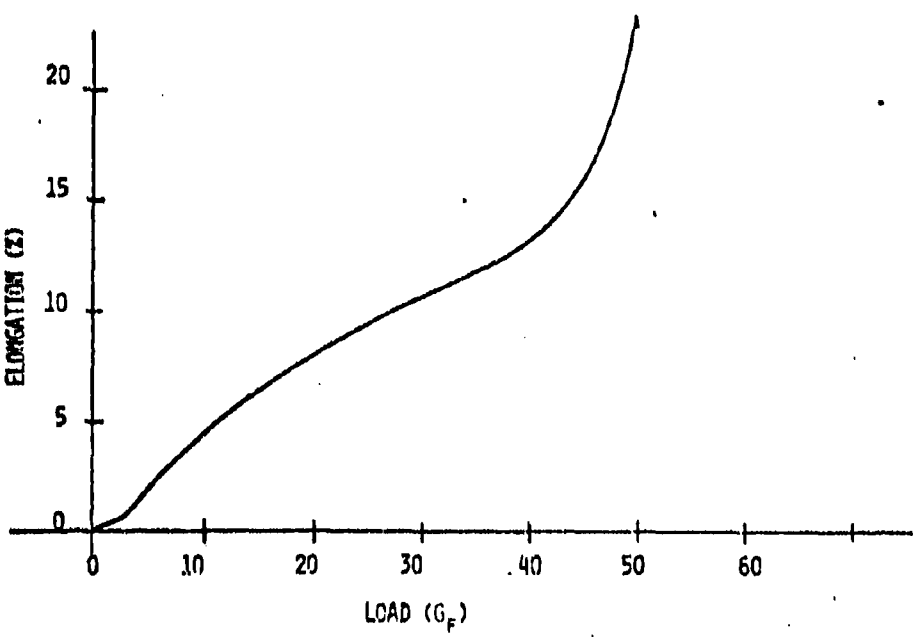

FIG. 3.61B FILAMENT FROM PROTECTED STRAND SURFACE LAYER FROM ROPE #10

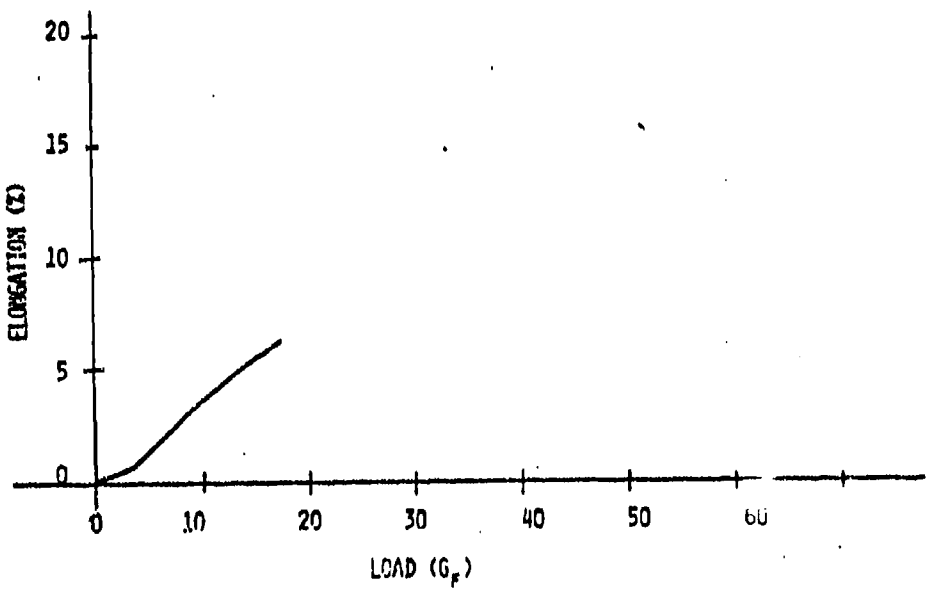

FIG. 3.62A FILAMENT FROM EXPOSED STRAND SURFACE LAYER FROM ROPE #9

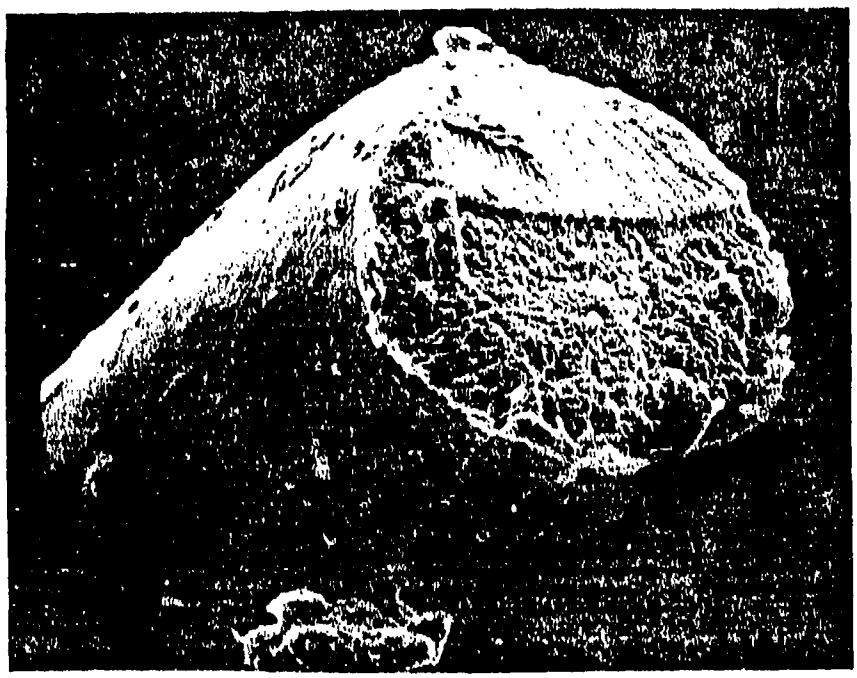

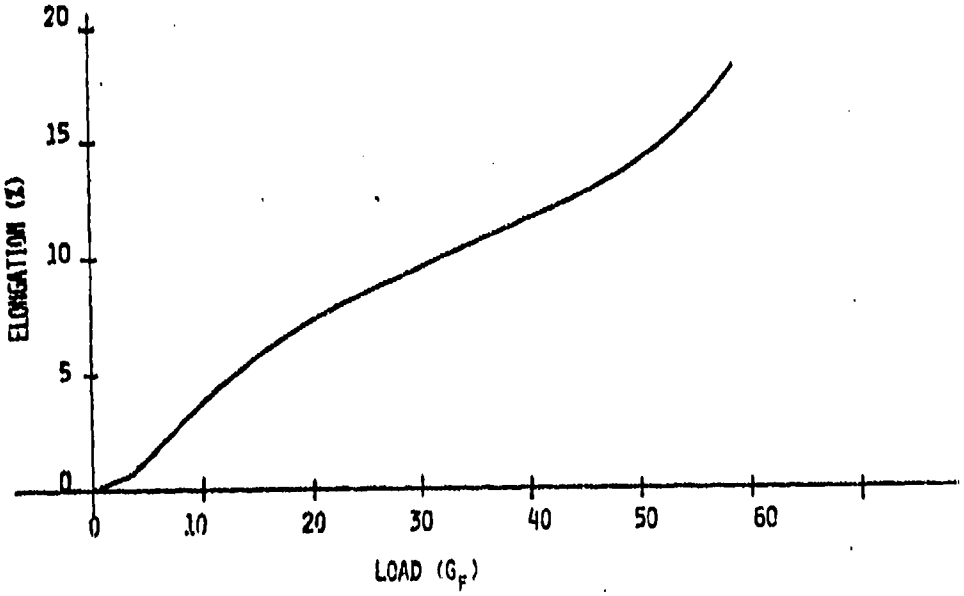

FIG. 3.62B FILAMENT FROM PROTECTED STRAND SURFACE FROM ROPE #9

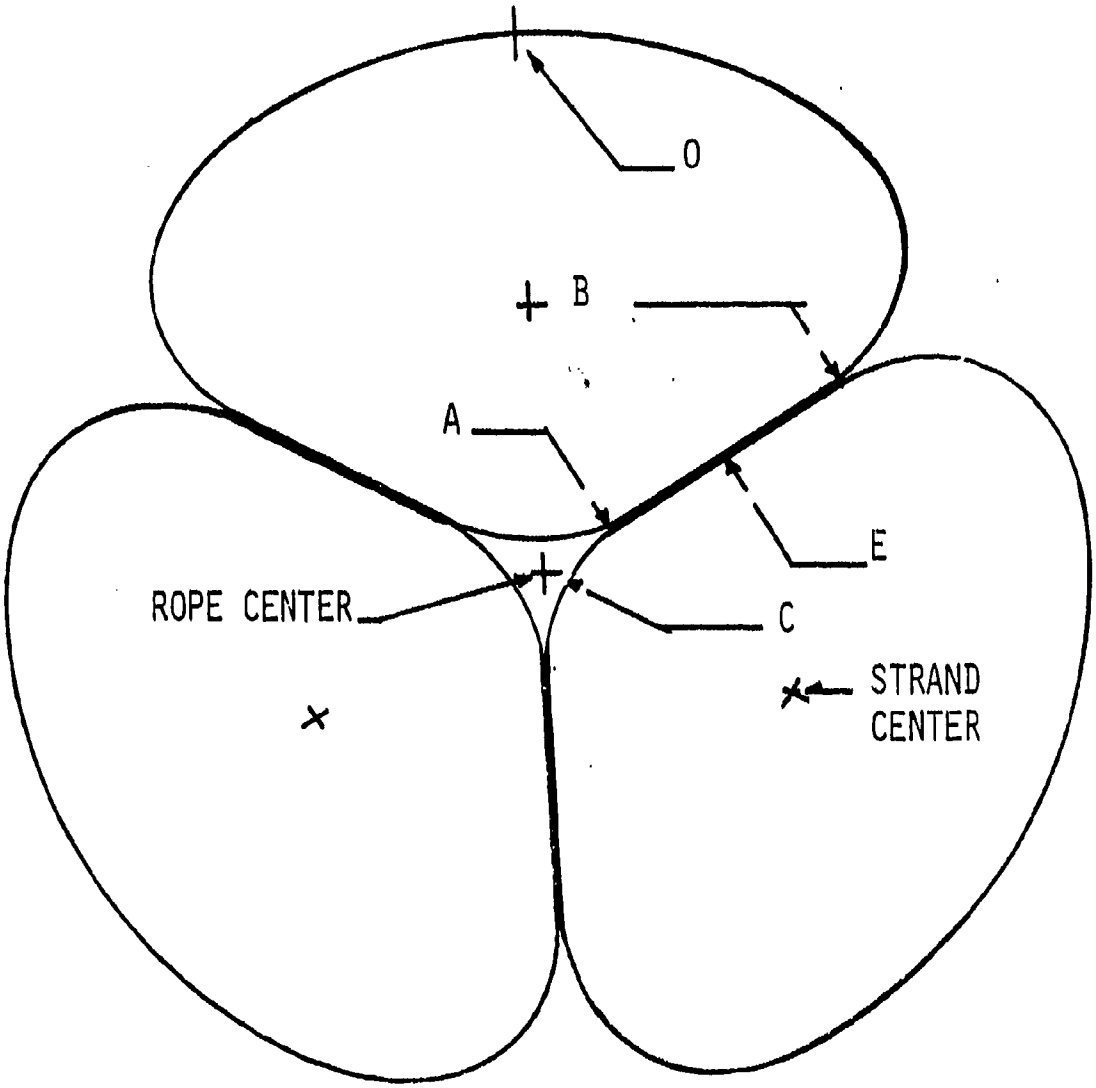

FIG. 3.63 CROSS SECTION MAP OF 3-STRAND TWISTED ROPE

3.64A

3.64B

FIG. 3.64 SURFACE OF ROPE STRAND AT POSITION 0
A. ROPE 7; B. ROPE 4

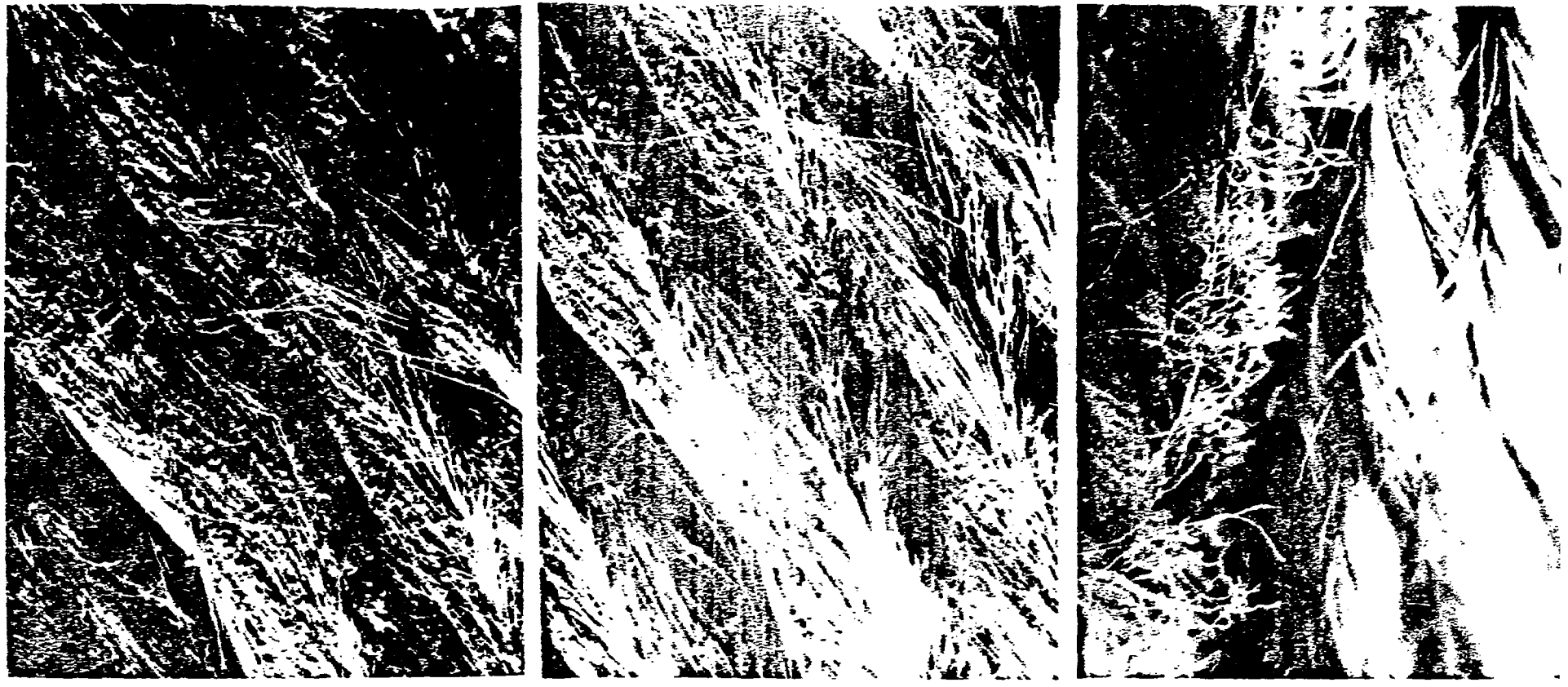

FIG. 3.65 SURFACE OF ROPE STRAND
A. POSITION B, ROPE 8; B. POSITION B, ROPE 7; C. POSITION EB, ROPE 7

A

B

FIG. 3.66 SURFACE OF ROPE STRAND

A. POSITION E, ROPE 8; B. POSITION E, ROPE 7

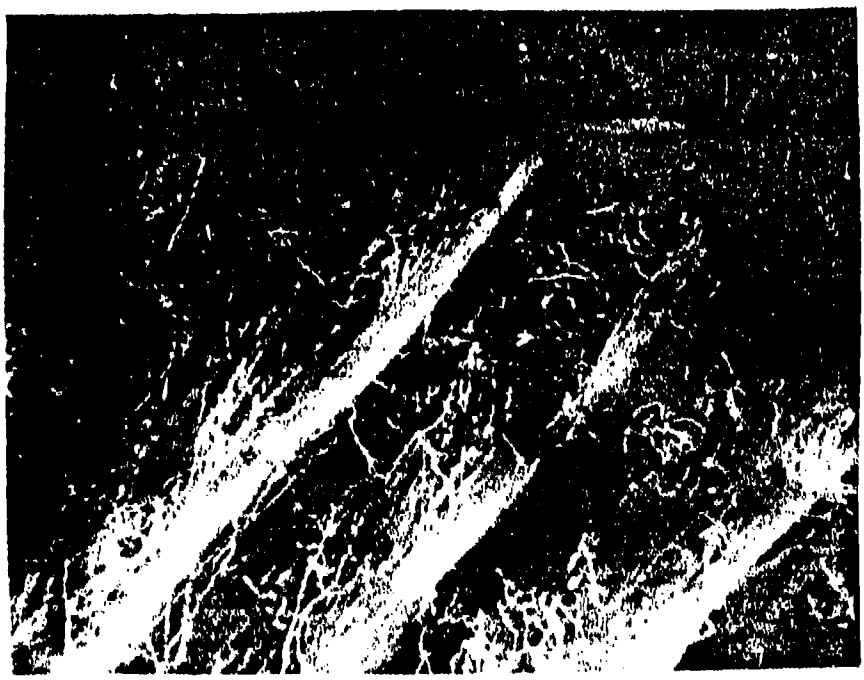

FIG. 3.67 SURFACE OF ROPE STRAND, POSITION AE, ROPE 7

A

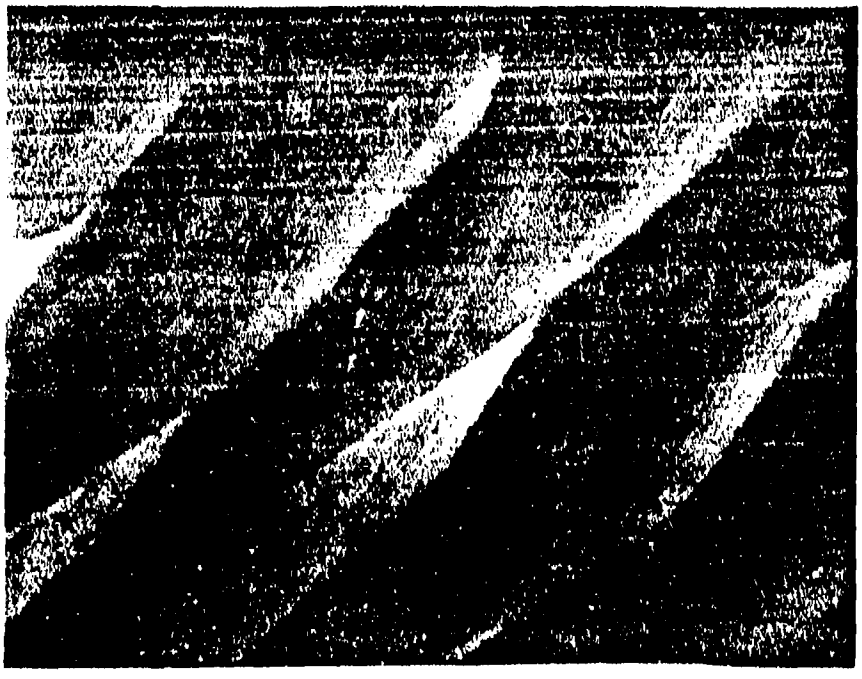

B

FIG. 3.68 SURFACE OF ROPE STRAND AT POSITION C
A. ROPE 8; B. ROPE 7

LIST OF TABLES

3.1a Identification of Used Ropes

3.1b Used Rope Identification Data

3.2a Structural Composition

3.2b Structural Composition

3.2c Structural Composition

3.2d Structural Composition

3.3 Distribution of Plied Yarn in Twisted Strand

3.4 Summary of Filament Strength from Worn Rope

3.5 Normalized Tensile Data for 3-Strand Ropes

3.6 Summary of Fiber Tensile Results (gf)

3.7 GPC Data for Worn Ropes; $\bar{M}_n$ (X1000)

3.8 GPC Data for Worn Ropes; $\bar{M}_n$ (X1000)

3.9 GPC Data for Worn Ropes; Polydispersity

3.10 GPC Data for Worn Ropes; ($\bar{M}_n$) Normalized

3.11 Melting Temperatures of Rope Fibers

3.12 Tensile Properties of Nylon 6.6 Monofilaments After Creep Tests

3.13 Mechanical Properties of Synthetic Monofilaments After Dry Creep

TABLE 3.1a Identification of Used Ropes

Rope Number	1	2	3	4	5
Size: no load circum(in)	9-1/8	9	7-1/2	8-1/2	6-3/8
nominal circum(in)	9	9	---	---	6-1/2
Naterial	Nylon	Nylon	Nylon	Nylon	PET
Construction	3-strand	3-strand	D-braided	3-strand	D-braided
Manufacturer	BNSR*	BNSR	Samson	Tubbs	---
Date of Manufacture	1971	1966	1972	1972	---
Specification	PNS**	PNS	PNS	PNS	PNS
Application	Mooring line	Mooring line	Mooring line	Mooring line	Tug Line
Type of Load	---	---	---	---	High dynamic
Years of Use	---	---	---	---	9-12 mos.
General Condition	Generally good	Good	Good	Fair	Good
Remarks	---	---	---	---	Soft, Pliable

* Boston Naval Shipyard Ropewalk; ** Philadelphia Naval Shipyard.

TABLE 3.1b Used Rope Identification Data

Rope Number	6	7	8	9	10
Size no load circum (in) nominal circum (in)	9-1/2	9-1/2	9-1/2	5-11/16	5-9/16
Material	Nylon	Nylon	Nylon	Nylon	Nylon
Construction	5-strand	3-strand	3-strand	3-strand	3-strand
Manufacturer	BNSR	BNSR	Cordage Group	BNSR	Aamstrand
Date of Manufacture	1961	1966	1978	1969	1979
Specification					
Source of Rope	BNS*	PNS**	PNS	PNS	PNS
Application	Docking Line	Mooring Line	Mooring*** Line	Mooring Line	Mooring Line
General Condition	Good, some Chafe	Old, Chafed, Weathered Mossy	Good, some Chafe	Good, some Chafe	Fair
Remarks	Some Burns				

*Boston Naval Shipyard; **Philadelphia Naval Shipyard

***Possibly from Battle Ships

TABLE 3.2a Structural Composition

	Element	Description	Twist Turns/ft	Diameter inches	Fibers Numbers	Denier
	Textile Yarn	Singles	---	---	140	840
	"Rope Yarn"	18 Singles	13S	0.06	2,520	15,120
#1	Plied Yarn	3 Rope Yarns	12Z	0.13	7,560	45,360
	Strand	127 Plied Yarns	2S	1.5	960,120	5,760,720
	Rope	3 Strands	1.67Z	3.0	2,880,360	17,282,160
	Textile Yarn	Singles	---	---	136	816
	"Rope Yarn"	18 Singles	17S	0.06	2,448	14,688
#6	Plied Yarn	3 Rope Yarns	9Z	0.13	7,344	44,064
	Strand	126 Plied Yarns	2S	1.5	925,344	5,552,064
	Rope	3 Strands	1.78Z	3.0	2,776,032	16,656,192
	Textile Yarn	Singles	---	---	210	1,260
	"Rope Yarn"	12 Singles	12S	0.06	2,520	15,120
#7	Plied Yarn	3 Rope Yarns	12Z	0.13	7,560	45,360
	Strand	124 Plied Yarns	2S	1.5	937,440	5,624,640
	Rope	3 Strands	1.78Z	3.0	2,812,320	16,873,920
	Textile Yarn	Singles	---	---	210	1,260
	"Rope Yarn"	24 Singles	13S	0.1	5,040	30,240
#8	Plied Yarn	3 Rope Yarns	10Z	0.2	15,120	90,720
	Strand	61 Plied Yarns	2S	1.5	922,320	5,533,920
	Rope	3 Strands	1.67Z	3.0	2,766,960	16,601,760
	Textile Yarn	Singles	---	---	68	884
	"Rope Yarn"	18 Singles	13S	0.06	1,224	15,912
#10	Plied Yarn	3 Rope Yarns	12Z	0.125	3,672	47,736
	Strand	44 Plied Yarns	3S	0.90	161,568	2,100,384
	Rope	3 Strands	3Z	2.00	484,704	6,301,152

TABLE 3.2b Structural Composition

	Element	Description	Twist Turns/ft	Diameter inches	Fibers Numbers	Denier
	Textile Yarn	Singles	---	---	210	1,260
	"Rope Yarn"	12 Singles	15S	0.06	2,520	15,120
#2	Plied Yarn	3 Rope Yarns	12Z	0.16	7,560	45,360
	Strand	123 Plied Yarns	2S	1.5	929,880	5,570,280
	Rope	3 Strands	2Z	3.0	2,789,640	16,737,840
	Textile Yarn	Singles	---	---	140	840
	Textile Plied Yarn	4 Singles	2S	0.04	560	3,360
	Rope Yarn	7 Textile Plied Yarns	8^{S}_{Z}	0.1	3,920	23,520
	Plied Yarn	Core-7 Rope Yarns		0.3	27,440	164,640
		Cover-3 Rope Yarns	6^{S}_{Z}	0.2	11,760	70,560
	Cover	16x2 Left Braided Yarns		2.5	752,640	4,515,840
#3		16x2 Right Braided Yarns	1.75^{S}_{Z}			
	Core	6x3 Left Braided Yarns		1.6	987,840	5,927,040
		6x3 Right Braided Yarns	2^{S}_{Z}			
	Rope	Cover and Core		2.5	1,740,480	10,442.880

TABLE 3.2c Structural Composition

	Element	Description	Twist Turns/ft	Diameter inches	Fibers Numbers	Denier
	Textile Yarn	Singles	---	---	136	816
	Rope Yarn(Core)	24 Singles	18Z	0.075	3,264	19,584
	Rope Yarn(in Ply)	36 Singles	11S	0.10	4,896	29,376
#4	Plied Yarn	3 Rope Yarns	12Z	0.20	14,688	88,128
	Strand	22 Rope Yarns in Core 56 Plied Yarns	2S	---	894,336	5,366,016
	Rope	3 Strands	1.5Z	3.0	2,683,008	16,098,048
	Cover: Text. Yarn	Singles 3 (Interlaced)	---	---	280	2,240
	"Rope Yarn"	64 Singles	6^{S}_{Z}	0.3	17,920	143,360
	Cover	12x12 Left Rope Yarns 12x12 Right Rope Yarns	1.5^{S}_{Z}	2.5	860,160	6,881,280
	Core: Text. Yarn	Singles	---	---	190	1,140
#5	"Rope Yarn"	10 Singles	4^{S}_{Z}	0.05	1,900	11,400
	Plied Yarn	22 Rope Yarns	3^{S}_{Z}	0.3	41,800	250,800
	Core	4x4 Left Braided Yarns 4x4 Right Braided Yarns	1^{S}_{Z}	1.5	1,337,600	8,025,600
	Rope	Cover and Core	---	2.5.	2,197,760	14,906,880

TABLE 3.2d Structural Composition

	Element	Description	Twist Turns/ft	Diameter inches	Fibers Numbers	Denier
	Textile Yarn	Singles	---	---	210	1,260
	"Rope Yarn"	12 Singles	14S	0.06	2,520	15,120
#9	Plied Yarn	3 Rope Yarns	10Z	0.125	7,560	45,360
	Strand	46 Plied Yarns	3S	0.90	347,760	2,086,560
	Rope	3 Strands	3Z	2.00	1,043,280	6,259,680

TABLE 3.3 Distribution of Plied Yarn in Twisted Strand

	Layer		Number/Layer	Total to this Layer
	5,6,7	Core	20	20
	4		15	35
#1	3		22	57
	2		30	87
	1	Surface	40	127
	1, 2, 3	Core	16	16
#2	4		16	32
	5		21	53
	6		30	83
	7	Surface	40	123
	4	Core	22	22
	3		12	34
#4	2		19	53
	1	Surface	25	78
	5,6,7	Core	21	21
	4		13	34
#6	3		25	59
	2		28	87
	1	Surface	39	126
	5,6,7	Core	19	19
	4		14	33
#7	3		24	57
	2		27	84
	1	Surface	40	124
	4,5	Core	10	10
	3		13	23
#8	2		16	39
	1	Surface	22	61
	4	Core	2	2
	3		9	11
#9	2		13	24
	1	Surface	22	46
	4	Core	2	2
	3		7	9
#10	2		16	25
	1	Surface	19	44

TABLE 3.4 Summary of Filament Strength from Worn Rope

		Surface Layer (Soft Spot)	Subsurface (Soft Spot)	Core	Subsurface (Hard Spot)	Ratio (A)*	Surface Layer (Hard Spot)	Ratio (B)*
1971	1E	29.4± 7.9	55.8±2.2	55.4± 2.3	54.3±1.9	0.975±0.025	38.2±10.1	1.360±0.378
1966	2D	37.8±16.0	56.2±9.3	54.5±14.7	57.0±6.8	1.022±0.062	53.0± 1.2	2.435±3.40
1972	4E	25.8±11.5	54.0±4.7	56.3± 3.6	55.6±4.2	1.033±0.078	51.3± 2.6	2.511±1.361
1966	7DA	32.0± 7.7	50.5±2.8	59.3± 6.9	52.8±3.5	1.045±0.037	51.9± 4.6	1.727±0.542
1966	7DB	41.6± 8.5	55.8±2.4	59.3± 6.9	58.7±2.3	1.053±0.058	48.7± 7.4	1.265±0.570
1978	8DA	46.4±15.2	60.9±2.7	61.6± 5.4	59.0±3.4	0.970±0.060	54.7±13.4	1.449±1.371
1978	8DB	38.9± 7.9	62.6±4.8	61.6± 5.4	63.2±4.5	1.011±0.044	61.8± 2.2	1.644±0.315
1969	9D	33.3±10.3	51.8±3.1	55.4± 5.6	55.3±4.4	1.072±0.117	43.0±14.4	1.488±0.963
1979	10D	82.0±18.4	102.8±5.6	111.4±10.2	102.0±8.2	1.000±0.040	109.2± 7.4	1.432±0.290

*(A) : Ratio of tensile values of hard/soft spots in the first subsurface layer.

(B) : Ratio of tensile values of hard/soft spots in the surface layer.

TABLE 3.5 Normalized Tensile Data for 3-Strand Ropes

Sample	Material	Surface Layer (Soft Spot)	Subsurface Layer (Soft Spot)	Core	Subsurface Layer (Hard Spot)	Surface Layer (Hard Spot)	Rope Identification
1E	N66	53.03	99.3	100	97.8	69.1	BMSR 1971, Generally Good PNS 9-1/2"
2D	N66	69.4	103.1	100	104.6	97.3	BNSR 1966, Good PNS 9"
4E	N6	46.1	95.9	100	98.7	91.1	TUBBS 1972, Fair PNS 8-1/2"
7D A	N66	53.9	85.2	100	89.0	87.5	BNSR 1966, Old, Chafed, Weathered Mossy PNS 9-1/2"
7D B	N66	70.2	94.2	100	99	82.2	"
8D A	N66	75.3	98.8	100	95.8	88.8	Cordage Group 1978 Good, Some Chafe PNS 9-1/2"
8D B	N66	63.1	98.3	100	89.7	100.3	"
9D	N66	60.2	93.4	100	99.8	77.6	BNSR 1969, Good Some Chafe PNS 5-11/16"
10D	N66	73.6	92.2	100	91.6	99.3	AAMSTRAND1979 Fair PNS 5-9/16"

Table 3.6

Summary of Fiber Tensile Results (gf)

3-Strand 9" Ropes

Sample Number	Layer 1 (surface)	Layer 2 (1st sub)	Layer 3 (2nd sub)	Layer 4 (3rd sub)	Core
1E	25.2±10.9	51.1±4.6	53.0±5.6	---	53.1±6.2
2D	31.8±10.8	49.4±8.2	---	---	50.1±3.8
4E	23.2±12.9	---	---	---	51.3±3.3
6A	29.7±10.6	51.1±5.9	---	53.3±4.6	51.9±5.0
7D	25.7±7.0	32.4±12.7	---	52.0±7.1	54.6±8.7
8D	50.4±6.5	59.2±3.2	57.2±10.6	---	62.4±3.9

3-Strand 6" Ropes

Sample Number	Layer 1 (surface)	Layer 2	Layer 3	Layer 4 (core)
9D	18.6±12.1	49.1±6.4	---	53.8±4.8
10D	42.8±20.0	103.2±6.4	---	102.0±16.3

Double-Braided 9" Ropes

Sample Number	Cover		Core	
	Outside	Inside	Outside	Inside
3E	41.1±9.9		47.7±7.8	53.7±3.4
5E	52.5±11.5	60.8±7.5	44.7±5.8	46.9±5.3

TABLE 3.7 GPC Data for Worn Ropes; $\bar{M}_n$ (X1000)

Sampling Position →→→ / Sample ↓	Surface Layer Rope Outside	Surface Layer Under-Part	1st Sublayer Rope Outside	Strand 1st Core	Sublayer Rope Center	Surface Layer Rope Center	Age of Rope
1E - N66	54.0	54.5	58.8	57.7	62.9	62.7	1971
2D - N66	51.1	61.3	51.8	59.7		62.5	1966
4E - N6	47.2	51.4	54.6	56.8	56.9	63.4	1972
7D A - N66	38.82	40.14	42.78	44.61	48.74	44.79	1966
7D B - N66	40.32		48.55		45.54	45.07	1966
8D A - N66	48.73	46.68	45.04	46.77	46.15	44.06	1978
8D B - N66	45.34		45.44		44.99	44.11	1978
9D - N66	40.09			44.81		44.27	1969
10D - N66	49.54			46.71		48.7	1979

TABLE 3.8 GPC Data for Worn Ropes; $\bar{M}_w$ (X1000)

Sampling Position → / Sample ↓	Surface Layer Rope Outside	Surface Layer Under-Part	1st Sublayer Rope Outside	Strand 1st Core	Sublayer Rope Center	Surface Layer Rope Center	Age of Rope
1E - N66	101.1	100.9	109.3	107.1	109.3	109.8	1971
2D - N66	94.9	104.9	92.8	114.4		105.7	1966
4E - N6	80.4	80.8	82.5	94.0	84.1	92.4	1972
7D A - N66	88.42	92.99	96.48	96.98	103.74	96.22	1966
7D B - N66	92.36		105.02		101.18	97.82	1966
8D A - N66	107.22	99.53	97.39	94.59	95.88	92.44	1978
8D B - N66	102.74		96.89		89.40	91.77	1978
9D - N66	87.57			92.84		92.39	1969
10D - N66	107.95			97.47		98.28	1979

TABLE 3.9 GPC Data for Worn Ropes, Polydispersity

Sampling Position → / Sample ↓	Surface Layer Rope Outside	Surface Layer Under-Part	1st Sublayer Rope Outside	Strand Core	1st Sublayer Rope Center	Surface Layer Rope Center	Age of Rope
1E - N66	1.87	1.84	1.86	1.86	1.81	1.76	1971
2D - N66	1.86	1.72	1.80	1.87		1.69	1966
4E - N6	1.71	1.57	1.51	1.66	1.60	1.46	1972
7D A - N66	2.28	2.32	2.26	2.17	2.16	2.15	1966
7D B - N66	2.29		2.17		2.22	2.17	1966
8D A - N66	2.20	2.13	2.16	2.02	2.08	2.10	1978
8D B - N66	2.27		2.13		1.99	2.08	1978
9D - N66	2.19			2.07		2.09	1969
10D - N66	2.18			2.09		2.01	1979

TABLE 3.10 GPC Data for Worn Ropes; $(\bar{M}_n)$ Normalized

Sampling Position →→→ / Sample ↓	Surface Layer Rope Outside	Surface Layer Under-Part	1st Sublayer Rope Outside	Strand Core	1st Sublayer Rope Center	Surface Layer Rope Center	Age of Rope
1E - N66	93.6	94.5	101.9	100	109.0	108.7	1971
2D - N66	85.6	102.7	86.8	100	95.3	104.7	1966
4E - N6	83.1	90.5	96.1	100	100.2	111.6	1972
7D A - N66	87.0	90.0	95.9	100	109.3	100.4	1966
7D B - N66	90.4		108.8	100	102.1	101.0	1966
8D A - N66	104.2	99.8	96.3	100	98.7	94.2	1978
8D B - N66	96.9		97.2	100	96.2	94.3	1978
9D - N66	89.5			100		98.8	1969
10D - N66	106.1			100		104.3	1979

TABLE 3.11 Melting Temperatures of Rope Fibers

Rope Number	Test 1	Test 2
1	259°C	259°C
2	254	253
	257	257
3	259	259
4	222	222
	215	215
5	262	262
6	259	259
7	258	258
8	254	254
	258	258
9	260	260
10	259	258
11	255	255
	265	265
	267	

TABLE 3.12 Tensile Properties of Nylon 6.6 Monofilaments After Creep Tests

Time (hrs)	U.T.S.* (lbs)	Elong. to Break ε_B^* (%)	U.T.S./(U.T.S.)$_{orig}$*** (%)	$\varepsilon_B/(\varepsilon)_{B_{orig}}$ (%)
After Creep in Air, at 40% U.T.S.**				
0	21	36	100	100
5	21	33	100	92
20	21	--	100	---
25	21	30	100	83
40	21	30	100	83
Original Properties in Water*				
40	20.5	78	98	217
After Creep in Water, at 20% U.T.S.*				
20	18.8	54	90	150
45	17.8	56	85	156
After Creep in Water, at 40% U.T.S.*				
20	17.8	51	85	142
50	17.2	54	82	150

*Averaged values for 2 to 3 tests.

**U.T.S., ultimate tensile strength.

***Tensile properties measured dry at room temperature.

TABLE 3.13 Mechanical Properties of Synthetic Monofilaments After Dry Creep*

PET				NYLON			
Time (hrs)	U.T.S. (lbs)	ε_B (%)	$\varepsilon_B/\varepsilon_{Bo}$ (%)	Time (hrs)	U.T.S. (lbs)	ε_B (%)	$\varepsilon_B/\varepsilon_{Bo}$
0	13.8	51	100	0	21	36	100
5	13.2	37	73	5	21	33	92
10	13.8	37	73	20	21	--	---
20	13.6	34	67	25	21	30	83
30	14.0	36	71	40	21	30	83
40	13.8	34	67				

*At 40% of U.T.S.

4. NONDESTRUCTIVE EVALUATION (NDE) OF SYNTHETIC ROPE

INTRODUCTION

Nondestructive Evaluation (NDE) is a branch of applied science that is concerned with all aspects of the uniformity, quality and serviceability of materials and structures. By definition, nondestructive techniques involve those processes by which materials and structures may be interrogated without damage or disruption of their use. At present, there are no standards relating to the implementation of NDE techniques or the interpretation of NDE results for either new or used rope.

The purpose of this phase of the research program is to develop quantitative NDE techniques for assessing the structural integrity and the safety of synthetic rope structures. To date, the primary emphasis has been on the development of phenomenological quantitative characterizations via ultrasonics and acoustic emission.

There is very little previous work on the nondestructive evaluation of synthetic ropes. A literature survey is provided in (4.1).

ULTRASONIC CHARACTERIZATIONS

Ultrasonic Attenuation

Ultrasonic wave propagation in a medium can be characterized by the wave velocity and attenuation characteristics. The attenuation property describes the ultrasonic wave energy dissipation behavior of the medium and has been found to be useful for the NDE of fiber composites (4.2-4.4).

An experimental technique for measuring the ultrasonic attenuation is to transmit a tone burst (a short duration sinusoidal wave) via an ultrasonic transducer into the specimen and observe the decrease in amplitude of the propagating ultrasonic wave as detected by a receiving ultrasonic transducer. A schematic of the ultrasonic attenuation measuring system used in these experiments is shown in Figure 4.1. The system consisted of a pulsed oscillator (Arenberg Model PG-652C) for generating the sinusoidal waves; a low frequency inductor (Arenberg Model LFT-500); broadband (0.1 to 3.0 MHz) transmitting and receiving transducers (Acoustic Emission Technology [AET] FC-500) having an approximately flat sensitivity of -85 dB (re 1 V/μBar); a transducer-specimen interface couplant (AET SC-6); and an oscilloscope (Textronix Model 455). Two step attenuators were also used. One attenuator, set at 10 dB, reduced the input signal to 100 V (peak-to-peak) into the transmitting transducer, while a second attenuator, set at 20 dB, reduced the 100 V signal to 10 V at the oscilloscope only. The signal from the receiving

transducer was amplified 60 dB by an AET Model 160B preamplifier with a plug-in band-pass filter (FL12X) of 0.125 to 2 MHz and further amplified an additional 40 dB by an AET Model 201 before being displayed on the oscilloscope. The background noise level (after amplification) observed on the oscilloscope was 0.8 V peak-to-peak. The ultrasonic transducers were clamped onto the rope with a clamping force of approximately 67 N (15 lb).

An unflawed Samson double-braided 2-in-1, 1/4" nylon rope was held at different levels of tension in an Instron tensile testing machine. The output signal amplitudes for various signal frequencies and rope tensions, at a transducer center-to-center spacing of 3.8 cm (1.5 in), are summarized in Table 4.1. In general, the output signal amplitude decreases with increasing frequency and increases with increasing tension. Similar data have been obtained for transducer center-to-center spacings of 2.9 cm (1-1/8 in) and 5.1 cm (2 in). In general, the output signal amplitude decreases with increasing transducers center-to-center spacing. However, the output signal is greatly distorted and it is difficult to estimate the absolute attenuation of the rope from these data.

Stress Wave Factor

Another ultrasonic NDE parameter called the "stress wave factor" (SWF) has been proposed by Vary et al. (4.5, 4.6). This NDE parameter has been used successfully by Williams and Lampert (4.3) in the characterization of impact damaged composites.

The stress wave factor is a complicated measure of the ultrasonic energy transmissibility of a structure. Basically, a large amplitude stress pulse (which may be repetitive) is introduced into the specimen via an input ultrasonic transducer which is usually a broadband type. The stress pulse propagates through the specimen and is detected by a receiving ultrasonic transducer which is usually a resonant type located on the same surface as the input transducer. The output of the receiving transducer is often a complicated enveloped waveform containing various numbers of oscillations of the resonant frequency of the receiving transducer. The SWF is defined as the number of times the individual oscillations of the output signal exceed a preset threshold voltage. A relatively larger SWF indicates that the specimen has relatively lower ultrasonic attenuation. Generally, flaws in a structure impede the ultrasonic wave propagation and so flawed specimens tend to have a comparatively lower SWF. A major advantage of the SWF technique is its ease of operation. With the commercial development of the (Acoustic Emission Technology) AET 206 AU SWF unit, a self-contained portable instrument provides a direct digital readout of the SWF.

Flawed and unflawed Samson double-braided 2-in-1, 1/4" nylon ropes with 32 yarns in the cover and 16 yarns in the core were tested.

Specified numbers of core yarns were cut at the same location in the gage section to produce flawed ropes. Ropes were pulled to failure in an Instron tensile testing machine. Stress wave factor (SWF) measurements were obtained using an AET 206 AU unit with a Model 206 FIX transducer holder as shown in Figure 4.2. The input transducer was an AET FC-500 and the output transducer was a resonant AET AC-375 with a peak response at 375 kHz at a sensitivity of -65 dB (re 1 V/μBar). Both transducers were provided with pre-mounted waveguides. A transducer-specimen interface couplant (AET SC-6) was used. The clamping pressure at the transducer (waveguide)-specimen interface was 1.0 MPa (150 psi).

For the flawed and unflawed nylon ropes, the SWF was measured using a 150 V amplitude input pulse, a 65 dB total gain for the output signal, and a 1 V threshold for SWF counting. The repetition of the input pulse was set at 1,000 pulses/second. Because the output signals due to the individual input pulses did not overlap, if each pulse generated 5 SWF, the rate of SWF was 5,000/sec. The value of the digital readout for the SWF per second from the AET 206 AU unit was adjusted to reflect this nonoverlapping of output signals. So, from now on, the SWF data reported are actually the SWF per second due to 1,000 pulses/second. The SWF was measured at load levels of 2,220 N (500 lb), 4,450 N (1,000 lb) and 6,670 N (1,500 lb), unless the rope had already failed, or was near failure. The flaw was located at mid-distance between the two transducers.

The stress wave factor data at various load levels and the ultimate rupture load for the flawed and unflawed ropes are given in Table 4.2. SWF measurements have been made on the core-damaged samples at different load levels. These results can be plotted versus the load at which the measurement is taken. Figure 4.3 shows such a plot where the load level has been normalized with respect to the ultimate load of each individual rope sample. A straight line has been fitted by eye to the data. An example of using this correlation in Figure 4.3 is illustrated as follows: if a rope under tension produces a stress wave factor of 8,000; thus, the rope is at approximately 50% of its ultimate load, independent of core damage.

ACOUSTIC EMISSION CHARACTERIZATIONS

Acoustic Emission Parameters

When a rope structure is loaded, local redistributions of stress, such as filament rupture, release stress waves that propagate to the surface of the rope where they may be detected by a surface-mounted ultrasonic transducer. The electrical output signal from such a transducer is called acoustic emission (AE). In analyzing

the acoustic emission signals, there are various parameters that are commonly used. These parameters are shown in Figure 4.4. Essentially, what is shown is one event. This event begins when the signal first crosses the threshold. The event ends when the signal falls back below the threshold for a specified time. The length of the event is called the AE event duration. Each individual cycle of an event that crosses the threshold is called a ringdown count. The two parameters of AE event count and AE ringdown count are most commonly used. The AE peak amplitude is the highest amplitude the signal reaches. Generally, the AE peak amplitude is expressed in decibels (dB). As indicated by Figure 4.4, the rise time is the elapsed time between the initial threshold crossing and the peak amplitude, while the AE slope is equal to the AE peak amplitude divided by the AE rise time, in units of dB/sec.

Computer-Based Acoustic Emission System (CAES)

The computer-based AE system (CAES) accepts, conditions, analyzes and stores processed acoustic emission (AE) data from up to four channels of AE signals simultaneously. However, only two channels are utilized in these tests. Graphic data displays are provided in real time as well as after the completion of the test (that is, in a post-processing mode).

The CAES is based on a 16-bit LS14/10 microcomputer that resides within a bench-top mainframe of approximately 71 cm x 46 cm x 28 cm (28 in x 18 in x 11 in). Within the mainframe there are a time clock, an input-output interface, 36k words of memory for data and display, 16k words of memory for program storage, and various plug-in modules for AE date processing.

Each AE sensor output is preamplified 60 dB and frequency filtered before it is fed into the CAES. The CAES provides each channel with an adjustable postamplification of up to an additional 40 dB. For a preselected signal threshold level, each AE event is classified according to ringdown counts, peak amplitude, event duration, rise time and slope. Further, with its multichannel capability, the CAES evaluates the spatial location of the AE source (linear location for a two-channel system).

A vital feature of the CAES is its capability of signal and/or noise discrimination. The CAES can be set to accept data only from preselected spatial regions, as well as from preselected ranges of ringdown counts per event, peak amplitude, event duration, rise time, slope, and external analog signal level.

Data can be processed and displayed in a large variety of formats. The rate of events, rate of ringdown counts, rate of ..., cumulative events, cumulative ringdown counts, cumulative..., mean ringdown counts per event, mean peak amplitude per event,

mean..., etc., can be displayed versus time or an external analog parameter. The distribution (and cumulative distribution) of events by spatial location, ringdown counts..., etc., can also be displayed. All displays are automatically presented fully-scaled and the linear or logarithmic scale can be selected at will. Any display can be requested in real time or after the completion of the test, provided memory space has been allocated for that display prior to the initiation of the test.

Communications with the computer are accomplished through a separate graphic display terminal. Simple keyboard commands control the CAES. Test parameters such as the threshold level are set through the keyboard. Data displays are presented on a 30.5 cm (12 in) (diagonally-measured) screen of the graphic display terminal. All displays can be further annotated (say, with rope manufacturer, material or geometric information) by the user before the hard copy is obtained from the separate hard copy unit. The hard copy unit is a video printer that prints on a 12.5 cm (5 in) wide electrosensitive paper roll.

The CAES is a fully functional computer-based system that represents the state-of-the-art of AE test instrumentation.

Experimental Procedures

Two transducers (AET AC-375 LM) with resonant frequencies at 375 kHz at a sensitivity of -60 dB (re 1V/μBar) were attached to the gage section of Samson 2-in-1, 1/4" nylon rope specimens at a separation of 7.6 cm (3.0 in) at the low load of approximately 220 N (50 lb). An interface couplant (AET SC-6) was used. Clamps provided a clamping force of more than 67 N (15 lb) at the transducer-specimen interface. The transducers were protected from damage due to rope snapback by sponge covers. After a pre-amplification of 60 dB, the output from each transducer was post-amplified either an additional 34 dB or 40 dB producing a total system (post-transducer) gain of 94 dB or 100 dB. The AE threshold level was fixed at 1.0 V after total amplification. Peak amplitude results were obtained from AE signals directly after preamplification (and before postamplification) and the dB level was computed such that a 10 V signal corresponded to 64 dB. No special AE signal discrimination was used in this study other than discrimination by AE source location. Based upon calibration measurements using the CAES and the pulser of the AET 206 AU unit on unflawed rope at a 6670 N (1500 lb) load, the wave speed was taken to be 2.97×10^5 cm/sec (117,000 in/sec).

The rope specimens were pulled to failure in an Instron tensile machine using 10.2 cm (4 in) diameter capstan jaws at a constant crosshead speed of 0.085 cm/sec (2.0 in/min). Various AE data displays were recorded during and after each test.

Rope with Damaged Core

Samson double-braided 2-in-1, 1/4" nylon ropes with 32 yarns in the cover and 16 yarns in the core were tested. Specified numbers of yarns from the core were cut at the same location at the gage section of the rope. A total AE system gain of 94 dB was used.

Figure 4.5 shows a typical cumulative AE ringdown count versus time record obtained from a rope with ten (10) cut core yarns. The rope ruptured at 6230 N (1400 lb) at the section containing the cut yarns. A plot similar to Figure 4.5 can be obtained for the cumulative AE event count versus time. Both the cumulative AE ringdown and event counts curves rise rapidly as the core rupture load is approached and both curves rise rapidly as the cover rupture load is approached.

It can be seen that when a specimen is loaded gradually from zero load, AE will begin to be detected at a particular time which corresponds to a particular load. The corresponding load level is defined by the authors as the "AE load delay". Because of potential noise problems and the intrinsic threshold limitations of the AE test system, a convenient and practical level of AE activity is defined to be the load delay. Specifically, the load delay is defined as the load required to produce a specified low level of cumulative AE event or ringdown counts. Thus, the AE load delays based on the cumulative AE event and ringdown counts from the same specimen may be different, depending on the specified levels set for the cumulative AE event and ringdown counts, respectively.

For the ropes tested, the specified levels for the cumulative, AE event and ringdown counts are (tentatively) set at 2 and 75, respectively. The AE load delays for the flawed ropes obtained according to these criteria and the corresponding ultimate rupture loads are presented in Table 4.3. The AE load delay based on the cumulative AE ringdown counts is plotted versus ultimate rupture load in Figure 4.6. Straight lines have been fitted by eye to the data. A similar correlation can be obtained for the AE load delay based on the cumulative AE event counts. A potential application of the data in Figure 4.6 is the interrogation of ropes for core damage. For example, if a rope that is suspected of core damage is loaded to 4000 N and the AE ringdown counts load delay is not reached, then the rope can be predicted to support, at least, 8000 N.

Knotted Ropes

Various types of knots were introduced into Samson double-braided 2-in-1, 1/4" nylon ropes. The knotted ropes were pulled to failure in an Instron tensile testing machine. Acoustic emission (AE) testing were conducted on each knotted rope with a

total AE system gain of 100 dB.

Two classes of knots were tested, namely, a knot in a single rope and a knot for tying two ropes together. Various types of knots in a single rope and knots for tying two ropes together are shown in Figures 4.7 and 4.8, respectively (4.7).

For the knotted ropes tested, the specified levels in defining the AE load delay based on the cumulative AE event and ringdown counts are (tentatively) set at 2 and 25, respectively. The AE load delays for the knotted ropes obtained according to these criteria and the corresponding ultimate loads are presented in Table 4.3. Based on the previously measured unflawed new rope ultimate strength of 10,000 N (2250 lb), a knot efficiency can be calculated and is also shown in Table 4.4. Also, the industry's (4.7) suggested knot efficiency is given in Table 4.4.

The AE load delay based on the cumulative AE ringdown counts is plotted versus ultimate load in Figure 4.9. A straight line has been fitted by eye to the data. A similar correlation can be obtained for the AE load delay based on the cumulative AE event.

CONCLUSIONS

Preliminary nondestructive evaluation (NDE) has been conducted on synthetic ropes. The NDE techniques so far considered include ultrasonics and acoustic emission (AE). The NDE testing so far has been conducted on Samson double-braided 2-in-1, 1/4" nylon rope.

In ultrasonic attenuation testing with a transducer arrangement as shown in Figure 4.1, it has been found that the output signal amplitude decreases with increasing frequency and increases with increasing rope tension in an unflawed rope. In stress wave factor testing, a correlation has been found between the SWF and the SWF measurement load level normalized with respect to the ultimate load of each individual rope sample with cut core yarns. In AE testing, an "AE load delay" has been defined corresponding to the load level required to produce a specified low level of AE activity. It has been observed that the AE load delay can be correlated with the ultimate rupture load of a rope with cut core yarns and also of knotted ropes.

FUTURE PLANS

Based on the results of this preliminary study, further investigations into the AE load delay parameter will be pursued. Because AE signals are complex in nature, any progress towards maximizing the amount of information obtained from AE testing

relies on the understanding of the AE signal in greater detail. Also, the stress wave factor effort will be continued. The NDE testing so far has been conducted on Samson double-braided 2-in-1, 1/4" nylon rope. Future tests will include ropes of different sizes. Future tests will also include flaw configurations in addition to cut core yarns and knots.

REFERENCES

4.1 J.H. Williams, Jr. and S.S. Lee, "Acoustic Emission/Rupture Load Characterizations of Double-Braided Nylon Rope", (accepted for publication in Marine Technology).

4.2 J.H. Williams, Jr. and B. Doll, "Ultrasonic Attenuation as an Indicator of Fatigue Life of Graphite Fiber Epoxy Composite", Materials Evaluation, Vol. 38, No. 5, May 1980, pp. 33-37.

4.3 J.H. Williams, Jr. and N.R. Lampert, "Ultrasonic Nondestructive Evaluation of Impact-Damaged Graphite Fiber Composite", Materials Evaluation, Vol. 38, No. 12, December 1980, pp. 68-72.

4.4 J.H. Williams, Jr., S.S. Lee and T.K. Wang, "Quantitative Nondestructive Evaluation of Automotive Glass Fiber Composites", Journal of Composite Materials, Vol. 16, January 1982, pp. 20-39.

4.5 A. Vary and K.J. Bowles, "Ultrasonic Evaluation of the Strength of Unidirectional Graphite-Polyimide Composites", NASA Technical Memorandum 73646, April 1977.

4.6 A. Vary and R.F. Lark, "Correlation of Fiber Composite Tensile Strength with the Ultrasonic Stress Wave Factor", Journal of Testing and Evaluation, Vol. 7, No. 4, July 1979, pp. 185-191.

4.7 "Rope Knowledge for Riggers", The Cordage Group, Division of Columbian Rope Co., Auburn, New York 13021 (1977).

LIST OF FIGURES

4.1 System for Ultrasonic Attenuation Measurements in a Rope

4.2 AET 206 AU System for Stress Wave Factor Measurements

4.3 Stress Wave Factor vs. Load as a Percentage of Individual Ultimate Load at which Stress Wave Factor is Taken for Flawed and Unflawed Samson Double-Braided 2-in-1 0.635 cm (1/4-in) Nylon Rope

4.4 A Typical Acoustic Emission Signal with Some Common AE Parameters Indicated.

4.5 Cumulative AE Ringdown Counts vs. Time (extension) for a Samson Double-Braided 2-in-1, 0.635 cm (1/4-in) Diameter Nylon Rope with 10 Yarns Cut in Core

4.6 Cumulative AE Ringdown Counts Load Delay vs. Rupture Load of Samson Double-Braided 2-in-1, 0.635 cm (1/4-in) Diameter Nylon Rope with Various Numbers of Core Yarns Cut

4.7 Various Types of Knots in a Single Rope with Loading Directions Indicated by Arrows

4.8 Various Type of Knots for Tying Two Ropes Together with Loading Directions Indicated by Arrows

4.9 Cumulative AE Ringdown Counts Load Delay vs. Ultimate Load of Knotted Samson Double-Braided 2-in-1, 0.635 cm (1/4-in) Diameter Nylon Rope

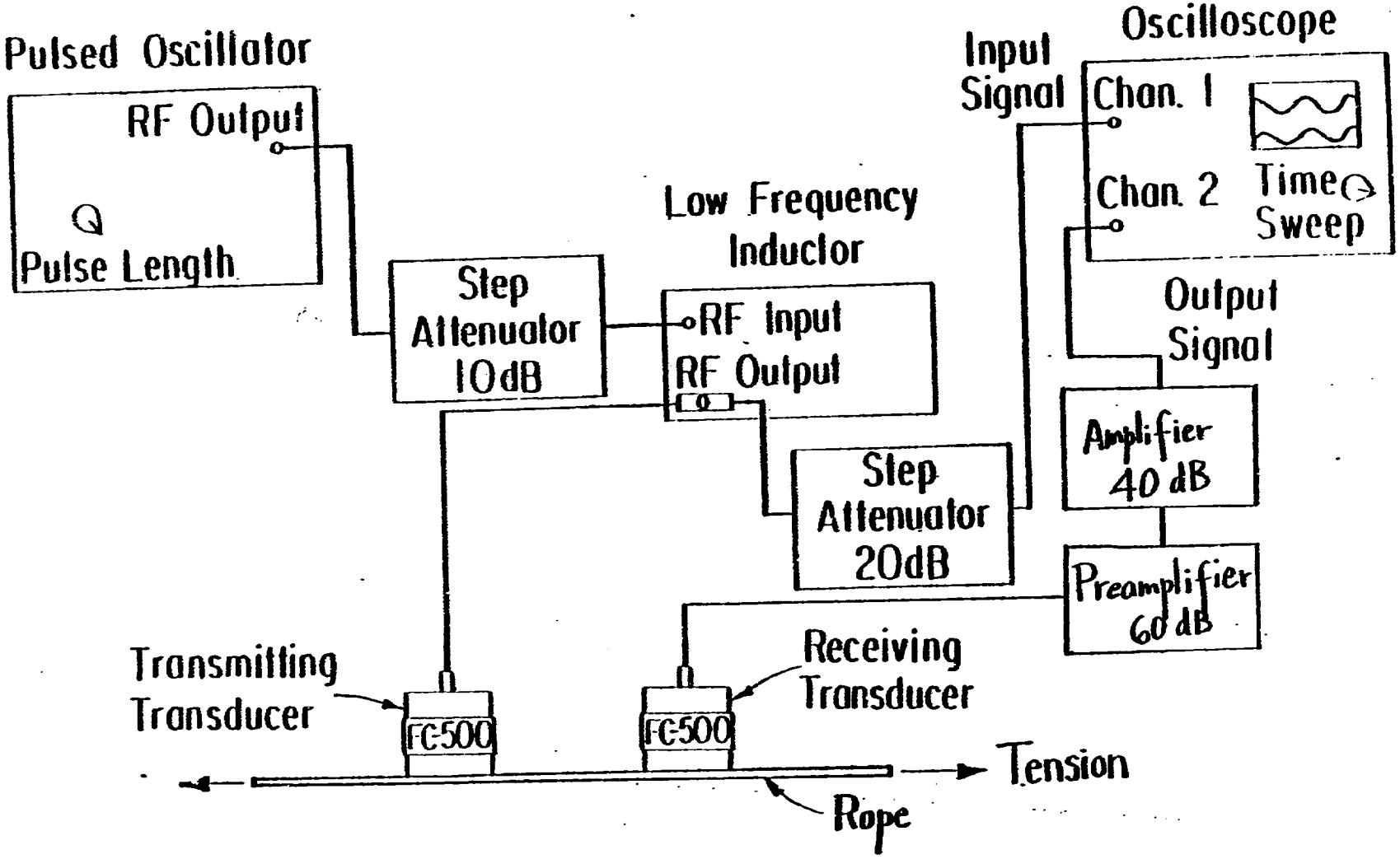

Fig. 4.1 System for ultrasonic attenuation measurements in a rope.

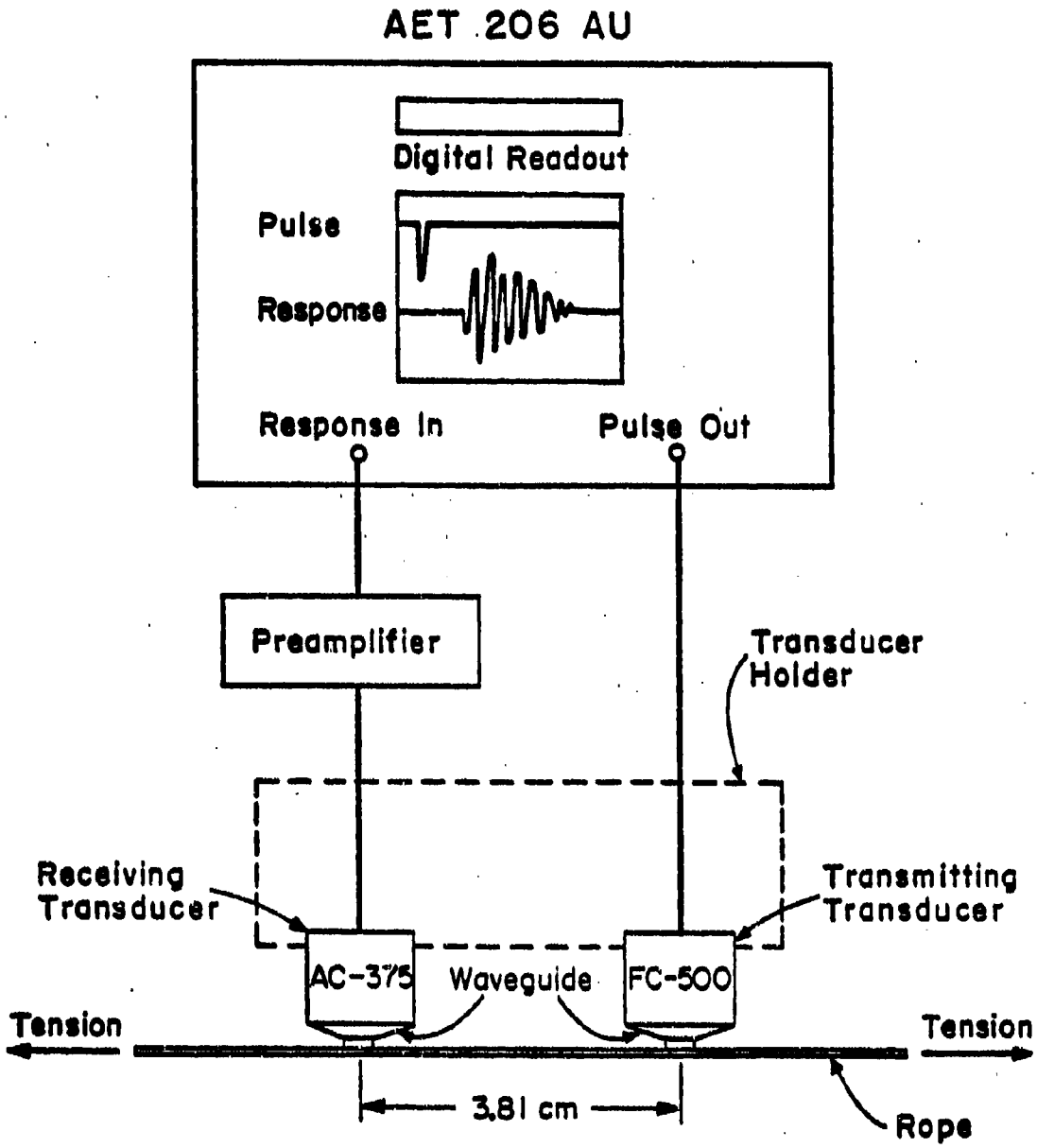

Fig. 4.2 AET 206 AU system for stress wave factor measurements.

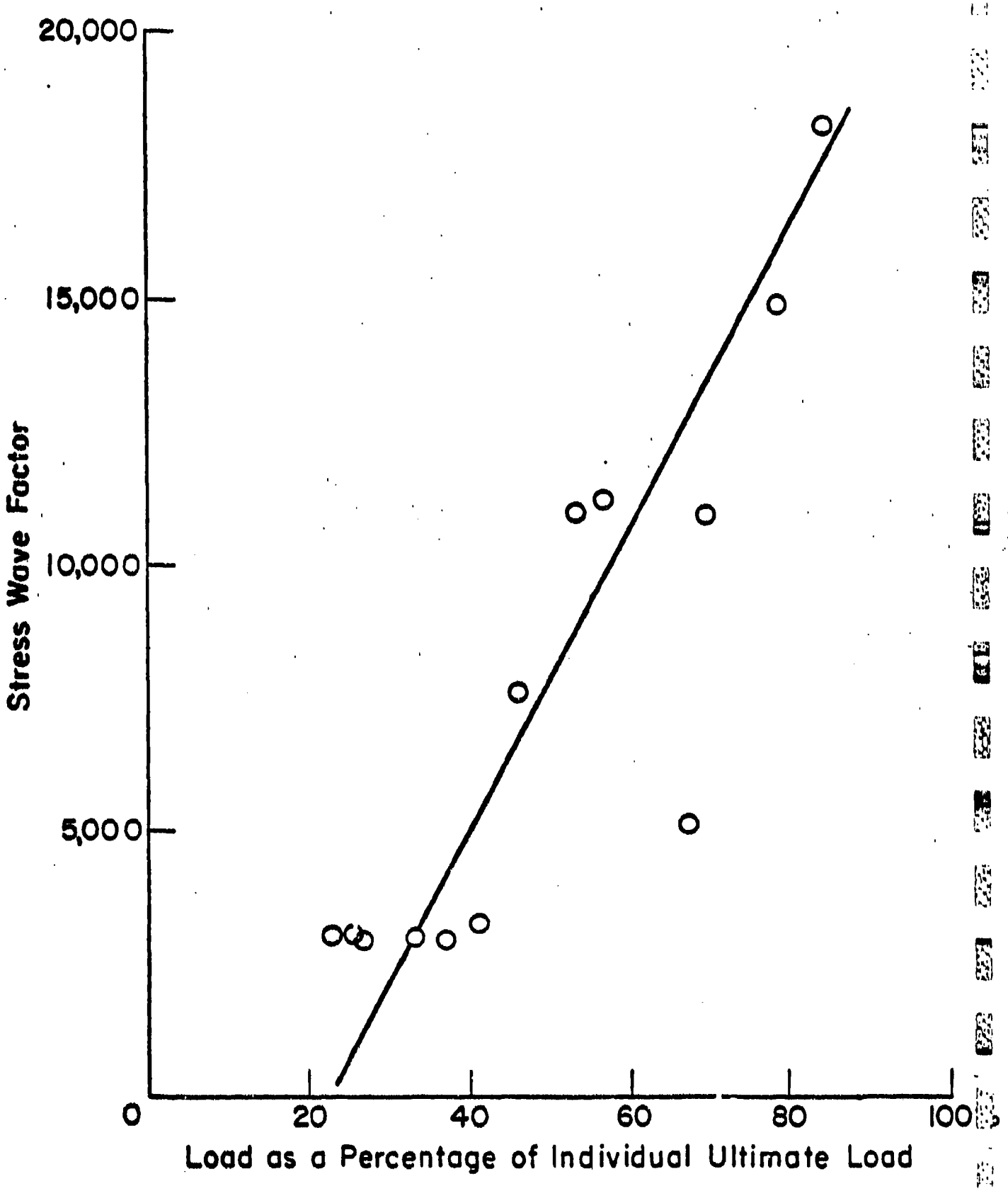

Fig. 4.3 Stress wave factor versus load as a percentage of individual ultimate load at which stress wave factor is taken for flawed and unflawed Samson double-braided 2-in-1, 0.635 cm (1/4 in) nylon rope.

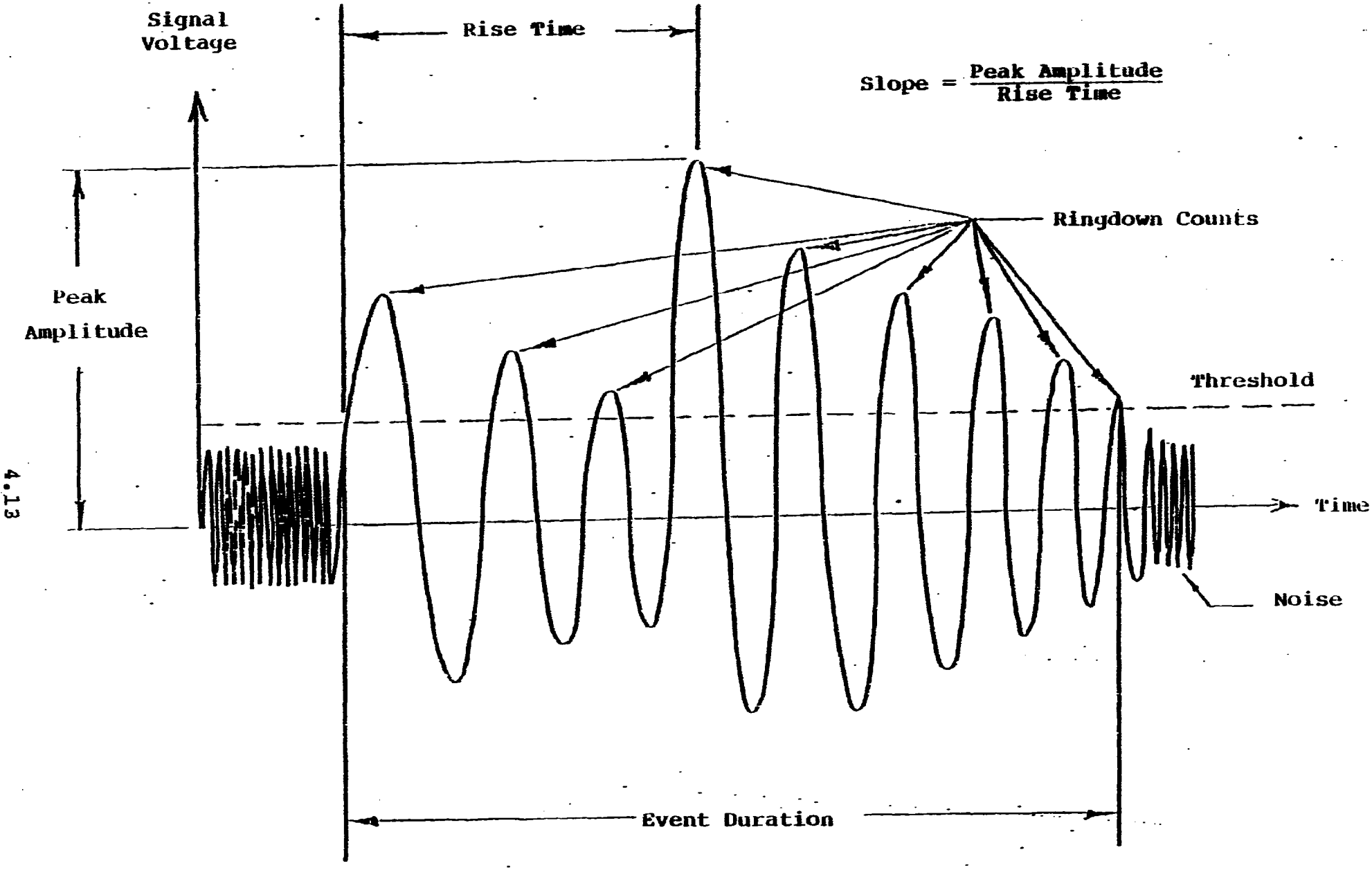

Fig. 4.4 A typical acoustic emission signal with some common AE parameters indicated.

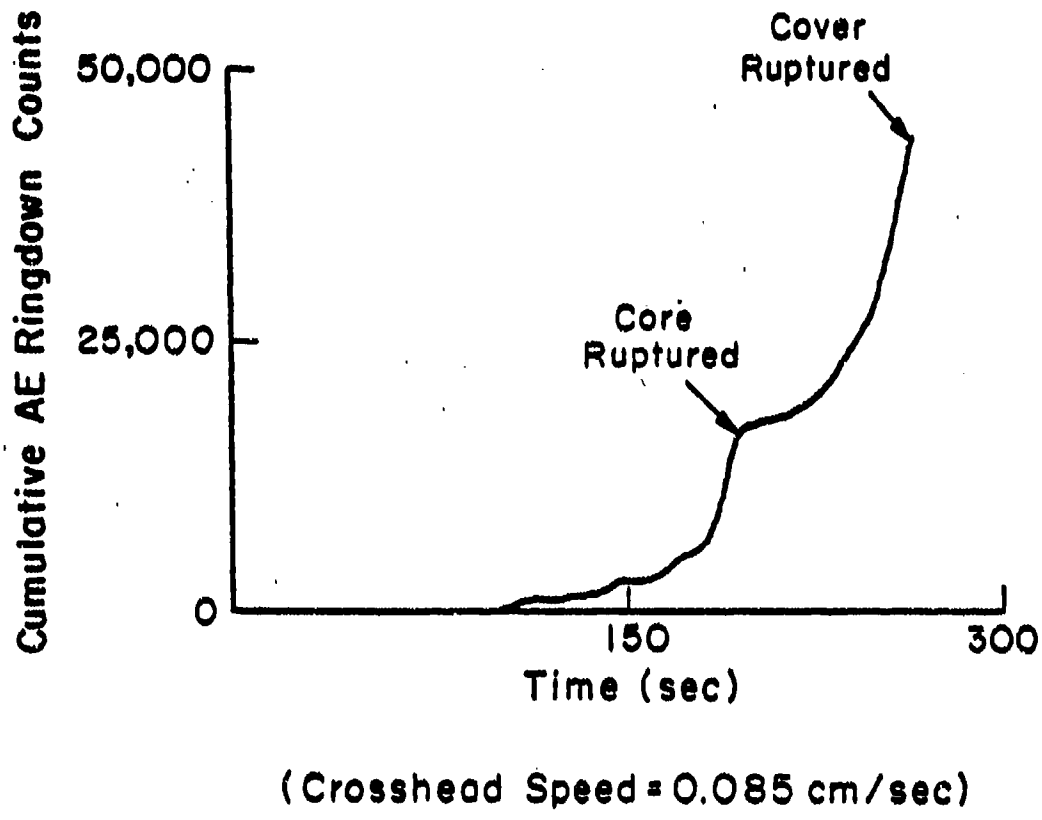

Fig. 4.5 Cumulative AE ringdown counts versus time (extension) for a Samson double-braided 2-in-1, 0.635 cm (1/4 in) diameter nylon rope with 10 yarns cut in core.

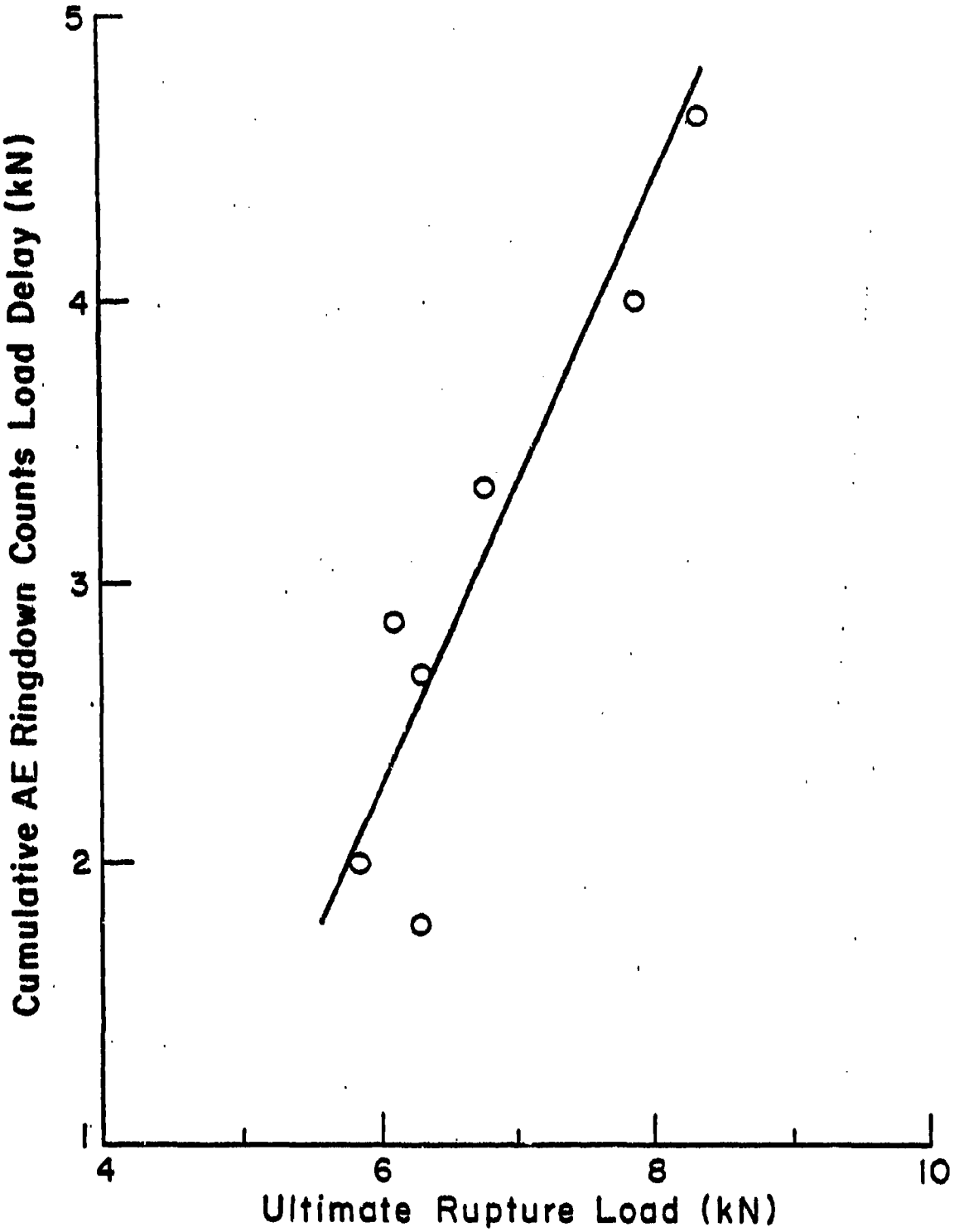

Fig. 4.6 Cumulative AE ringdown counts load delay versus rupture load of Samson double-braided 2-in-1, 0.635 cm (1/4 in) diameter nylon rope with various numbers of core yarns cut.

Overhand

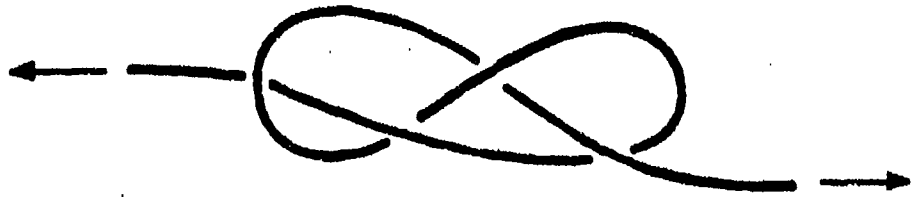

Figure Eight

Stevedore's

Fig. 4.7 Various types of knots in a single rope with loading directions indicated by arrows.

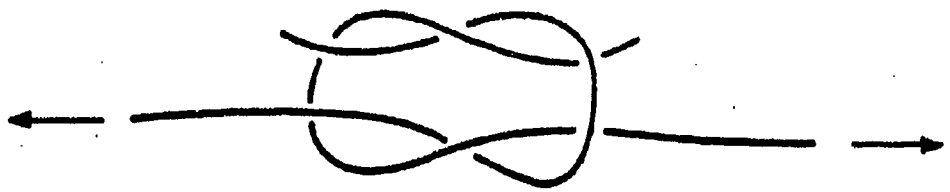

Square

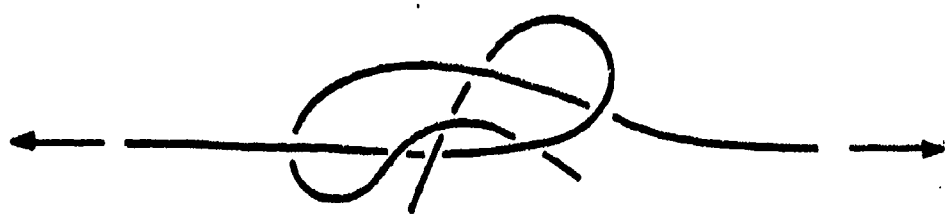

Sheet Bend

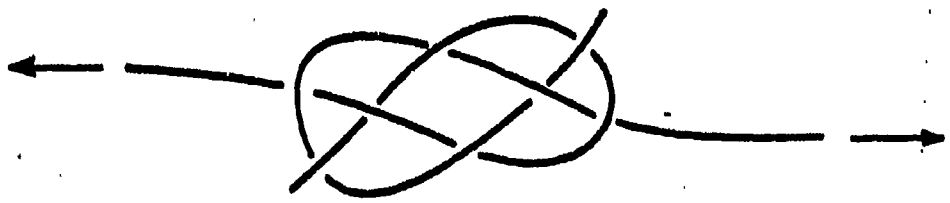

Carrick Bend

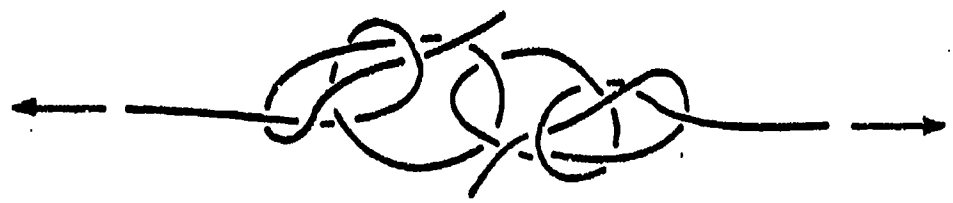

Interlocking Bowlines

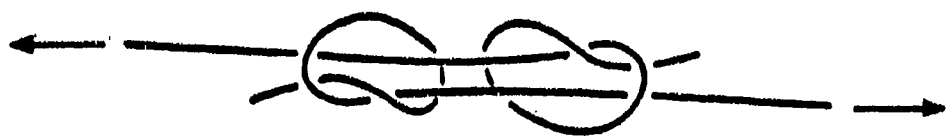

Fisherman's

Fig. 4.8 Various types of knots for tying two ropes together with loading directions indicated by arrows.

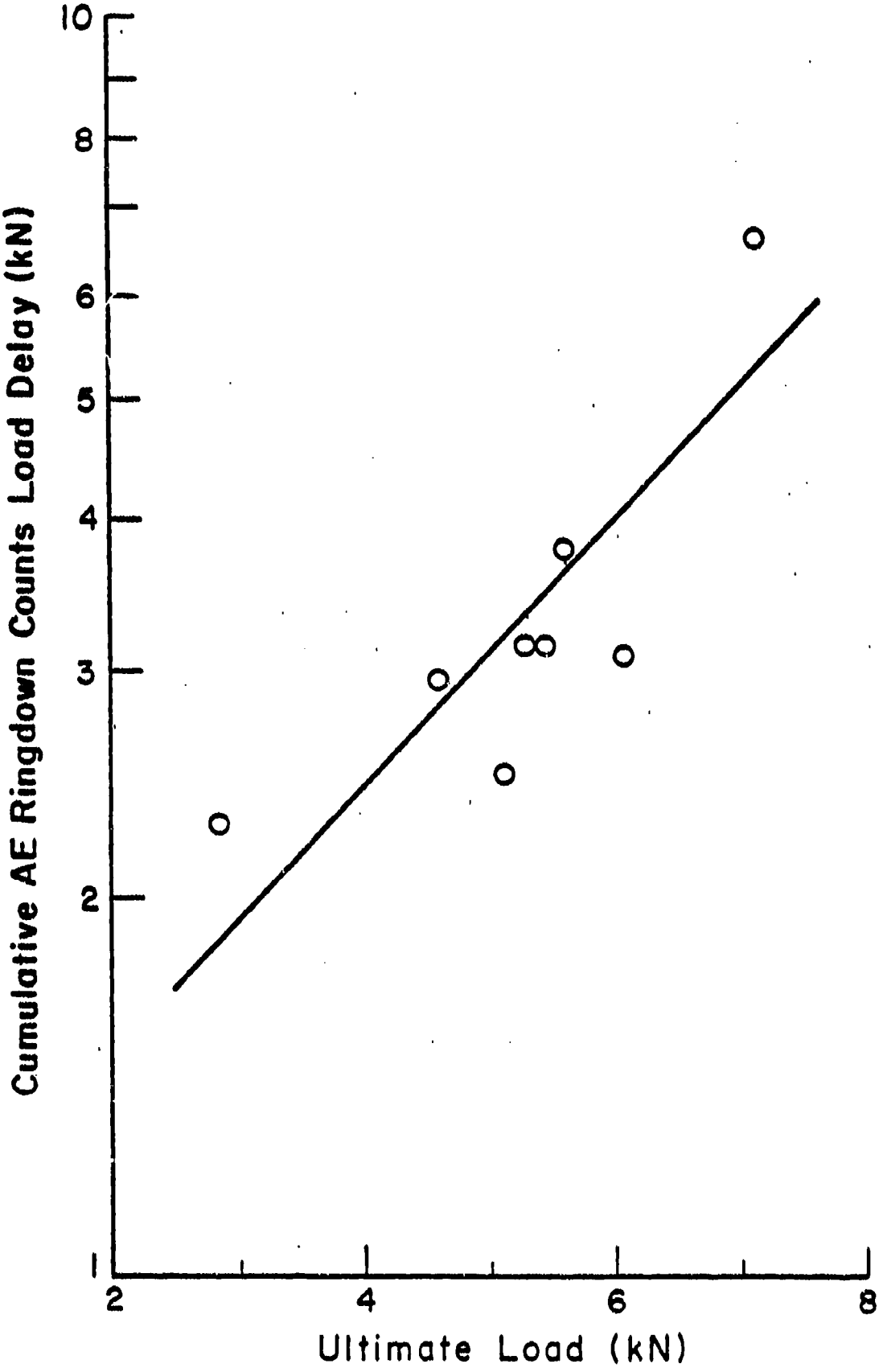

Fig. 4.9 Cumulative AE ringdown counts load delay versus ultimate load of knotted Samson double-braided 2-in-1, 0.635 cm (1/4 in) diameter nylon rope.

LIST OF TABLES

4.1 Output Signal Amplitude Data for Various Signal Frequencies and Rope Tensions at a Transducer Center-to-Center Spacing of 3.8 cm (1.5 in)

4.2 Summary of Strength and Stress Wave Factor Data for Samson Double-Braided 2-in-1, 0.635 cm (1/4 in) Nylon Ropes

4.3 Summary of Strength and Acoustic Emission Data for Samson Double-Braided 2-in-1, 1/4 in) Nylon Ropes

4.4 Summary of Strength, Acoustic Emission and Knot Efficiency Data for Knotted Samson Double-Braided 2-in-1 (1/4 in) Nylon Ropes

TABLE 4.1 Output Signal Amplitude Data for Various Signal Frequencies and Rope Tensions at a Transducer Center-to-Center Spacing of 3.8 cm (1.5 in).

Rope* Tension (N)	Output Signal Amplitude (V peak-to-peak) at Frequency					
	0.2 MHz	0.3 MHz	0.4 MHz	0.5 MHz	0.6 MHz	0.7 MHz
2220	2.4	2.0	1.6	1.2	1.0	-
4450	3.2	4.0	1.4	1.0	-	-
6670	6.7	15.0	1.4	2.5	1.2	1.0

* Unflawed Samson double-braided 2-in-1, 1/4" nylon rope.

- Less than 1.0 V peak-to-peak.

TABLE 4.2 Summary of Strength and Stress Wave Factor Data for Samson Double-Braided 2-in-1, 0.635 cm (1/4 in) Nylon Ropes.

Number of Yarns Cut in Core	Ultimate Rupture Load (N)	Stress Wave Factor Measured at		
		2,220 N	4,450 N	6,670 N
0	9,560	3,000	7,700	11,000
1	7,780	3,000	11,200	18,300
2	8,450	3,100	11,000	15,000
4	6,450	3,000	5,100	---
6	5,340	3,200	---	---
10	6,000	3,000	---	---

TABLE 4.3 Summary of Strength and Acoustic Emission Data for Samson Double-Braided 2-in-1, 1/4" Nylon Ropes.

Number of Yarns Cut in Core	Ultimate Rupture Load (N)	AE Load Delay (N)	
		Based on Cumulative AE Event Counts	Based on Cumulative AE Ringdown Counts
0*	8230	4230	4670
7	6670	3340	3340
8	5780	2000	2000
10	6230	1780	1780
12	6230	2670	2670
14	7780	3560	4000
16	6000	2220	2890

* The core was pulled out and then replaced without cutting any yarn.

TABLE 4.4 Summary of Strength, Acoustic Emission and Knot Efficiency Data for Knotted Samson Double-Braided 2-in-1, 1/4" Nylon Ropes.

Knot Type (4.7)	Ultimate Load (N)	AE Load Delay (N)		Knot Efficiency (%)	
		Based on Cumulative AE Event Counts	Based on Cumulative AE Ringdown Counts	Measured**	Industry's Suggested (4.7)
Overhand	5120	1790	2490	51.2	—
Figure Eight	5380	2180	3110	53.8	—
Stevedore's	5490	3140	3140	54.9	—
Square	2890*	2180	2270	28.9*	43-47
Sheet Bend	4670	2980	2980	46.7	48-58
Carrick Bend	6120	3070	3070	61.2	55-60
Interlocking Bowlines	7210	6740	6610	72.1	65-75
Fisherman's	5690	3870	3780	56.9	50-58

* Knot failed by slipping rather than breaking.

** Normalized with respect to 10,000 N.

5. FATIGUE LOADING AND ENVIRONMENTAL EFFECTS

INTRODUCTION

Marine ropes experience a complex history of static and cyclic loading (5.1) and environmental exposure. Some aspects of this history apparently combine to sufficiently weaken some ropes so that unexpected failures occur. This part of the project is concerned with determining the possible role played in the weakening process by static and cyclic fatigue loading in air and salt water environments. An understanding of the mechanisms by which these factors degrade ropes requires a thorough characterization of their effects at the more basic structural levels of fibers and yarns, as well as small ropes. Thus, the experimental program includes characterization at each level of structure of the fatigue lifetime over a broad range of static and cyclic loads in air and salt water environments; changes in the stress-strain curves and residual strength and elongation will also be determined at various fractions of the lifetime. The mechanisms of degradation will be studied microscopically and models will be developed for each case. These will be integrated with the other parts of the rope project to establish a more general understanding of the effects of fatigue loading and environmental factors on rope reliability.

The fatigue loading of polymers has received considerable attention in some areas such as fatigue crack growth (5.2), but experience with polymers is much less extensive than with metals. In inert environments, ductile polymers commonly fail by two distinct modes depending upon loading conditions. In a cyclic creep mode, failure is dominated by time under load, and in some cases occurs more rapidly with a constant load than with a cyclic load which allows some relaxation during the unloading parts of the cycle (5.3, 5.4). The other failure mode is associated with fatigue crack initiation and propagation, and occurs much more rapidly with cyclic loads (5.2,5.4), although very slow crack growth can also occur at low static loads, sometimes termed creep cracking (5.5).

Environmental effects (excluding ultraviolet degradation) generally depend upon the mode of failure involved. Environmental agents may plasticize the material, as with water in nylon, so that molecular motion and resulting deformation occur more readily. In nylon the effects of moisture are associated with the interruption of hydrogen bonding between nylon molecules (5.6). More severe effects may occur with specific chemical agents, as with the effects of certain metal salts on nylon (5.7-5.10) which interact with moisture and hydrogen bonding. If the polymer fails in a cyclic creep mode, then plasticization decreases the time to failure at a given static or cyclic stress as it also decreases the yield stress (5.6). The elastic modulus may also decrease under

these conditions. Fatigue crack generated failures may have a more complex response to environmental agents. Nylon 66 is reported (5.2) to show a minimum crack growth rate around 2% moisture, apparently due to embrittlement below this value and excessive softening above it. A phenomenon called environmental stress cracking (5.11) occurs when polymers, frequently ductile under normal conditions, fail by brittle cracking in the presence of long term low tensile stresses and specific environmental agents. Examples of this are metal salt solutions with nylon (5.7-5.10) and detergents with polyethylene (5.11).

The foregoing fatigue and environmental effects relate to bulk polymers. The fibers from which ropes are constructed behave very differently from bulk forms of the same materials. The strength of nylon 66 fibers is typically more than ten times higher than the yield strength of the bulk polymer, and the elastic modulus is several times higher. These differences reflect the oriented molecules and microfibers in the drawn fiber structure (5.6, 5.12) which give much higher mechanical properties along the fiber axis. It is doubtful that the fatigue and environmental effects observed for bulk polymers apply directly to their fibers due to the great difference in structure and resulting deformation mechanisms. Furthermore, ropes are constructed from many fibers arranged in substructures as discussed in other sections of this report. Many fatigue effects may be expected from interactions between fibers and larger scale structures within the rope.

A number of studies have been made of the fatigue of nylon and other fibers using several techniques (see for example Ref. 5.13-5.18). While various degrees of fatigue resistance are reported, it is clear from the more standard tests (5.13,5.14) that nylon fibers lose a substantial amount of their strength when subjected to cyclic loading, apparently losing on the order of half of the initial strength after 10^5 to 10^6 cycles. Failure modes in fibers are reported to shift from a transverse crack in a simple strength test to axial splitting in fatigue (5.16). It is also reported (5.16) that the fiber must become slack on each cycle for significant fatigue degradation to occur. The very limited data available on the effects of the environment on the fatigue behavior indicates some loss in lifetime associated with water immersion in a complex test involving rotation over a pin (5.17).

Several studies have also been reported on synthetic fiber ropes varying in size from 1/2 inch to 8 inch diameter. The most extensive data are reported by Bidding (5.19) for 1/2 inch diameter 8-strand plaited nylon rope tested in sea water. These results indicate a more severe degrataion of ropes in fatigue than that usually reported for single fibers. Other tests reviewed by Paul (5.20) show changes in the stress-strain behavior of fatigued ropes which diminish their subsequent energy absorbing ability.

The available literature indicate that fatigue loading is probably an important factor in degrading the properties of fibers and ropes. The importance of sea water in this process is uncertain, but general experience with the environmental stress cracking of polymers and the specific effects of moisture and some metallic salts on nylon suggest that this subject deserves careful consideration. Environmental and fatigue effects on ropes cannot be understood without study of their effects on single fibers. However, consideration must also be given to the complications which may arise due to the rope structure and interactions between fibers. Some effects may occur only in association with fiber-fiber contact and shifts in the geometry of the rope structure. In an effort to include these interactions, the study involves yarns as well as single fibers, and will later include small ropes. The work has been limited to nylon 66 based materials.

EXPERIMENTAL PROCEDURES

Gripping Methods

Correct gripping is particularly important for valid fatigue results. Considerable time was devoted to correct gripping in the early phases of the project and it continues to be a concern. For valid testing, breakage should occur within the specimen gage length, rather than at the grips (under conditions of unknown stress concentration). A tabbing method is used for testing of nylon yarns and single fibers; tabs differ for wet and dry conditions, but are generally similar to Figure 5.1. Cardboard tabs and Eastman 910 adhesive are preferred for dry testing as no visible slippage occurs. The flexible silicone sealant is used to modulate slight misalignment errors and stress transfer at the tab end, as well as to protect the sample from abrasion. With this system, grip breaks occur in less than 20% of the specimens. The tab for wet testing is constructed of PVC, sanded and acetone cleaned prior to fiber bonding. Thinning of the rigid PVC tab edges is also necessary for more gradual stress transfer. Epon 828/TETA is used as the adhesive.

Fatigue Testing

Fatigue testing is conducted on an Instron Model 1331 servo-hydraulic machine. Tests may be run in load, stroke or strain control in a variety of functions (eg. sine, haversine, ramp). Most tests were conducted in the load control mode, using a sine wave function.

Ultimate tensile load was evaluated using a single ramp test to failure with a loading rate equivalent to the loading portion of the fatigue cycle (approximated by one-half of a sine wave). Subsequent cycling was then conducted at various percentages of ultimate tensile load. The specimens were cycled between limits of

the given maximum load and one-tenth of this value, i.e. the stress ratio, R = minimum load/maximum load, was set equal to 0.1. A master cycle of 1 Hz was used for most testing. Master cycle is used here to refer to the frequency which would be obtained in theoretical cycling at 100% of ultimate tensile strength. Actual test frequency at each percentage of ultimate tensile load was then adjusted upward to maintain a constant loading rate. Test frequency was kept as close as possible to this level, except in the case of single fiber or sea water testing, where machine resonances required slightly lower values.

For single fiber fatigue testing a specially designed support frame was constructed to minimize vibrations transmitted from the hydraulics. The support is a free-standing steel W-beam construction on pneumatic shock absorbers. A 2000-gram load cell suspended from this frame registers approximately 1.5 gram noise on the lowest possible calibration.

Computer assisted data acquisition uses a Digital Minc minicomputer and the 1331 Instron. A program which detects maximum and minimum load, maximum and minimum displacement, and energy at designated cycle intervals has been developed; the program is useful for detailed sample monitoring and subsequent ease of data manipulation.

Sea Water Testing

ASTM standard formulation D1141 was used for sea water composition. A specially designed plexiglas chamber and grips for sea water fatigue are shown in Figure 5.2. The chamber is mounted with the fixed grip positioned on the Instron piston and the freely travelling rod attached to the load cell suspended from a separate support stand. During cycling the entire chamber moves up and down on the piston, around the rod. This configuration is necessary when using sensitive load cells which cannot support the weight of the chamber. For smooth operation, careful adjustment of the gain is required, and the upper grip must remain above water to avoid control problems from hydrodynamic effects.

RESULTS AND DISCUSSION

S-N Data

Fatigue S-N curves (maximum stress vs. log cycles to fail) have been obtained for DuPont 707 nylon 66 yarns and fibers extracted from them. The 1260 denier yarns (210 fibers) are lightly interlaced at intervals of several inches, so that an interlace point normally occurs somewhere in the gage section of yarn specimens. The S-N data are presented as normalized plots where the maximum load is divided by the single cycle ultimate tensile load for the conditions of that particular data set. Table 5.1 gives values of ultimate tensile load and strain at failure for the conditions tested; these can be used to determine absolute load values for the S-N data if desired.

Figure 5.3 gives the baseline S-N fatigue data for single fibers and yarns in laboratory air. The solid lines are least-squares fits to the data. The S-N curve for the yarns is relatively steep compared with the single fiber data after a plateau where the yarns show no apparent loss in strength for the first 1-2 decades of cycles. This plateau appears to result from structural effects related to straightening of the fibers in the yarn, as will be discussed later. The yarns can only carry 40% of their initial strength out to 10^5 or 10^6 cycles; it is not yet clear whether any fatigue limit is reached at loads below 40%. These S-N curves are generally comparable to those given in Refs. (5.13) and (5.14), and appear to be approximately linear on the semilog plots.

The effect of short term exposure to sea water on the S-N curve of single fibers is indicated in Figure 5.4. The sea water tests were conducted on specimens immersed for only five minutes before testing, as well as during the tests. Longer exposure times will be used in future work. The results in Figure 5.4 and Table 1 show some loss in initial strength and fatigue lifetime for fiber specimens exposed to sea water. Figure 5.5 gives the corresponding results for yarn tests. The wet yarns do not show the high stress plateau of the dry yarns, but the data converge at lower stresses. The wet yarns fail up to a decade sooner than dry yarns at high stress. Figure 5.6 compares the sea water data for yarns and single fibers; unlike the dry case in Figure 5.3, the wet fiber and yarn data are nearly the same on the normalized plot.

The dry yarn data appear to be different from the other cases in that there is a plateau at high stress and a relatively steep S-N curve. The static test results for the dry yarns do not appear unusual (Table 1) in that the strength and strain to failure are similar to the values for the wet case. Typical load-displacement curves for dry and wet yarns are given in Figure 5.7. These curves are also similar except for the bump in the dry curve at low load. This bump is less prominent for the wet yarn and for single fibers. One explanation for the dry yarn data may be that the fibers are difficult to straighten, especially with interlaced cases. Water may lubricate the yarn and fatigue cycling may also help to shake down the structure. If the dry yarns have a lower single cycle strength due to this effect, then the plateau may simply indicate that the shaken down or lubricated strength would be higher, and the S-N data in Figure 5.3 may extrapolate to this ficticious value. Results for residual strength to be given later appear to support this hypothesis, but further investigation is required. The dry yarn S-N curve may be steeper due to more severe fiber-fiber interactions as will be supported later by fractographic evidence.

Reference has been made in the literature (5.16,5.19) as to the significant effects of reaching a slack condition during each fatigue cycle. The results given here are generally for cases where a minimum tensile load of 10% of the maximum value is maintained. The effects of a slack load on dry yarn fatigue were investigated by testing in displacement control using manual adjustments to maintain the maximum load. Figure 5.8 indicates no significant effect

of reaching zero load and allowing the yarn to go slack on each cycle, as compared with the usual conditions. The effect of a slack load could prove to be more significant with rope tests, where more relaxation of the structure is possible.

Figure 5.9 compares the sea water results for yarns and fibers with the mean lifetimes reported by Bidding (5.19) for 1/2 inch, 8 strand plaited nylon rope. The rope tests included a slack load on each cycle, and were conditioned for one week in sea water prior to testing, as compared with the yarn and fiber tests which were conditioned for only five minutes. The ropes were also tested with an eye-splice at the ends which may influence the results. Despite the many differences in testing conditions and structure, wet yarn and fiber data appear to agree surprisingly well with Bidding's rope data. Future work on this project will also involve small rope testing.

As mentioned earlier, the fatigue lifetime of polymers may be dominated either by time under load (cyclic creep) or may be more typical of metals, involving crack initiation and growth which depends most heavily on the number of stress reversals. The dominance of either effect may be determined by varying the fatigue loading parameters and frequency. Figure 5.10 gives fatigue data for single fibers tested in air as a function of log time to failure rather than cycles. The total test lifetime is apparently similar regardless of test frequency or even for constant force, creep rupture tests. While more study is required to form definite conclusions, it appears that the single fiber lifetime is controlled to a first approximation by the cumulative time under load rather than the number of fatigue cycles.

Figure 5.11 gives comparable data for dry yarns. Here the creep rupture curve is much less steep than the cyclic fatigue curves, but is similar to the single fiber creep rupture curve. The cyclic results show a sensitivity of total test lifetime to frequency. The same data plotted vs. log cycles to fail in Figure 5.12 tend to fall in a similar range independent of frequency. Thus, it appears that the yarn lifetime in fatigue is determined by the number of cycles while the fiber lifetime is determined by the total loading time. This implies that the steeper S-N curves found for dry yarns as compared with fibers may derive from fiber-fiber damage effects which would be expected to depend on the number of cycles. This may become even more important in tests of ropes.

Residual Property Tests

The residual property tests are conducted to follow changes in the properties of the specimen at various fractions of its lifetime, typically 25, 50 and 75% of the mean lifetime at a particular load. These properties are important in rope applications since they give an indication of what load, strain, or energy absorption the rope is capable of after a period of use. Figure 5.13 shows typical load vs. displacement data during the fatigue of a yarn. The first loading-unloading cycle contains significant hysteresis (enclosed area) and permanent strain (which could relax given more

time at low load). Further cycling tends to shift the curve to the right, and a typical hysteresis loop is developed representing the cyclic stress-strain behavior for an intermediate cycle. This may continue until failure occurs, as in a normal S-N test, or the cycling may be stopped and the stress-strain curve to failure measured at that point, as in Figure 5.13. The final ramp test to failure then gives the residual strength and failure strain.

Figures 5.14 - 5.16 give data for the residual strength at a variety of load levels (% ultimate load) and cycles (cycle ratio = number of cycles of fatigue divided by the expected lifetime at that load level). The single fiber data in Figure 5.14 show that the residual strength is almost equal to the original ultimate strength at all conditions. Thus, failure must occur in a sudden-death fashion, with little decrease in strength before the fiber suddenly fails. The data in Figure 5.15 for dry yarns show some initial increase in residual strength at high loads and few cycles over the normal ultimate strength. At longer cycling times and lower loads some slight decrease in residual strength then occurs. The initial increase in residual strength is consistent with the shakedown process and S-N plateau discussed earlier. The decrease at higher numbers of cycles is associated with the appearance of some individual broken fibers. The wet yarn data in Figure 5.16 is similar to the dry yarn data except that the residual strength does not increase at short cycling times. This is consistent with the lack of a plateau in the S-N curve for wet yarns, apparently due to the lubricating effect of water on the single cycle ultimate strength,which precludes the shakedown process. The details of the shakedown behavior may become more clear when rope tests are run.

Figure 5.17 shows typical changes in the cumulative displacement for a given cycle during typical fatigue tests to failure. The elongation is similar for yarns and fibers at their corresponding loads (70% of ultimate). The dry yarn shows some increase in elongation beyond the single fiber just before failure, apparently due to the breakage of some of the fibers in the yarn. Figure 5.18 gives the change in hysteresis loop energy (area under the load-displacement curve for a loading-unloading cycle), for wet and dry yarns. The curves are similar except for the large initial hysteresis for the dry yarn, which may just occur on the first cycle. This is another manifestation of the shakedown process in dry yarns.

Table 5.2 gives data for the strains during cycling of dry yarns taken from curves like Figure 5.13. The data at various cycle ratios at a load of 50% of the initial strength are all similar, showing about 3% permanent strain on the first cycle, 10% residual strain in the final ramp test, and a total cumulative strain of 16% at failure. Approximately 3% additional "permanent" strain accumulates between the first cycle and the ramp test. The total cumulative strains at failure are all similar, and are close to the single cycle strain to failure in Table 5.1.(Measured strains are slightly greater for the computer acquired data shown in Figure 5.17 as a more refined procedure is used with a slightly lower initial load as the starting point). These data indicate that the

residual strain decreases during fatigue, particularly on the first cycle. While the residual strength may not change greatly, the strain capability and apparent energy absorbing capability are reduced measurably, even after only a small fraction the lifetime is consumed.

Fractographic Study

The study of damage and fracture surfaces by scanning electron microscopy is essential in understanding the mechanisms of degradation. The work done to date is preliminary to a greater effort anticipated in future work. The fracture surfaces of fibers observed in this study are generally similar to those reported in the literature (5.16). Figure 5.19 shows the most typical geometry, involving a generally transverse failure with an obvious slow crack growth region initiating at one surface. No unique features have been identified on fatigue vs. static strength specimens. Figure 5.20 shows a second type of fracture which is dominated by splitting generally parallel to the fiber axis. Both types of failure have been found on single fibers failed in fatigue at various load levels and in air or sea water. This finding is not in agreement with literature reports (5.16) which identify the axial cracking mode as indicative of fatigue failures and requiring a slack load condition. Figure 5.21 shows evidence of fiber-fiber wear in a dry yarn specimen after fatigue cycling; while this may indicate the origin of the steep S-N curve for this case, it is the only example found to date and its significance has not been established.

Failures of the type shown in Figures 5.19 and 5.20 suggest a fatigue crack growth controlled failure. In bulk polymers this would also suggest a cyclic rather than creep dominated behavior which could be considered in a fracture mechanics context. However, the results for the strains and elongations in Figure 5.17 and Table 5.2 indicate that fiber failure occurs at the achievement of some cumulative strain condition typical of creep rupture. The similar times to failure under differing conditions in Figure 5.10 are also consistent with a creep rupture mode. While cracks are clearly associated with eventual failure of the fibers, they may not represent the typical fatigue cracks which dominate bulk polymer breakdown (5.2). It is not clear how fiber-fiber damage which may occur in yarns or especially in ropes would change this process.

CONCLUSIONS

Nylon fibers and yarns lose a significant fraction of their strength when subjected to cyclic fatigue loads. Single fibers appear to fail according to the total time under load, regardless of the frequency or stress amplitude. Yarns are more sensitive to cyclic loading than are single fibers, losing approximately 60% of their initial strength after 10^5 cycles; yarn failure appears dominated by the number of cycles rather than total time under load, possibly due to fiber-fiber interactions. Dry yarns go through a shakedown process which results in a plateau on the S-N curve at high loads. Short term seawater immersion causes a modest reduc-

tion in lifetime under some conditions, but also may lubricate yarn structures. The residual strength of fibers and yarns remains close to the initial strength up to at least 75% of their lifetime; the residual strain to failure is reduced by approximately 40% in cycling, but the cumulative strain to failure is close to the strain to failure in a single cycle. Preliminary fractographic work indicates possible fiber-fiber damage and fracture surfaces which are not unique to fatigue loading.

FUTURE PLANS

Emphasis in future work will be in three areas: (1) generating similar data for small diameter ropes, (2) studying the long term effects of sea water on fibers, yarns, and ropes under static and cyclic loads, and (3) developing conceptual models for the mechanisms of degradation at each level of structure under various loading and environmental conditions. The results of this work will be considered in the context of the work of other groups in the rope project, including the rope mechanics studies, comparison of residual property data with used rope pathological studies, and nondestructive evaluation of damage generated in fatigue.

REFERENECES

5.1 Starsmore, N., Halliday, M.G. and Ewers, W.A., "Barge Motions and Towline Tensions Measured During a North Sea Tow," Proc. Int. Symp. Ocean Engr.-Ship Handling," Gothenberg, Sweden (1980), paper 13.

5.2 Hertzberg, R.W. and Manson, J.A., "Fatigue of Engineering Plastics," Academic Press, New York (1980).

5.3 McKenna, G.B. and Penn, R.W., "Time-Dependent Failure in Poly(methyl methacrylate) and Polyethylene," Polymer, 21 (1980) p. 213.

5.4 Mandell, J.F., Smith, K.L., and Huang, D.D., "Effects of Residual Stress and Orientation on the Fatigue of Injection Molded Polysulfone," Poly. Engr. Sci, 21 (1981) p. 1173.

5.5 Kausch, H.H., "Polymer Fracture," Springer-Verlag, Berlin (1978).

5.6 Kohan, M.I., ed., "Nylon Plastics," Wiley, New York (1973).

5.7 Dunn, P., Sansom, G.F., "The Stress Cracking of Polyamides by Metal Salts, Part I, Metal Halides," J. App. Poly. Sci. 13, (1969), 1641-1655.

5.8 Dunn, P., Sansom, G.F., "The Stress Cracking of Polyamides by Metal Salts, Part II, Mechanism of Cracking," J. Appl. Poly. Sci. 13 (1969), 1657-1672.

5.9 Kramer, E.J., "Environmental Cracking of Polymers," Developments in Polymer Fracture, E.H. Andrews, ed., Applied Sci. Publishers Ltd., London (1979).

5.10 Reimschuessel, A.C., Kim, Y.J., "Stress-Cracking of Nylons Induced by Zinc Chloride Solutions," J. Mat. Sci., 13 (1978), 243-252.

5.11 Howard, J.B., in "Engineering Design for Plastics," E. Baer, ed., Reinhold, New York (1964) pp. 742-794.

5.12 Peterlin, A., "Mechanisms of Deformation in Polymeric Solids," in Polymeric Materials, E. Baer and S. Radcliffe, eds., Am. Society for Metals, Metals Park, Ohio, 1975, 175-238.

5.13 Narisawa, I., Ishikawa, M., Ogawa, H., "The Fatigue Process in Highly Oriented Nylon 6," J. Poly. Sci., 15 (1977), 1055-1066.

5.14 Kelley, W.T., "Some Effects of Repeated Loading on Filament Yarns," TRJ 35 (1965), 852-854.

5.15 Hearle, J.W.S, Plonsker, H.R., "Behavior of Fibers in Cumulative Extension Cycling," J. Appl. Poly. Sci., 10 (1966), 1949-1971.

5.16 Bunsell, A.R., Hearle, J.W.S., "A Mechanism of Fatigue Failure in Nylon Fibres," J. Mat. Sci., 6 (1971), 1303-1311.

5.17 Bunsell, A.R., Hearle, J.W.S., "The Fatigue of Synthetic Polymer Fibers," J. App. Poly. Sci., 18 (1974), 267-291.

5.18 Waller, R.C., Roseveare, W.E., "Fatigue Failure of Rayon Tire Cord," J. App. Physics, 17 (1946), 482-491.

5.19 Bitting, K.R., "The Dynamic Behavior of Nylon and Polyester Line," USCG Report CG-D-39-80 (ADA 087 106), April 1980.

5.20 Paul, W., "Review of Synthetic Fiber Ropes," USCG Academy, New London, CT, Govt. Report ADA 084 622, Aug. 1970, 2.1-2.67.

5.21 Flory, J.F., Denham, F.A., Marcello, J.T., Porancki, P.F., Woehleke, S.P. "Guidelines for Deepwater Port Single Point Mooring Design," USCG Report CG-D-49-77 (ADA 050 182), Sept. 1977, 5.1-5.54.

LIST OF FIGURES

5.1 Sea Water Test Tab

5.2 Sea Water Test Chamber, Front View

5.3 Comparative Fatigue Lifetimes, du Pont 707 Nylon Fiber and Yarn in Air

5.4 Fatigue Lifetime, du Pont 707 Nylon Fiber in Sear Water and Air

5.5 Fatigue Lifetime du Pont 707 Nylon Yarn in Sea Water and Air

5.6 Comparative Fatigue Lifetimes, du Pont 707 Nylon Fiber and Yarn in Sea Water

5.7 Representative Load - Displacement Curves. Yarn in Sea Water and Air

5.8 Effect of Slack Load on the Fatigue Lifetime of du Pont 707 Nylon Yarn in Air

5.9 Comparative Fatigue Lifetimes of du Pont 707 Nylon Fiber and Yarn in Sea Water with Fatigue Data from K.R. Bitting [5.19] for 1/2 inch, 8-strand Plaited Nylon Rope

5.10 Frequency Effects, du Pont 707 Single Fiber in Air

5.11 Frequency Effects on Test Duration for du Pont 707 Yarn in Air

5.12 Frequency Effects on Fatigue Lifetime, du Pont 707 Nylon Yarn in Air

5.13 Typical Clyclic and Residual Load-Displacement Curves for a Dry Yarn Cycled at 90% of its Ultimate Load for 50% of Its Expected Lifetime

5.14 Residual Tensile Strength After Fatiguing, du Pont 707 Nylon Fiber in Air

5.15 Residual Tensile Strength After Fatiguing, du Pont 707 Nylon Yarn

5.16 Residual Tensile Strength after Sea Water Fatiguing, du Pont 707 Nylon Yarn

5.17 Elongation During Cycling, du Pont 707 Yarn and Fiber in Air and Sea Water

5.18 Hysteresis Energy During Cycling, du Pont 707 Yarn in Air And Sea Water

5.19 Fatigue Fracture Surface of Single Dry Fiber Cycled at 90% of the Ultimate Load

LIST OF FIGURES

5.20 Fatigue Surface of Fiber from a Dry Yarn Cycled at 50% of the Ultimate Load

5.21 Surface of Unbroken Fiber in Yarn Fatigued at 70% Ultimate Load

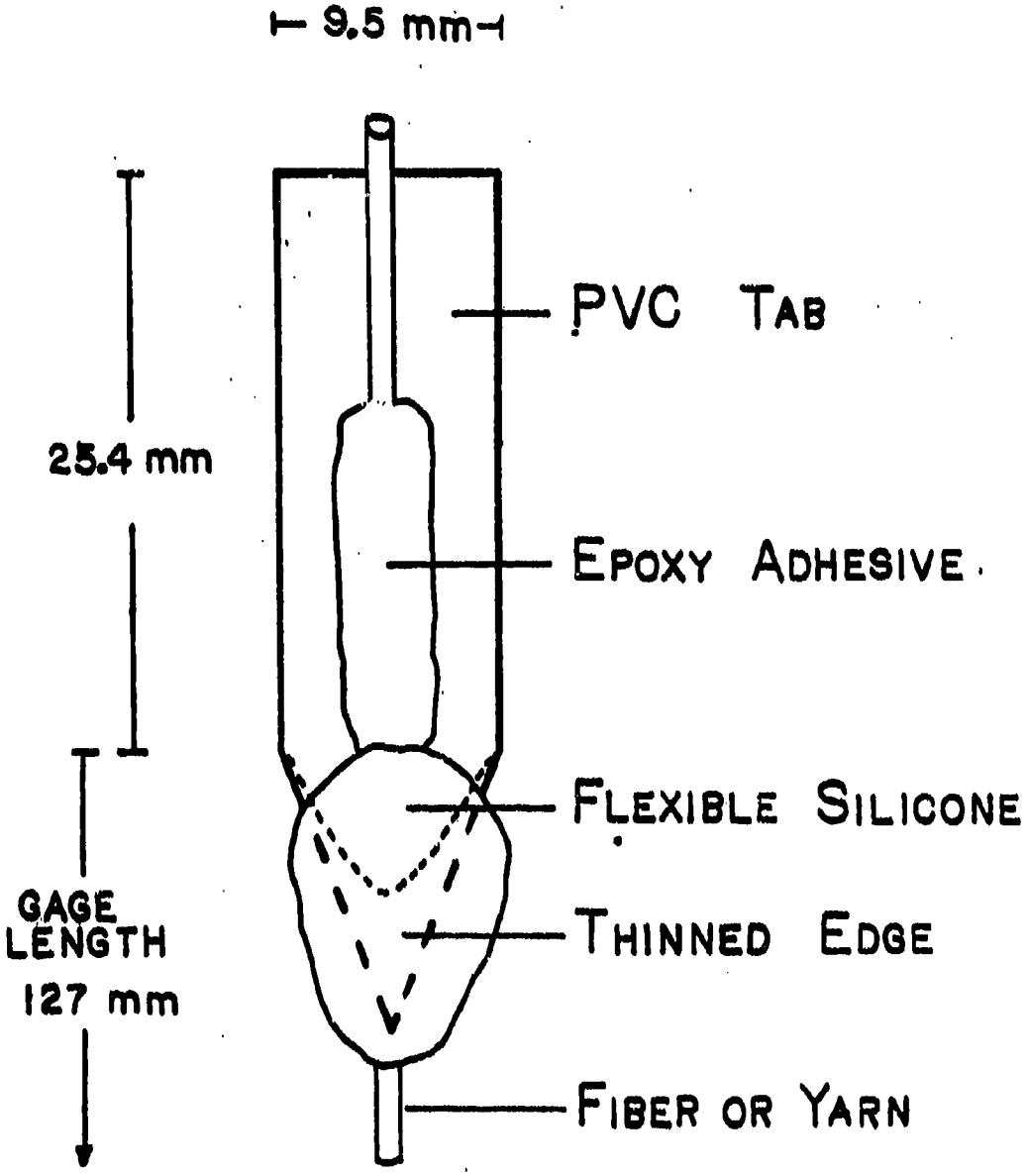

SEA WATER TEST TAB

FIGURE 5.1

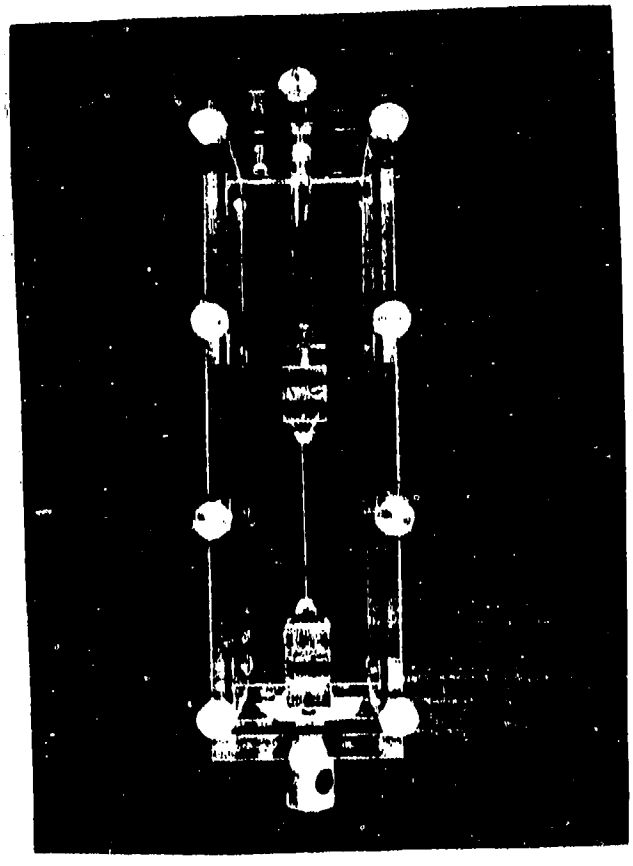

SEA WATER TEST CHAMBER

FRONT VIEW

FIGURE 5.2

FIGURE 5.3

COMPARATIVE FATIGUE LIFETIMES
DUPONT 707 NYLON FIBER AND YARN
IN AIR

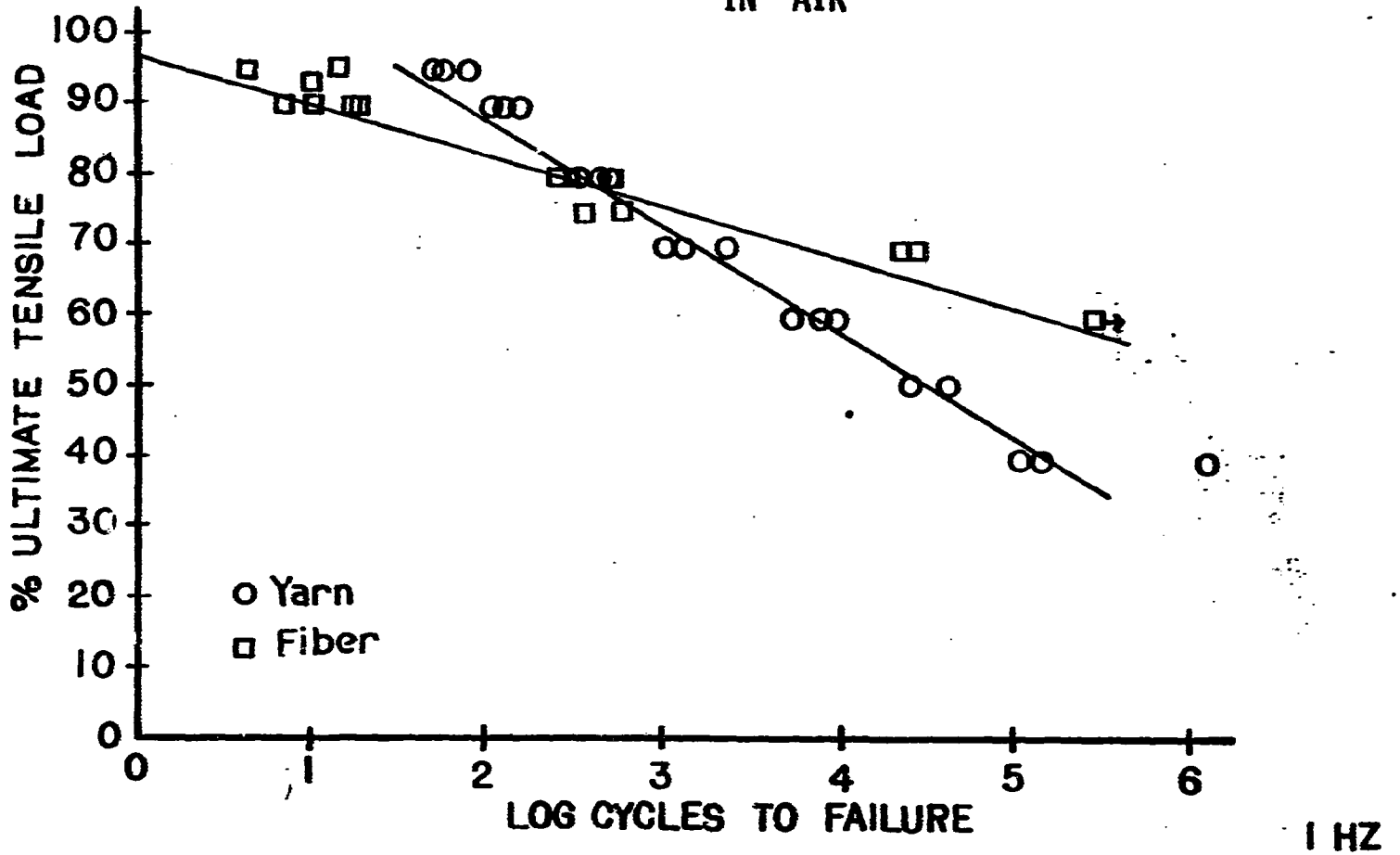

FIGURE 5.4

FATIGUE LIFETIME

DUPONT 707 NYLON FIBER

IN SEA WATER AND AIR

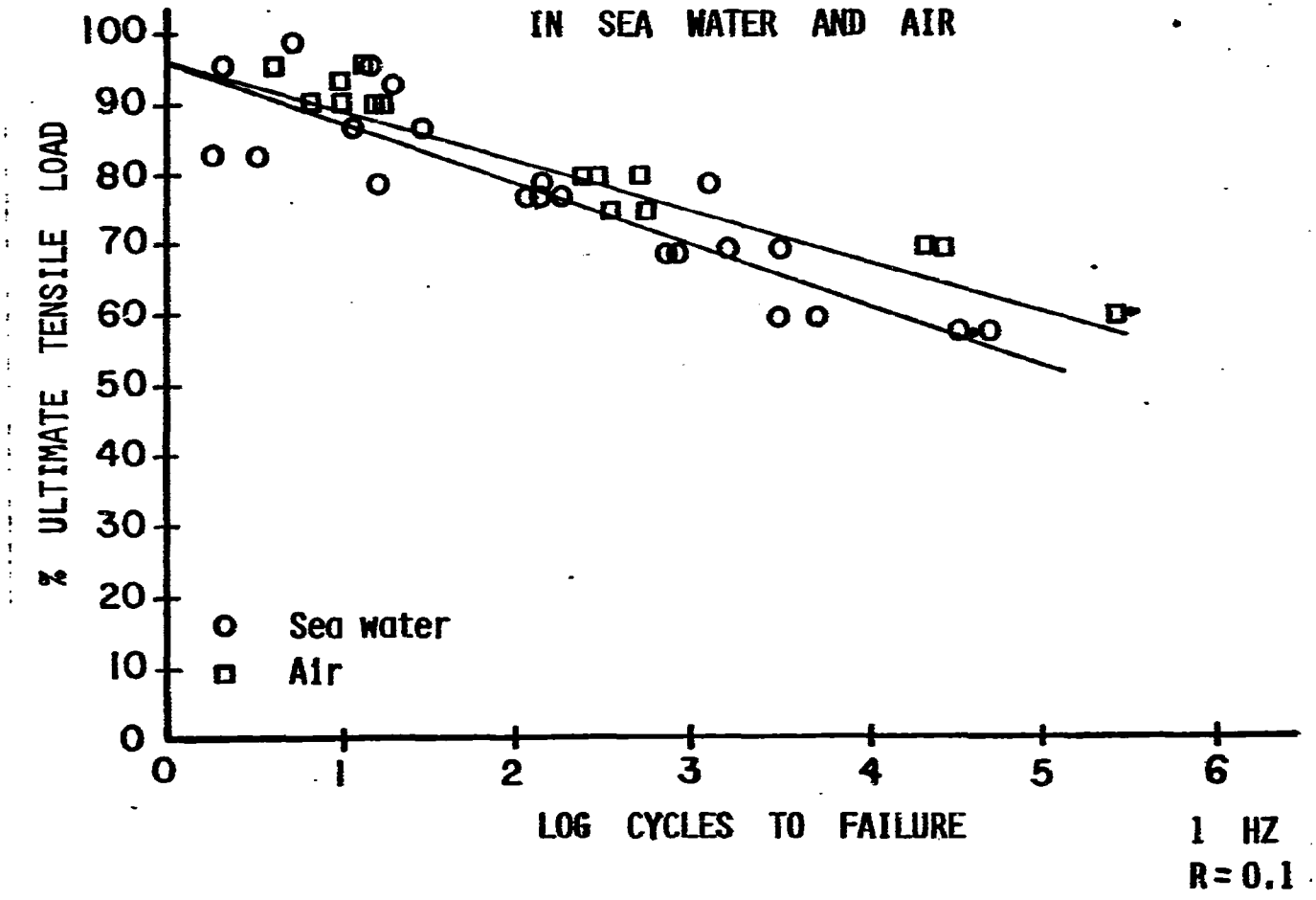

FIGURE 5.5

FATIGUE LIFETIME
DUPONT 707 NYLON YARN
IN SEA WATER
AND AIR

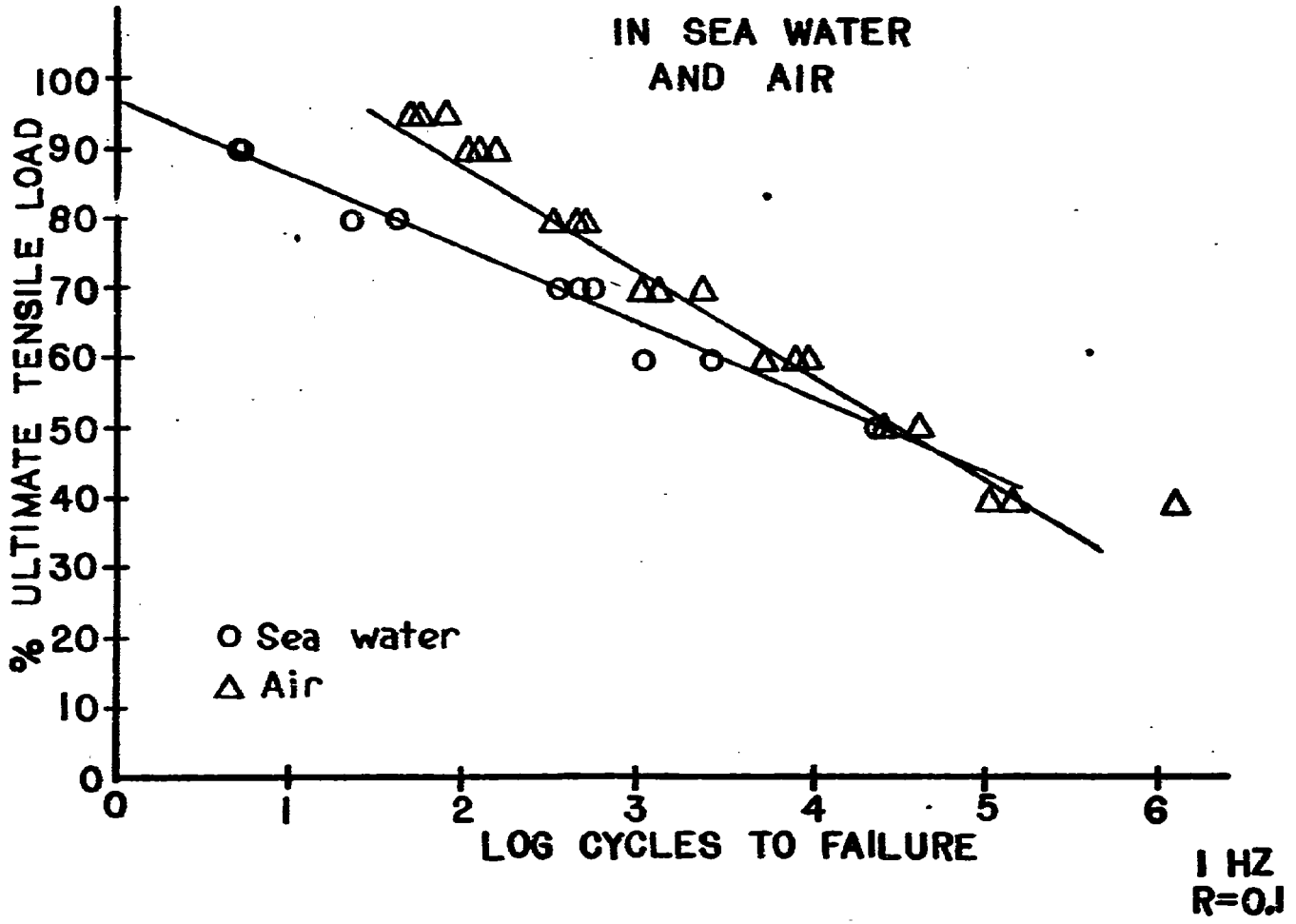

FIGURE 5.6

COMPARATIVE FATIGUE LIFETIMES

DUPONT 707 NYLON FIBER AND YARN

IN SEA WATER

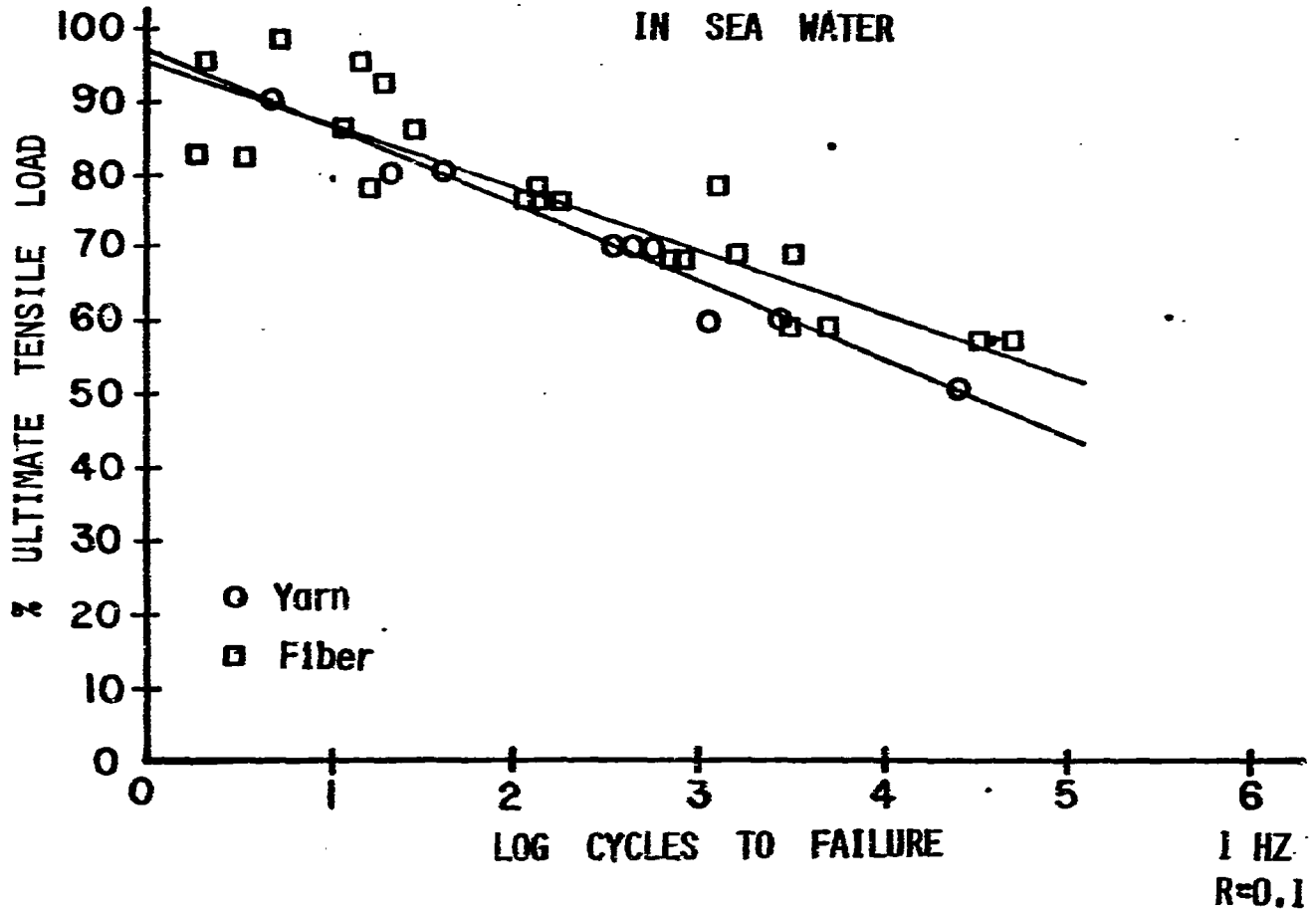

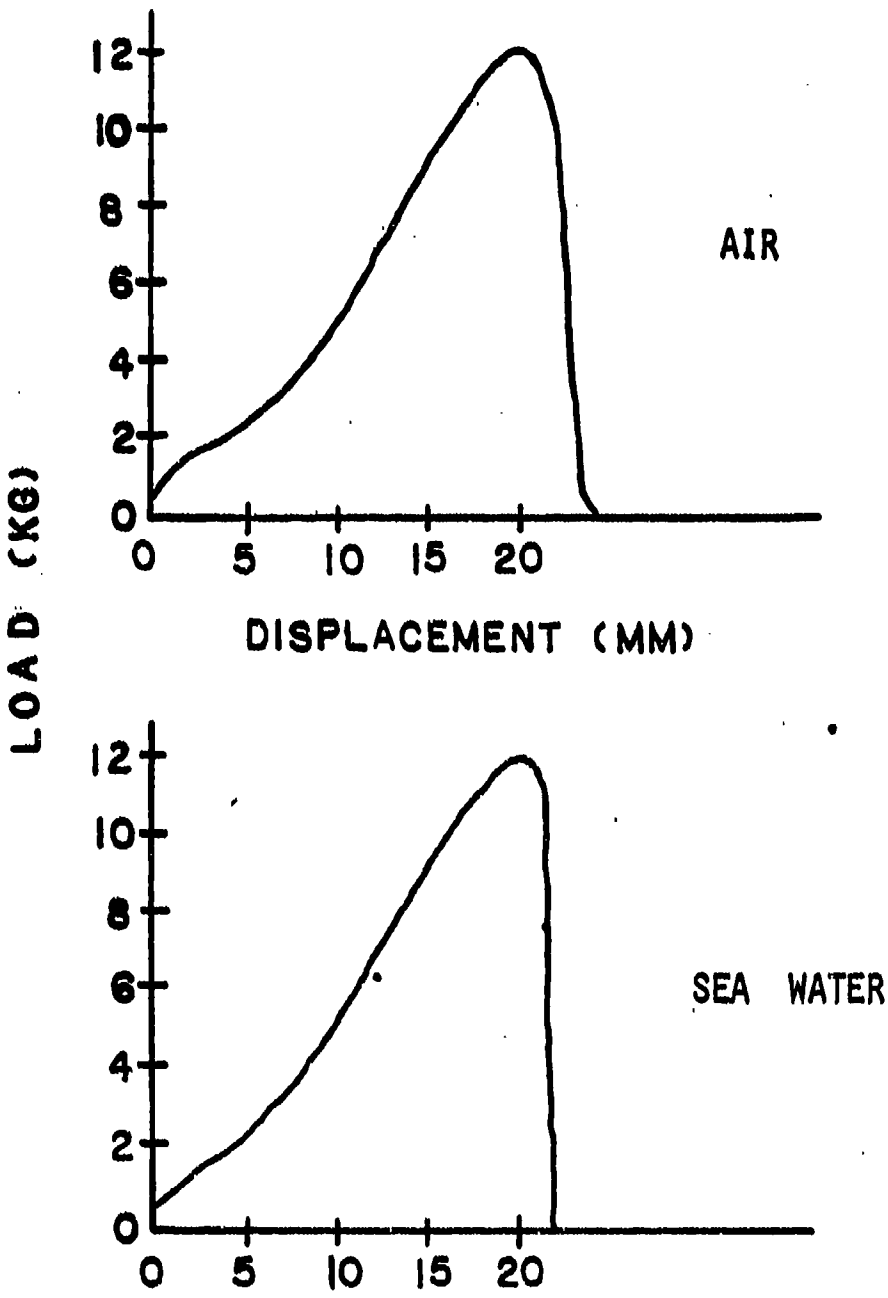

REPRESENTATIVE LOAD - DISPLACEMENT CURVES
YARN IN SEA WATER AND AIR

FIGURE 5.7

FIGURE 5,8

EFFECT OF SLACK LOAD ON THE FATIGUE LIFETIME OF DUPONT 707 NYLON YARN IN AIR

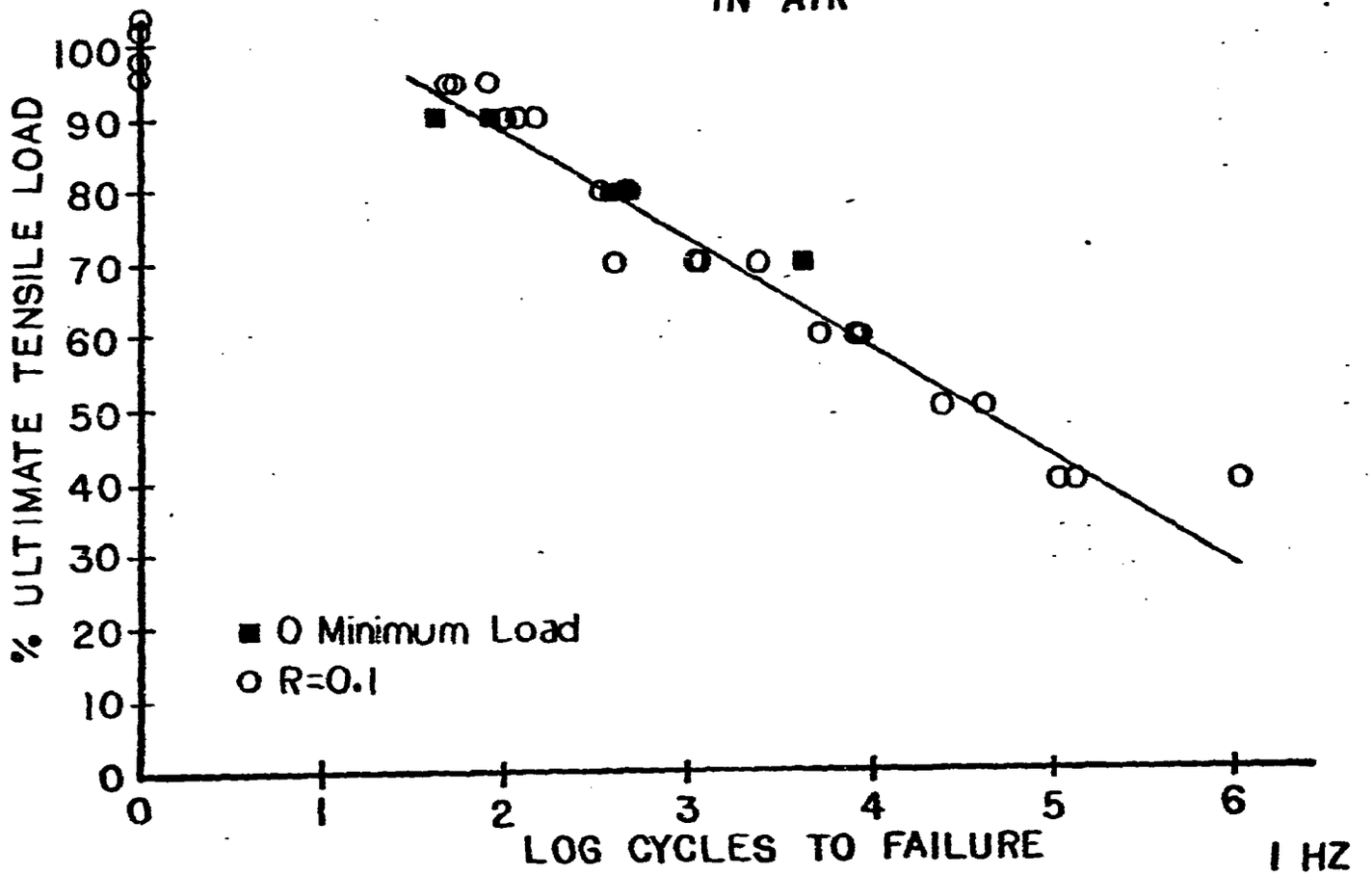

FIGURE 5.9

COMPARATIVE FATIGUE LIFETIMES OF
DUPONT 707 NYLON FIBER AND YARN
IN SEA WATER WITH FATIGUE DATA FROM K.R.BITTING (5.19)
FOR 1/2 INCH, 8-STRAND PLAITED NYLON ROPE

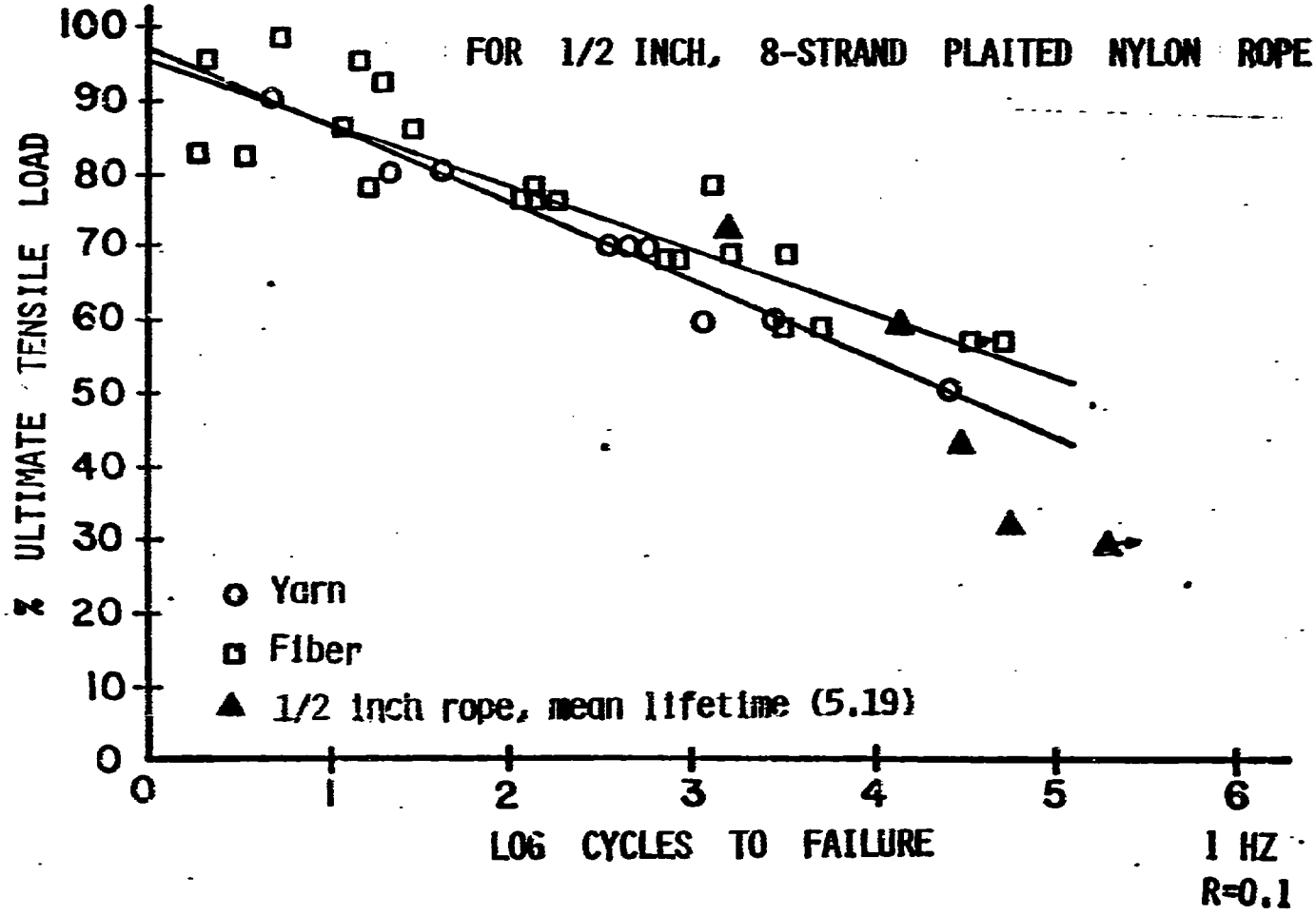

FIGURE 5.10

FREQUENCY EFFECTS

DUPONT 707 SINGLE FIBER IN AIR

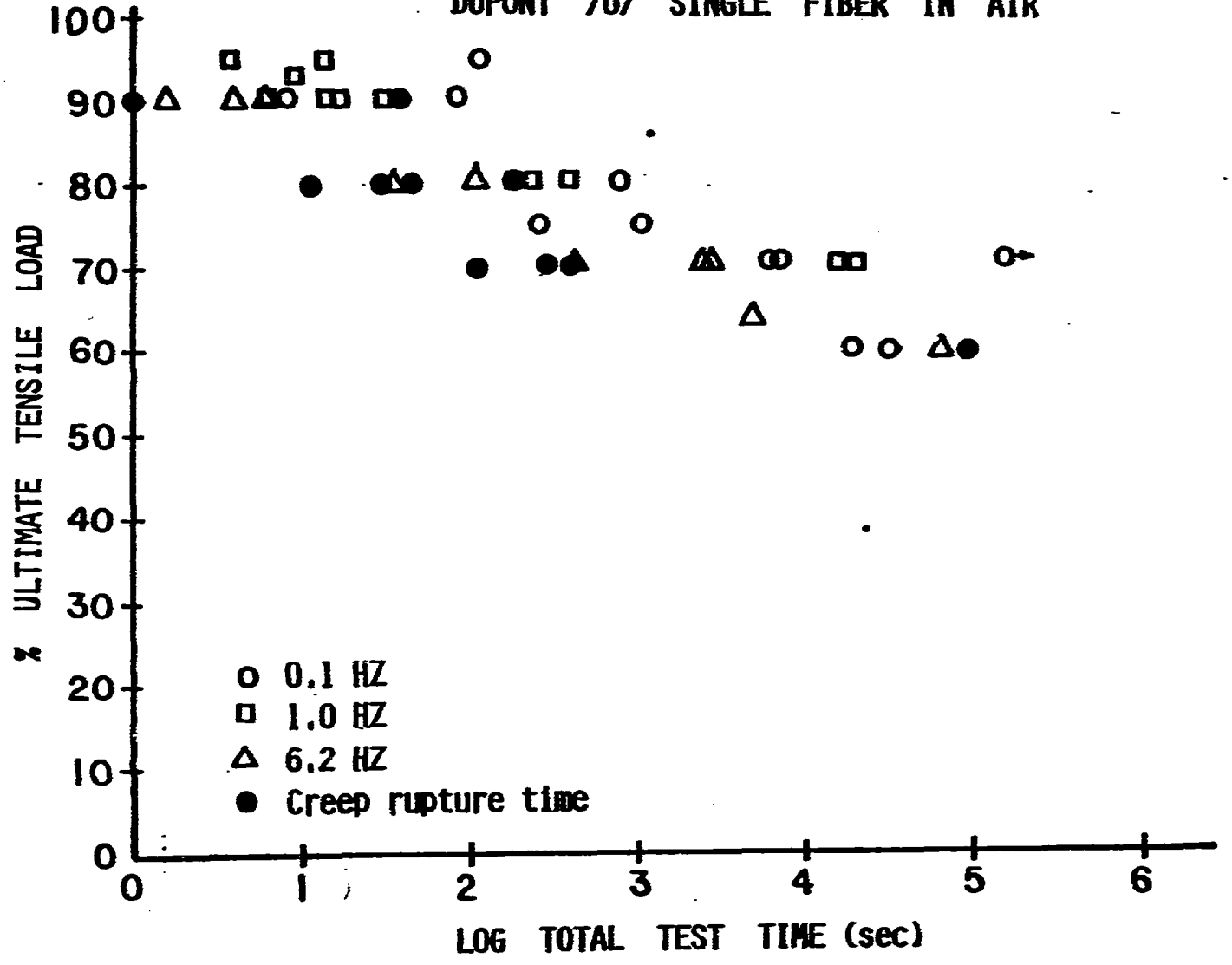

FIGURE 5.11

FREQUENCY EFFECTS ON TEST DURATION FOR DUPONT 707 YARN IN AIR

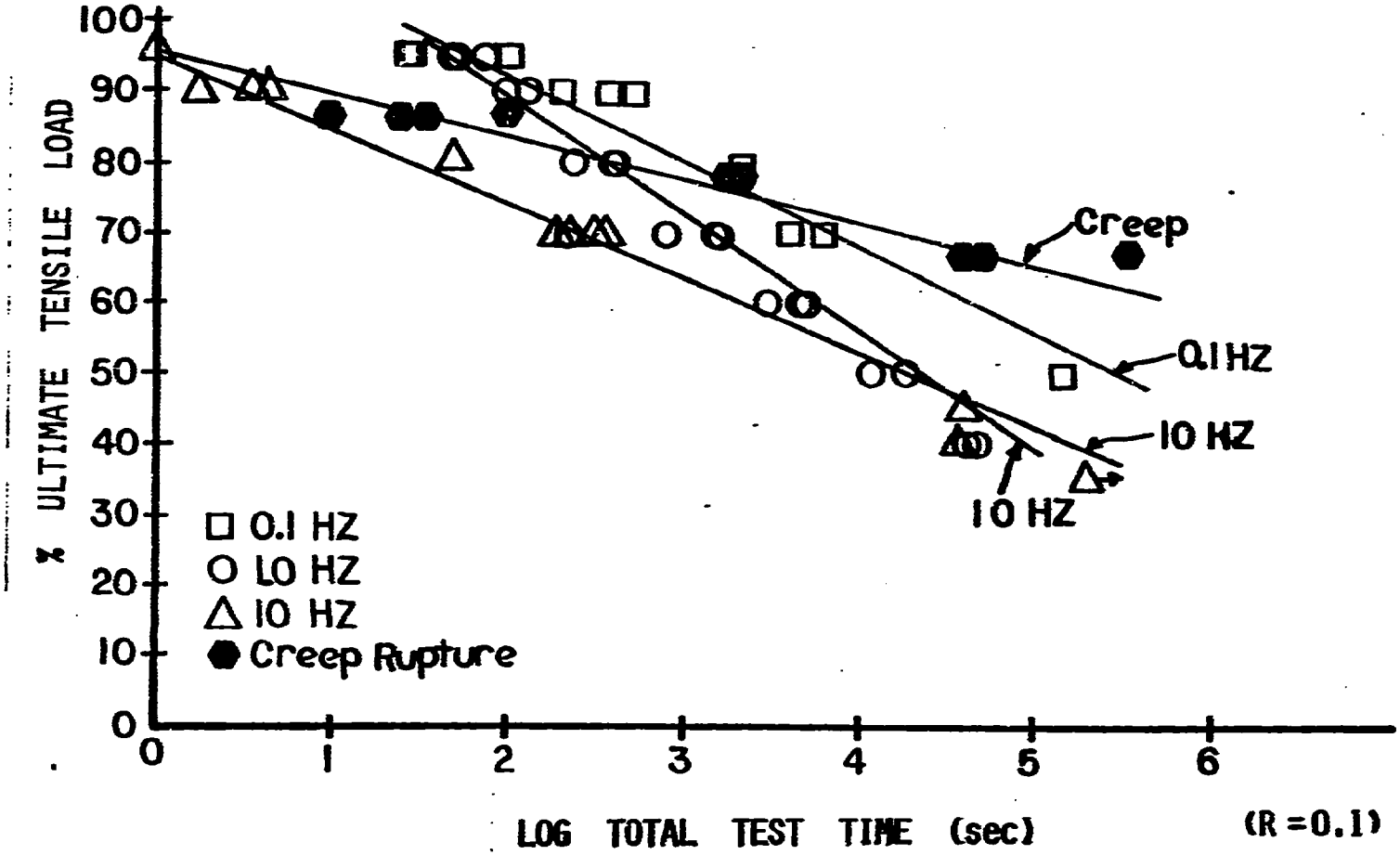

FIGURE 5.12

FREQUENCY EFFECTS ON
FATIGUE LIFETIME
DUPONT 707 NYLON YARN
IN AIR

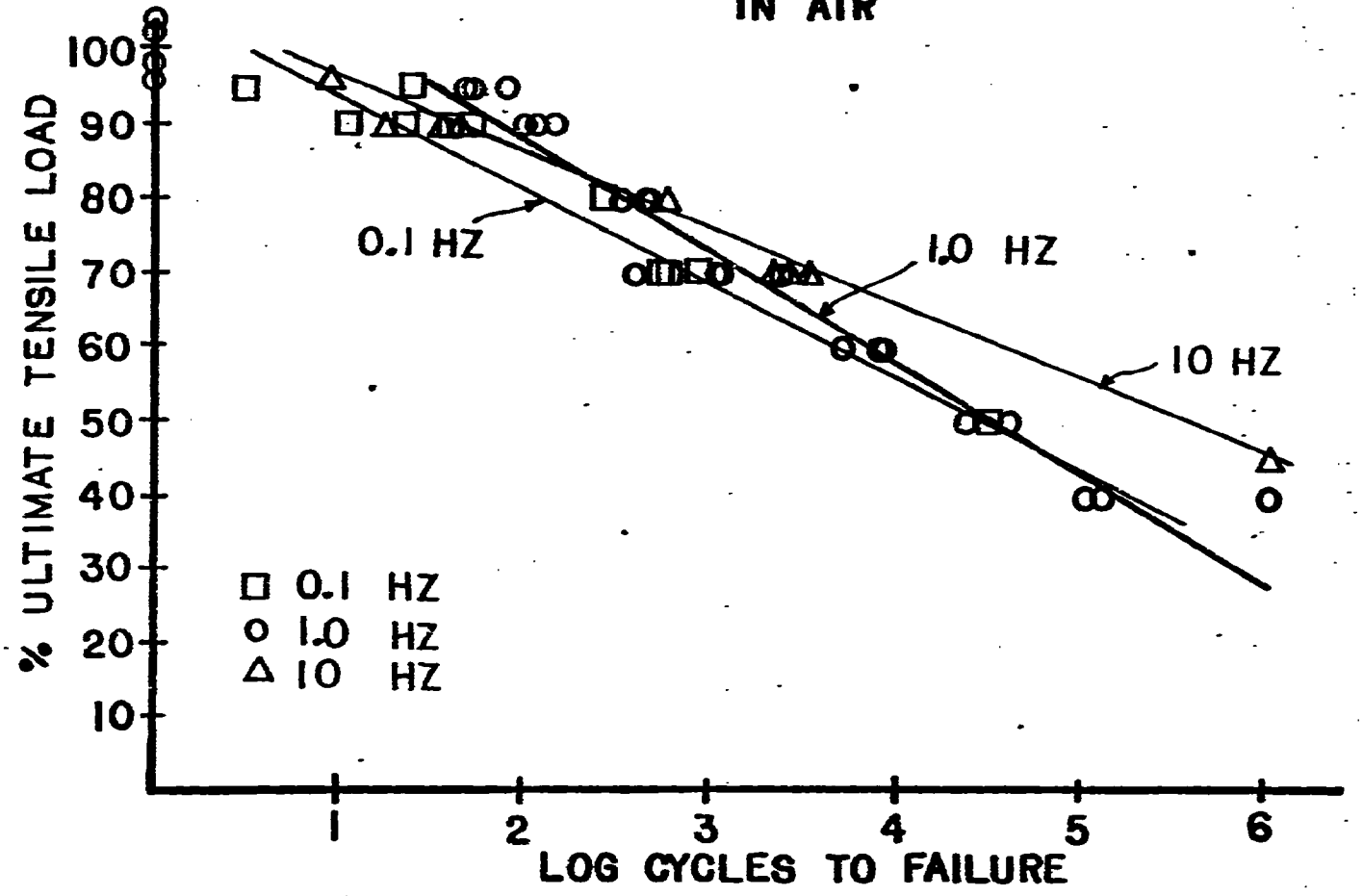

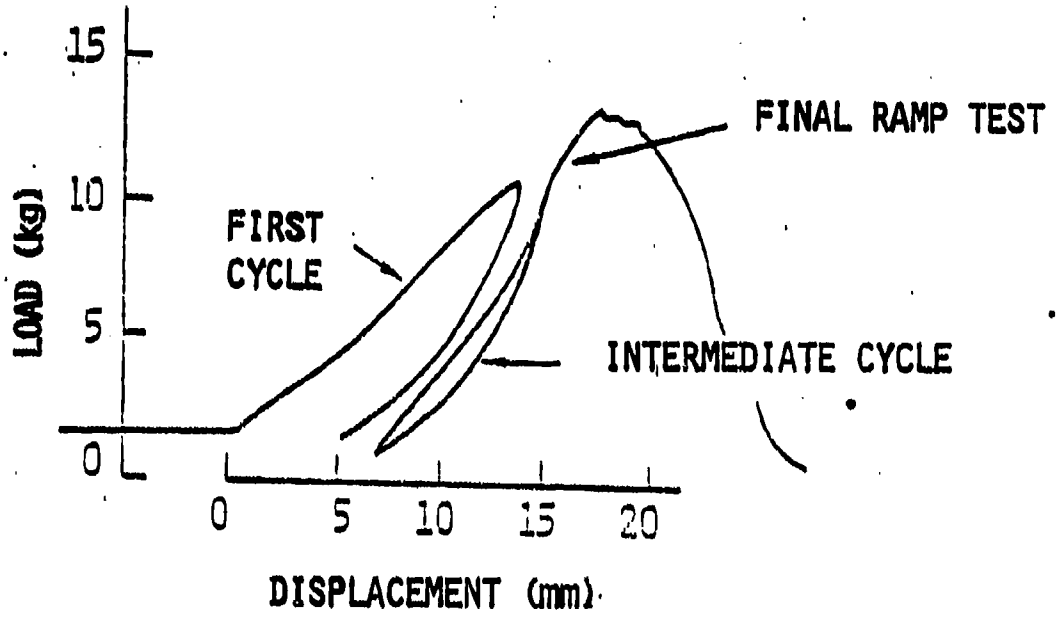

FIG. 5.13 TYPICAL CYCLIC AND RESIDUAL LOAD-DISPLACEMENT CURVES FOR A DRY YARN CYCLED AT 90% OF ITS ULTIMATE LOAD FOR 50% OF ITS EXPECTED LIFETIME

FIGURE 5.14

RESIDUAL TENSILE STRENGTH AFTER FATIGUING

DUPONT 707 NYLON FIBER IN AIR

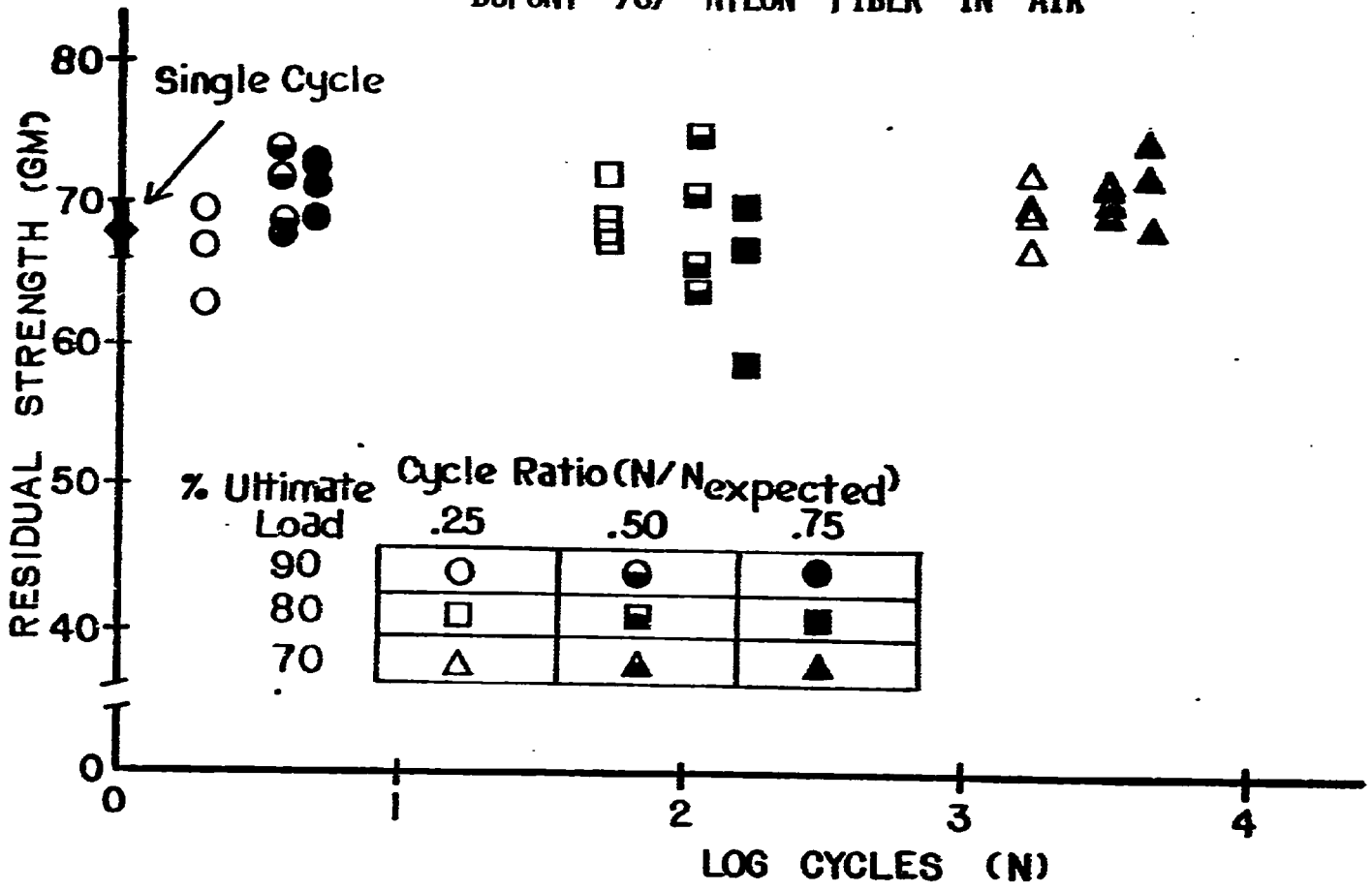

FIGURE 5.15

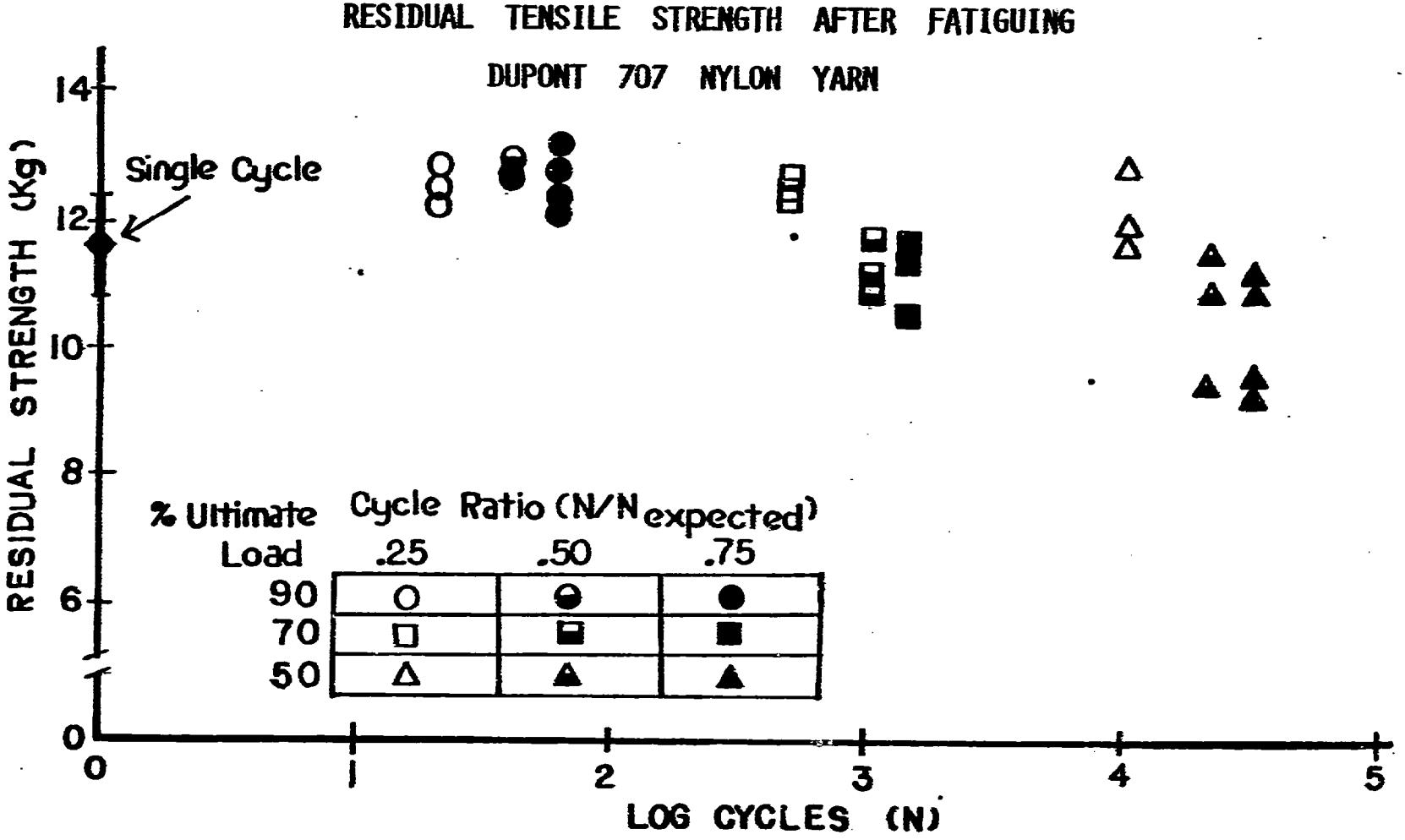
RESIDUAL TENSILE STRENGTH AFTER FATIGUING
DUPONT 707 NYLON YARN
RESIDUAL STRENGTH (Kg)
Single Cycle
14
12
10
8
6
0
0
1
2
3
4
5
LOG CYCLES (N)
% Ultimate Load
Cycle Ratio (N/N expected)
.25
.50
.75
90
70
50

FIGURE 5.16

RESIDUAL TENSILE STRENGTH
AFTER SEA WATER FATIGUING
DUPONT 707 NYLON YARN

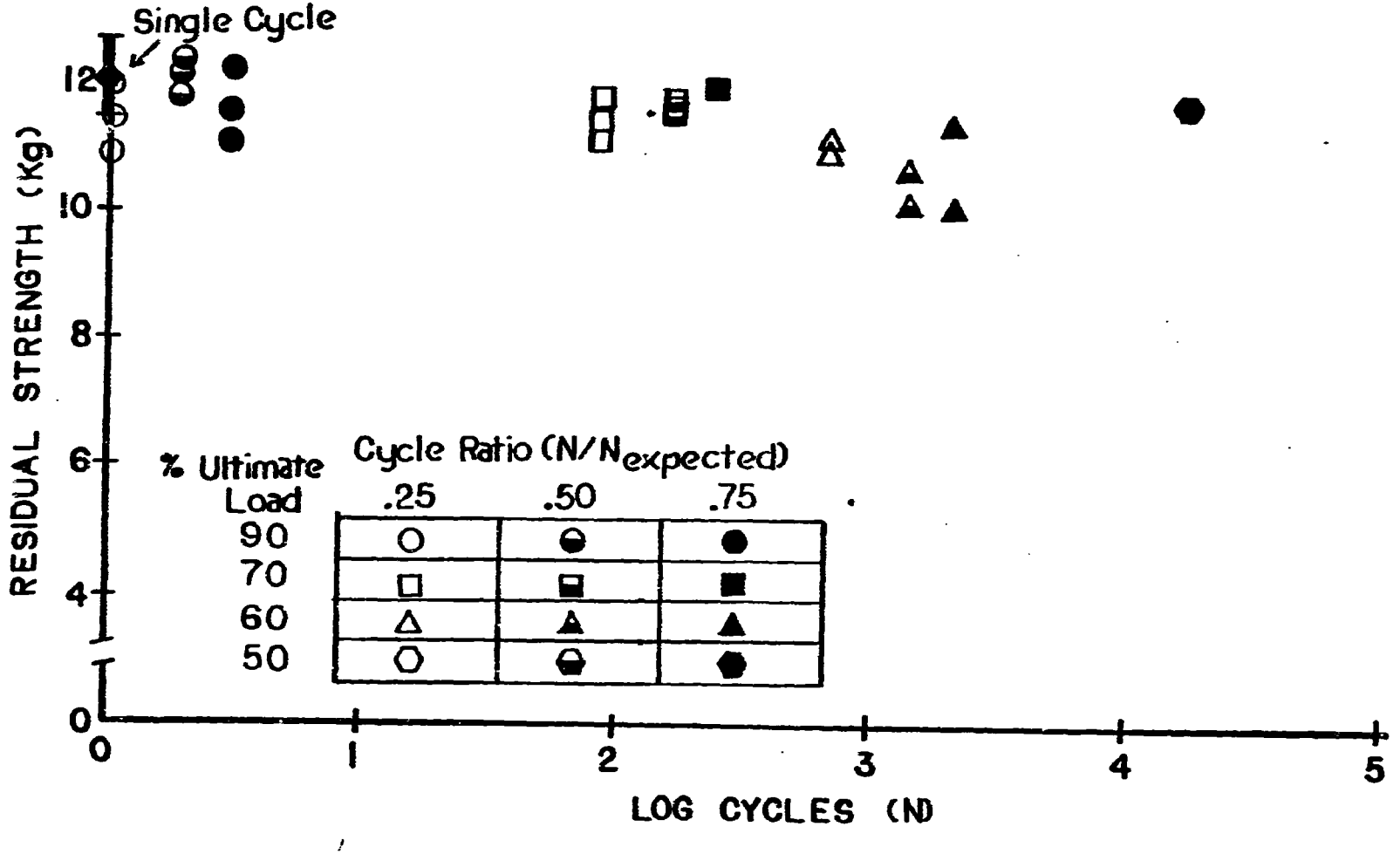

FIGURE 5.17

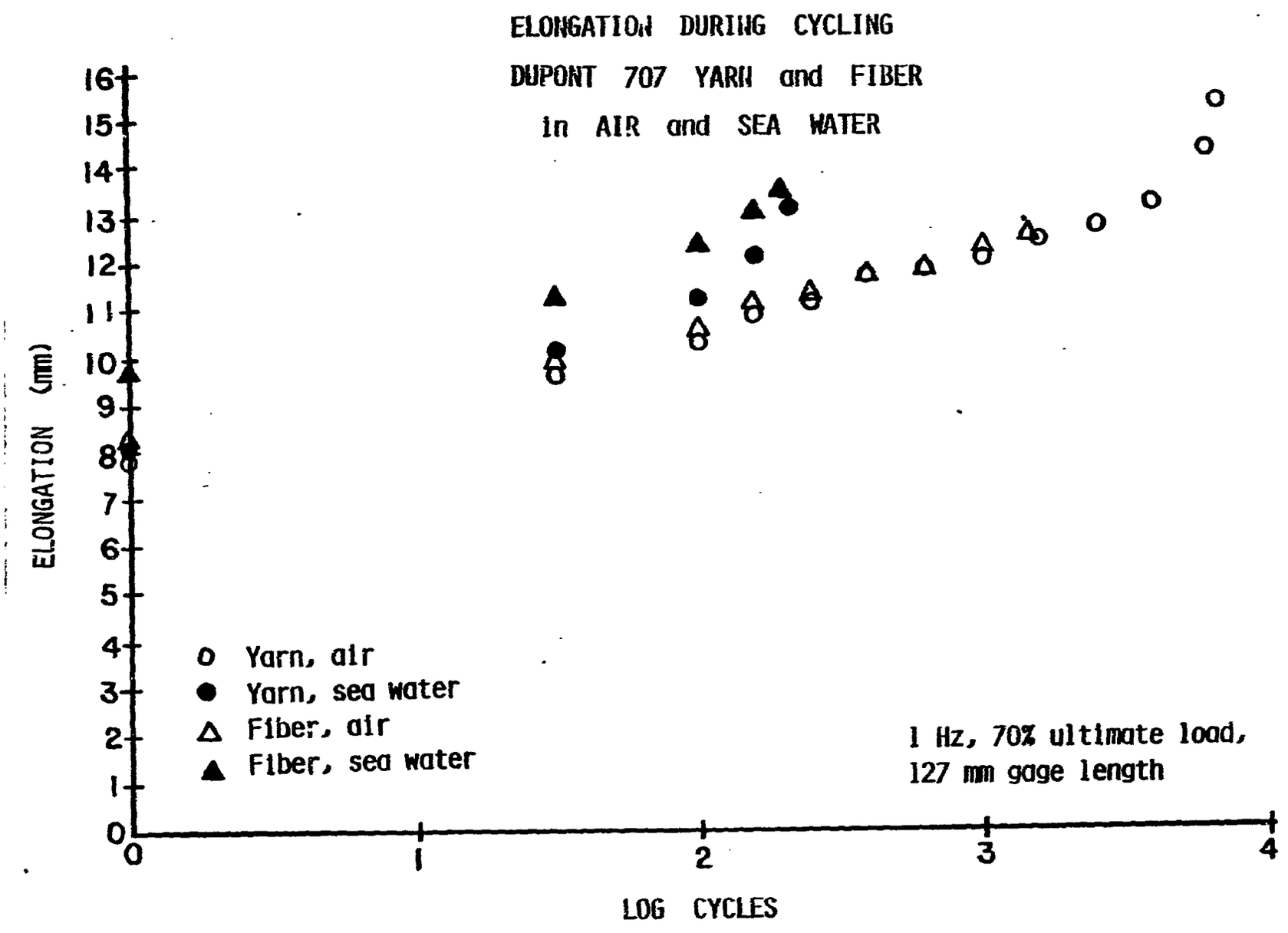
ELONGATION DURING CYCLING
DUPONT 707 YARN and FIBER
in AIR and SEA WATER
ELONGATION (mm)
0
1
2
3
4
5
6
7
8
9
10
11
12
13
14
15
16
0
1
2
3
4
LOG CYCLES
o Yarn, air
● Yarn, sea water
△ Fiber, air
▲ Fiber, sea water
1 Hz, 70% ultimate load,
127 mm gage length

FIGURE 5.18

HYSTERESIS ENERGY DURING CYCLING
DUPONT 707 YARN in AIR and SEA WATER

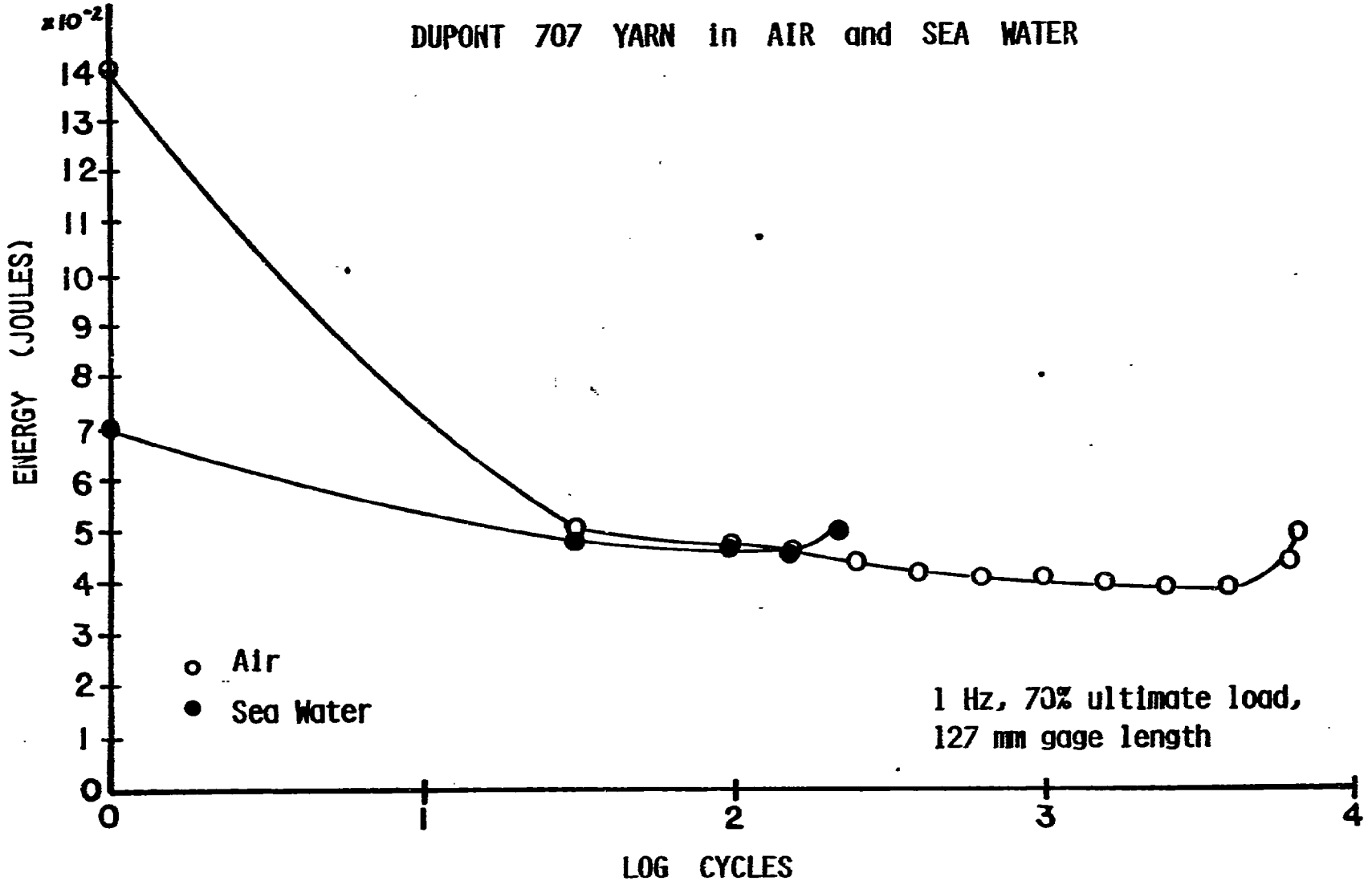

FATIGUE FRACTURE SURFACE OF SINGLE DRY FIBER CYCLED AT 90% OF THE ULTIMATE LOAD

FIGURE 5.19

FATIGUE FRACTURE SURFACE OF FIBER FROM A DRY YARN CYCLED AT 50% OF THE ULTIMATE LOAD

FIGURE 5.20

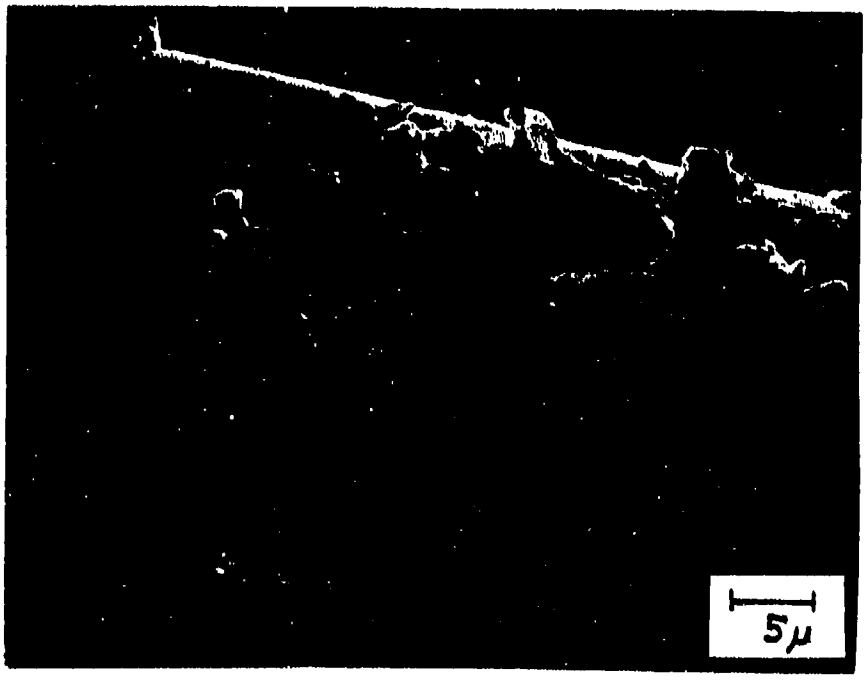

SURFACE OF UNBROKEN FIBER IN YARN
FATIGUED AT 70% ULTIMATE LOAD

FIGURE 5.21

LIST OF TABLES

5.1 Ultimate Load and Elongation, Single Cycle Ramp Tests

5.2 Average Elongation During Cycling at Cycle Loading of 50% UTC, du Pont 707 Yarn in Air

Table 5.1

Ultimate Load and Elongation

Single Cycle Ramp Tests

		Ultimate Load	Ultimate Elongation (%)
FIBER	Air	68.1 gm (±2.0)	15.0 (±.75)
	Sea Water	60.4 gm (+3.2)	14.4 (±1.2)
YARN	Air	11.61 kg (±.43)	17.0 (±1.4)
	Sea Water	12.11 kg (±.26)	17.8 (±1.4)

Table 5.2

Average Elongation During Cycling

At Cycle Loading of 50% UTS

DuPont 707 Yar In Air

Cycle Ratio[1]	After First Cycle (%)	Residual Strain (%)	Total/Cumulative Strain to Failure (%)
25	3.2 (.4) n=2	10.2 (1.6)	16.3 (.35)
50	2.6 (.2) n=3	9.7 (.7)	15.0 (.4)
75	2.8 (.2) n=3	10.7 (1.7)	15.8 (1.21)

n: number of tests

( ) : standard deviation

[1] Cycle Ratio = $\frac{\text{test cycles}}{\text{predicted lifetime}}$

1 Hz Master Cycle

Sine Wave, Load Control

6. MECHANICAL STUDY OF NEW ROPES

This section contains short reports on a variety of activities relating to different phases of this program. However, none of the studies here described has been developed to the point where it warrants presentation in a separate section.

Structural Changes Incurred During Loading

It has been shown in Figs. 3.2 and 3.30 that plied yarn cross sections in various locations in a 3-strand twisted rope are drastically altered from a circular (or trilobal) form as a result of lateral pressures. These pressures vary from location to location, hence the cross sectional yarn shapes likewise change significantly. Such departures from the ideal geometry of multiple helical structures must be accounted for analytical approaches to rope mechanics.

Since such embedded yarn sections were not easily made for the two double braided rope samples in the study, it was decided to observe the compressional behavior of small diameter new double braided ropes. Towards this end, samples of 1/4-in. double braided nylon rope were embedded in polyester resin, in some cases without tension and in other cases with a constant tensile load. After hardening of the polyester, the embedded specimen was cut, polished, photographed, then traced in profile. The resulting cross sectional profiles are seen in the following figures.

Figure 6.1A shows a cross section of a hollow braid (double braid with the center braid removed) under high tension (100 lbs) and Fig. 6.1B shows the same hollow braid under negligible (20 gf) tension. The lateral contraction due to the application of tension is drastic and suggests the importance of lateral pressures between cover and core in analysis of double braided ropes.

Figures 6.2A and B show the full 1/4-in double braided rope with both cover and core at 200 and at 600 lbs tension, respectively. The lateral contraction due to the load increase is evident, as is the change in the core yarn section shapes at the higher tensile load.

Next embedded was a specimen of 1/4-in double braided rope which was then sectioned, polished, and profiled. Traces of the cover yarns only are shown in Figs. 6.3A to F. Each successive figure represents a new cut just below the previous cut. Thus, the sequence of Figs. 6.3A to 6.3F permits the reader to trace the relative movement of four pairs of yarns as they move helically around the cover braid. One pair has a left hand cross-hatch, the other a right hand cross-hatch. Note in the lower part of Fig. 6.3A there are two pairs of yarns lying one above the other. In Fig. 6.3B the lower left hand cross-hatch pairs move to the left, while the right cross-hatch pair moves to the right. This same movement continues in

Figure 6.3C, further in Fig. 6.3D, still further in Fig. 6.3E, and so on. Notice also that each pair not only moves helically around the invisible cylinder constituting the core braid, but also each pair alternates from the inside of the braid cover to the outside.

The patterns of Fig. 6.3 strongly suggest that the path of the yarn pairs moving about the braid cover can be approximated by superimposing a sinusoidal motion along the direction of the principal helix normal, as the yarns helically encircle the braid cover. By connecting the sections of yarns moving in the same direction in a single cross sectional view, as is done in Fig. 6.4, one sees the potential of the superposition of helical and sinusoidal motion. This superposition can be carried out going back to the differential geometry of the helix, noting that for a single helix we have:

$$\bar{R}_s = r\cos\theta\ \hat{i} + r\sin\theta\ \hat{j} + r\theta\ \cot q\ \hat{k}$$

where

$\bar{R}_s$ = the position vector of the helix

r = the mean radius of the braided structure (core or cover

θ = the rotation angle along the Z axis.

with

$$\bar{T}_s = \frac{d\bar{R}_s}{d_s}$$

$$\bar{N}_s = \frac{1}{k}\frac{d\bar{T}_s}{d_s}$$

we have

$$\bar{N}_s = -\cos\theta\ \hat{i} - \sin\theta\ \hat{j}$$

Let us assume the sine waves are superimposed onto the single helix in the normal direction with a frequency of T. Then, we have the position vector $\bar{R}_{DB}$ for the double braided rope as:

$$\bar{R}_{DB} = \bar{R}_s + r_y \sin T\theta\ \bar{N}_s$$

$$= (r - r_y \sin T\theta)\cos\theta\ \hat{i} + (r - r_y \sin T\theta)\sin\theta\ \hat{j} + r\theta\ \cot q\ \hat{k}$$

where r_y is the radius of the plied yarn.

This implies:

$$\frac{d\bar{R}_{DB}}{d\theta} = [-r\sin\theta - r_y T\cos T\theta\cos\theta + r_y \sin T\theta \sin\theta]\hat{i}$$

$$+ [r\cos\theta - r_y T\cos T\theta \sin\theta - r_y \sin T\theta \cos\theta]\hat{j}$$

$$+ r\cot q\,\hat{k}$$

since

$$\frac{dS_{DB}}{d\theta} = \sqrt{\frac{d\bar{R}_{DB}}{d\theta} \cdot \frac{d\bar{R}_{DB}}{d\theta}}$$

$$\frac{dS_{DB}}{d\theta} = [r^2 + r_y^2 T^2 \cos^2 T\theta + r_y^2 \sin^2 T\theta - 2rr_y \sin T\theta + r^2\cot^2 q]^{1/2}$$

$$S_{DB}\Big|_{\theta_1}^{\theta_2} = A^{1/2}\int_{T\theta_1}^{T\theta_2} (1 + B\sin T\theta + C\sin^2 T\theta)^{1/2} dT\theta$$

where

$$A = \frac{1}{T^2}(r^2 + r_y^2 T^2 + r^2\cot^2 q)$$

$$B = -2rr_y/A$$

$$C = (r_y^2 - r_y^2 T^2)/A$$

$$S_{DB}\Big|_{\theta=0}^{\theta=2\pi} = 2\pi(r^2 + r_y^2 T^2 + r^2\cot^2 q)^{1/2}$$

Comparisons between experimental data and the results calculated from this equation for Samson 2-in-1 1/4-in double braided rope have been found to agree within a few per cent.

Hardness and Bending Rigidity Scanner

The extensive data reported in Section 2 and relating to properties of fibers from worn ropes, obviously suffer from significant sampling problems. The primary sampling decision was already completed when one 15-ft sample of each of the ropes was selected and forwarded to M.I.T. Records indicated, with a few descriptions, that the remaining segments were in fair condition, or worn, or fuzzy, etc. No further data were available as to the state of the rope in specific locations.

To provide such data on an objective basis, it was considered desirable to design and construct an instrument to scan specific properties of rope in a continuous run. Such a device was constructed to measure the thickness, the lateral hardness and the bending rigidity of rope on a continuous basis. The device was assembled at the end of the year and preliminary experiments were run on 9" 3-strand twisted rope, and on 9" double braided rope. A sketch of the device is shown in Fig. 6.5. It consists of two freely revolving grooved wheels, one weighted, freely revolving, grooved wheel and one freely revolving disk. The thickness tests are run with the rope placed between the weighted grooved wheel and the (raised) disk, with a displacement sensor provided, as well as a recorder to document the vertical displacement of the weighted roller during passage of the rope through the instrument. Thickness scans run at different weight levels provide a continuous measure of rope deformation under different lateral loads, hence a hardness-related quantity.

The bending tests are conducted with the disk in the lower position shown in Fig. 6.5. The rope is now moved over the roller on the right, under the center, weighted roller and over the roller on the left. The displacement record now represents the deformation of a fixed span of rope under given central loads, a quantity related to the bending rigidity of the rope. Care is taken to feed the rope from a horizontal plane directly onto the pulley at the right and tensions are maintained at a minimum.

Tests have been conducted thus far in the bending and in the hardness mode, employing manual feed. This aspect introduces a potential time shift in the hardness trace. Nonetheless, it is possible to demonstrate the reproducibility of the measure in a series of tests conducted on a worn 9" double braided rope as shown in Fig. 6.6. In this plot are reported the results of five test scans of hardness--three on one arbitrary orientation of the rope (Position 1) and two on an orientation at 90° to the first run (Position 2). To aid the reader in recognizing the pattern similarity in the three repeat tests and in the two repeat tests, numbers are added to the plot to identify unique peaks and valleys of vertical displacement. The reproducibility of the patterns is evident, allowing for the horizontal shift due to variations in rate of manual feed.

Tests of this type are to be applied to the set of worn ropes waiting for strength tests at the Coast Guard Research Center in Groton. And arrangements have been made to follow the change in successive rope scans during actual use life of selected ropes.

Crushing of Filaments

Scanning Electron Microscopy photographs of Section 3 indicate the presence of lateral compression and embossing of filaments in the high pressure zones of the 3-strand twisted rope. There is some evidence of filament strength loss in the presence of such compression. But it is not known whether such axial strength reduction is directly caused by the lateral deformation or indirectly caused by increased frictional attrition accompanying the high lateral pressures. To help answer this question a number of compressional tests were conducted on 20 mil PET monofilaments.

The monofilaments were first compressed laterally between flat platens without axial tension. They were released and tested for tensile strength, and SEM examinations were then conducted at fracture points. In a second series of tests, the monofilaments were tensile tested on the Instron during application of lateral compression from surrounding monofilaments.

The two testing modes are shown in Fig. 6.7A for platen compression before tensile testing and 6.7B for tensile testing in the presence of lateral compression. The results for platen compression followed by tensile tests are shown in Fig. 6.8A,B. Residual or plastic lateral deformation is plotted against total applied deformation in Fig. 6.8A and residual tensile strength vs. residual lateral deformation in Fig. 6.8B. Surprisingly, little tensile strength loss is observed for residual deformations up to 4 mils (20% diameter reduction) corresponding to applied deformations up to 8 mils (or 40%, based on the original diameter). Between residual deformations of 4 mils to 7 mils, strength losses of 10% to 20% are recorded.

In the presence of a low residual lateral deformation of 1.2 mils, longitudinal axial cracks are in evidence in the fractured end view of the monofil. Such cracking can be seen in Fig. 6.9A,B yet lateral bonding between "fibrillar" components is still strong enough to hold the structure together. Once failure takes place in such a structure, the locally released stress is transferred to adjacent fibrillar components, leading to their failure and to fracture propagation across the filament section in a well defined fracture surface, e.g. in Fig. 6.9A,B. However, as lateral crushing increases, the lateral bonding forces are reduced and the monofilaments behave more like loosely bonded "fibrillar" components. Now, upon initial failure of one segment of the filament, cracks tend to propagate along the filament, as well as across its section. The sequence of fracture surfaces seen in monofilaments exposed to successively higher lateral deformations is seen in Figs. 6.9C,D,E,F which manifest striational structures and "tailing" breaks. The delamination present in Fig. 6.10A is not unlike the delamination shown in Fig. 6.10B representing the chafing of a filament at a "hard" zone in a 3-strand twisted rope.

The lateral load deformation behavior of monofilaments (similar to those used in the rope study) has been studied in the

Fibers and Polymers laboratory and reported earlier [3.3]. Figure 6.11A,B provides a summary of such measurements, indicating a moderately linear behavior in lateral compression up to the order of 10% change in diameter. This is consistent with the results of the current study plotted in Fig. 6.8A.

These data are limited, but they do indicate that axial strength reduction for the one monofilament studied is limited for residual diametral deformations of less than 20%. They also indicate that its axial strength loss for extreme lateral compressions is of the order of less than 20%. Such observations, coupled with the evidence of linear elastic behavior in lateral compression up to 10% diametral reduction for four different monofilaments, suggests in a preliminary way that the direct effect of inner rope pressure on filament axial strength may not be a serious factor in deterioration of synthetic fiber rope. It remains, however, to conduct further tests according to the method of Fig. 6.7B, or by similar technique. The effect of lateral pressure on the local frictional attrition is an entirely different matter, also a subject for further investigation.

Self Induced Twisting of Ropes

It has been noted that ropes being pulled over curved surfaces will tend to twist under certain running conditions. Such twisting may lead to excessive torque, even to torsional buckling or hockling with subsequent localized rope damage. In the case of a mountaineer rapelling down a cliff face and controlling his rate of descent by looping his rope around a metal pin or ring, the torsion thus induced could cause him to rotate about the axis of the supporting line, creating a dangerous situation. A like danger is present for personnel descending from a helicopter, or for firefighters descending the wall of a building. Accordingly, it was deemed worthwhile to study this phenomenon of induced twisting.

The study has been experimental thus far, with some analytical components. The experiments have been conducted in both unsteady and steady state running conditions. In all cases, the rope specimen (1/4" diameter) has been wrapped 360° around a metal or plastic (PMMA) rod and relative translational motion has been effected, either by moving the pin along a rope held at both ends, or by maintaining the pin in a fixed position with rope motion induced by pulley rotation. The variables of the system were: the type of rope (i.e. whether double braided or 3-strand twisted), the pin diameter and material, the angle between the pin axis and the rope path (upstream and downstream) and the rope tension. The dependent variable in these experiments was the rate of rope rotation, determined by counting the revolutions of a flag or a marker on the rope during a given test sequence.

During transient runs, the test set-up was that sketched in Fig. 6.12 showing rope positions at which rotations were measured. Figure 6.13 presents typical results of rope rotation vs. rope position as a function of pin angle (to rope path). It is clear

that the induced twist increases significantly as the pin angle is reduced from 90° to 45°. This dependence on pin angle is confirmed in steady state tests using rope pulleys. It is noted that the starting rope tension in the tests of Fig. 6.13 was 10 lbs. When this initial tension was decreased to 5 lbs, the same effect of pin angle was observed, but with a drastic reduction in the magnitude of rotation at all positions and at all angles. In contrast, when the starting tension was raised to 15 lbs and to 20 lbs, the same trends and the same magnitudes of rotation rates were observed as at 10 lbs tension. In short, a step increase in rotation occurred above 5 lbs initial tension, then the rotation rate was essentially constant with further increases in tension.

The effect of pin diameter was noted to be significant, with a doubling of the pin diameter resulting in a halving of the rotation rate in a given rope. Further, it was noted that shifting from a steel pin to a PMMA rod significantly increased the rotation rate. And, finally, it was observed that changing the direction of pin wrap for the braided 1/2-in diameter rope simply changed the direction of rotation, but not the magnitude of rotation rate. A similar change for the 1/4" 3-strand twisted rope resulted in significant differences in the rate of rotation.

The behavior of the rope about the pin is deemed to be caused by the forced geometric path of the helical pin wrap, in short, by the induced geometric torsion of the rope. This torsion is known to equal $\sin 2\theta/2R$ (where θ is the helix angle of wrap and R is the combined pin and rope radius). Thus, the geometric torsion is observed to peak at $\theta = 45°$, a feature partially observed in the transient test data of Fig. 6.13 and fully observed in the transient test data of Fig. 6.13 and fully observed in subsequent tests under steady state conditions.

The rope twist which is manifested upstream in the steady state test and both upstream and downstream in the transient test is caused by rotational slippage of the rope over the pin-contact entry zone and the pin-contact exit zone. In short, the frictional restraint on rope rotation in the entry and exit zones is not sufficient to effect a sudden step drop in rope torque from the helical path zone to the straight entry end zones. The transient occurrence of this phenomenon has been studied by D. Skeels [6.1] and the investigation of the steady state condition is being continued by M. Oliviera.

Structural Mechanics of Ropes

Major emphasis in the initial mechanics studies of this program has been given to the 3-strand twisted rope, although some preliminary geometric consideration has been given to the double braided rope structures of Figs. 6.1, 6.2 and 6.3.

The basic structure of the 3-strand rope can be displayed in

a variety of ways, as has been done in Fig. 3.1 and Fig. 3.3. The basic geometry of the rope is displayed in Fig. 6.14 with conventional notations from differential geometry of a circular helix. It is seen that the basic helix is that formed by the strand about the rope axis. A secondary helix is formed by the plied yarn axis about the strand axis and a tertiary helix by the rope yarn around the plied yarn axis. One can go on concerning the path of the textile yarn about the rope yarn axis and the filament about the textile yarn axis, but the double (or, at most, the triple) helix of Fig. 6.14 should suffice for the purpose of predicting rope behavior in monotonic tension or in cyclic loading.

The key geometric parameters of these various components of the 3-strand rope are the local orientation (or obliquity) angle, the local path curvature and path torsion, and the path length within given limits. The exact expressions for these geometric parameters have been published in the tire cord literature [6.2] and will not be repeated here. Suffice to say that lengths of plied yarns in various layers of a strand of rope 4 have been calculated according to the geometric relationships for a full turn of the strand about the rope. Direct measurements made of the corresponding lengths at the surface and in first and second sublayers are in agreement with the calculated values to within 6%.

The tensile mechanics of the plied yarns can be approached by use of energy methods as proposed by Treloar [6.3], but it is doubtful that these methods can be extended for the treatment of fracture initiation and fracture propagation in plied yarns. Nonetheless, the energy method may be applied to the two extreme instances in yarn mechanics, first for the case of frictionless filaments, where tensions are constant along the length of each filament, and second for the case of total friction (no freedom of movement) where local component strain is a function primarily of local obliquity to the axis of the next higher order component.

The real situation in 3-strand ropes obviously lies between these two extremes and permits some filament and yarn slippage from locations of low tension to those of high tension. Clearly, the degree of slippage in any instant is dependent on the relative levels of tension in the two zones and on the degree of slippage restraint related to local lateral pressures and frictional coefficients. The role of friction can be easily demonstrated by removing the finish and/or waxes from a rope and then replacing them with various levels of lubrication.

The approach which is being taken at present is to determine the lateral pressure distribution based on the alternate assumptions of (1) complete freedom of filament slippage and (2) complete restraint. The potential for slippage between tension extremes in the no-slip case will then be determined, based on the restraints possible under the alternative pressure distribution assumptions. The reordering of the stress distributions will follow based on the slippage patterns established. The process will be reiterated until a steady state is determined.

As to rupture initiation, efforts will be directed towards superposition of the damage distributions such as have been observed in the pathological studies of Section 3. At this point, resort will be had to recently developed statistical techniques of numerous other workers in the field. Particular emphasis is being given to the works of Zweben and of Phoenix.

The remaining important aspect of mechanics of rope structures is that of tensile fatigue of twisted structures. An extensive study of fiber fatigue has been presented in Section 5 with emphasis on single fiber and low twist yarn fatigue, as well as on stress corrosion cracking in synthetic filaments. A study is also underway to explore the fatigue behavior of higher order rope structures, both in theory and in experiment.

The approach being taken is to consider fatigue failure as consisting of two elements: first, a pure tensile cycling fatigue (as discussed in Section 5) occurring in a twisted structure whose lateral pressures vary as a function of local geometry. The model for simple tensile fatigue is based on the assumption of earlier failure of filaments at maximum cycling stress, followed immediately by redistribution of relieved stresses to adjacent rings. In effect, then, cyclic stresses on middle zone filaments will not maintain constant stress amplitudes but, rather, increasing stress amplitudes as ruptures sequentially propagate outward from the initial failure zone. Clearly, the pure tensile fatigue behavior of single filaments under monotonically increasing stress amplitudes must be determined experimentally as a basis for this model development.

Summary/Conclusions/Future Plans

The departure from ideal cross sectional yarn geometry upon application of rope tension has been illustrated for double braided ropes. And residual cross sectional deformations have been recorded for 3-strand twisted rope. The importance of these departures from round or elliptical or trilobal geometries has not been established, but it will be a subject for further study.

Hardness and bending rigidity scans along a rope length have been made possible by construction of a special deformational scanner working in two possible modes. A variety of 3-strand ropes and double braided ropes has been scanned in repeat tests of hardness or of bending rigidity, and good reproducibility of the data has been noted. At the same time, it was noted that entry and exit conditions, e.g. initial curvature, and back tension both influenced the resulting scans. Future tests will be modified to control these features. At the same time it should be stressed that the bending test gauge length is short (i.e. $\ell/d \approx 6$) and the deformation angles are small, thus suppressing the effect of line tension.

Scans are to be made of the remaining rope specimens retained by the Coast Guard Laboratories at Groton. And these worn ropes will be subjected to tensile tests by Mr. Bitting. This affords

a good opportunity to determine the potential utility of the scanning tests. For the time, it can be stated without reservation that each worn rope has its own fingerprint as determined by a hardness or bending rigidity scan. It remains to establish the significant parameters of such scans.

Crushing of filaments in a rope center due to tension-induced lateral pressures does not appear to be a serious problem for nylon and PET ropes. Still, some evidence of filament compression was seen in filaments extracted from the worn rope series. The importance of lateral stresses may be expected to increase as one moves from nylon or PET to aramid filaments known to have compressional vulnerability. For this reason, some additional work is planned concerning compressional effects on filament performance.

Self-induced twisting of ropes has been reproduced under laboratory conditions and a good start has been made on analysis of the phenomenon. Completion of the analysis and of verifying experiments is planned for the current year.

Study of the structural mechanics of rope structures has been initiated this year, but kept at a low level, while emphasis was put on mechanical pathology of worn ropes. During the coming year, this emphasis will be reversed, and structural mechanics will receive major attention. The subjects to be considered are: (1) tensile strength of rope structures based on knowledge of average filament properties and of rope geometry, (2) tensile strength of worn ropes with patterns of deterioration such as reported in Section 3 of this report, (3) cyclic tension fatigue behavior of new ropes based on knowledge of fatigue properties of individual yarns, and (4) cyclic bending fatigue behavior of worn ropes with patterns of deterioration such as reported in Section 3.

6. REFERENCES

6.1 F. Doyle Skeels, Torsion Induced in a Rope Wrapped Helically Around a Guide Pin, 2.32 Laboratory Report, Department of Mechanical Engineering, 1981.

6.2 Backer, S., Tire Cord Structure and Properties, in Mechanics of Pneumatic Tires, Edited by S. Clark, N.B.S. Monograph 122, Washington, D.C. (1971).

6.3 Treloar, L.R.G. and Riding, G., A Theory of the Stress-Strain Properties of Continuous Filament Yarns, J. Textile Inst. 54, 156-170 (1963).

LIST OF FIGURES

6.1A,B	Cross Sectional Profiles of 1/4-in Double Braided Rope with Core Removed A. At 300 lbs Tension; B. At 20 gf
6.2A,B	Cross Sectional Profiles of 1/4-in Double Braided Rope at A. 200 lbs; B. 600 lbs.
6.3A,B	Cross Sectional Profiles Successively Cut in a 1/4-in Double Braided Rope (Core is Omitted)
6.3C,D	Cross Sectional Profiles Successively Cut in a 1/4-in Double Braided Rope
6.4	Locus of Yarn Movement in Cover of a Double Braided Rope
6.5	Hardness-Bending Rigidity Scanning Instrument
6.6	Hardness and Profile Test of a Used Double Braided Rope
6.7	Testing Modes
6.8a b	Plastic Deformation vs. Total Deformation Breaking Strength vs. Plastic Deformation
6.9	Fractography of Laterally Crushed Monofilaments
6.10	Fractography of Laterally Crushed Monofilaments
6.11a	Load Deformation Behavior of PET Monofilaments (1,2) in Lateral Compression
6.11b	Load Deformation Behavior of Nylon 66 Monofilaments (1,2) in Lateral Compression
6.12	Test Equipment to Measure Induced Twist
6.13	Effects of Varying Pin Angle with Constant Tension
6.14	Geometry of Three-Strand Twisted Rope

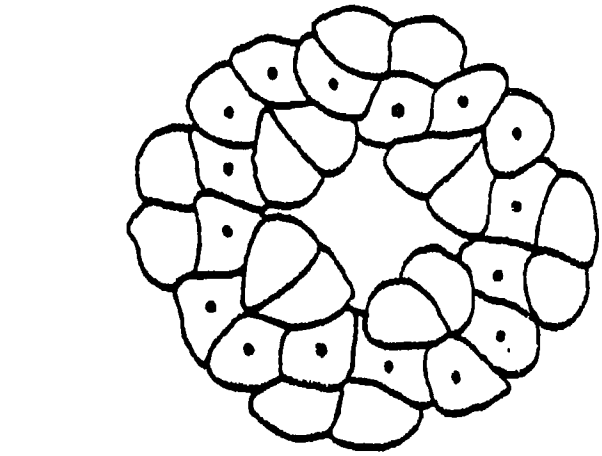

(A)

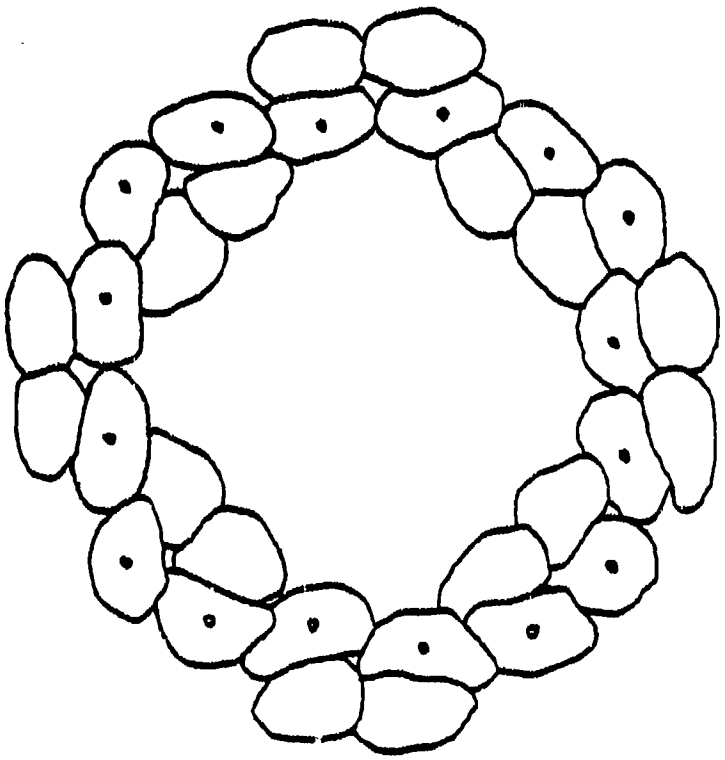

(B)

FIG. 6.1 A AND B. CROSS SECTIONAL PROFILES OF 1/4 IN. DOUBLE BRAIDED ROPE WITH CORE REMOVED (A) AT 300 LBS TENSION, (B) AT 20 GF

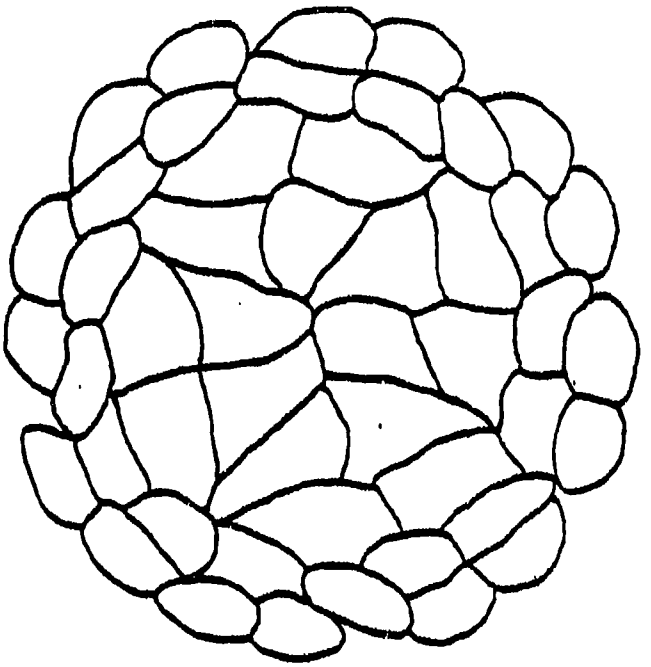

(A)

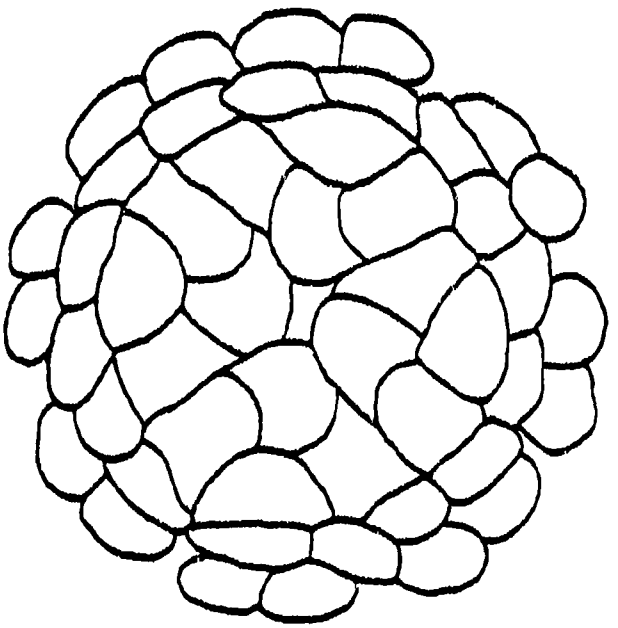

(B)

FIG. 6.2 A AND B. CROSS SECTIONAL PROFILES OF 1/4 IN. DOUBLE BRAIDED ROPE AT (A) 200 LBS AND (B) 600 LBS.

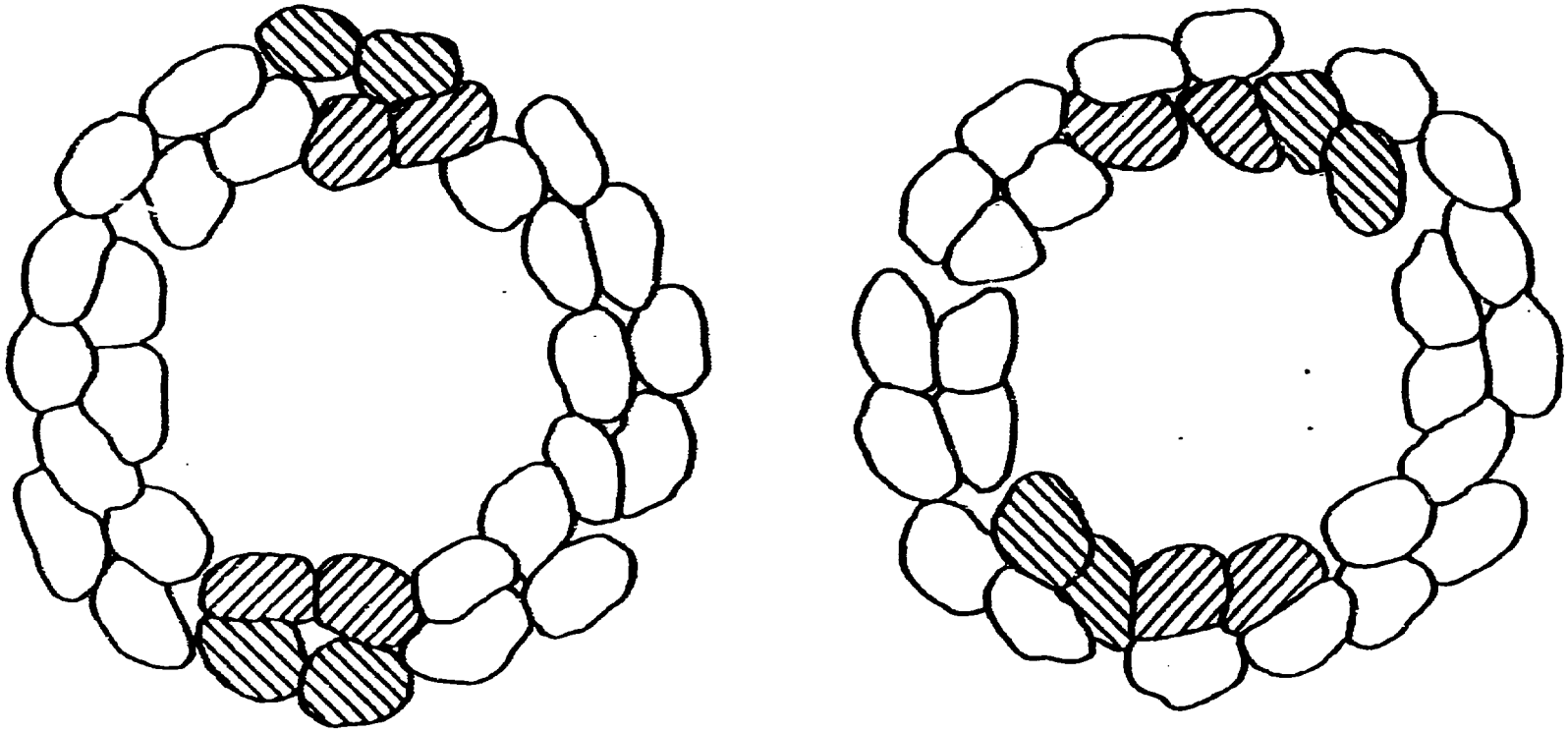

(A) (B)

FIG. 6.3 A AND B. CROSS SECTIONAL PROFILES SUCCESSIVELY CUT IN A 1/4 IN. DOUBLE BRAIDED ROPE (CORE IS OMITTED).

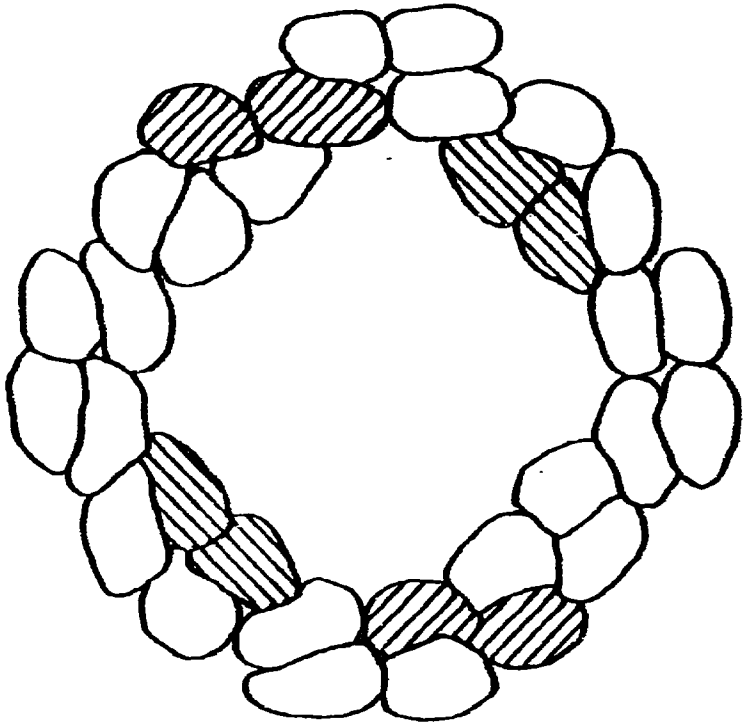

(C)

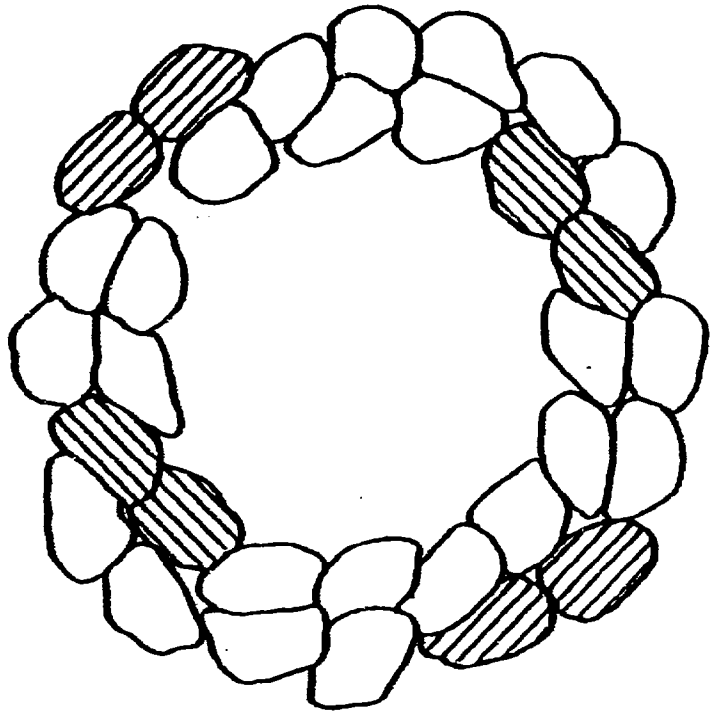

(D)

FIG. 6.3C AND D. CROSS SECTIONAL PROFILES, SUCCESSIVELY CUT IN A 1/4 IN. DOUBLE BRAIDED ROPE.

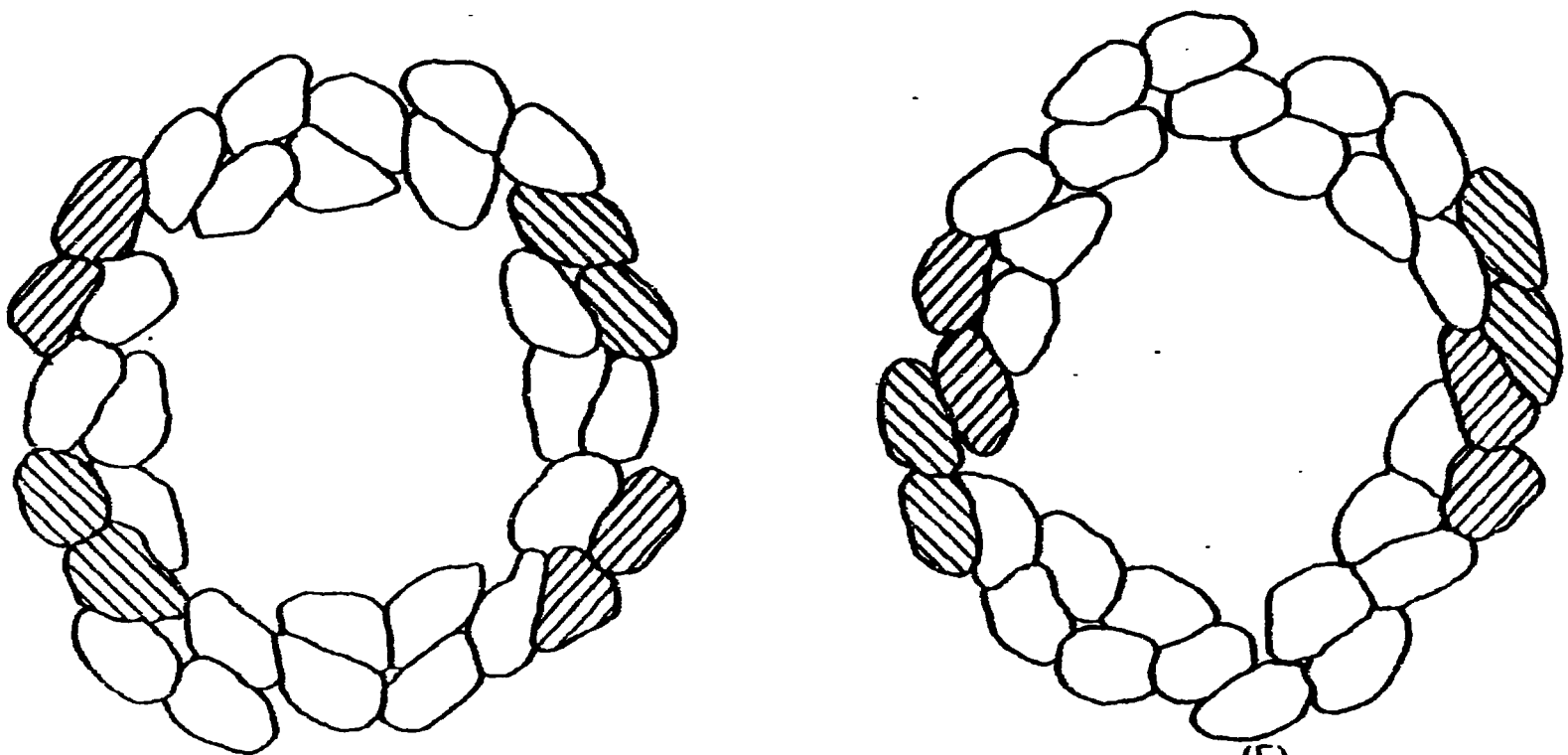

FIG. 6.3 E AND F. CROSS SECTIONAL PROFILES SUCCESSIVELY CUT IN A 1/4 IN. DOUBLE BRAIDED ROPE.

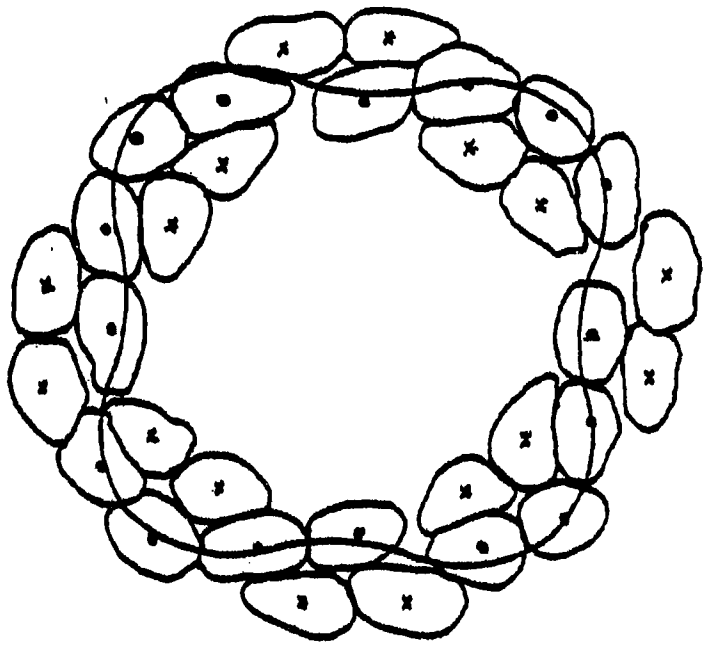

FIG. 6.4. LOCUS OF YARN MOVEMENT IN COVER OF A DOUBLE BRAIDED ROPE.

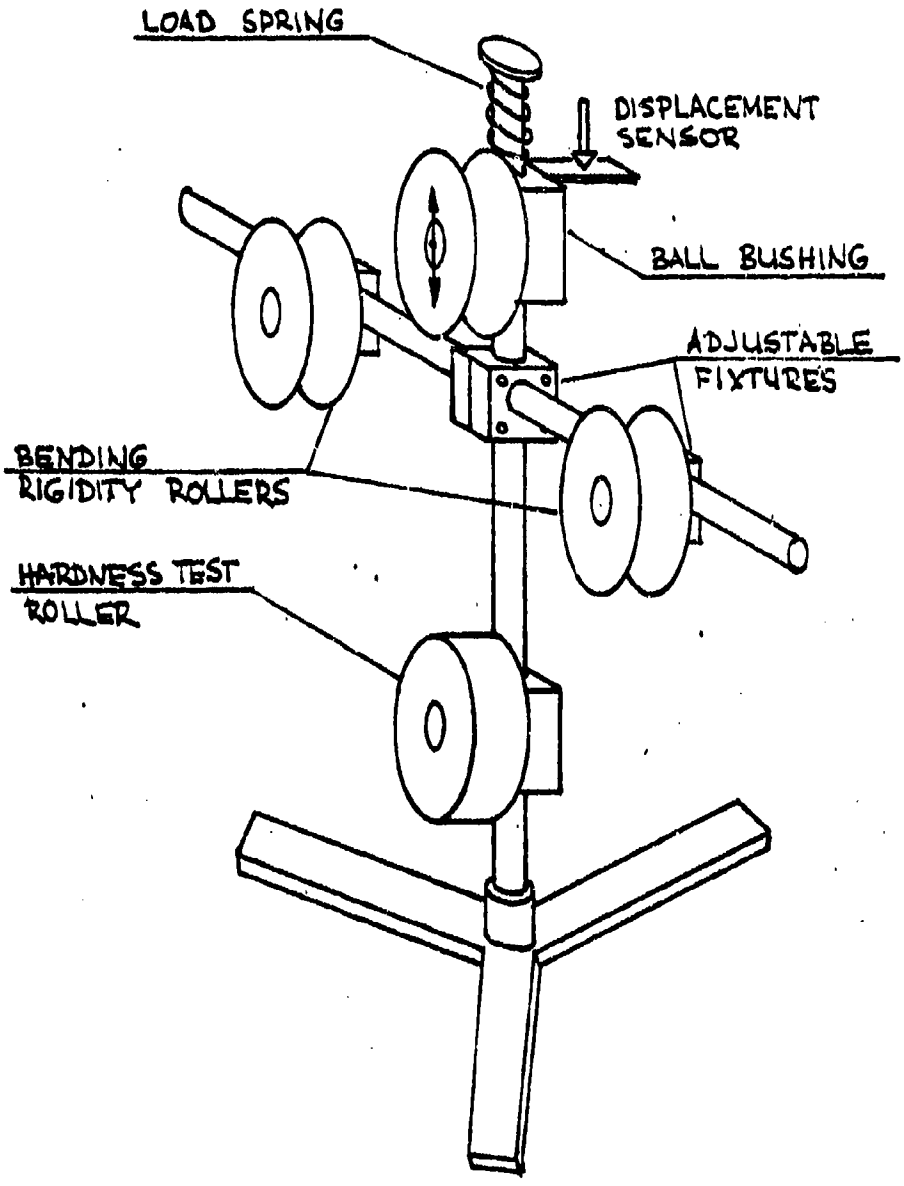

FIG. 6.5 HARDNESS-BENDING RIGIDITY SCANNING INSTRUMENT

FIG. 6.6

HARDNESS AND PROFILE TEST OF AN USED DOUBLE BRAIDED ROPE (9" CIRCUMFERENCE, DELIVERED 2/20/82

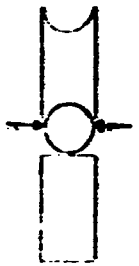

6.20

POSITION 1

POSITION 2
(ROPE TURNED BY 90°)

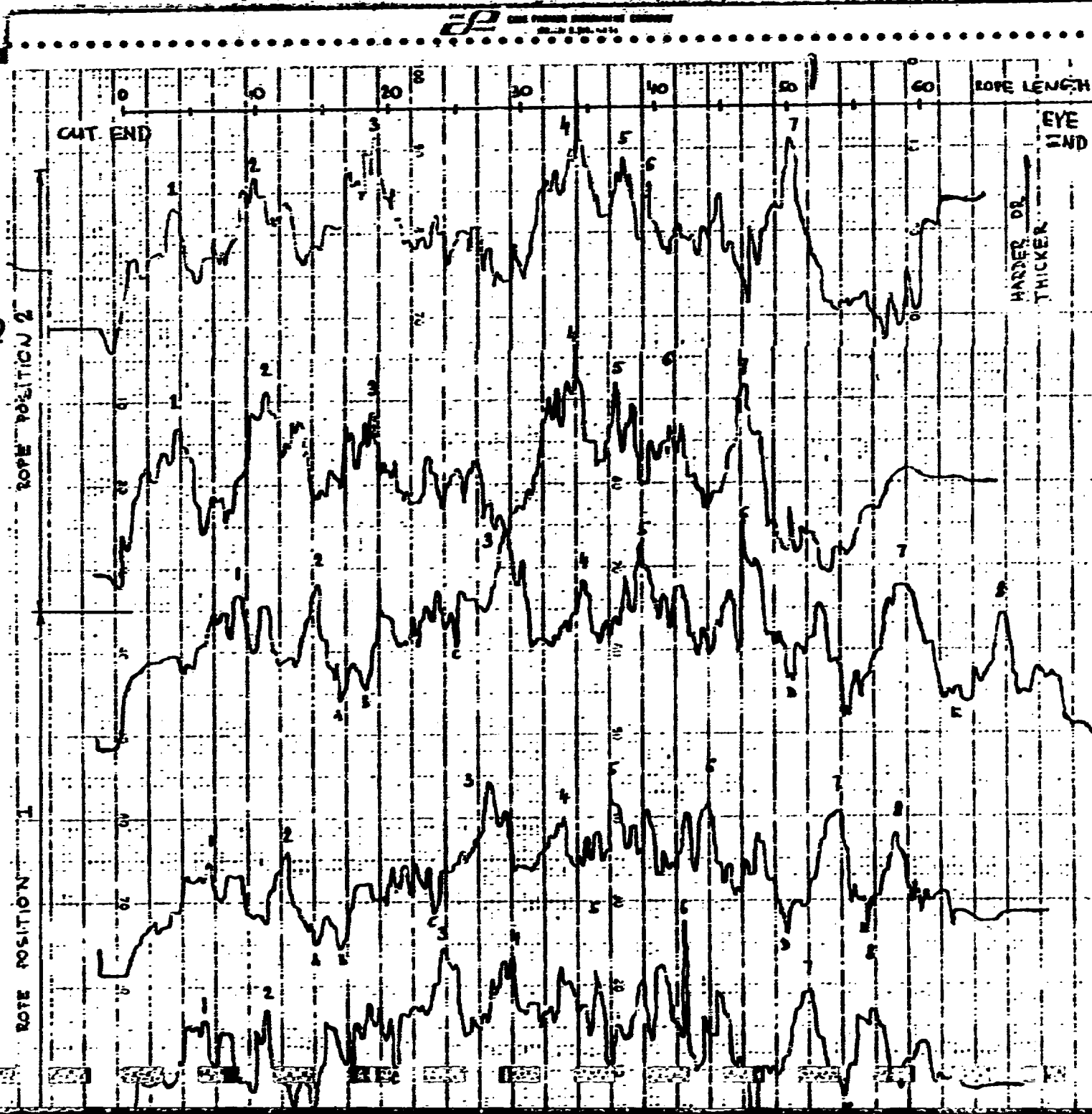

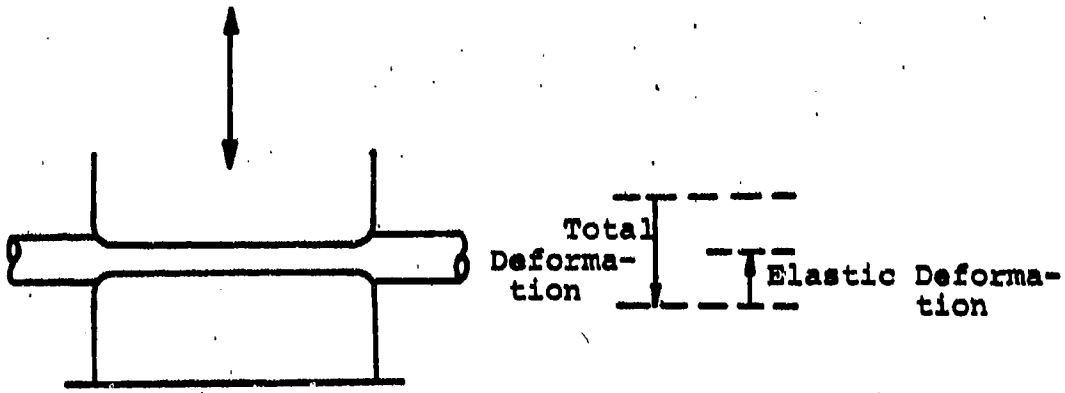

(a)

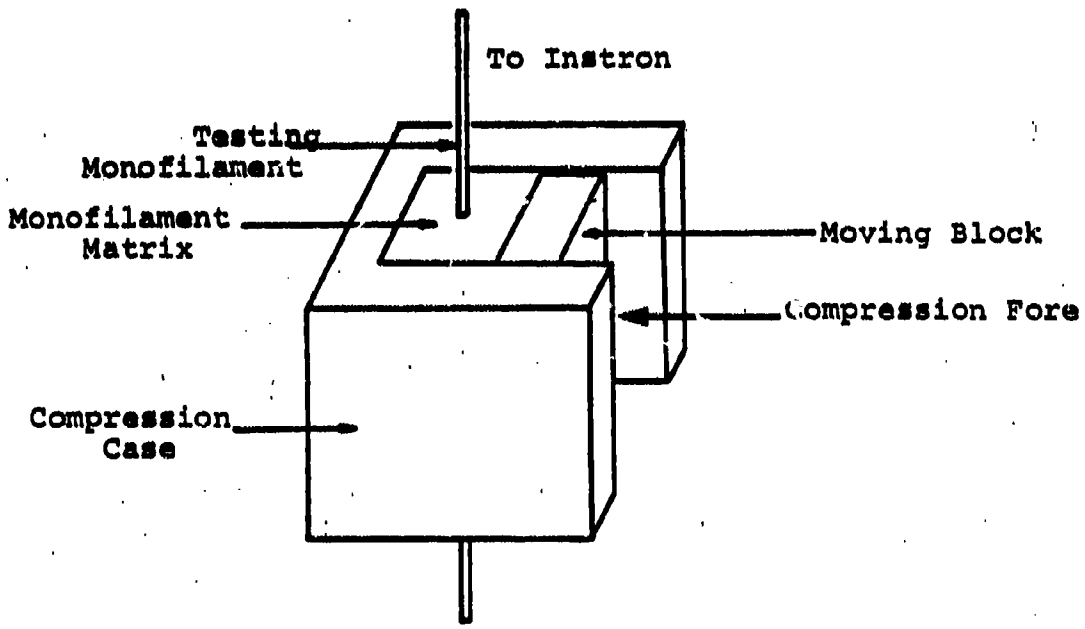

(b)

Fig. 6.7 Testing Modes

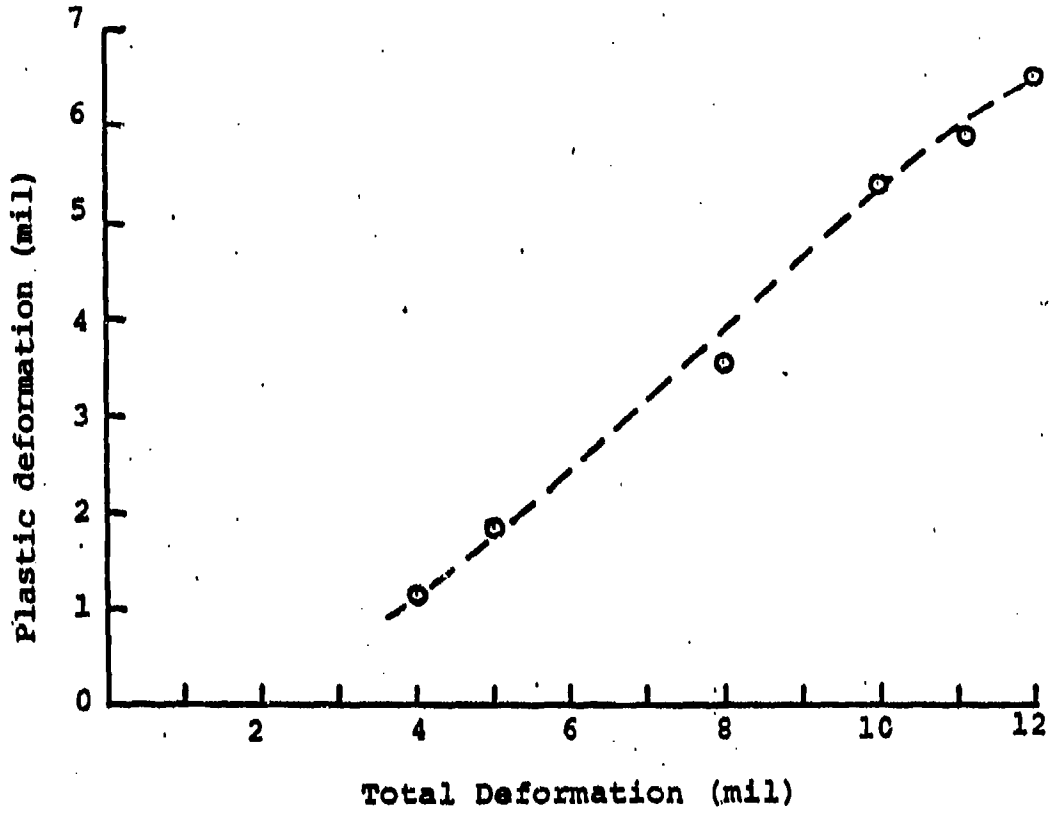

(a)

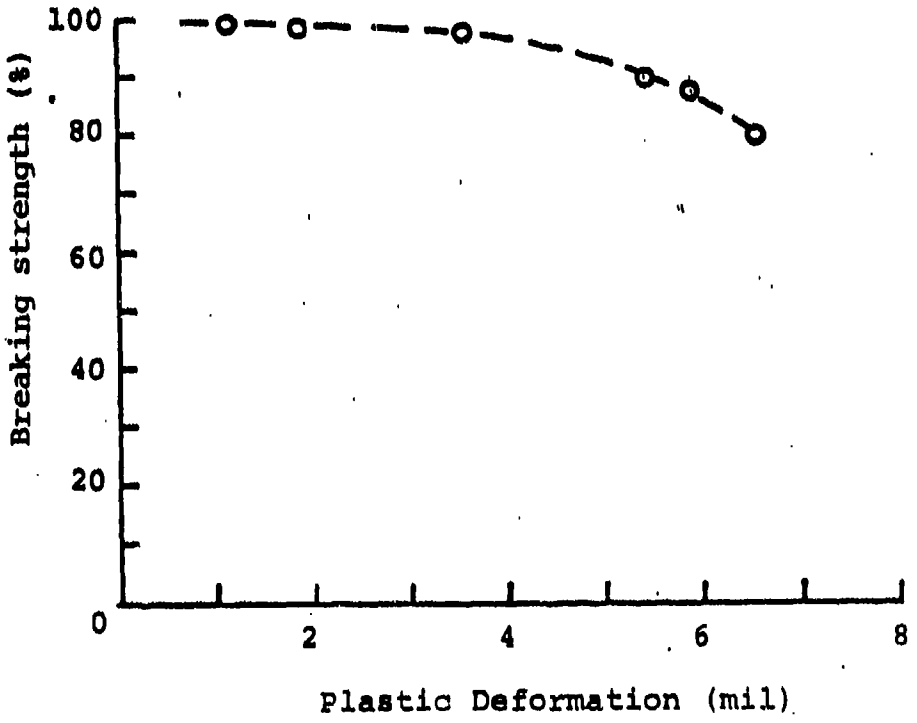

(b)

Fig. 6.8 (a) Plastic deformation vs. total deformation
(b) Breaking strength vs. plastic deformation

(a) Plastic Deformation 1.2 mil, x100

(b) Plastic Deformation 1.2 mil, x500

Fig. 6.9 Fractography of Laterally Crushed Monofilaments

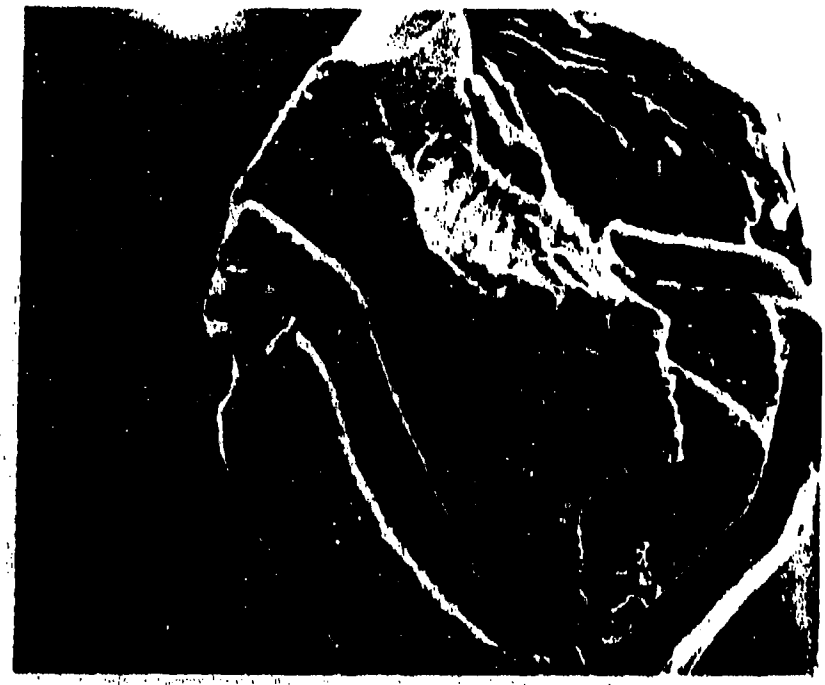

(c) Plastic Deformation 3.6 mil, x100

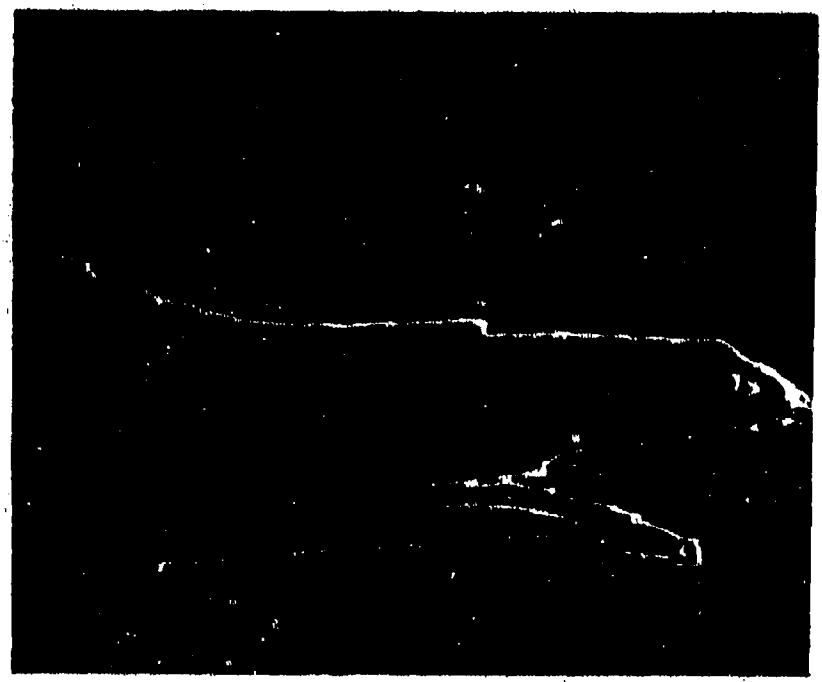

(d) Plastic Deformation 5.4 mil, x100

Fig. 6.9 Fractography of Laterally Crushed Monofilaments

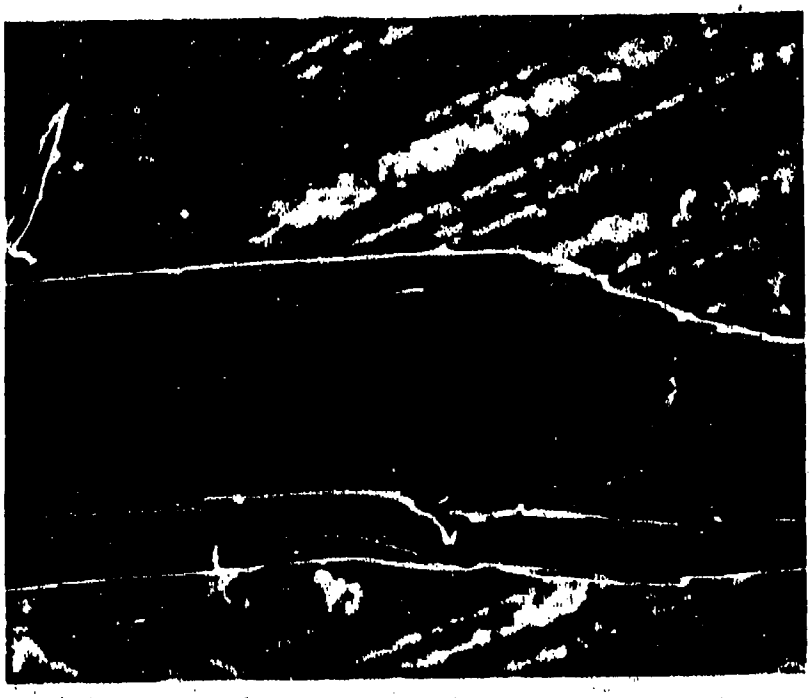

(e) Plastic Deformation 5.4 mil, x100

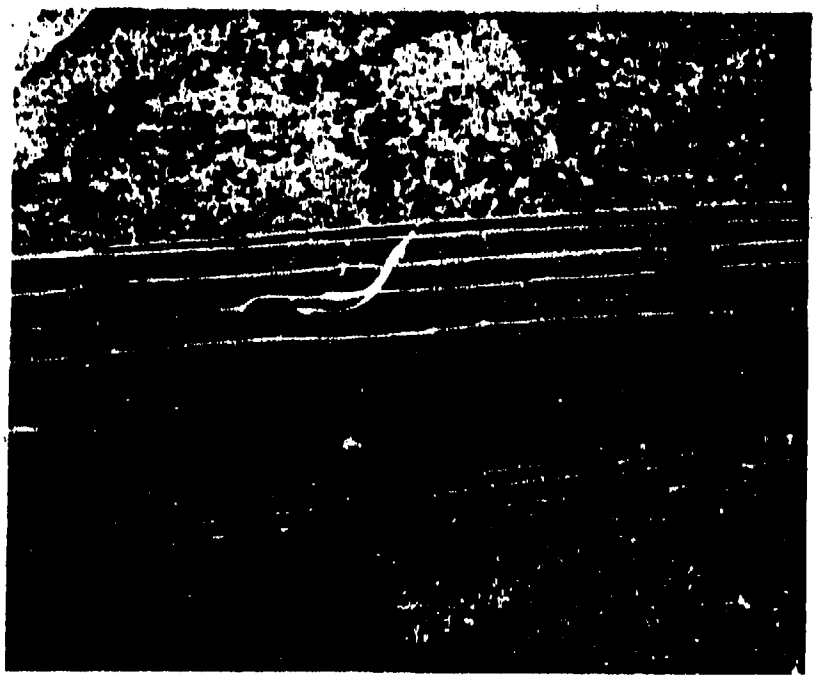

(f) Plastic Deformation 6.5 mil, x100

Fig. 6.9 Fractography of Laterally Crushed Monofilaments

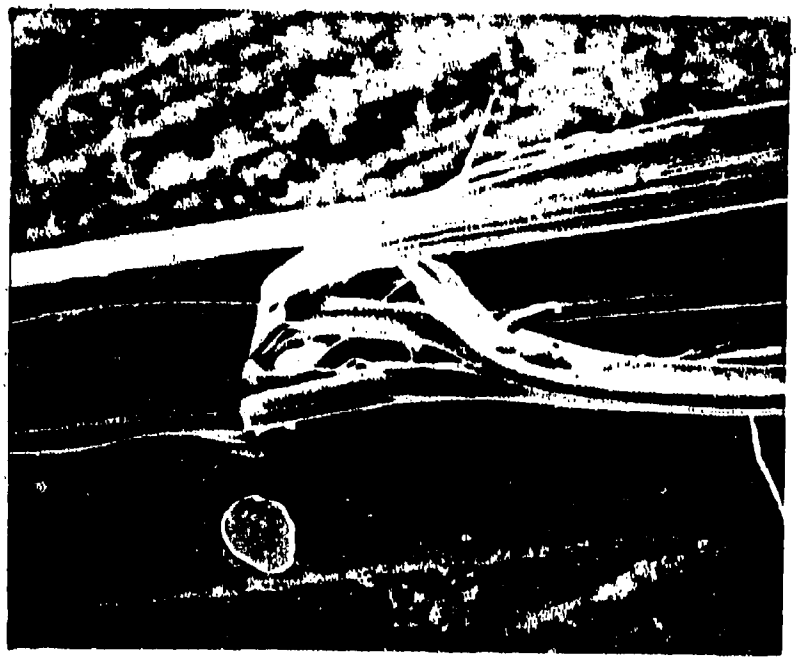

A

Plastic Deformation 6.5 mil, x100

B

Chaffing Spot of Hard Zone

Fig. 6.10 Fractography of Laterally Crushed Monofilaments

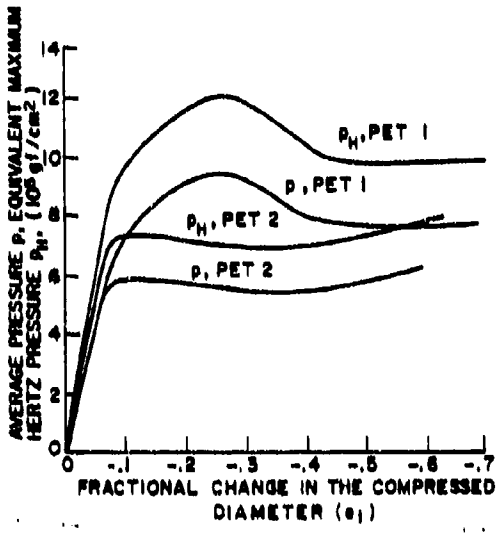

FIG. 6.11a Load Deformation Behavior of PET Monofilaments (1,2) in Lateral Compression

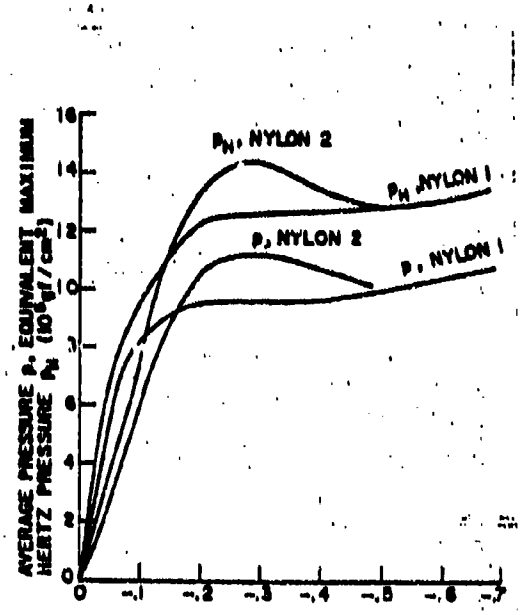

FIG. 6.11b Load Deformation Behavior of Nylon 66 Monofilaments (1,2) in Lateral Compression

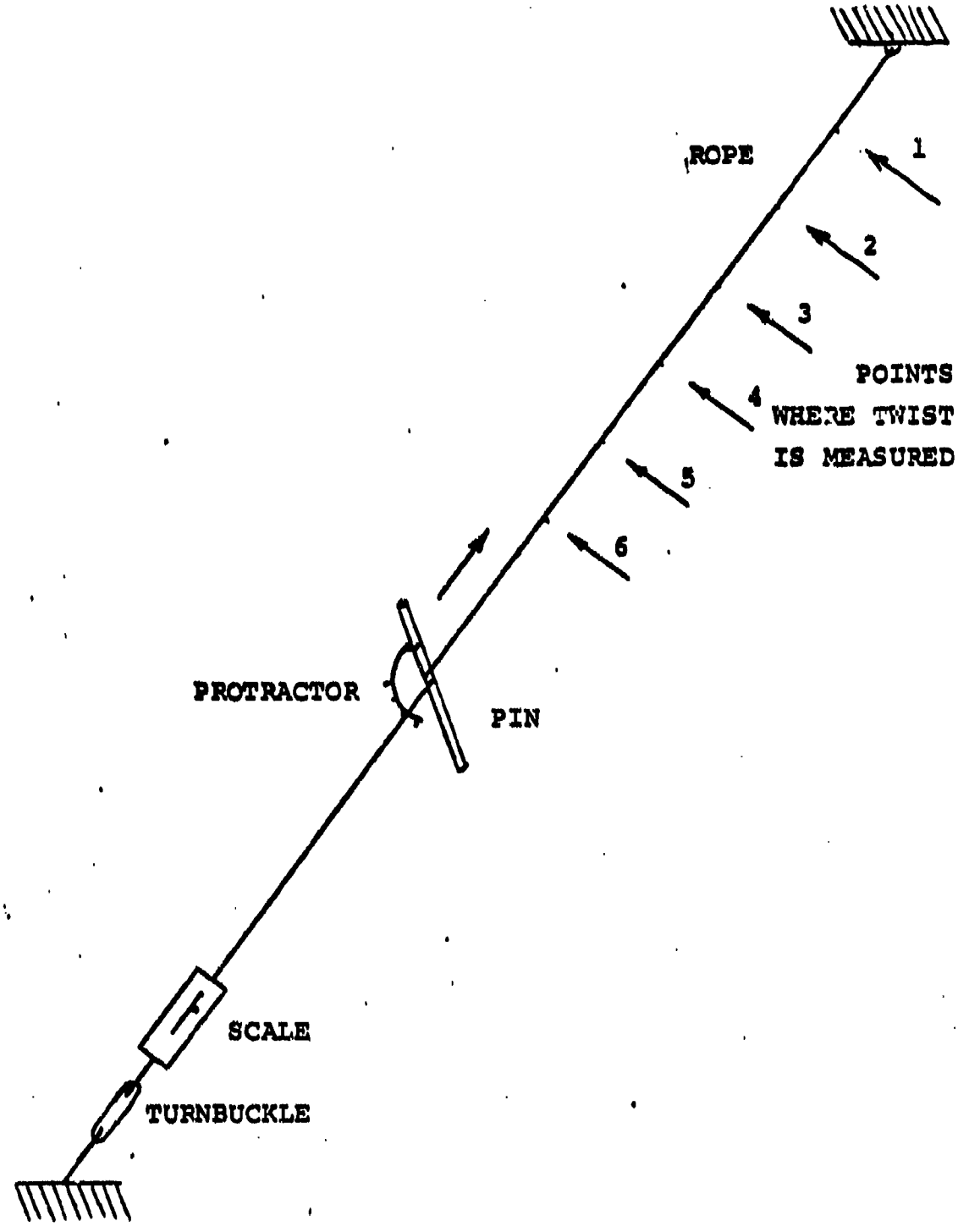

FIG. 6.12 TEST EQUIPMENT TO MEASURE INDUCED TWIST

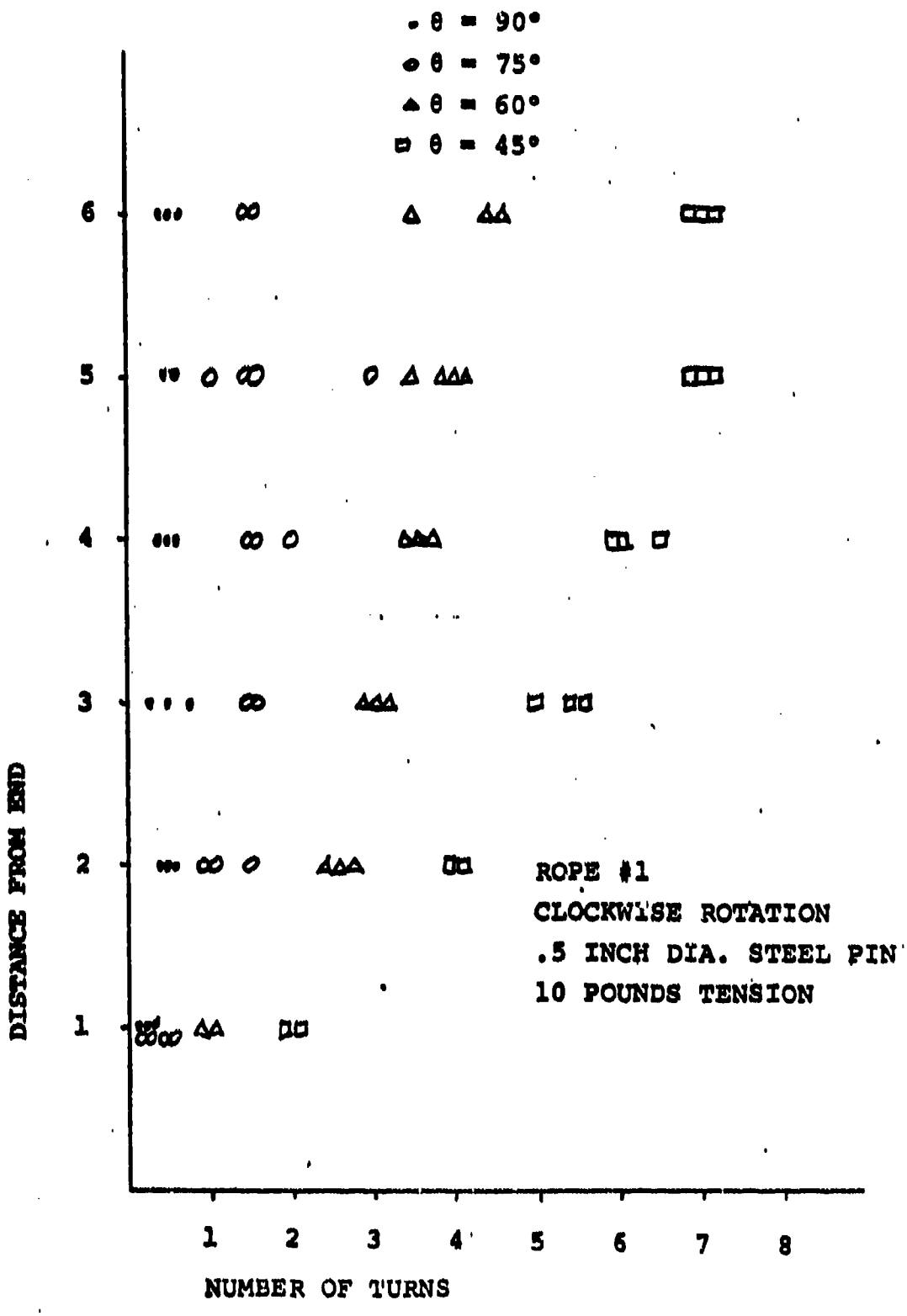

FIG. 6.13 EFFECTS OF VARYING PIN ANGLE WITH CONSTANT TENSION

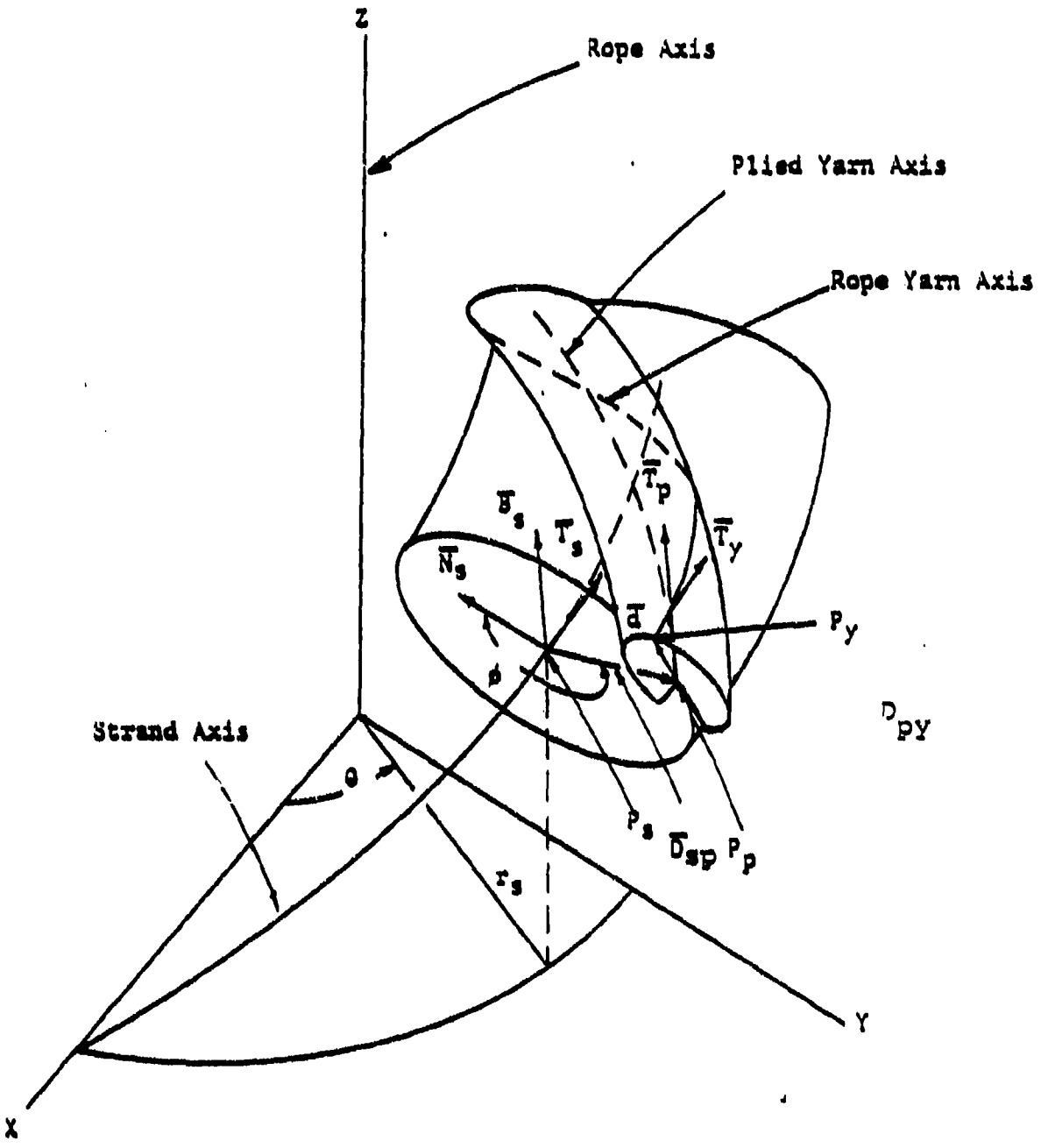

FIG. 6.14 GECMETRY OF THREE-STRAND TWISTED ROPE